

THE UNIVERSITY OF SOUTHERN CALIFORNIA
AERODESIGN TEAM PRESENTS

EMERGENSC

2023-2024 AIAA DESIGN, BUILD, FLY COMPETITION

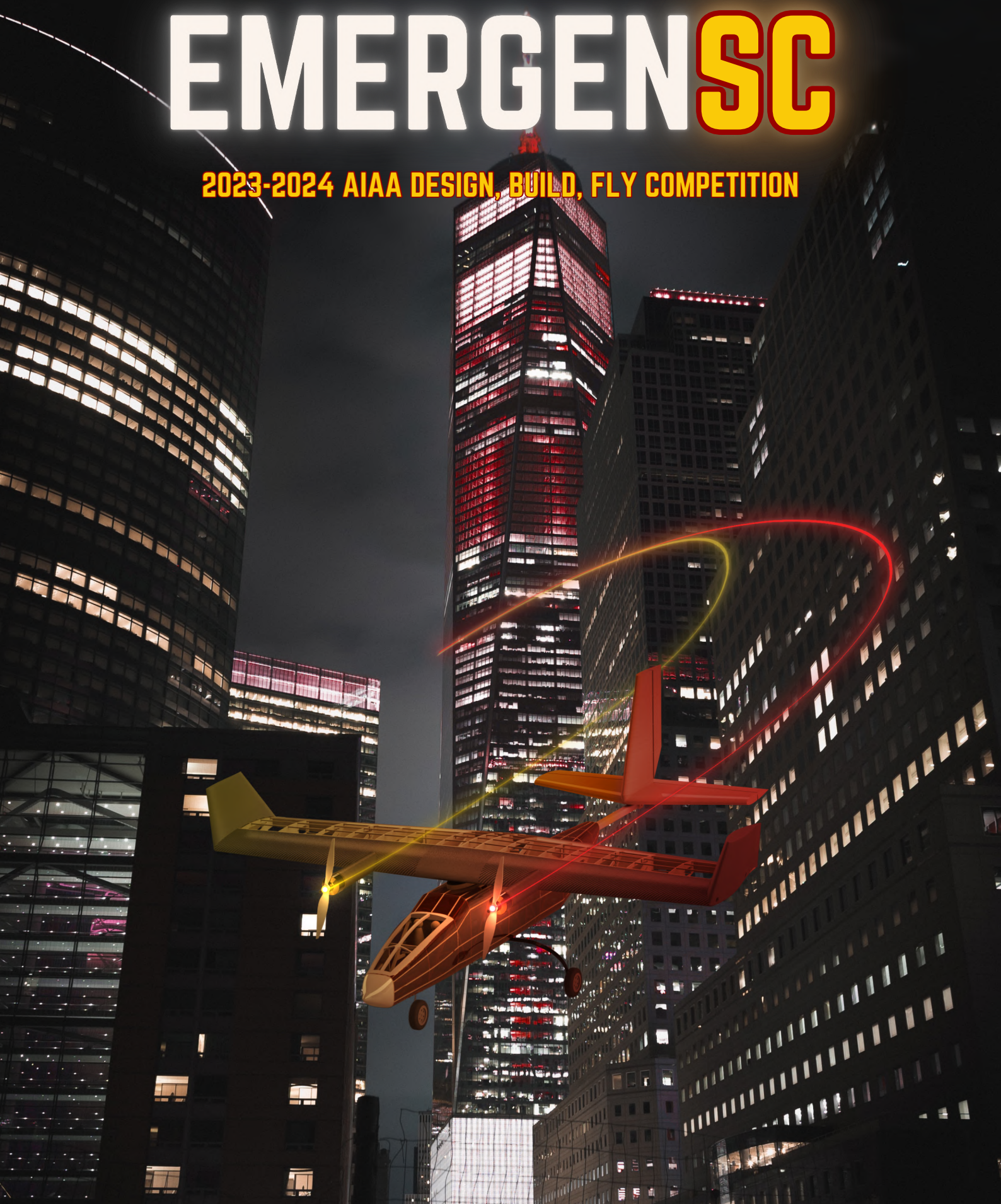


Table of Contents

Acronyms, Abbreviations, and Symbols	3
1.0 Executive Summary	4
2.0 Management Summary	5
2.1 Team Organization	5
2.2 Milestone Chart.....	6
3.0 Conceptual Design	7
3.1 Mission Requirements	7
3.2 Design Requirements	9
3.3 Configuration Selection.....	10
3.4 Final Conceptual Design.....	14
4.0 Preliminary Design	14
4.1 Design Methodology	14
4.2 Wing Geometry	15
4.3 Stability and Control.....	20
4.4 Trade Studies.....	22
4.5 Propulsion	25
4.6 Predicted Flight and Mission Performance	27
5.0 Detailed Design	28
5.1 Dimensional Parameters Table	28
5.2 Structural Characteristics and Capabilities	28
5.3 Subsystem Design.....	29
5.4 Weight and Mass Balance	38
5.5 Drawing Package.....	38
6.0 Manufacturing Plan	43
6.1 Manufacturing Processes Investigated	43
6.2 Manufacturing Processes Selected	44
6.3 Manufacturing Milestones.....	47
7.0 Testing Plan	48
7.1 Test Objectives	49
7.2 Subsystem Testing	49
7.3 Flight Test Schedule and Flight Plan	54
7.4 Flight Checklists.....	55
8.0 Performance Results	55
8.1 Demonstrated Performance of Key Subsystems	56
8.2 Demonstrated Flight Performance of Completed Aircraft	57
9.0 Bibliography	60

ACRONYMS, ABBREVIATIONS, AND SYMBOLS

a	Aileron	LiPo	Lithium Polymer
α	Angle of Attack	M#	Mission #
A	Amps	m_{MSC}	Mass of Medical Supply Cabinet
Ah	Amp-hour	MSC	Medical Supply Cabinet
AIAA	American Institute of Aeronautics & Astronautics	n	Load Factor
AR	Aspect Ratio	n_{laps}	Number of Laps
AVL	Athena Vortex Lattice	n_{pax}	Number of Passengers
b	Span	ρ	Air Density
β	Sideslip Angle	psi	Pounds per Square Inch
BC	Battery Capacity	q	Dynamic Pressure
BWB	Blending Wing Body	r	Rudder
c	Chord	RPM	Rotations per Minute
c/4	Quarter Chord	s	Seconds
C_L	Lift Coefficient	S_g	Takeoff Ground Roll
c_l	2D Lift Coefficient	SM	Static Margin
$C_{l\beta}$	Sideslip Rolling Moment Derivative	S_{ref}	Reference Area
$C_{l\delta r}$	Rudder Yaw Moment Control Derivative	S_X	Surface Area of X component
C_D	Drag Coefficient	t/c	Thickness to Chord
C_{D_0}	Parasite Drag Coefficient	TE	Trailing Edge
c_d	2D Drag Coefficient	t_{GM}	Ground Mission Time
$c_{d_{airfoil}}$	Winglet Parasite Drag Coefficient	TOFL	Takeoff Field Length
$C_{m\alpha}$	Angle of Attack Pitching Moment Derivative	t_{M2}	Mission 2 Time
$C_{n\beta}$	Sideslip Yaw Moment Derivative	T/W	Thrust to Weight Ratio
CA	Cyanoacrylate	USC	University of Southern California
CAD	Computer-Aided Design	V	Volts
CFRP	Carbon-Fiber Reinforced Polymer	V#	Version # of Team Aircraft
CG	Center of Gravity	V	Volume Coefficient
COTS	Commercial Off-the-Shelf	V_e	Propeller Velocity
δ	Control Deflection	VT	Vertical Tail
DBF	Design, Build, Fly	V_{TO}	Effective Takeoff Velocity
deg	Degrees	V_{TO1}	Takeoff Velocity
e	Elevator	V_X	Characteristic Velocity (i.e. V_{stall})
e	Oswald Efficiency Factor	W	Watts
FG	Fiberglass	W_0	Gross Takeoff Weight
FoM	Figures of Merit	W_p	Payload Weight
FoS	Factor of Safety	Wh	Watt-hours
ft	Feet	W/S	Wing Loading
fwd	Forward		
g	Acceleration Under Gravity		
GM	Ground Mission		
HT	Horizontal Tail		
in	Inches		
k	Lift-induced Factor		
lb	Pounds		
L/D	Lift to Drag Ratio		
LE	Leading Edge		
LG	Landing Gear		

1.0 EXECUTIVE SUMMARY

This report details the design, manufacturing, and testing of *EmergenSC*, the University of Southern California aircraft for the 2023-24 American Institute of Aeronautics and Astronautics (AIAA) Design, Build, Fly (DBF) competition. This radio-controlled aircraft was designed to perform four Urban Air Mobility missions. Mission 1 (M1) is a delivery flight to demonstrate operational capabilities. Mission 2 (M2) is an urgent transport flight of medical personnel, a Patient on a gurney, and a Medical Supply Cabinet (MSC). Mission 3 (M3) is an urban taxi flight with Passengers. Finally, the Ground Mission (GM) is a demonstration of efficient transitions between the flight mission configurations. In addition to the mission profiles, the aircraft is required to fit within a 2.5 ft (0.76 m) wide parking spot and takeoff within 20 ft (6.1 m) [1].

EmergenSC was designed in three phases: conceptual, preliminary, and detailed design. The purpose of the conceptual design was to determine the ideal aircraft configuration based on system requirements and sensitivity studies. The preliminary phase sized the aircraft weight, wing, empennage, and propulsion system using constraint analysis and performance trade studies. The detailed design phase focused on the internal structure of each component and payload integration. The resulting design was a dual-motor monoplane with a pivoting high wing, conventional tail, and tricycle landing gear as shown in Fig. 1. A high wing was chosen to maximize the internal fuselage volume for payloads and maintain propeller ground clearance. The wing was designed to pivot about the aircraft centerline to fit within the parking spot without compromising the wing structure by hinging at the spar. A conventional tail was selected for manufacturability and stall recovery. A dual-motor propulsion system was chosen to improve takeoff performance with blown lift. Finally, a tricycle gear was selected for stability during wing pivoting and payload loading. The manufacturing process aimed to investigate methods and materials for fabricating *EmergenSC* to its designed specifications while minimizing weight. The team implemented balsa and plywood built-up structures for all major components and employed new procedures such as steam-bending. A thorough test campaign was conducted, from component-level validation to flight performance tracking. The demonstrated capabilities of *EmergenSC* are shown in Table 1.

Table 1. Predicted performance of *EmergenSC*

Data	M1	M2	M3	GM
Gross Weight [lbf]	13.6	19.3	15.0	-
TOFL [ft]	15	20	16	-
Mission Time [s]	92.9	75.9	269.1	95
Cruise Airspeed [ft/s]	119	163	110	-
Number of Laps [-]	3	3	8	-
Payload	-	4.85 lbm	18 pax	-



Figure 1. USC 2023-24 aircraft: *EmergenSC*

2.0 MANAGEMENT SUMMARY

The 2023-24 USC AeroDesign Team consists of 50 students who contribute on an extracurricular basis. Four are graduate students, 11 are seniors, and 35 are underclassmen. The team is entirely student-led, but receives guidance from faculty, alumni, and industry advisors at weekly meetings and design reviews.

2.1 TEAM ORGANIZATION

The AeroDesign Team of USC employs a matrix leadership structure like the management hierarchy of most aerospace firms. Team leadership for the 2023-24 competition is outlined in Fig. 2.

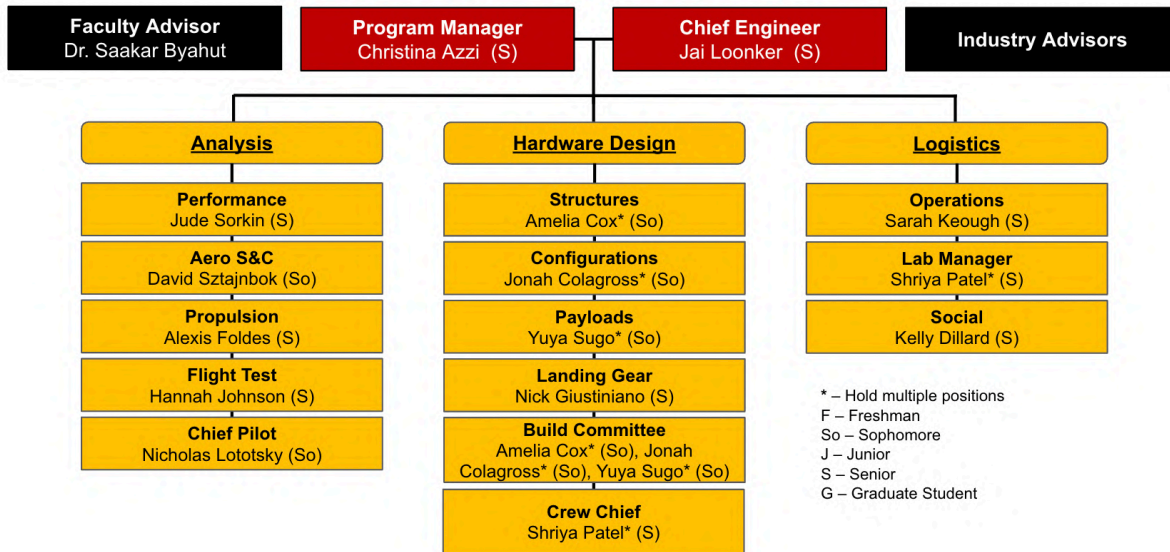


Figure 2. AeroDesign Team Organization Chart

The *Chief Engineer* leads design, build, test, and analysis efforts while the *Program Manager* sets major milestones, and coordinates documentation efforts. The two team leaders (**red**) receive suggestions from team advisors (**black**) and coordinate the design effort with 12 sub-team leaders (**gold**). The 12 sub-team leaders are organized into three distinct sub-teams: analysis, hardware design, and logistics.

The analysis sub-team conducts trade studies on wing and payload sizing (*Performance Lead*), performs stability and control analysis (*Aero S&C Lead*), selects a suitable propulsion package (*Propulsion Lead*), develops flight test schedules for data processing (*Flight Test Lead*), and trains new pilots (*Chief Pilot*). The *Chief Pilot* is selected at the start of the flight-testing regime while reserve pilots continue training. The analysis sub-team requires skills in aircraft sizing, simulation, propulsion, data acquisition, along with practical experience in model aircraft flying.

The hardware design sub-team designs all aircraft components (*Structures Lead*) and subsystems (*Payloads Lead*), models components in Computer-Aided Design software (*Configurations Lead*), produces the landing gear (*Landing Gear Lead*), manufactures components with knowledge in 3D-printing, composites, and woodworking (*Build Committee*), while also integrating the aircraft avionics (*Crew Chief*). The hardware design team possesses a range of skills including proficiency in component modeling,

knowledge of various manufacturing techniques, and expertise in system testing to ensure reliability of the designed hardware.

Lastly, the logistics sub-team obtains sponsorship funding and oversees the annual budget (*Operations Lead*), manages team involvement (*Social Lead*), while enforcing safe lab practices in an organized lab space (*Lab Manager*). The logistics sub-team requires skills such as familiarity with funding streams, excellent communication abilities, and strong organizational skills.

2.2 MILESTONE CHART

The *Program Manager* maintains a high-level schedule, shown in Fig. 3, that is used to plan workflow, allocate resources, and track tasks to completion. The manufacturing schedule set at the beginning of the year is updated accordingly, as shown by “Actual Timing”. Note that “Actual Timing” is not shown for future tasks. The design process was conducted to focus on wing and fuselage sizing during the Conceptual and Preliminary Designs respectively, while refining subsystem designs, such as the payload system and parking spot mechanism during the Detailed Design. The schedule allows for the construction of five aircraft. The main purpose of the Version 0 aircraft was to confirm Takeoff Field Length (TOFL) and overall aircraft dimensions. Version 1 introduced the assembly of the initial built-up fuselage to assess aerodynamics and determine Passenger capacity. Version 2 focused on integrating the rotating wing and securing device to fit in the parking spot configuration, and Version 3 aims to enhance optimization for all missions and payloads. Looking forward, the competition aircraft, *EmergenSC*, is set to leverage manufacturing learnings from earlier versions, incorporate mission performance enhancements from Version 3, as well as utilize results from all system tests, presented in more detail in Section 7.0.

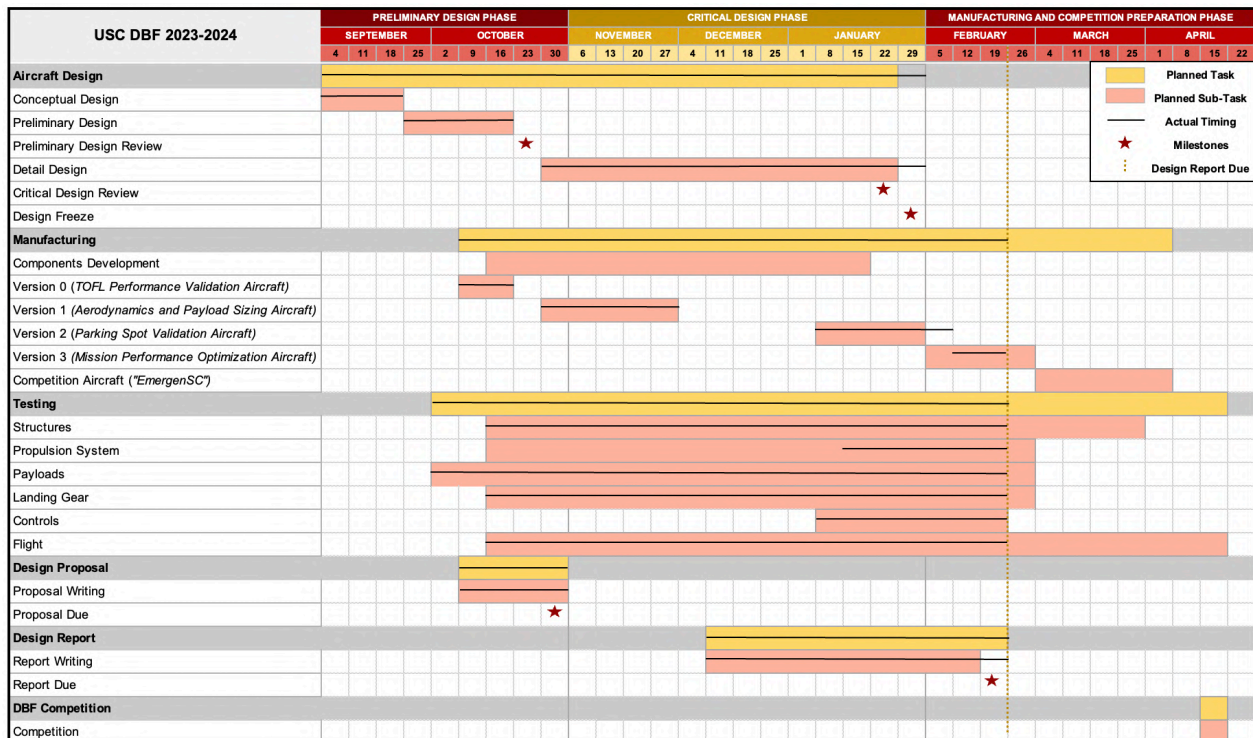


Figure 3. Master schedule showing the planned and actual timing for team tasks

3.0 CONCEPTUAL DESIGN

During the conceptual design phase, the team identified key design objectives by analyzing the scoring equations and competition requirements. The highest-scoring aircraft configuration was then derived by comparing relevant Figures of Merit (FoM). The final conceptual design is a high-wing monoplane, dual-motor tractor, with a conventional tail and tricycle landing gear, as presented in Section 3.5.

3.1 MISSION REQUIREMENTS

The 2023-24 AIAA DBF competition challenges teams to design an aircraft for Urban Air Mobility missions. The competition consists of three flight missions and one ground mission: a proof of flight (M1), a medical transport flight (M2), an urban taxi flight with Passengers (M3), and a configuration demonstration (GM).

3.1.1 MISSION AND SCORING SUMMARY

The Competition Score is a function of Report Score, Mission Score, and Participation Score, as seen in Eq. 1. The Total Mission Score is the sum of flight and ground mission scores, as in Eq. 2. A Participation Score of 1 is given for attending, 2 for passing tech inspection, and 3 for attempting a mission.

$$\text{Competition Score} = \text{Design Report Score} \times \text{Total Mission Score} + \text{Participation Score} \quad \text{Eq. 1}$$

$$\text{Total Mission Score} = M_1 + M_2 + M_3 + GM \quad \text{Eq. 2}$$

Staging

Prior to each flight, the aircraft is placed in a 2.5 ft (0.76 m) wide parking spot with the propulsion battery and Crew removed. In five minutes, the team must transition the aircraft to a flight-ready configuration, install the battery, and position two Crew members in the cockpit. Then, the team will have another five minutes to complete the flight mission, with the time starting when the throttle is advanced for takeoff. All flight missions are flown along the same path, as shown in Fig. 4. Before takeoff, all ground contact points must be forward of the start line, and the aircraft must takeoff within the 20 ft (6.1 m) takeoff field length (TOFL). Laps consist of two 1,000 ft (304.8 m) straightaways, two 180° turns, and one 360° turn in the opposite direction of the 180° turns. The completion of a lap is defined by crossing the finish line, either airborne or on the ground. A successful landing is required to receive a mission completion score.

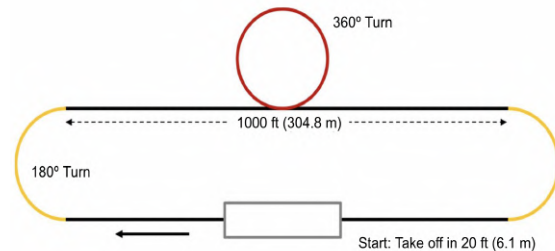


Figure 4. Flight path

Mission 1 – Delivery Flight

The objective for M1 is to fly three laps with no payload. One point is awarded if successful.

$$M_1 = 1.0 \quad \text{for successful mission} \quad \text{Eq. 3}$$

Mission 2 – Medical Transport Flight

M2 simulates the urgent transport of a Patient with two EMTs and a Medical Supply Cabinet (MSC). The score is determined by MSC mass and time to fly three laps, normalized by the highest score.

$$M_2 = 1 + \frac{(m_{MSC} / t_{M2})_{USC}}{(m_{MSC} / t_{M2})_{MAX}} \quad \text{Eq. 4}$$

Mission 3 – Urban Taxi Flight

The payload for M3 is Passengers, with the number of Passengers (n_{pax}) carried decided by the team. The score depends on n_{pax} , the number of laps flown in five minutes (n_{laps}), and the battery capacity (BC). The score is normalized by the maximum score achieved by any team, as shown in Eq. 5.

$$M_3 = 2 + \frac{(n_{laps} \times n_{pax} / BC)_{USC}}{(n_{laps} \times n_{pax} / BC)_{MAX}} \quad \text{Eq. 5}$$

Ground Mission – Configuration Demonstration

GM tests the ability of the aircraft to change mission configurations quickly. Only one team member is allowed to handle the aircraft during the GM. The aircraft begins stowed in the parking spot with all payloads in a triage area. Once time starts, the aircraft is transitioned to M2 flight configuration with Crew, EMTs, and a Patient on gurney, and MSC installed. The time then pauses for flight control verification. Once demonstrated successfully, time resumes and the team member replaces the M2 payloads with those for M3, or the maximum number of Passengers declared in Tech Inspection. The time then pauses again to check all flight controls. Finally, the time resumes, and the team member returns the aircraft to parking configuration with Crew and Passengers removed. The mission score is total time to transition between configurations (t_{GM}), normalized by the lowest time recorded by any team, as seen in Eq. 6.

$$GM = \frac{(t_{GM})_{MIN}}{(t_{GM})_{USC}} \quad \text{Eq. 6}$$

3.1.2 AIRCRAFT CONSTRAINTS

Constraints for the aircraft are defined by the AIAA and summarized in Table 2.

Table 2. Aircraft constraints (ACs)

Category	AC	Requirement
Configuration	1	Wingspan cannot exceed 5 ft (1.52 m).
	2	Aircraft must fit inside a parking spot 2.5 ft (0.76 m) wide while on its landing gear in the upright orientation, with no components removed aside from mechanical retention devices.
	3	Fuselage must have two compartments separated by a solid bulkhead. The forward (fwd) cockpit will seat Crew and the aft compartment will carry mission-dependent payloads.
	4	Each compartment in the fuselage must have a horizontal floor that need not be coplanar.
	5	Crew must sit in a cockpit such that their heads are above the fuselage fwd of the cockpit.
Structure	6	Aircraft must pass a wingtip load test with the maximum designed takeoff weight.
Payload	7	Gurney must be at least the same width and length as the Patient with a minimum height of 1.5 in (3.8 cm).
	8	MSC must have a minimum width and length of 3 in (7.6 cm) and height of 3.5 in (8.9 cm).
	9	Crew, EMTs, and Passengers must be mounted upright and perpendicular to the floor. The Patient must be horizontal on the gurney parallel to the direction of flight. EMTs must be alongside the patient. Payloads can only touch the floor or insert.
	10	The aft compartment must be accessed via a hinged hatch on the side of the aircraft, limited to a width of 6 in (15.2 cm) without extending past the fuselage vertical centerline.
	11	The cockpit must be accessed via a separate hinged hatch fwd of the required bulkhead.
Propulsion	12	Aircraft must be propeller driven and electric powered.
	13	Total stored propulsion energy must not exceed 100 Wh.
	14	The maximum current rating for the arming fuse is 100 A.
	15	Batteries must be commercial off-the-shelf (COTS) and unaltered.

The Crew, EMTs, and Passengers, provided at competition, have their dimensions presented in Fig. 5. Apart from the constraints, the rules allow flexibility in certain subsystems, as seen in Table 3.

Table 3. Aircraft design allowance

Category	Allowance
Propulsion	Propeller diameter and pitch may be changed for each flight attempt.
	Battery(ies) may be changed for each flight attempt.
Payload	A separate insert on top of the horizontal floor specific to each mission may be used.
	The MSC can be fwd or aft of the EMTs/Patient.
	There is no limit to number of hatches, but they must be on the same side of the aircraft.



Figure 5. Crew, EMTs, Passengers (left), and Patient (right)

3.2 DESIGN REQUIREMENTS

Design goals were defined using the mission scoring equations with constraints outlined in Table 4.

Table 4. Mission to Design Translation

Mission	Scoring	Design Goals	Relevant Constraints
M1	1.0 for successful mission	<ul style="list-style-type: none"> Stable flight 	<ul style="list-style-type: none"> TOFL
M2	$1 + \frac{(m_{MSC} / t_{M2})_{USC}}{(m_{MSC} / t_{M2})_{MAX}}$	<ul style="list-style-type: none"> Maximize m_{MSC} Maximize cruise speed (V_{cruise}) 	<ul style="list-style-type: none"> TOFL Fuselage structure Propulsion package
M3	$2 + \frac{(n_{laps} \times n_{pax} / BC)_{USC}}{(n_{laps} \times n_{pax} / BC)_{MAX}}$	<ul style="list-style-type: none"> Maximize n_{pax} Maximize endurance Select efficient propulsion package 	<ul style="list-style-type: none"> TOFL Fuselage volume Propulsion package
GM	$\frac{(t_{GM})_{MIN}}{(t_{GM})_{USC}}$	<ul style="list-style-type: none"> Fast payload un/loading Easy access to payload Quick storage mechanism for parking 	<ul style="list-style-type: none"> Aircraft configuration n_{pax}

3.2.1 SCORE SENSITIVITY ANALYSIS

Score sensitivity analysis was conducted on flying missions to observe the relative impact of scoring parameters on overall mission performance. M1 was excluded due to its binary scoring and assumed completion. Assumptions for the maximum scoring team in each mission were derived from previous Design, Build, Fly (DBF) aircraft. Figure 6 shows that decreasing t_{M2} and BC yields the highest percent increase in score.

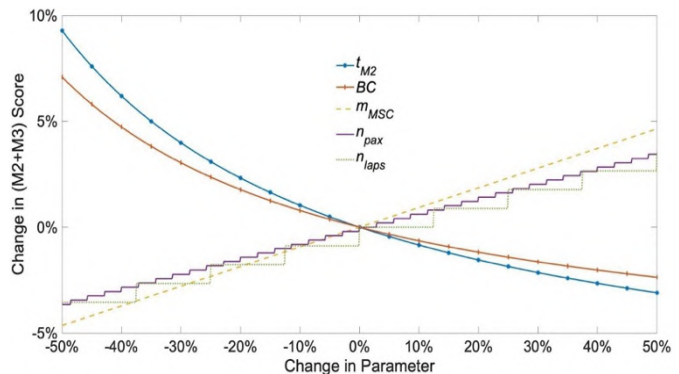


Figure 6. Score sensitivity

Table 5. Energy analysis

Mission	Parameter	Relation to Energy Consumption
M2	m_{MSC}	Quadratic, $E \sim W^2$
	t_{M2}	Cubic, $E \sim V^3$
M3	n_{pax}	Quadratic, $E \sim W^2$
	n_{laps}	Cubic, $E \sim V^3$

Since optimizing score is highly dependent on assumptions for the best performing plane in each mission, energy consumption

was investigated to further focus the design. The relationships between scoring parameters and energy consumption are summarized in Table 5. It should be noted that $E \sim W^2$ only at low speeds and during turns where induced drag is dominant. When the aircraft is in high-speed cruise, which occupies most of

flight time, parasite drag is the primary contributor to energy consumption, suggesting that increasing weight has an even smaller energy cost than the quadratic relationship in Table 5. Although initial score sensitivity drives a decrease in t_{M2} , flying faster consumes more energy than increasing aircraft weight. Energy is also critical because it directly affects M3 scoring. Therefore, the team decided to optimize for m_{MSC} and n_{pax} to efficiently use available energy.

3.3 CONFIGURATION SELECTION

An optimal aircraft configuration and its components were determined through the downselect process outlined in Table 6. Selected FoM are listed below along with their impact on scoring.

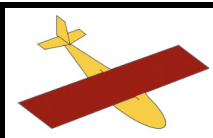
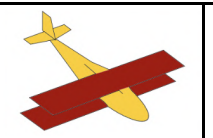
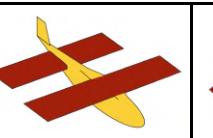
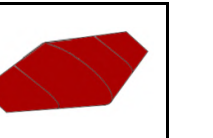
Table 6. Configuration downselect process

Step 1	Identify high-level aircraft subsystems that require a configuration downselect.
Step 2	Select relevant FoM for each subsystem and assign a weight between 0 and 1 for importance.
Step 3	Grade configuration options with a -1, 0, or 1 in comparison to a baseline configuration.
Step 4	Calculate total score for each option by multiplying FoM weights with grades and summing the scores.

3.3.1 AIRCRAFT CONFIGURATION

Table 7 shows the four aircraft configurations analyzed: monoplane, biplane, tandem, and blended wing body (BWB). The highest-weighted FoM were TOFL, flight speed, and weight as they directly impact flying mission scores. Although the increased wing area in biplane and tandem configurations are beneficial in reducing TOFL, both configurations increase weight, drag, GM complexity, and manufacturing time. The BWB was comparable to the monoplane in numerous aspects, but increased complexity in stability, control, and manufacturing. Furthermore, the team steered away from the BWB due to the risk of violating the AIAA rules, which reference a fuselage. The conventional monoplane configuration offered the best flight characteristics, GM handling, and manufacturability.

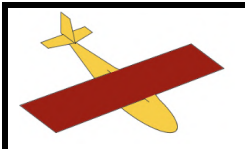
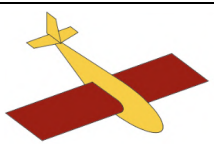
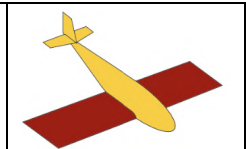
Table 7. Aircraft configuration downselect

					
FoM	Weight	Monoplane	Biplane	Tandem	BWB
TOFL	0.2	0	1	1	0
Flight Speed	0.2	0	-1	-1	0
Weight	0.2	0	-1	-1	-1
Payload Access	0.1	0	-1	-1	-1
Parking Complexity	0.1	0	-1	-1	0
Stability & Control	0.1	0	0	-1	-1
Manufacturability	0.1	0	-1	-1	-1
		0	-0.5	-0.6	-0.5

3.3.2 WING LOCATION

Wing placement options included low-wing, mid-wing, and high-wing configurations, as shown in Table 8. Impact on payload access and volume were highly considered for GM scoring. The mid-wing configuration was eliminated because it decreased available fuselage volume for payloads. The high-wing and low-wing configurations did not interfere with payloads, but the low-wing limited parking spot designs due to its proximity to the landing gear. Further, manufacturing a low wing posed more challenges for less propeller ground clearance and fewer stability and control benefits. A high-wing configuration was selected primarily for flexibility in payload and parking spot designs, with added benefit in flight handling and manufacturing.

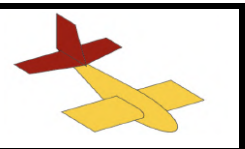
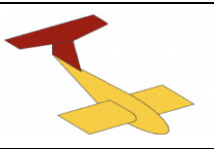
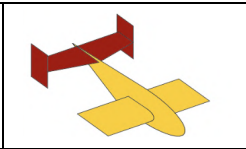
Table 8. Wing location downselect

				
FoM	Weight	High	Mid	Low
Payload Access	0.3	0	0	1
Payload Volume	0.3	0	-1	0
Parking Options	0.2	0	-1	-1
Propeller Ground Clearance	0.1	0	-1	-1
Manufacturability	0.1	0	-1	-1
		0	-0.7	-0.1

3.3.3 TAIL CONFIGURATION

Tail configuration options included conventional tail, T-tail, and H-tail, as shown in Table 9. Due to the TOFL constraint, weight was of crucial importance. T-tail and H-tail configurations come with the added structural weight of reinforcements towards the tip of the vertical and horizontal stabilizers, respectively. The conventional tail is lighter, since the horizontal stabilizer is attached to an already reinforced station, and easier to manufacture. The stability and control benefits of the T-tail and H-tail were also considered, resulting from advantageous stall and post-stall characteristics due to the placement of the horizontal and vertical tails outside the wake of a stalled wing. However, these benefits were far outweighed by the manufacturability and weight for TOFL. Therefore, a conventional configuration was selected for the tail.

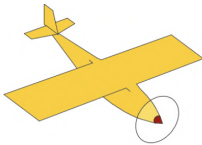
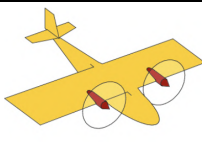
Table 9. Tail configuration downselect

				
FoM	Weight	Conventional	T-Tail	H-Tail
Weight	0.5	0	-1	-1
Stability & Control	0.3	0	1	0
Manufacturability	0.2	0	-1	-1
		0	-0.4	-0.7

3.3.4 PROPULSION

Single-motor and dual-motor configurations were compared in Table 10. Addressing TOFL and propeller torque were high priorities due to the team's struggle with takeoff in previous years [2]. The use of counter-rotating propellers in a dual-motor configuration would negate propeller torque and increase dynamic pressure over the wing flaps for a higher lift coefficient during takeoff. This benefit outweighed the lower cruise efficiency and higher mass of two motors, making dual-motor the preferred configuration.

Table 10. Propulsion configuration downselect

			
FoM	Weight	Single	Dual
TOFL	0.3	0	1
Propeller Torque	0.3	0	1
Cruise Efficiency	0.2	0	-1
Weight	0.2	0	-1
		0	0.2

3.3.5 PAYLOAD

The payload system affects structural design and fuselage volume; therefore, different concepts were considered to support both M2 and M3 payload inserts while allowing for low GM time (t_{GM}).

Table 11. Payload system downselect

				
FoM	Weight	Rail and Bottom Hold	Rail and Neck Hold	Hatch Per Insert
Reliability	0.3	0	1	-1
System Weight	0.3	0	0	-1
t_{GM}	0.3	0	1	-1
Adaptability	0.1	0	0	-1
		0	0.6	-1

For the rail and bottom hold design, Passengers are held from their base and inserts are pushed along a floor-mounted rail from a hatch in the aft of the fuselage. For the rail and neck hold, Passengers are secured from their neck and inserts are pushed along a rail suspended in the fuselage from a hatch in the aft. The hatch per insert has Passengers held from their base, with inserts placed through side fuselage hatches.

Friction from sliding the inserts along the floor and the increased complexity of having more hatches favor a design with a rail that suspends the inserts within the fuselage in reliability, weight, and t_{GM} . A significant variance in the base diameter of the purchased Passengers can be seen, as shown in Fig. 7. This makes

a friction-fit restraint method at the base of the Passengers unreliable. Additionally, in the event of changes with the target n_{pax} , the rail will adapt to these changes easily rather than redetermining the structure to hold another hatch. For these reasons, the rail and neck hold design was selected.

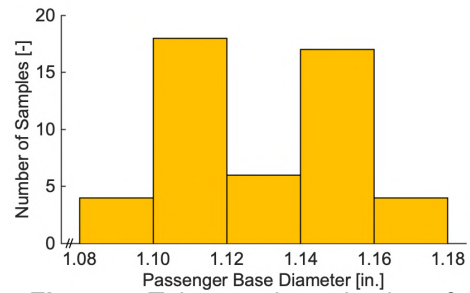
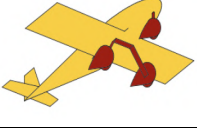
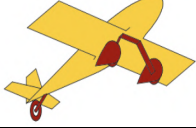


Figure 7. Tolerance investigation of Passenger base

3.3.6 LANDING GEAR

The two landing gear configurations considered were tricycle and tail dragger. This selection was especially critical due to its impact on TOFL and payload access. The AIAA rules mention that prior to takeoff, the aircraft must be positioned with all ground contact points ahead of the start line. Therefore, a tricycle configuration would maximize effective TOFL due to the smaller wheelbase. Additionally, a tricycle gear keeps the fuselage parallel to the ground, which makes payload operations easier given the rail system selection. These benefits outweighed the drag, weight, and manufacturability concerns of this configuration.

Table 12. Landing gear configuration downselect

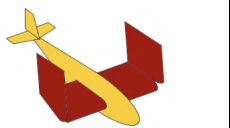
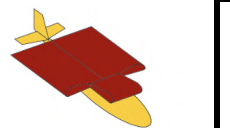
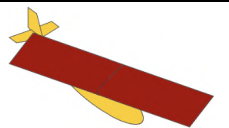
			
FoM	Weight	Tricycle	Tail Dragger
TOFL	0.3	0	-1
Payload Access	0.3	0	-1
Weight	0.2	0	1
Drag	0.1	0	1
Manufacturability	0.1	0	1
		0	-0.2

3.3.7 PARKING CONFIGURATION

The team approached the parking configuration selection by first considering which aircraft dimension to constrain. Longitudinal constraints implied splitting the fuselage or constraining the usable fuselage length to 2.5 ft (0.76 m) as required by AIAA rules. Lateral constraints implied splitting or constraining the wing. The team eliminated longitudinal constraints as AIAA rules already limited the span to 5 ft (1.52m) and would require reinforcement of multiple fuselage structural members, increasing fuselage weight. Additionally, the cavity created by the fuselage hinge could not be used for Passenger loading per AIAA rules, providing no overall benefit for the structural compromise. With the constraint dimension chosen, the team explored three parking configurations. Because parking configuration directly affects t_{GM} , the team placed emphasis on designs that could be stored in a single manual motion. Additionally, a configuration that would promote minimal mechanical components and minimize weight was preferred to mitigate

mission-critical failures. These considerations led to the selection of a rotated wing, as the entire wing could be manually stored in one movement with minimal mechanical linkages and no compromise to the spar.

Table 13. Parking configuration downselect

				
FoM	Weight	Folding	Swept	Rotated
Weight	0.3	0	1	1
Time to Store	0.3	0	0	1
Structural Compromise	0.2	0	-1	0
Mechanical Complexity	0.2	0	-1	0
		0	-0.1	0.6

3.4 FINAL CONCEPTUAL DESIGN

The final aircraft configuration was a monoplane with a pivoting high-wing, dual tractor motors, conventional tail, and tricycle landing gear, as shown in Fig. 8 (in its parking configuration).

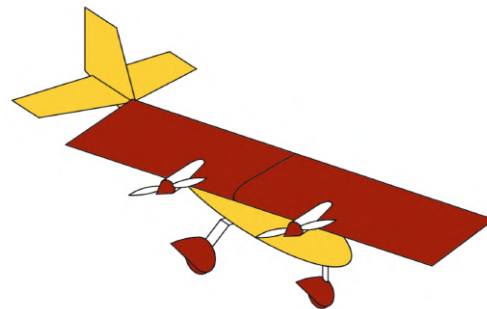


Figure 8. Conceptual aircraft design

4.0 PRELIMINARY DESIGN

The preliminary design aimed to converge on an aircraft optimized for cabinet mass and number of Passengers. Several trade studies were conducted across disciplines using simulations and models to size each major component. Methods and outcomes of this design phase are outlined below.

4.1 DESIGN METHODOLOGY

The design methodology was an iterative process inspired by industry and the team's previous design cycles. First, an aircraft configuration was selected by deriving design requirements from the rules and conducting score analysis. A preliminary weight estimation and constraint diagram were then utilized to assess design space and size the wing. Aerodynamic studies followed to determine airfoil geometry, tail volumes, and a stable center of gravity (CG) location. A team-developed mission model in MATLAB [3] predicted aircraft performance with varying payload configurations to maximize score. The propulsion system was sized to provide required thrust for takeoff and efficient cruise. With initial sizing complete, the Computer-Aided Design (CAD) was developed in collaboration with structure and payload requirements. Wiring and integration were heavily considered during detailed design given the parking spot and internal fuselage constraints of the competition. Upon freezing the design, manufacturing began involving laser cutting, 3D-printing, and composite layups. After final assembly, ground and in-flight tests were conducted. Test results were compared with initial design requirements. Methodology is outlined in Fig. 9.

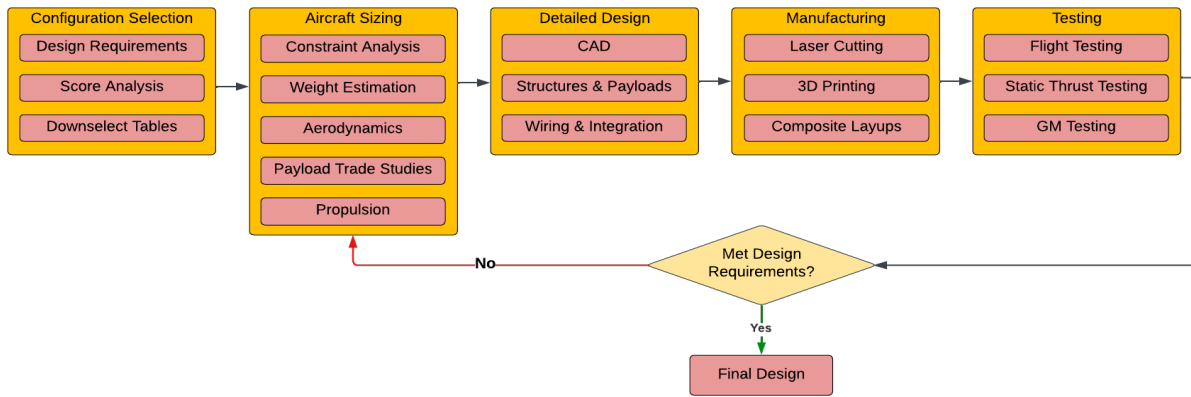


Figure 9. Design methodology

4.2 WING GEOMETRY

4.2.1 CONSTRAINT ANALYSIS

To assess the design space of the first iteration of the aircraft, a constraint analysis was performed, investigating the relationship between the thrust-to-weight ratio (T/W) and wing-loading (W/S). Expressions can be derived for different performance metrics and plotted in a T/W vs W/S plot:

$$\frac{T}{W} = \frac{1.21}{g\rho C_{L_{max}} S_g} \times \frac{W}{S} + \frac{0.605}{C_{L_{max}}} (C_{D_{TO}} - \mu C_{L_{TO}}) + \mu \quad \text{Eq. 7}$$

$$\frac{T}{W} = q C_{D_{min}} \times \frac{1}{W/S} + k \times \frac{1}{q} \times \frac{W}{S} \quad \text{Eq. 8}$$

$$\frac{W}{S} = \frac{1}{2} \rho V_s^2 C_{L_{max}} \quad \text{Eq. 9}$$

where Eq. 7 - 9 refer to desired takeoff ground roll (S_g), cruise speed (V_{cruise}) and stall speed (V_{stall}) [4].

To make valid assumptions about target performance for the first iteration, similar aircraft from the 2022 DBF Competition were studied. These aircraft had similar geometric, payload, and takeoff field length (TOFL) constraints. Additionally, the ERAU and WashU entries applied similar build techniques as USC's current design. This enabled a fair comparison of parameters such as wing loading and T/W .

Table 14. Analysis of comparable competitive aircraft

	ERAU 2022	WashU 2022	Johanneum 2022
Stall Speed	33.4 ft/s (10.2 m/s)	31.1 ft/s (9.5 m/s)	32 ft/s (9.8 m/s)
Cruise Speed	110 ft/s (33.5 m/s)	71.9 ft/s (21.9 m/s)	91 ft/s (27.7 m/s)
TOFL	25 ft (7.62 m)	25 ft (7.62 m)	25 ft (7.62 m)
W/S	1.8 lb/ft ² (86.5 N/m ²)	1.4 lb/ft ² (64.9 N/m ²)	2.3 lb/ft ² (110.1 N/m ²)
T/W	1.37	1.51	-

From the study of the aircraft above as well as historical USC designs, similar takeoff and cruise performance as the studied aircraft was expected. Similar weights and propulsion packages yield similar V_{cruise} , and similar aerodynamic parameters such as wing loading yield similar stall speeds. Therefore,

target V_{stall} and V_{cruise} were selected to be 32.81 ft/s (10 m/s) and 114.83 ft/s (35 m/s) respectively based on the comparisons above.

Additional assumptions were made in Eq. 7-9. A preliminary investigation of candidate airfoils allowed for the assumption of a $c_{l \text{ max}} = 1.6$ while a takeoff drag coefficient of $C_{DT0} = 0.04$ was assumed from previous aircraft and suggestions in literature [4]. Thus, the constraint diagram, was plotted using the required S_g of 20 ft (6.1 m) with a factor of safety (FoS) of 0.8, yielding 16 ft (4.88 m).

Analysis of the constraint diagram yielded $W/S = 0.012$ psi (83 N/m²) and $T/W = 1.3$. An FoS of 0.8 was applied to W/S in the optimal location of the diagram, where the stall speed and TOFL constraints intersect, since it was critical to meeting TOFL. The T/W was kept at the indicated optimal value of 1.3 given its proximity to the other aircraft compared. This analysis allowed an initial study of the design space as it related to scoring – higher W/S for a fixed sized wing yielded a heavier payload and thus, higher score. A heavier payload also decreased T/W , affecting takeoff and cruise performance. Therefore, varying payload weight for a given W/S and T/W to identify the highest-scoring aircraft was key and discussed in Section 4.4. To determine the required wing area and static thrust, a preliminary weight estimation was conducted.

4.2.2 PRELIMINARY WEIGHT ESTIMATION

The gross takeoff weight (W_0) can be calculated using a modified version of methods in Raymer [5]. The modified expression for W_0 , sometimes denoted as the unity equation in literature, is shown in Eq. 10:

$$W_0 = \frac{W_p}{1 - \frac{W_e}{W_0} - \frac{W_{a\&p}}{W_0}} \quad \text{Eq. 10}$$

where W_p is payload weight (Passengers, cabinet, etc.), W_e/W_0 is the empty weight fraction, and $W_{a\&p}/W_0$ is the avionics and propulsion weight fraction. The last of these values includes the motor, propeller, batteries, and servos/avionics.

Historical values for these weight fractions were estimated by analyzing similar competitive aircraft from the 2022 competition. The aircraft analyzed featured similar manufacturing techniques that would later be used, and similar W_p . This would yield similar W_e and propulsion weight as expected from the first iteration of the aircraft. The weight fractions for the aircraft studied are shown in Table 15.

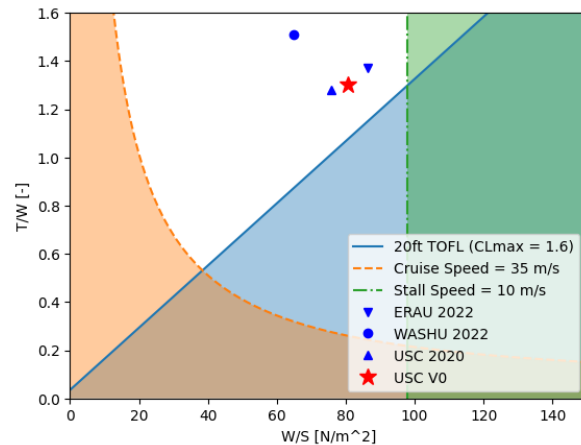


Figure 10. Constraint diagram

Table 15. Weight fractions of comparable competitive aircraft

	ERAU 2022	WashU 2022	MIT 2022
W_e/W_0	0.44	0.56	0.48
$W_{a\&p}/W_0$	0.21	0.22	0.21

Therefore, intermediate empty weight fractions were estimated to be $W_e/W_0 = 0.52$ and $W_{a\&p}/W_0 = 0.21$. With an initial guess of 50 Passengers based on the team's previous designs and other top reports, an initial W_0 estimate of 12.35 lbm (5.6 kg) was yielded, per Eq. 10. With W_0 and W/S determined, the wing geometry was found with hand calculations and experience that maximizing wingspan was favorable for TOFL. Thus, the maximum span of 5 ft was assumed, yielding the following final dimensions for the zeroth iteration of the aircraft, V0, shown in Table 16.

Table 16. V0 Wing Dimensions

Span	5 ft (1.52 m)
Wing Area	6.9 ft ² (0.641 m ²)
AR	3.5
Chord	1.427 ft (0.435 m)

4.2.3 AERODYNAMICS

The aerodynamics were designed and analyzed using XFLR5 [6] and Athena Vortex Lattice (AVL) [7]. XFLR5 uses XFOIL [8] to analyze the drag and lift characteristics of airfoils to aid airfoil selection. AVL uses a vortex-lattice model to define the lifting surfaces of an aircraft to analyze its static and dynamic stability as well as the induced drag of the aircraft and stabilizer. In addition, calculations were used to trade the drag of different winglets, and flight testing verified the flight characteristics of the full aircraft.

4.2.3.1 AIRFOIL SELECTION

The selection of an airfoil depended on the maximum lift of the airfoil during takeoff and parasitic drag at the design cruise lift coefficient (C_L). High-lift devices were studied to achieve a high $C_{L,max}$ and minimize TOFL. To select an initial airfoil, a team-developed Python code iterated through airfoils [9], targeting high $c_{l,max}$. Candidates were analyzed for their drag at the design lift coefficient, maximum lift to drag ratio, and takeoff performance with flaps. Considered airfoils are included in Fig. 11.

The team proceeded with the Eppler 1230 airfoil for V0. Flight testing and further analysis confirmed that the Eppler's $c_{l,max}$ of 1.8 and a wing area S_{ref} of 7.15 ft² (0.664 m²) met TOFL with ease but lacked V_{cruise} . Therefore, a trade study was conducted to evaluate the drag benefit of thinner airfoils with reduced c_{d0} using PlaneGeometry, an Excel tool developed by team advisor, Prof. Blaine Rawdon [10].

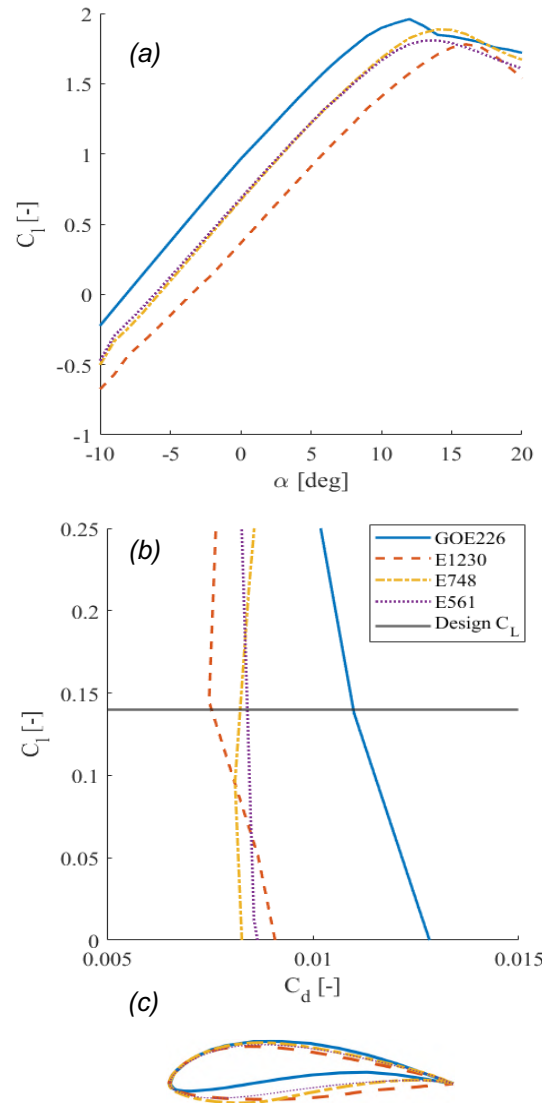


Figure 11. (a) Lift curves at takeoff conditions, $Re = 3 \times 10^5$, and (b) drag polars at cruise conditions, $Re = 1 \times 10^6$, of the (c) GOE226, E1230, E748, and E561 airfoils

Aircraft with selected airfoils were designed in the software, which includes the wings, tail, and fuselage. The airfoils analyzed were selected for their similar range of operational 2D lift coefficient (c_l), all close to the design c_l but with differing thicknesses and 2D drag coefficient (c_d) values. The spreadsheet also calculates the parasitic drag coefficient of all surfaces of the aircraft. To apply the increased S_{ref} penalty for airfoils with reduced c_{lmax} , $c_{lmax} \times S_{ref}$ was kept constant for all aircraft, using the Eppler 1230 as a baseline.

The resulting polars of all aircraft with their respective airfoils are illustrated in Fig. 12. The aircraft's sink rate is directly proportional to the power required. Therefore, the glide polar is a measure of the aircraft's endurance. Lower sink rate at a given airspeed is desired since it yields higher endurance. Alternatively, for a given sink rate (or power required) a higher airspeed is desired.

The polars show that the Eppler 1230 was outperformed, having a higher sink rate at the target V_{cruise} . The SM701 performed the best at higher airspeeds being a moderately thick airfoil ($t/c = 16\%$) yet still thinner than the previously selected Eppler 1230 ($t/c = 18\%$). The SM701 also provides high lift for short takeoff and has gentle stall characteristics.

The AG35 was close in performance, but still worse than the SM701. It was initially suspected that the very low thickness of the AG35 ($t/c = 9\%$) would make it more streamlined with a lower drag coefficient. However, the wing area required to meet TOFL outweighed its drag benefit. Therefore, the SM701 was selected for later versions of the aircraft. Its lift and drag polars are outlined in Fig. 13.

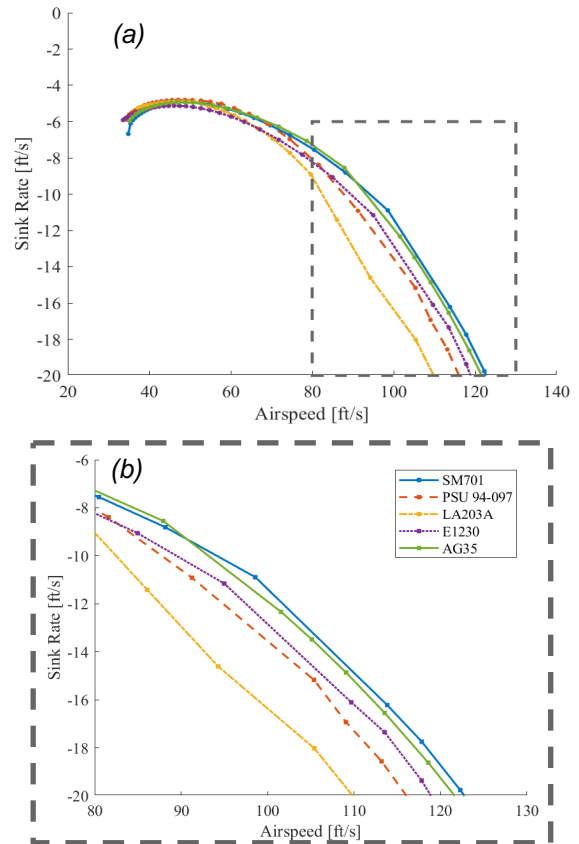


Figure 12. (a) Glide polar of aircraft with different candidate aircraft and (b) zoomed in version at high airspeeds, representative of the target V_{cruise} of 114 ft/s (35m/s)

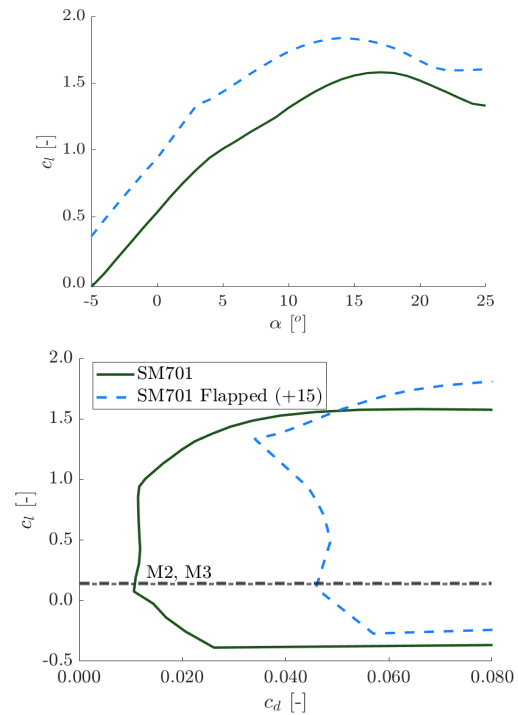


Figure 13. Lift and drag performance, including flapped performance, of SM701 airfoil

4.2.3.2 AERODYNAMIC COMPONENT ANALYSIS

An effective way to increase the aerodynamic performance of a span-constrained aircraft is to use winglets. However, winglets carry a parasitic drag cost as well as a weight cost that may negate their reduction in lift-induced drag. Therefore, a trade study was conducted to evaluate their cost and benefit. To do so, the energy expended per lap due to drag, or drag energy, was calculated for different winglet height-to-semispan ratios. The drag coefficient of a winglet was calculated, as shown in Eq.11, where the winglet airfoil's 2D parasite drag coefficient $c_{d_{\text{airfoil}}}$ was assigned a value of 0.0080 (80 drag counts) based on the drag of the SM701 airfoil computed in XFLR5 [6].

$$C_{D_{\text{winglet}}} = \frac{c_{d_{\text{airfoil}}} \times S_{\text{winglet}}}{S_w} \quad \text{Eq. 11}$$

Then, the total drag of the aircraft is calculated using Eq. 12, where C_{D_0} is the aircraft's parasitic drag coefficient without winglets, C_L is the coefficient of lift, and k is the lift-induced factor:

$$C_D = (C_{D_0} + C_{D_{\text{winglet}}}) + kC_L^2 \quad \text{Eq. 12}$$

The change in the lift-induced factor k was assessed in AVL [7] for different flight conditions. This ensured the analysis accounted for the aerodynamic benefit of winglets. This benefit is more pronounced in high C_L conditions, like flight at low speeds and turns. Finally, the drag energy in Wh per lap is found using Eq. 13.

$$\text{Drag Energy} = C_D \times q \times S_{\text{ref}} \times \text{distance} \quad \text{Eq. 13}$$

where the distance is assumed for each leg of a competition lap, that is, 2000 ft (610 m) straightaways and $2 \times 2\pi r_{\text{turn}}$ for the two full turns at the higher, loaded coefficient of lift. The turn radii were assumed from test flight data, and therefore considered the pilot's typical turns. The V_{cruise} for C_L calculations were assumed to be the target design lift coefficient of 0.14. The results of the trade study are shown in Table 17. These indicate that the minimum energy expenditure per lap is attained at a winglet height-to-semispan ratio of 0.2, or 0.5 ft (0.15 m). It is important to note that these values do not include dissipative losses associated with the propulsion system. They also do not include losses from interference drag between the wing and the winglets but, they provide an insight into the losses from the parasitic drag of the winglets.

Table 17. Results of winglet height trade study

	No Winglet	$\frac{h}{b/2} = 0.1$	$\frac{h}{b/2} = 0.2$	$\frac{h}{b/2} = 0.3$
Straightaway Drag Energy [Wh]	2.29	2.33	2.38	2.43
Turns Drag Energy [Wh]	2.76	2.69	2.61	2.80
Total Drag Energy [Wh]	5.04	5.02	4.99	5.24

4.2.4 DRAG ANALYSIS

The main drag component across all missions is parasitic drag due to the low cruise coefficients of lift. Since all payloads are internal, the only difference in drag between missions is lift-induced drag caused by difference in weight, and hence cruise lift coefficient, of the payloads. Drag build ups are shown in Fig. 14. Note that the drag due to payload is negligible and shown as 0% on the charts.

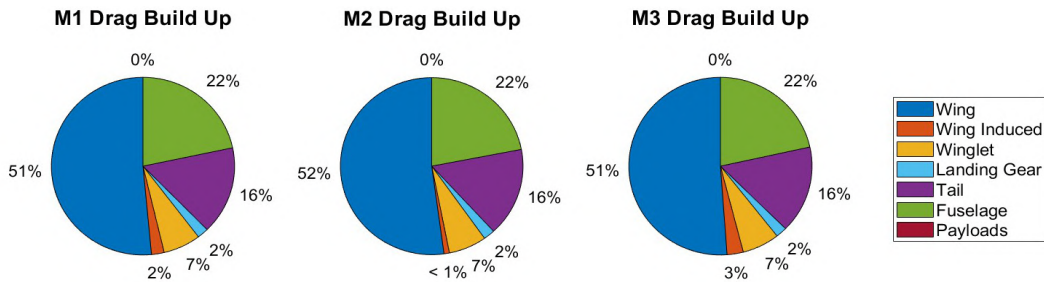


Figure 14. Drag breakdowns for Missions 1 (M1), Mission 2 (M2), and Mission 3 (M3)

The drag breakdown shown in Fig. 14 was used to conduct an analysis of the lift to drag ratio (L/D) vs. C_L of the aircraft during cruise for M2 and M3. The results are shown in Fig. 15. The aircraft flies at 44% of the maximum L/D during M2 and M3 cruise. For M2 and M3, the L/D is 5.4 during cruise and 10.6 during turns.

Trim conditions for M1, M2, and M3 were analyzed using AVL to determine the trimmed angle of attack, α , the elevator trim deflection, δ_e , and Oswald efficiency, e . The numerical outputs for each mission and Trefftz plot for M2 are shown in Table 18 and Fig. 16 respectively.

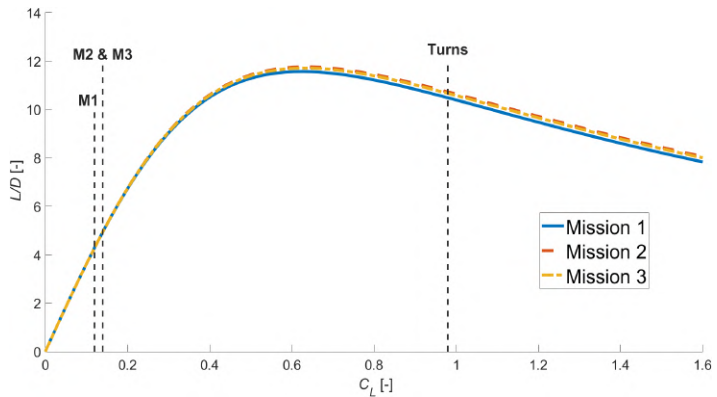


Figure 15. L/D plot to visualize efficiency of the aircraft in M1, M2, and M3, shown with the cruise and turn coefficients of lift for each mission

Table 18. Trim deflections with lift and drag coefficients for each mission during cruise

	M1	M2	M3
e [-]	1.21	1.25	1.24
α [°]	-1.12	-0.75	-0.86
δ_e [°]	-1.00	-1.14	-1.10
C_L [-]	0.12	0.14	0.14
C_D [-]	0.0325	0.0326	0.0325

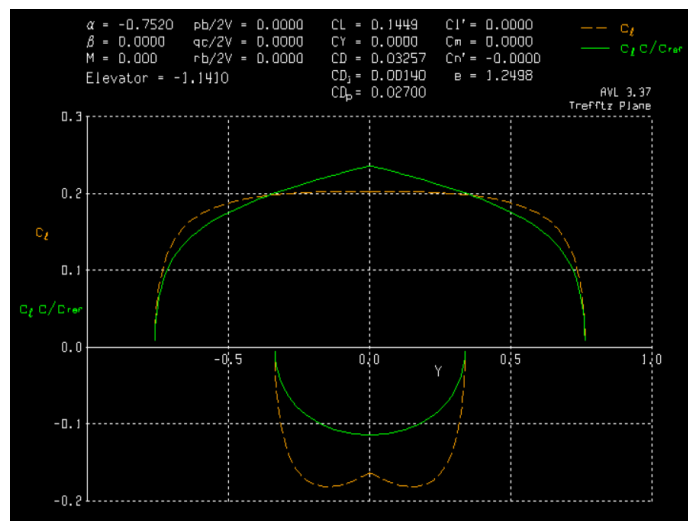


Figure 16. Trefftz plane analysis of the aircraft for M2 during cruise

4.3 STABILITY AND CONTROL

4.3.1 STATIC STABILITY ANALYSIS

Tail sizing and placement were initially determined with tail volume coefficients as defined in Eq. 14 and 15, where l_t is the tail moment arm, S_H is the planform area of the horizontal tail, and S_V is the planform

area of the vertical tail. Coefficients of $V_H = 0.6$ and $V_V = 0.05$ for the horizontal and vertical stabilizers were chosen from literature [5].

$$V_H = \frac{l_t \times S_H}{c \times S_w} \quad V_V = \frac{l_t \times S_V}{b \times S_w} \quad \text{Eq. 14, 15}$$

The tail volumes and CG location were later analyzed using AVL [7]. The tail moment arm and volume coefficients were parametrically varied, and the resulting e recorded. A heatmap of the study results is shown in Fig. 17.

The final tail volumes were $V_H = 0.7$ and $V_V = 0.075$. Analysis in AVL and PlaneGeometry showed that a CG placement for a 16% static margin (SM) in cruise yielded tail downloads within a safe range to avoid stalling the horizontal tail [7][10]. It also allowed enough δ_e to achieve the target V_{cruise} at the trimmed α .

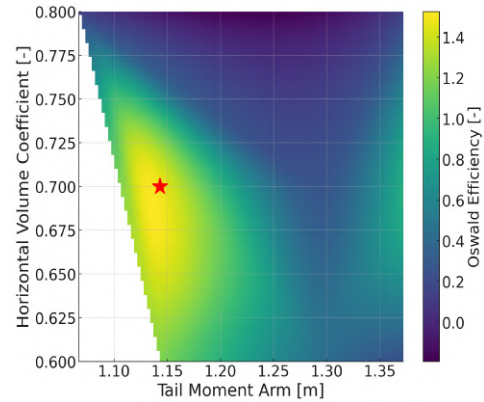


Figure 17. Tail sizing trade study

The static stability derivatives as calculated in AVL are shown in Table 19, and include the requirements for the pitching moment derivative with respect to angle of attack, $C_{m\alpha}$, roll moment derivative with respect to sideslip, $C_{l\beta}$, yaw moment derivative with respect to sideslip, $C_{n\beta}$, and rudder yaw moment control derivative, $C_{l\delta_r}$. Based on these AVL results, the aircraft is statically stable in all flight missions.

Table 19. Static stability derivatives for M1, M2, and M3

Derivative	$C_{m\alpha}$ (Longitudinal) [rad ⁻¹]	$C_{l\beta}$ (Lateral) [rad ⁻¹]	$C_{n\beta}$ (Directional) [rad ⁻¹]	$C_{n\delta_r}$ [deg ⁻¹]
Requirement	Negative	Negative	Positive	-
Mission 1	-0.640	-0.0044	0.164	0.013
Mission 2	-0.640	-0.0076	0.164	0.012
Mission 3	-0.640	-0.0067	0.164	0.013

4.3.2 DYNAMIC STABILITY ANALYSIS

The dynamic stability of the aircraft was analyzed using AVL for all missions. A root-locus plot was used to analyze the longitudinal and lateral-directional modes of the aircraft, as shown in Fig. 18. A mode is stable if its real component is negative. The five dynamic modes, roll, spiral, phugoid, Dutch roll, and short period were conducted for takeoff and cruise conditions for M1, M2, and M3.

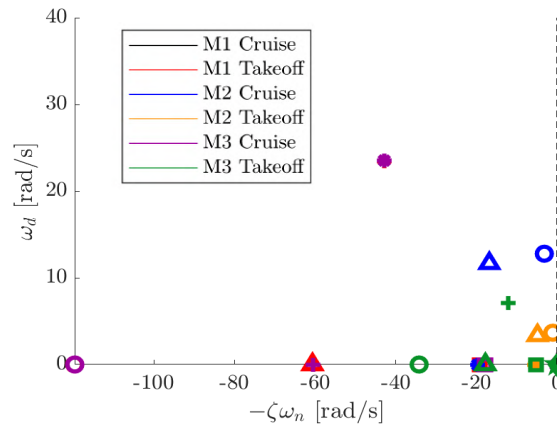


Figure 18. Root locus plot of the dynamic stability of the aircraft in roll (●), spiral (×), phugoid (◆), Dutch roll (▲), and short period (⊕)

The aircraft is shown to be dynamically stable in all modes across all missions. The aircraft meets the Level 1 flying qualities of a Class 1 aircraft described in MIL-F-8785C [11]. Characteristic values of these modes for M2 and M3 are shown in Table 20. The characteristics for M1 and M3 are comparable to those of M2 and are therefore not shown. The aircraft is dynamically stable in every mode for M2, except the slow spiral mode in takeoff and cruise, as defined by MIL-F-8785C [11].

Table 20. Dynamic stability results for Mission 2: values are listed as takeoff value / cruise value

Mode		ζ [-]	ω_n [rad/s]	$\zeta\omega_n$ [rad/s]	Time to Half Amplitude [s]
1	Roll	-	-	5.58 / 19.6	0.124 / 0.0345
2	Spiral	-	-	-0.232 / -0.0676	2.99 / 10.3
3	Phugoid	0.0451 / 0.345 ($\zeta > 0.04$)	0.623 / 0.0235	0.0281 / 0.00810	24.7 / 8.56
4	Dutch Roll	0.273 / 0.242 ($\zeta > 0.08$)	3.67 / 12.8 ($\omega_n > 0.4$)	1.00 / 3.10 ($\zeta\omega_n > 0.15$)	0.691 / 0.224
5	Short Period	1.431 / 1.436 ($0.35 < \zeta < 2.00$)	3.354 / 11.67	4.80 / 16.75	0.144 / 0.0414

4.4 TRADE STUDIES

To predict the performance of the preliminary aircraft design and explore optimization, the team developed a multidisciplinary design optimization tool in MATLAB [3] called PlaneTools, which is an object-oriented and time-based mission simulator with foundations in the physical models that govern aircraft dynamics. PlaneTools allows the team to explore the relationship between physical dimensions and mission score.

4.4.1 MISSION MODEL

To predict the aircraft performance, PlaneTools utilizes several fundamental physics equations along with simplifying assumptions. The methodology and assumptions for each physical model are outlined below:

Aerodynamics – Airfoil lift and drag coefficients were determined from airfoil geometry studies within XFLR5 [6]. To simulate blown lift, air velocity behind the propellers was calculated using Bernoulli's equation [5]. Lift was then calculated as a function of spanwise location along the wing and added up.

Drag – Aircraft geometry was used to calculate parasitic drag while considering Reynolds number, e , and flow transitions [5]. Interference drag and compressibility effects were ignored.

Propulsion – Static and dynamic thrust data for propellers, provided by UIUC Applied Aerodynamics Group [12], was integrated into propulsion models. Battery voltage decay was modeled as a function of temperature, current, and state of charge based on a curve fit model [13]. Propeller, battery, and motor outputs were verified through lab testing.

Mass – The weights of individual manufactured components were estimated based on aircraft sizing and build methods used by the team. Masses for commercial off-the-shelf (COTS) electronic components were input based on specification sheets.

Environment – Based on historical weather patterns during mid-April in Wichita, KS, headwinds of 0 to 16.2 ft/s (4.9 m/s) were assumed [14]. Elevation was set to 1300 ft (400 m) for calculating air density.

Physics models were used to simulate four segments of the competition course – Takeoff, Climb, Cruise, and Turns. Figure 19 displays the competition course as modeled. Assumptions for each flight segment are detailed below:

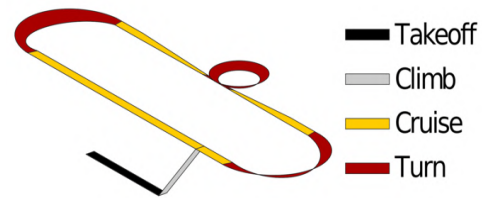


Figure 19. Competition course as simulated in PlaneTools

- 1. Takeoff** – Assumed throttle was linearly increased to 100% over 1.7 s to avoid a propeller torque impulse. The model accounted for a lab-measured rolling resistance coefficient of 0.03 while adjusting C_L and C_D based on speed. To incorporate a FoS, the rotation speed was set to 120% of the takeoff configuration V_{stall} with the wing's maximum C_L accounting for 20° slotted flaps. The assumed TOFL was 110% of the calculated length to account for rotation before liftoff.
- 2. Climb** – The aircraft was assumed to climb at full throttle until reaching a cruising altitude of 33 ft (10 m) above ground level. The rate of climb was calculated with excess power.
- 3. Cruise** – The aircraft was assumed to maintain steady, level flight with constant cruise throttle. Throttle settings were maximized for each mission while ensuring the battery state of charge remained above 15% until completing the mission (flying three laps for M2 or five minutes for M3), serving as reserves for landing.
- 4. Turn** – The aircraft was assumed to perform coordinated, max-lift, level turns for both the 180° and 360° turns. The maximum C_L used was determined with the chosen airfoil without flaps and reduced by the effects of the downforce created by the tail.

PlaneTools was developed to make component-specific trade studies and evaluate the effects of every dimension, allowing for large design spaces to be studied through multivariable trade studies. A simplified schematic of how PlaneTools simulates aircraft is in Fig. 20. The logic can be summarized as follows: for every plane traded, simulate takeoff. If successful, fly the mission until completed or stalled. Then, continue either with M3 or the next plane (as fit). This cycle is repeated until all planes in the study are simulated.

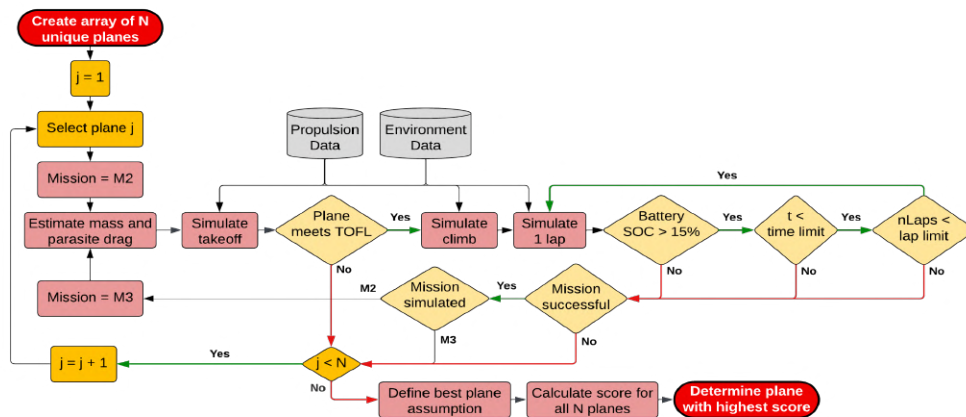


Figure 20. PlaneTools logic applied for evaluating aircraft

In this flow, the battery state of charge is only allowed to reach a minimum of 15% (instead of 0%) to allow adequate charge for landing. The goal of PlaneTools is to rule-out as many non-competitive planes as fast as possible to quickly analyze complete design spaces.

4.4.2 PAYLOADS

Given a wing geometry and target weight for the aircraft (Section 4.2), trade studies were conducted to determine the optimal payload configuration for both M2 and M3. To account for the internal volume required for M3 payloads, the fuselage length (and therefore weight and C_{D_0}) was assumed to be linearly proportional to the number of Passengers (n_{pax}). The final assumption was that Ground Mission (GM) loading time was independent of n_{pax} due to the loading mechanism described in Section 5.3.6, so increasing n_{pax} would not decrease total mission score.

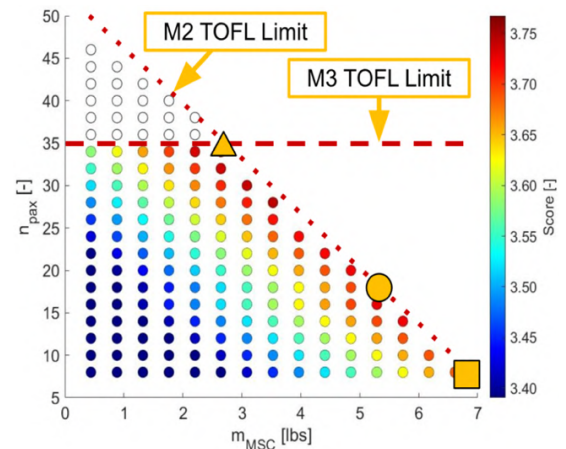


Figure 21. PlaneTools study of score as a function of payloads carried

From the initial studies, the score is maximized along the M2 TOFL limit, beyond which the plane fails takeoff preventing it from completing both M2 and M3, seen in Fig. 21. At a value of $n_{pax} = 34$, the fuselage becomes too heavy and drag-inducing to achieve TOFL in M3 while continuing the M2 scoring trend. These planes are considered non-competitive and are therefore ignored, depicted by colorless circles in Fig. 21. As expected, the highest scoring aircraft are carrying the $W_{p,max}$ while still taking off in under 20 ft (6.1 m). The best scoring plane has multiple optimum scoring configurations including being M2 and M3 oriented. An M2 focused aircraft is depicted by the square, carrying a heavier Medical Supply Cabinet (MSC) by carrying fewer n_{pax} . An M3 oriented aircraft is deprecated by the triangle, carrying more n_{pax} , at the cost of a lighter MSC mass (m_{MSC}). A well-rounded plane will balance the two extremes. All high scoring configurations lay along the M2 TOFL limit line.

For Figure 20, the overall score was dependent upon the assumption made about the best plane at competition. Based on previous years, the best planes for M2 and M3 were assumed to score as seen in Table 21. Note that these planes are assumed to be two separate planes, optimized for M2 or M3 alone.

The “factor” is the value used to normalize all planes’ scores. While USC’s overall score varies as these assumptions change, the same trend from Fig. 21 remains with changing best plane assumptions. This was verified through a score sensitivity chart in Fig. 22, with the baseline plane being a balanced M2 and M3 plane marked by the circle in Fig. 21.

Table 21. Best plane assumptions

Mission	Score	Factor
M2	$\frac{(4.0 \text{ kg})}{(66 \text{ s})}$	0.061
M3	$\frac{(60 \text{ nPax})(10 \text{ laps})}{(2.7 \text{ Ah})(8 \text{ cells})(3.7 \text{ volts/cell})}$	7.508

If the team's best plane assumptions are incorrect, the inherent risk of choosing a single-mission-oriented plane becomes clear – if USC's plane is optimized with the goal of being the highest scoring plane for one mission (at the cost of worse performance metrics in the other mission) and the best competing plane for the same mission is better than our prediction, USC's total mission score drops drastically relative to the

competition. However, score sensitivity indicated that the aircraft is more sensitive to the assumed best-performing plane in M2, so the aircraft should be closer to the square than the triangle in Fig. 21. Additionally, since the fuselage size will be fixed once the aircraft is built, the design was driven towards M2 in which the team can optimize m_{MSC} as a function of wind speed at competition, something which cannot be done with n_{pax} without changing fuselage length. Thus, 18 Passengers and a m_{MSC} of 4.85 lbs (2.2 kg) were chosen.

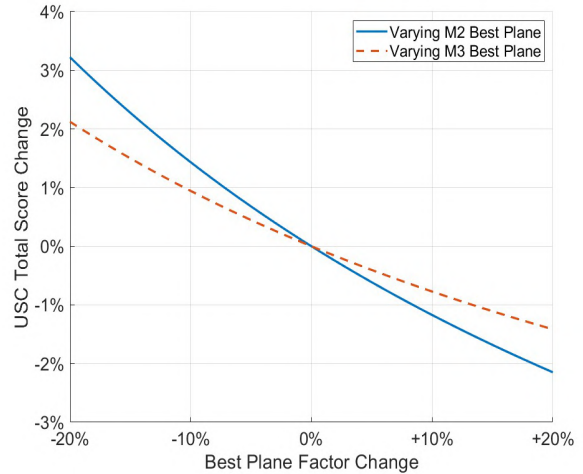


Figure 22. Score sensitivity to varying best plane assumptions

4.5 PROPULSION

M2 requires more static thrust due to the higher W_p and prioritizes dynamic thrust to increase the allowable V_{cruise} to reduce the time to fly the three mission laps. To maximize range on M3, it was found to be optimal to fly for the entirety of the allowed 5-minute window. To achieve this and take full advantage of the 97.7 Wh propulsion battery, an ideal power consumption of 1170 W calculated for cruise. A slower V_{cruise} was selected for M3 to increase endurance and max number of laps (n_{laps}) with max payload within the energy limit. Therefore, the propulsion package needed to satisfy high static thrust as well as efficient low-power cruise.

4.5.1 STATIC THRUST REQUIREMENT

The propulsion package, including a motor, ESC, battery, propeller, and fuse combination, was balanced to optimize score on M2 and M3. It was assumed that the aircraft took off 20% faster than V_{stall} with a C_{Lmax} of 1.6 obtained through XFLR5. Utilizing a W_0 of 19.3 lbm (8.77 kg) for M2 and 15.4 lbm (6.97 kg) for M3, the takeoff velocity, V_{TO1} , was calculated using Eq. 16 to be 42.3 ft/s (12.9 m/s) for M2 and 37.7 ft/s (11.5 m/s) for M3.

$$V_{TO1} = \sqrt{\frac{2W}{\rho S C_{Lmax}}} \quad \text{Eq. 16}$$

Since the aircraft is designed to take advantage of blown lift, the propeller accelerated wake is considered. The accelerated velocity of the propeller, V_e , was found from disk theory seen in Eq. 17, where T is the thrust, ρ is the air density, and A is the propeller circular area.

$$V_e = \sqrt{\frac{2T}{\rho A (V_{TO1})^2}} \quad \text{Eq. 17}$$

To account for blown lift generated and lower the V_{TO1} requirement, an effective takeoff velocity, V_{TO} , was used as denoted by Eq. 18.

$$V_{TO} = V_{TO1} - V_e \quad \text{Eq. 18}$$

Static thrust was calculated using Eq. 19, with initial velocity, V_0 , equal to the assumed 16.4 ft/s (5 m/s) wind speed. An additional margin, FS_{TOFL} , of 10% was assumed. A static thrust, T_{static} , of 15.8 lbf (70.5 N) for M1, 32.5 lbf (144.4 N) for M2, and 20.3 lbf (90.5 N) for M3 was found sufficient for a 20 ft (6.1 m) TOFL.

$$T_{static} = ma = m \frac{V_{TO}^2 - V_0^2}{2 \left(\frac{TOFL}{FS_{TOFL}} \right)} \quad \text{Eq. 19}$$

4.5.2 MOTOR SELECTION

The motor cannot be changed between missions and therefore must be sufficient for all flight missions. Motors were compared using the aircraft configuration tool eCalc [15] and weighed by their M3 endurance at V_{cruise} and M2 speed at maximum throttle. Reliable brands based on team experience were selected and the best-suited motors that could deliver the required static thrust maximize endurance

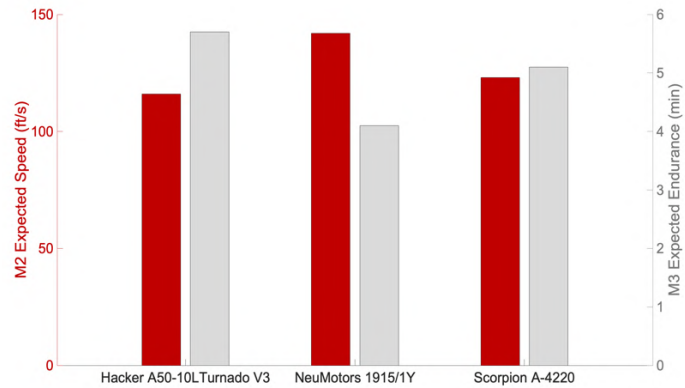


Figure 23. Endurance and speed performance motor comparison

were compared [2][13]. The Scorpion A-4220 540 kV motor was found to be the best motor for both missions, as shown by the comparisons of expected speed and endurance in Fig. 23.

4.5.3 ELECTRONIC SPEED CONTROLLER (ESC) SELECTION

The team selected KDE Direct ESCs for their reliable data logging and straightforward user interface. During flight testing, each motor sustained a current of 70A during cruise at 50% throttle setting and a maximum current of 110A during takeoff, proving the suitability of the 130A ESC.

4.5.4 BATTERY AND PROPELLER SELECTION

The contest rules allow for commercial off-the-shelf (COTS) Lithium Polymer (LiPo), Nickel-Cadmium, or Nickel-Metal-Hydride propulsion batteries with an energy limit of 100 Wh. LiPo batteries were selected for propulsion due to their higher specific energy compared to other battery types and superior discharge rate [16]. LiPo batteries are sized by their cells they have which have a nominal voltage of 3.7 V per cell. Energy in Watt-hours is calculated as $Wh = Voltage \times Capacity$, where $Voltage = n \times 3.7$, n is the number of cells in series, and capacity is in Ampere-hours (Ah). Only using reliable brands restricted the competitive M2

and M3 battery selection to a 6S LiPo with a battery capacity of 3000-4500 mAh or an 8S LiPo with a battery capacity of 2250-3300 mAh.

Propulsion performance results were initially gathered from eCalc and verified experimentally as seen in Section 8.1.2 [15]. When comparing M2 packages, the primary goal was to maximize V_{cruise} . A factor of 1.15 was applied to predicted electrical power from eCalc to correct the model to match experimentally collected data. This was used in conjunction with predicted maximum V_{cruise} to arrive at a package of an 8S 3300 mAh battery, an 11x7 in clockwise pusher propeller, and an 11x7 in counterclockwise sport propeller from APC Props. These propellers were selected such that they counter-rotate to negate torque. Using Eq. 20, the predicted V_{cruise} is 123 ft/s (37 m/s), with each lap taking an estimated 33.6 s. For M3, the analysis converged to a combination of an 8S 3300 mAh LiPo battery with an 11x6 in APC pusher propeller and sport propeller. This would allow for counter rotation to negate propeller torque. Using Eq. 21, the aircraft was predicted to complete 8 laps for M3, with an average time of 37.5 s per lap.

$$\text{Speed} = \frac{\text{Range}}{\text{Total Energy}} \times \frac{\text{Power}}{\text{Efficiency}} \quad \text{Eq. 20}$$

$$\text{Range} = \frac{\text{Energy Limit}}{\text{Power}} \times \text{Speed} \times \text{Efficiency} \quad \text{Eq. 21}$$

For M3, propellers were sized to be 11x6 in so the pitch speed, 117 ft/s (36.7 m/s), matched the V_{cruise} , maximizing endurance. This led to a predicted M3 endurance of 269.1 seconds, as in Section 4.6.

4.5.5 FINALIZED PROPULSION PACKAGES

The final propulsion packages are seen in Table 22. The fuse was selected from a 2023 team study comparing fuse brand sensitivity to current, in which the 100 A Stinger fuse was selected [2].

Table 22. Propulsion packages for each flight mission

Mission	Motor	ESC	Battery	Propeller	Fuse
1 & 2	Scorpion A-4220 540 kV	KDE Direct 130 A ESC	Thunder Power RC 8S 3300 mAh	[1] APC 11x7S & [1] APC 11x7P	Stinger 100A MAXI Fuse

4.6 PREDICTED FLIGHT AND MISSION PERFORMANCE

Utilizing PlaneTools (see Section 4.4.1), the performance of the preliminary design was simulated. Shown in Table 23 are the relevant aircraft performance values with all FoS included. Overall, the aircraft performs well in both M2 and M3. However, due to the higher takeoff weight (TOW) and payload (Section 4.4.2), M2 has a higher static thrust requirement and thrust settings for takeoff and cruise.

Table 23. Simulated Mission Performance

	M1	M2	M3
Payload	[-]	4.85 lbm (2.2 kg)	18 pax
TOW	13.6 lbm (6.17 kg)	19.3 lbm (8.77 kg)	15.0 lbm (6.97 kg)
TOFL	15 ft (4.5 m)	20 ft (6.1 m)	16 ft (4.9 m)
Cruise Throttle	70%	100%	70%
Cruise Speed	119 ft/s (36.2 m/s)	163 ft/s (49.6 m/s)	110 ft/s (33.5 m/s)
Cruise C_L	0.13	0.07	0.15
Battery Usage	43.5%	48.7%	82.9%
Number of Laps	3	3	8
Mission Time	92.9 s	75.9 s	269.1 s
Score	1	1.5	2.4

5.0 DETAILED DESIGN

Once conceptual and preliminary design were completed, detailed design involved further analysis and testing of individual components, both on-ground and in-flight. A particular focus was given to weight reduction. Impacts to aircraft performance and structure were also considered.

5.1 DIMENSIONAL PARAMETERS TABLE

Table 24 lists the characteristics of each subsystem for *EmergenSC*. The subsystems are explored in more detail in the subsequent sections.

Table 24. Characteristic properties for each major subsystem for *EmergenSC*

Wing		Tail	
Airfoil	SM701	Airfoil	NACA 0014
Span, b	5 ft (1.52 m)	Horizontal Span	26.5 in (0.674 m)
MAC	1.33 ft (0.405 m)	Horizontal Chord	9.02 in (0.229 m)
Planform Area, S	6.58 ft ² (0.611 m ²)	Vertical Span	13.0 in (0.330 m)
Aspect Ratio, AR	3.8	Vertical Chord	9.02 in (0.229 m)
Incidence Angle	-2°	Planform Area	1.63 ft ² (0.151 m ²)
Static Margin	16-20%	Incidence Angle	0°
Fuselage and Tail Boom		Tail Arm	44.9 in (1.14 m)
Total Length	70.1 in (1.78 m)	Controls and Power	
Width	5.89 in (0.149 m)	Receiver	RadioMaster ER8
Maximum Height	7.70 in (0.195 m)	Servos	HS7955TG x 2; D485HW x 5
Tail Boom Length	15.8 in (0.402 m)	Battery Model	Thunder Power
Tail Boom Width	0.83 in (0.021 m)	Cell Count	8S
Motor		Pack Voltage	29.6 V
Model	Scorpion A-4220	Pack Weight	1.59 lbm (0.72 kg)
kV	540	Propeller	
Power Rating	2553 Watts	Manufacturer	APC Propellers
No-Load Current, I_0	1.54 Amps	Mission 1 (M1)	11x7S & 11x7P in
Internal Resistance	18.2 mΩ	Mission 2 (M2)	11x7S & 11x7P in
Weight	10.16 oz (288 g)	Mission 3 (M3)	11x6S & 11x6P in

5.2 STRUCTURAL CHARACTERISTICS AND CAPABILITIES

The aircraft structure was designed to withstand aerodynamic, inertial, and landing loads while minimizing weight and drag. In-flight aerodynamic loads act primarily on the wing and empennage. The aerodynamic surfaces were designed to withstand load factors of up to 6g at maximum cruise velocities. The empennage and wing structures house servos and allow for proper hinging and deflection of control surfaces. The fuselage serves as the load junction for all other subcomponents. The fuselage structure was designed to accommodate payloads and avionics. It was sized to withstand a 6g turning load factor, maximum aerodynamic down-loading on the tail, and a 3g landing.

5.3 SUBSYSTEM DESIGN

Built-up structures were used for the fuselage, wing, and tail to minimize empty weight (W_e). The fuselage and empennage were balsa, plywood, and spruce built-up with Solarfilm Lite (Solite) skins. A tail boom increased the fuselage length for tail attachment. The landing gear (LG) was an S-Glass bow gear and 1/8-in steel wire nose gear.

Laser-cut plywood and 3D-printed polylactic acid (PLA) components were used to make the payload rail that supports both M2 and M3 inserts while minimizing Ground Mission time (t_{GM}). Mission-specific payloads were designed from laser-cut plywood and rubber gasket material to restrain Passengers and EMTs. The M2 Medical Supply Cabinet (MSC) has a laser-cut plywood enclosure housing stainless steel bars to increase m_{MSC} . The Patient gurney was 3D-printed, and the hatch was built-up using laser-cut wooden components. The Passenger and Crew floor were laser-cut from balsa, with the Crew restrained at the base by friction-fit rubber inserts.

5.3.1 WING AND MOTOR MOUNTS

The wing was designed to withstand 6g turning loads and support wing mounted motors with a factor of safety (FoS) of 1.3. Figure 24 shows the bending and shear loads along the wing semispan based on lifting loads, outboard rotating motor torque, as well as motor and ESC weight. The wing needed to withstand a maximum allowable bending moment of 45 lb-ft (61 Nm) and a maximum allowable shear load of 36 lbf (160 N).

A commercial off-the-shelf (COTS) composite tube was selected as the main wing spar due to its manufacturing reliability and weight. The selected spar was round carbon fiber reinforced polymer (CFRP) with an inner diameter of 0.75 in (1.9 cm) and an outer diameter of 0.83 in (2.1 cm). This spar was selected since it satisfied strength and stiffness requirements based on the loading shown in Fig. 24, as determined through testing discussed in Section 8.2.3. Torsional loads were handled by a 1/8-in plywood aft spar and a +45°/-45° twill-weave CFRP D-Box at the leading edge of the wing. To save weight, the ribs were mainly 1/8-in balsa with cutouts but were

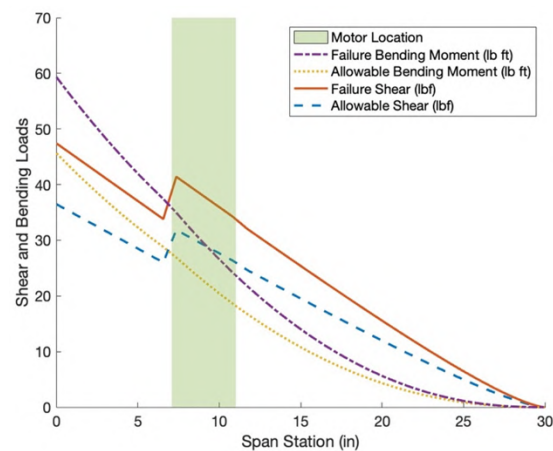


Figure 24. Loading along semispan in 6g turn

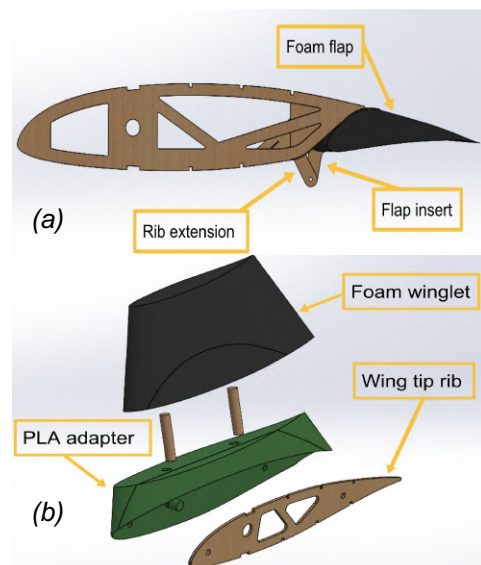


Figure 25. (a) Flap hinging method and (b) winglet attachment method

designed individually based on their unique functions. Balsa stringers supported a Solite skin for the aft of the wing.

The control surfaces and winglets utilized fiberglass-reinforced polystyrene foam, with ailerons hinged using fiberglass tape. As seen in Fig. 25, the slotted flaps, hinged through plywood extensions from the rib, attached to plywood parts in the flaps. Winglets were affixed via a 3D-printed PLA adapter, bolted onto the plywood wingtip rib with nylon bolts.

The motors are mounted forward of the leading edge via a custom-made CFRP tube, shown in Fig. 26, with twill plies oriented at $+45^\circ/-45^\circ$. The same motor diameter was used for the motor mount to decrease drag and manufacturing complexity. Components were sized to withstand torque, thrust, and weight from the motor, which was epoxied to a plywood plate bonded to the front of the tube. The aft of the tube was mounted to a plywood plate which slotted into plywood ribs on each side, transferring the motor loads into the spar.

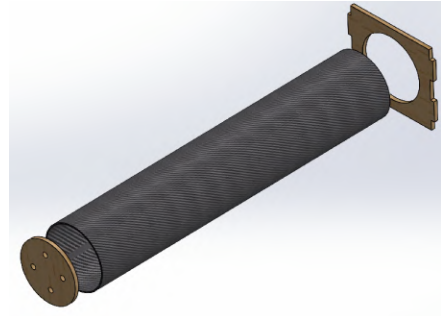


Figure 26. Motor mount design

Using a Wing Upwash and Speed Calculator [17] from Prof. Blaine Rawdon, based on lifting line theory, the motors and propellers were mounted 8 in (20.3 cm) forward of the leading edge (LE) at a 3.4° downward incidence angle to the LE. This minimized wing blockage of the prop wash, align the thrust vector upwash in front of the wing during cruise, and take advantage of blown lift during takeoff and turns.

5.3.2 TAIL

A built-up tail design was selected to minimize weight and was sized for down-loading on the tail at maximum cruise speeds (V_{cruise}). Two spars were used due to the swept and tapered tail planform and were sized to handle all bending loads. 1/4-in thick balsa was selected for the forward spar using Eq. 22 with a yield strength of 145 psi (1 MPa) and a wooden dowel was tested and validated to act as the middle spar. 1/8-in balsa ribs and a 1/4-in balsa aft spar handled torsional loads. 1/32-in balsa sheeting was selected as the skin to create a light, aerodynamic surface. The vertical stabilizer spars attach to the horizontal stabilizer spars. Together, these connect to the tail boom through dropdowns from the root ribs, which are reinforced with 1/16-in plywood on each side.

$$\sigma_{\text{max}} = \frac{Mc}{I} \quad \text{Eq. 22}$$

5.3.3 FUSELAGE

The fuselage, shown in Fig. 27, is a built-up structure designed to accommodate M2 and M3 payloads, support Ground Mission (GM) loading, and transfer tail, wing, and LG loads. The cross-sectional shape of the fuselage is held by formers (red). These parts serve mainly as a construction tool, but some are also reinforced (green) and used as integration points for other subcomponents and for the payloads rail. Attachment points for the wing (blue) and LG connect to formers in the middle of the fuselage. The

longitudinal bending loads were handled using four longerons (orange), which extend the length of the fuselage and slot into the corners of the formers.

Shear loads were handled by a truss structure (yellow) between longerons. To create a rounded aerodynamic shape to support the Solite skin, balsa stringers extended between balsa shapers (pink).

The loading cases discussed in Section 5.2 were used to size the components of the fuselage. The resultant bending moment and shear force are shown in Fig. 28 and Fig. 29 with a 1.3 FoS. Sizing for the fuselage was completed assuming that loading may be completely asymmetrical.

The longerons were sized under the assumption that the top and bottom longerons act as a force couple, creating a moment to withstand the local expected bending moment. Balsa and spruce were considered due to their weight and capacity for axial loading. The required side length for a square longeron cross-section was calculated based on the expected local bending moment, the distance between the top and bottom longerons, and an axial yield strength of 145 psi (1.0 MPa) for balsa and 230 psi (1.6 MPa) for spruce. Based on these calculations, 1/4-in spruce was selected for the majority of the longeron, with a transition to lighter 1/4-in balsa at the nose to minimize weight. The truss components are used to transfer shear loads along the fuselage and withstand any torsional loads, with their individual orientations influenced by local concentrated loads. The truss members were assumed to be loaded axially to withstand

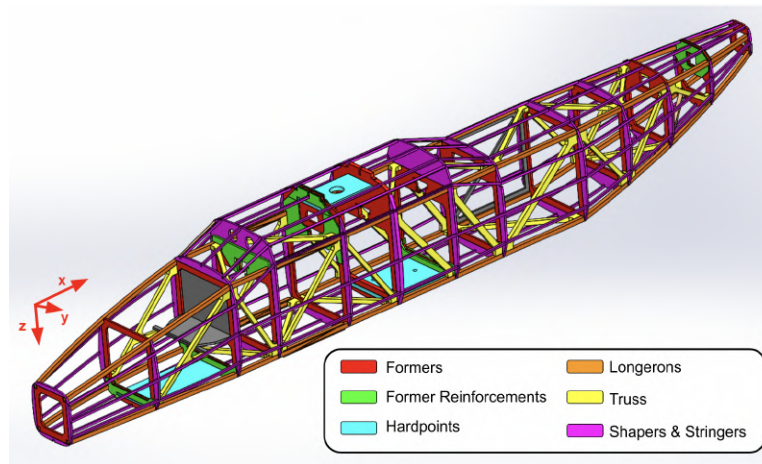


Figure 27. Fuselage components

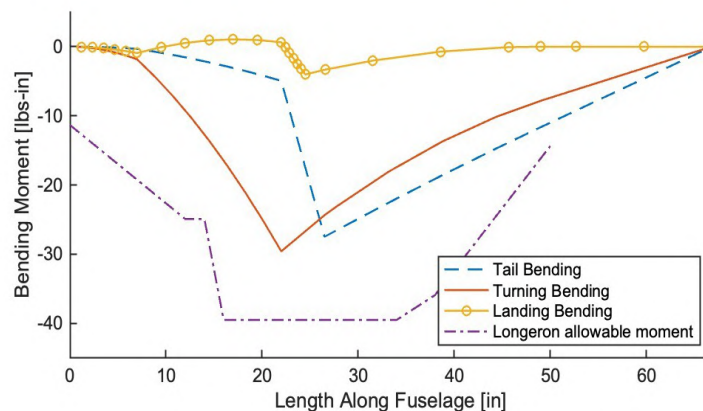


Figure 28. Bending moment along fuselage with 1.3 FoS

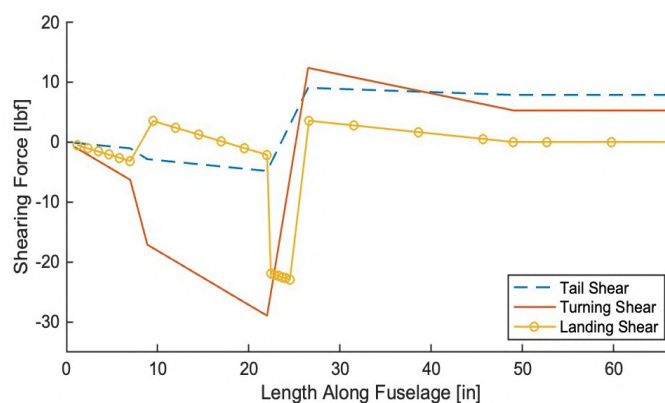


Figure 29. Shear force along the fuselage with 1.3 FoS

the local shear, and the required load supported by each component was used to determine its optimal material and dimension - from 1/4-in x 1/4-in balsa, 1/4-in x 3/4-in balsa, and 1/4-in x 1/4-in plywood. Truss members are filleted at the ends to prevent buckling.

Most formers were made of 1/8-in balsa to minimize weight. However, the structural formers had additional plywood sandwiching reinforcement on either side of the balsa former to transfer loads into the longerons and truss structure. The shape and thickness of these reinforcements was determined using simple shear and bending calculations from Eq. 23 and 24 with a FoS of 3 to account for stress concentrations. The wing and LG hardpoints are made of plywood and tested to validate their strength as shown in Section 7.2.3.

$$\tau = V/A \quad \sigma = My/I \quad \text{Eq. 23, 24}$$

5.3.4 PARKING SPOT MECHANISM

A rotating wing mechanism was selected during the conceptual design phase to fit the aircraft in the 2.5 ft (0.76 m) parking spot. In the selected design, shown in Fig. 30, the wing rotates on a flat interface with the fuselage around a pipe and is held in place with a spring-loaded anti-rotation pin when in flight configuration.

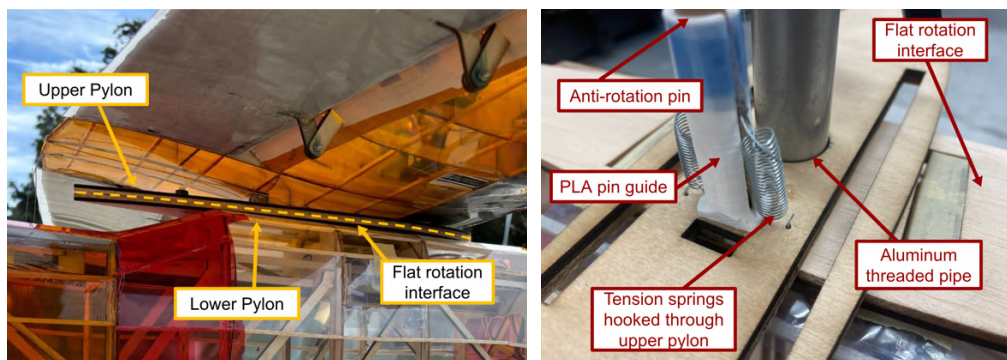


Figure 30. External (left) and internal (right) view of parking spot mechanism

A threaded pipe was selected as the point of rotation with wiring passing directly through it to prevent tangling during GM. The pipe handles all tensile loads between the wing and the fuselage and is secured by brass nuts to hardpoints in the wing and fuselage shown in Fig. 31. The coefficient of friction between the upper and lower pylon was low enough to fully tighten the nuts without preventing rotation. The strength of the pipe and hardpoints are validated in Section 7.2.3.3. All compressive loads were distributed through contact of reinforced ribs and formers. Pitching and rolling moments were handled by the pipe and pylon.

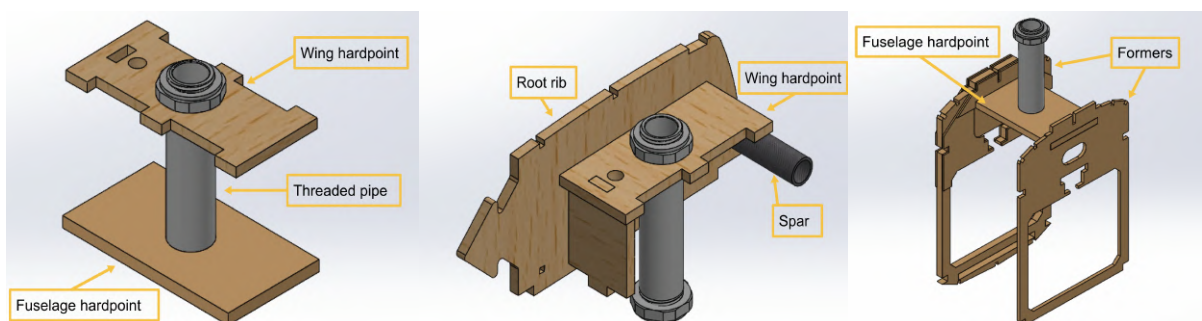


Figure 31. Threaded pipe integration into wing and fuselage

A spring-loaded anti-rotation pin restrains the wing in yaw in the flight configuration. The mechanism involves a dowel held vertically in the wing, pulled down by two tension springs. When the wing is set in the flight configuration, a hole in the upper and lower pylon aligns. This allows the pin to be pulled through the bottom pylon and lock the wing in place. To store the wing, a string is attached to the pin and extended through the top skin of the wing for the pin to be pulled out of the bottom pylon.



Figure 32. Pylon in parking configuration (left) and flight configuration (right)

5.3.5 LANDING GEAR

The main bow gear was designed using GearSizer, a dynamic spreadsheet created by Prof. Blaine Rawdon [18]. The gear was sized for a maximum aircraft weight of 15.3 lbm (6.9 kg), a 4.91 ft/s (1.50 m/s) sink rate, and a 2.1g loading limit. Sink rate and loading limit decisions were driven by team experience [2]. The bow was designed with a 16.8 in (0.43-m) track and a height of 4.0 in (0.10 m), shown in Fig. 33. Parameters for the gear were determined using Sadraey [19].



Figure 33. GearSizer model of the landing gear (left) and constructed fiberglass gear (right)

S-glass was chosen for its lower stiffness over carbon fiber and high strength compared to other fiberglass types. This allows for a lower bounce frequency upon landing, which absorbs more energy, preventing fuselage damage and increasing landing control. As shown in Fig. 34, the shear stress of the gear was kept under 500 psi (3.5 MPa), with a built-in FoS of 1.4, resulting in a maximum stress of 360 psi (2.5 MPa).

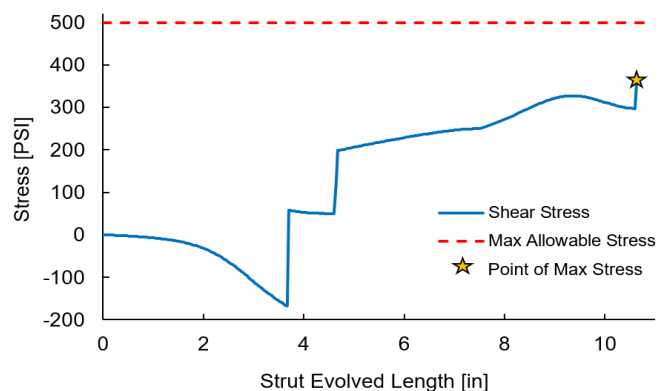


Figure 34. Calculated Stress Along Bow Gear

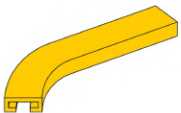
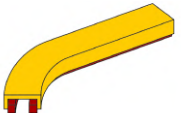
5.3.6 PAYLOADS

The payload system includes a longitudinal rail that suspends both M2 and M3 payload inserts in the fuselage from the top, as traded in Section 3.3.5.

5.3.6.1 PAYLOADS RAIL

The rail was designed to support all payload inserts and minimize t_{GM} while supporting in-flight loads and minimizing system weight. The rail holds square aluminum nuts connected to each insert, allowing for smooth unrestricted motion along the rail when loading and unloading, while also restraining the inserts in position during flight. Different materials were considered for the payload rail with system weight, strength, and manufacturability as figures of merit (FoM) in Table 25. Three options were considered: a fully 3D-printed PLA rail with a curved section, a COTS aluminum rail cut at an angle to create the aft curved segment, and a custom-sized built-up wooden rail with PLA contact points and square aluminum nuts. The fully 3D-printed PLA rail was the baseline for comparison.

Table 25. Material downselect for payload rail

				
FoM	Weight	Fully 3D-Printed PLA	COTS Aluminum Rail	Wooden Rail + PLA Contact
Weight	0.4	0	-1	0
Strength	0.4	0	1	1
Manufacturability	0.2	0	0	-1
		0.0	0.0	0.2

While both the COTS aluminum rail and the wooden rail with PLA contact can withstand the loads during a 6g turn, the custom-sized wooden rail was 78% lighter than the COTS aluminum rail. This benefit overcame the drawbacks of increased manufacturing complexity. Thus, the custom-sized wooden rail with PLA contact that reduces the friction

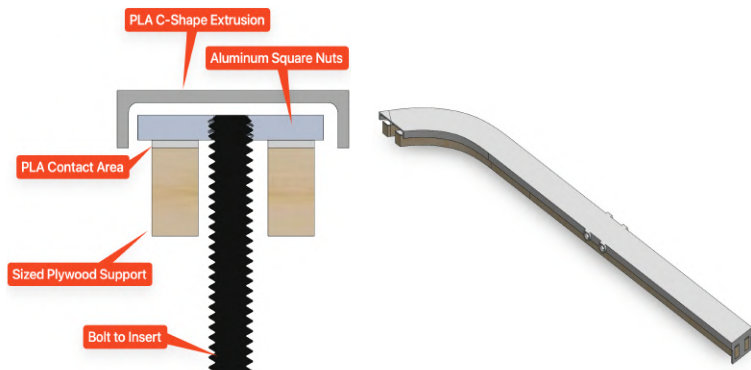


Figure 35. Rail cross-section with aluminum square nut (left), and entire payload rail assembly (right)

between the aluminum inserts and the plywood supports, shown in Fig. 35, was selected. To restrain the square nuts in the upward and lateral directions, a custom PLA C-shape extrusion was 3D-printed and attached to the fuselage formers. Plywood rail supports were sized to hold m_{MSC} in a 6g turn with a 1.5 FoS to restrain the inserts in the downward direction under in-flight loads. To restrain the inserts in the longitudinal direction during flight, the front end of the rail is closed off with a wall from the 3D-printed C-shape

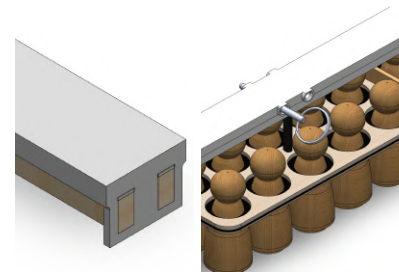


Figure 36. (Left) Front End PLA Cap (Right) M3 Restraining Pin

extrusion, as seen in Fig. 36, and the aft section has holes cut for restraining pins. These pins are removed to load the inserts and re-positioned in their respective location (forward hole for M2, aft hole for M3) to restrain the inserts. The rail curves towards the payload hatch to load and unload the inserts. The rail cross-section was lofted to meet the hatch after the required payload inserts.

5.3.6.2 M2 MEDICAL SUPPLY CABINET (MSC)

The M2 MSC was designed as a separate insert from the Patient and EMT. With varying headwind conditions in Wichita, KS, the goal for the MSC was to enable quick m_{MSC} adjustments before flights without changing insert dimensions. The MSC was manufactured to have 24 slots, as seen in Fig. 37, where additional weight can be inserted to increase m_{MSC} . The empty weight of the cabinet is 0.575 lbm (0.261 kg) and the maximum weight that can be achieved by adding 24 1/2-in x 1/2-in x 6-in 304 stainless steel bars is 10.9 lbm (4.94 kg) with increments of 0.43 lbm (0.195 kg). Thus, this insert can meet the target m_{MSC} of 4.85 lbm (2.2 kg) while allowing for incremental increase. The insert is held on the payload rail through two square aluminum nuts, while being able to rotate about the axis of the bolt to ensure smooth loading and unloading around the curved section of the rail. The door of the MSC is held by a 5/8-in stainless steel fabric snap and hinged at the bottom using tape.

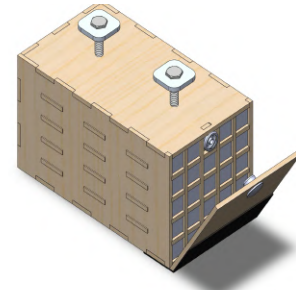


Figure 37. M2 MSC fully loaded to 10.9 lbm (4.94 kg)

5.3.6.3 M2 PATIENT/EMT INSERT

For the M2 Patient and EMTs, an insert was designed to hold the gurney with the Patient and EMTs as instructed by the rules - shown fully loaded in Fig. 38. Since the base diameter of the Passenger/EMTs were not toleranced to allow a friction-fit of the inserts, the EMTs are restrained from their necks with a custom rubber gasket cut from a 1/32-in thick sheet of multipurpose neoprene rubber. The cutouts open out around their heads and close around their necks to hold them in place. The gurney is made from 3D-printed PLA to match the Patient's shape. The Patient is held down to the gurney with rubber bands guided by slots on the bottom of the gurney. The gurney is secured to the insert with Velcro.

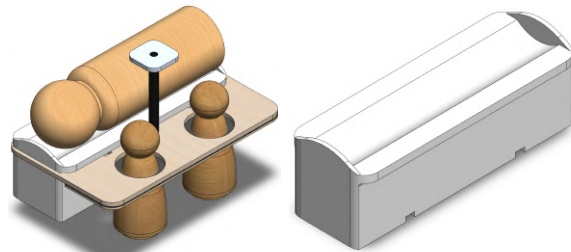


Figure 38. M2 Patient/EMT insert with rubber band restraint not shown (left), Gurney (right)

5.3.6.4 M3 PASSENGER INSERTS

The design focus for the M3 Passenger inserts was minimizing t_{GM} and insert weight. Since large quantities of Passengers were expected to be loaded quickly, the goal was to design a method to load multiple Passengers at once. With the base diameter of the as-received Passengers having around a 0.1 in (0.4 mm) variation, a friction-based restraint method was avoided.

Thus, like the M2 EMT restraint method, the Passengers were held from their necks with rubber gasket holes of diameters 1.25 in (3.18 cm). A 10-Passenger insert is shown in Fig. 39. Thin separators can be added to prevent collisions, should the Passengers touch each other in-flight.



Figure 39. Fully loaded 10-Passenger insert with bumper CAD for M3

This push-down method allows for the entire insert-worth of Passengers to be loaded in one motion by pushing the inserts from above the Passengers' heads downwards until the inserts reach their necks, as seen in Fig. 40. This greatly reduces t_{GM} when compared to individually loading each Passenger. While loading individual Passengers took around 1.5 seconds per Passenger, the push-down method could load all 10 Passengers in around 2.0 seconds (or 0.2 seconds/passenger). Inserts may come with a built-in bumper made of 1/8-in laser-cut piece to ensure the inserts can push each other along.



Figure 40. Three stages of M3 with 8-Passenger insert loading with inserts placed above Passengers (left), inserts pushed down to open rubber gasket (middle), and Passengers ready for loading (right)

When evaluating passenger layout in the fuselage, t_{GM} , system weight, and fuselage cross-section were considered, since weight and drag would be affected. A 2x5 + 2x4 layout was chosen over a 2x3 + 2x3 + 2x3 and a 3x3 + 3x3 layout. This selection allowed for the quickest t_{GM} to load 18 Passengers with the fewest inserts.

5.3.6.5 PAYLOADS HATCH

The rear payload hatch serves as an entry point for mission-specific inserts to be un/loaded while minimizing t_{GM} . The goal is to meet rule specifications for the hatch while maintaining its reliability. Since magnetic latching mechanisms are specifically prohibited by the rules and Velcro may be deemed unfit by the technical inspection line judge, a conservative approach to avoid these options were taken. A leather fabric snap fastener was integrated into the hatch and fuselage to ensure a positive latching mechanism while closing. As the hatch is closed, the male end snaps into the female end, locking the hatch in place. Testing showed that 10.8 lbf (48.0 N) would separate fasteners away from each other, signifying that an inadvertent opening of the hatch would be unlikely under normal operating conditions. Like the fuselage, a Solite skin was adhered to the balsa components. Figure 41 shows the aft fuselage hatch.



Figure 41. Payload hatch (fabric snaps not shown)

5.3.6.6 PASSENGER AND CREW COMPARTMENTS

The Crew compartment meets the requirements for all missions while minimizing weight. Laser-cut 1/32-in balsa was selected for the Passenger floor, while 1/8-in balsa was selected for the Crew floor. The floor is supported with extensions from the adjacent truss. Since the base diameter of the Crew varies, the Crew members were restrained with a hollow cylinder made from neoprene rubber for a friction fit between the side of the Crew and the rubber. These rubber cylinders were attached to the Crew floor with CA adhesive. The Crew Hatch was 3D-printed from PLA to fabricate the complex geometry of the hatch while meeting the requirements and was hinged with tape to the fuselage for easy internal access.

5.3.7 PROPULSION SYSTEM

Each propulsion component was tested to best optimize advance ratio, J , for each mission. Flight testing confirmed that power, current, and TOFL requirements would be met for each mission. The mission breakdown is shown in Table 26.

Table 26. Package breakdown by mission

	M1 & M2	M3
Motor	[2] Scorpion A-4220-540 kV	
Propeller	[1] APC 11x7S (Right) [1] APC 11x7P (Left)	[1] APC 11x6S (Right) [1] APC 11x6P (Left)
Battery	Thunder Power RC 8S, 3300 mAh	
ESC	[2] KDE Direct 130A ESC	
Fuse	[1] Stinger 100A MAXI	

5.3.8 WIRING

The wiring for the avionics and motors can be seen in Fig. 42.

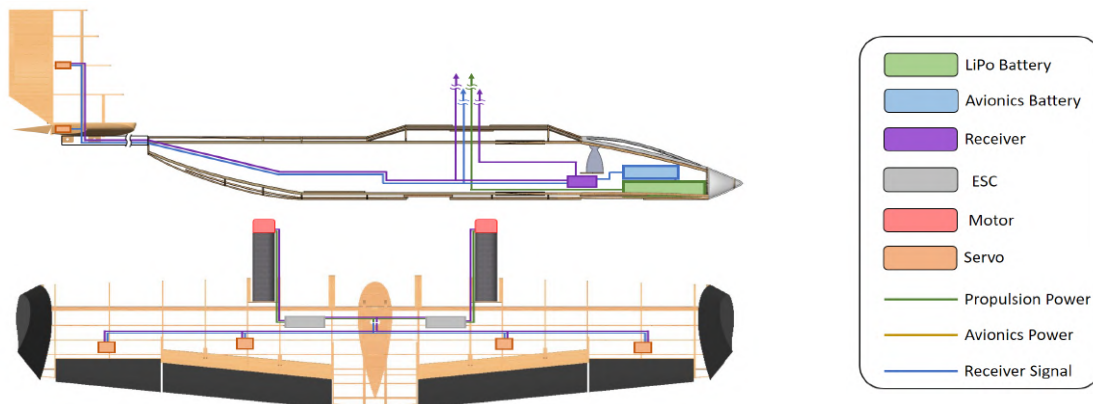


Figure 42. Wire Routing Diagram

Each motor was connected to an electronic speed controller (ESC), connected in parallel to the propulsion Lithium Polymer (LiPo) battery and to the RadioMaster ER8 receiver. A separate battery powers the avionics servos through a battery eliminator circuit and signals sent from the receiver. Servos were sized with an Excel-based tool that calculates hinge moment created by surface deflection at a given airspeed. A required torque of 14.16 lb-in (1.60 N-m) for the flaps and 8.37 lb-in (0.95 N-m) for the rest of the control surfaces was shown. The flaps used stronger servos (D950TW) to resist large hinge moment loads due to propeller wash, while all other control surfaces used D485SW servos. The avionics battery was sized to ensure sufficient energy for the entire duration of the mission without the addition of unnecessary weight. Based on servo stall currents and receiver current draw over the duration of staging and 5-minute mission with a FoS of 2, a 3S 1100 mAh battery was found sufficient for all missions.

5.4 WEIGHT AND MASS BALANCE

The empty weight (W_e) for *EmergenSC* is 11.5 lbs (5.21 kg). The battery was used as a ballast to ensure the CG was within the static margin (SM), described in Section 4.3.1, for all mission configurations. The coordinate system used is shown in Fig. 43. Table 27 shows the mass of

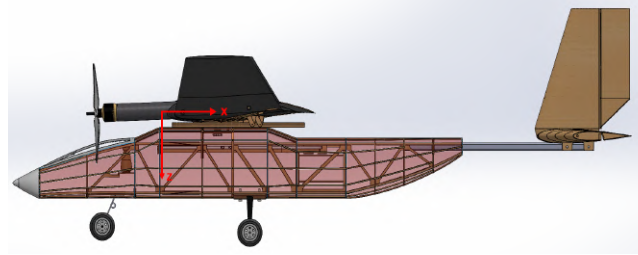


Figure 43. Aircraft coordinate system with origin placed at the leading edge of the wing

each component and CG location relative to this coordinate system centered at the root leading edge. The mass balance for *EmergenSC* was analyzed using measured component weights and empirical material measurements. For M2, the MSC location was chosen to ensure CG would stay within the SM. The M3 configuration described in Table 27 considers the maximum 18-Passenger loading case. The Passenger and inserts CG was taken at the center of the system of multiple inserts and Passengers. Table 28 shows the CG and stability margins for each mission configuration in the coordinate system shown in Fig. 43.

Table 27. Mass balance table for all missions

Mission	Aircraft Component	Mass		X Displacement		Z Displacement	
		[lb]	[g]	[in]	[cm]	[in]	[cm]
General	Fuselage with Boom	2.37	1107	13.1	33.4	4.57	11.6
	Wing (Includes Motors and wiring)	4.16	2470	2.32	5.90	-0.45	-1.15
	Tail	0.91	414	51.2	130.0	1.46	3.70
	Main Landing Gear	0.22	125	9.88	25.1	12.5	31.8
	Nose Landing Gear	0.07	34	-9.06	-23.0	10.9	27.8
	Fixed Avionics	0.41	209	-9.84	-25.0	7.48	19.0
	Crew	0.17	78	-5.12	-13.0	5.28	13.4
M1	Propellers	0.18	80	-8.46	-21.5	0.20	0.50
	Battery	1.49	720	-9.45	-24.0	8.11	20.6
	Total	11.5	5210	6.33	16.1	2.70	6.87
M2	Propellers	0.18	80	-8.46	-21.5	0.20	0.50
	Medical Supply Cabinet	4.85	2200	6.30	18.0	6.14	15.6
	EMT + Gurney +Patient + Insert	0.63	286	-0.79	-2.00	6.46	16.4
	Battery	1.49	720	-8.66	-22.0	8.11	20.6
Total	17.02	7720	6.33	16.1	3.82	9.71	
M3	Propellers	0.18	80	-8.46	-21.5	0.20	0.50
	Passengers (18) and Inserts	1.74	788	6.10	15.5	6.38	16.2
	Battery	1.49	720	-9.05	-23.0	8.11	20.6
	Total	13.3	6028	6.33	16.1	3.19	8.09

Table 28. CG Location and SM per Mission

	M1	M2	M3
CG Location	6.33 in (0.161 m)	6.33 in (0.161 m)	6.33 in (0.161 m)
Stability Margin	16%	16%	16%

5.5 DRAWING PACKAGE

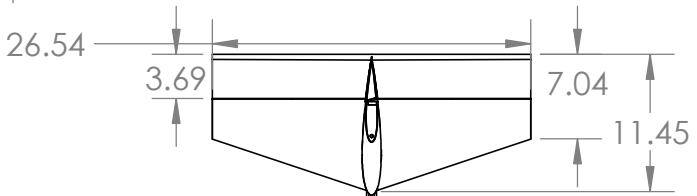
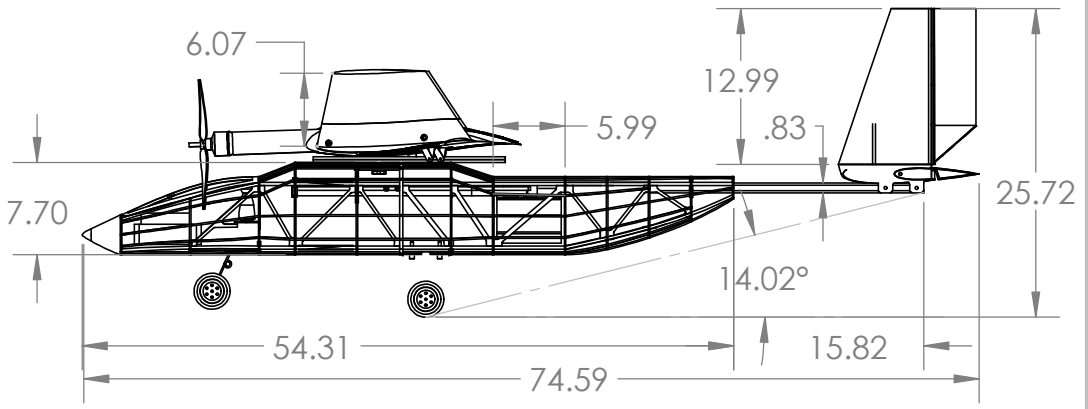
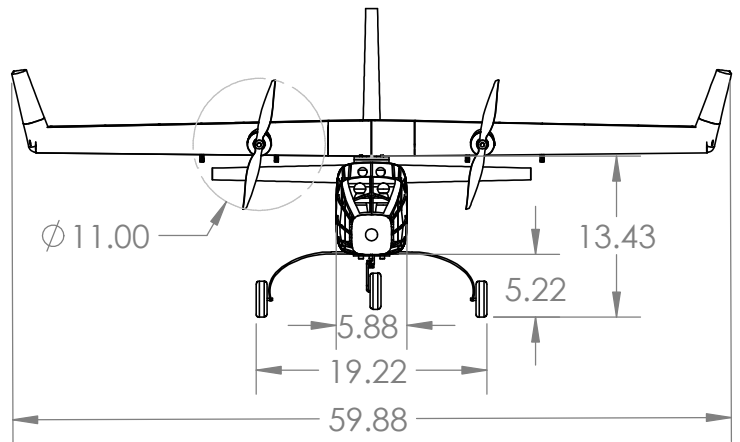
The following package includes a dimensional 3-View, structural arrangements, subassembly detail, mission-specific payloads, and parking configuration. All drawings were made using SolidWorks [20].

2

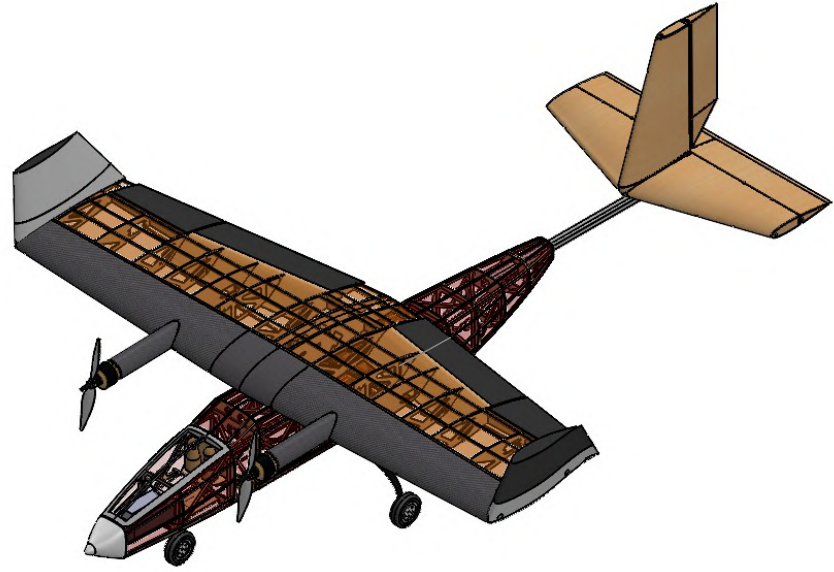
1

B

B

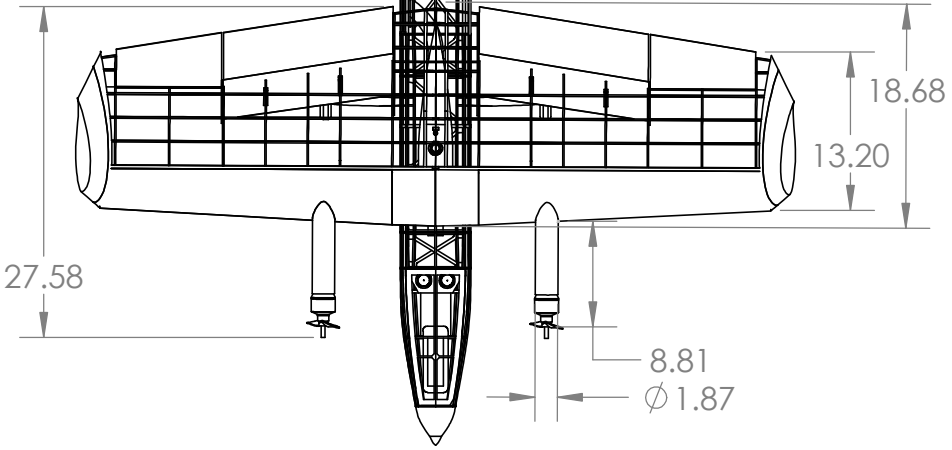


.83



A

A



NOTE: MISSION 1 CONFIGURATION



UNLESS OTHERWISE NOTED: ALL DIMENSIONS IN INCHES

2024 UNIVERSITY OF SOUTHERN CALIFORNIA
"EmergenSC"

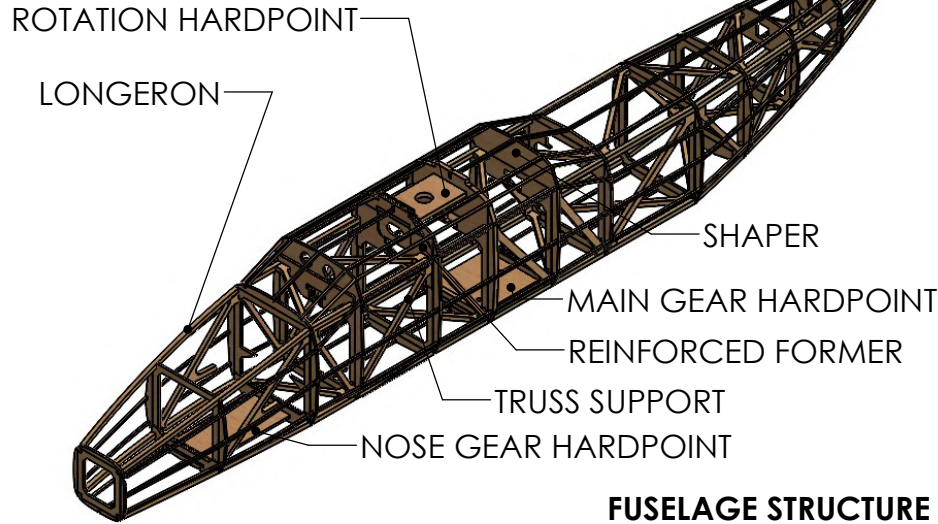
SIZE	DWG. NO.	REV
A	Aircraft 3-View	3

SCALE: 1:16 Drawing Package SHEET 1 OF 4

1

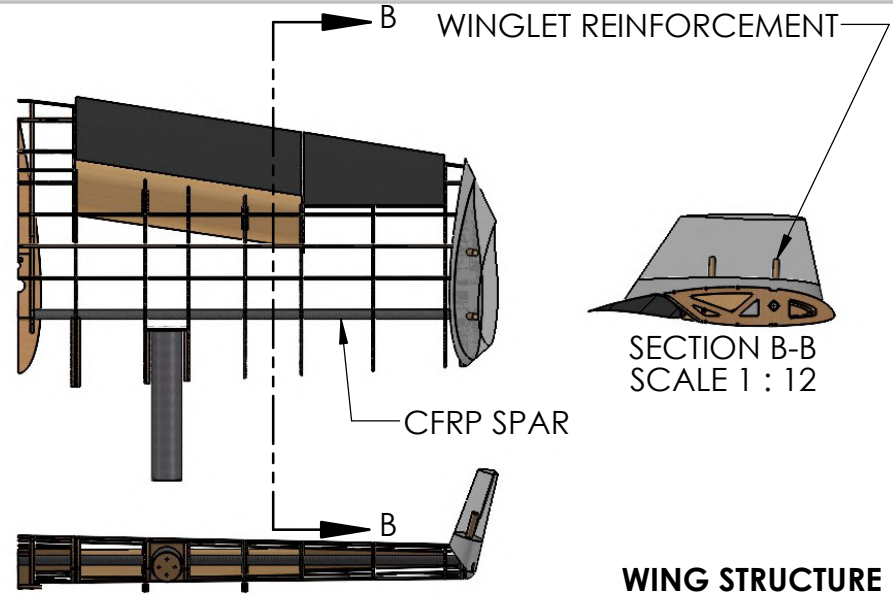
2

NOTE: BULKHEAD AND CREW FLOOR HIDDEN



FUSELAGE STRUCTURE

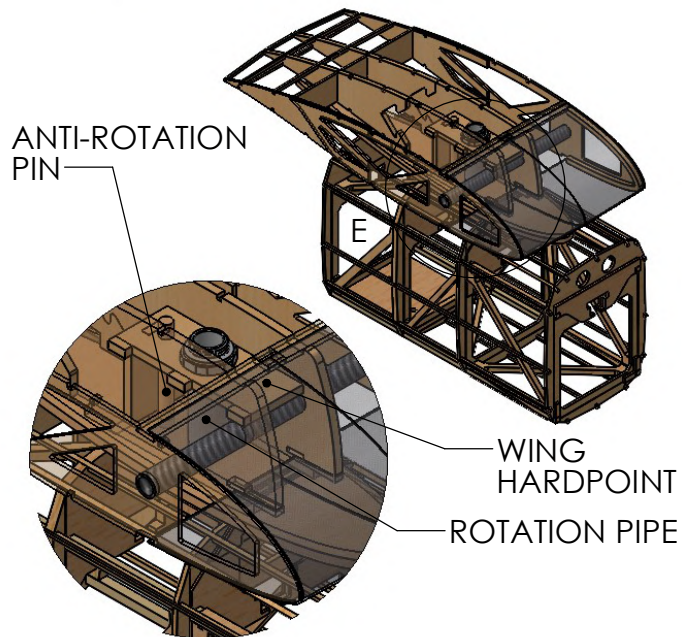
1



WING STRUCTURE

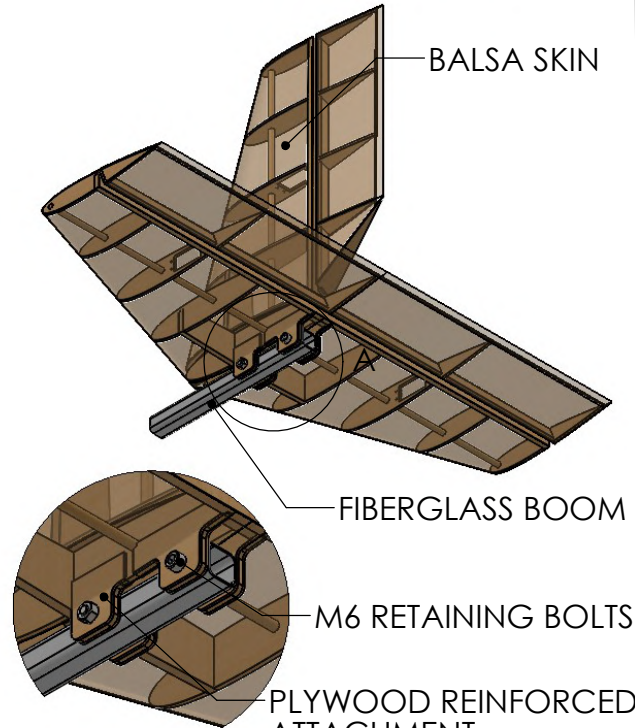
B

B



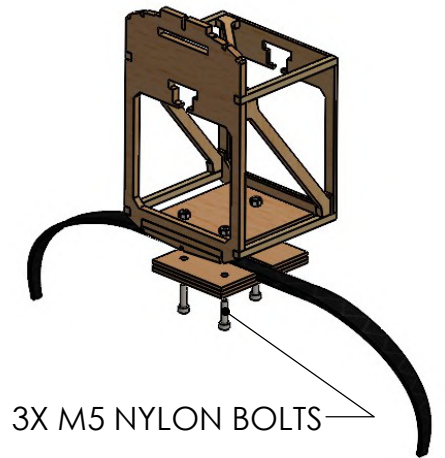
DETAIL E
SCALE 1 : 4

WING ROTATION MECHANISM



DETAIL A
SCALE 1 : 4

TAIL STRUCTURE



LANDING GEAR ATTACHMENT

A

A



UNLESS OTHERWISE NOTED: ALL DIMENSIONS IN INCHES
 2024 UNIVERSITY OF SOUTHERN CALIFORNIA
 "EmergenSC"

SIZE	DWG. NO.	REV
A	Structural Layout	3

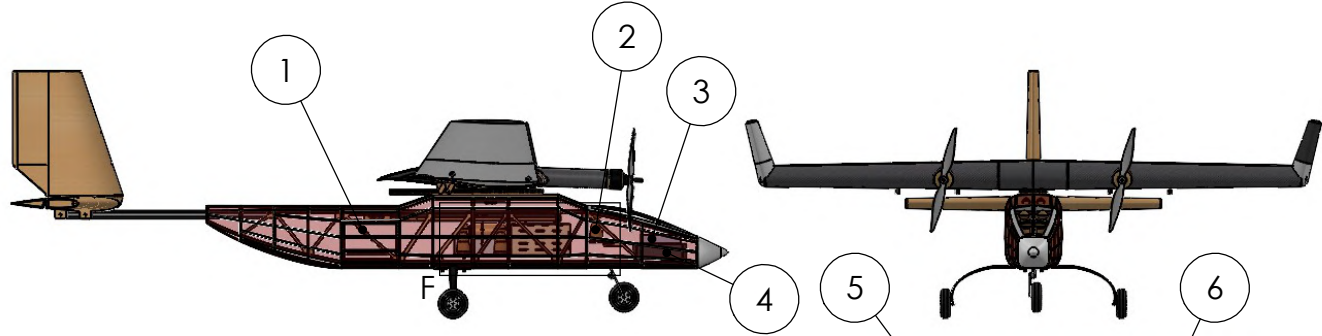
SCALE: 1:16 Drawing Package SHEET 2 OF 4

1

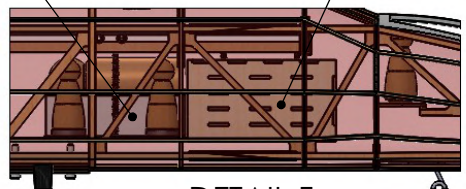
2

1

B

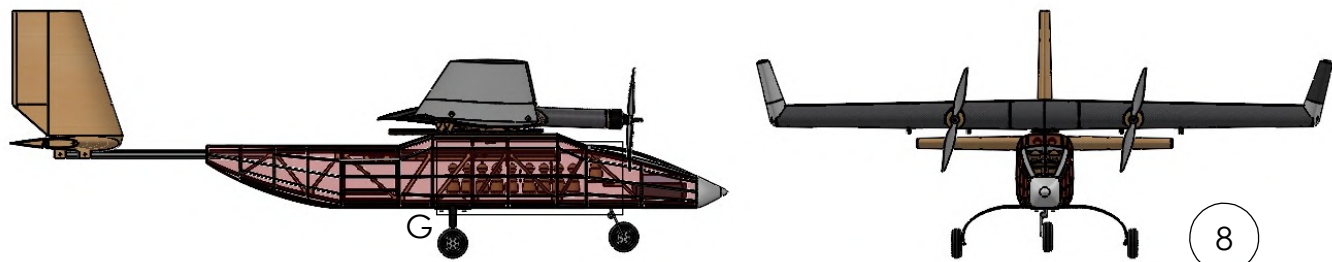


ITEM NO.	NAME
1	PASSENGER HATCH
2	CREW
3	BATTERY - 8S 3300 mAh
4	AVIONICS BATTERY
5	EMT + PATIENT GURNEY INSERT
6	CABINET MASS INSERT

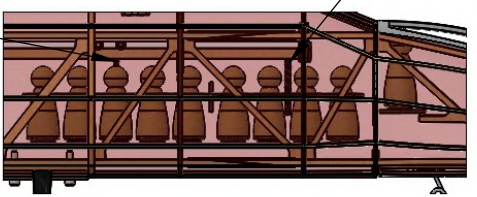


DETAIL F
SCALE 1 : 8
M2 CONFIGURATION

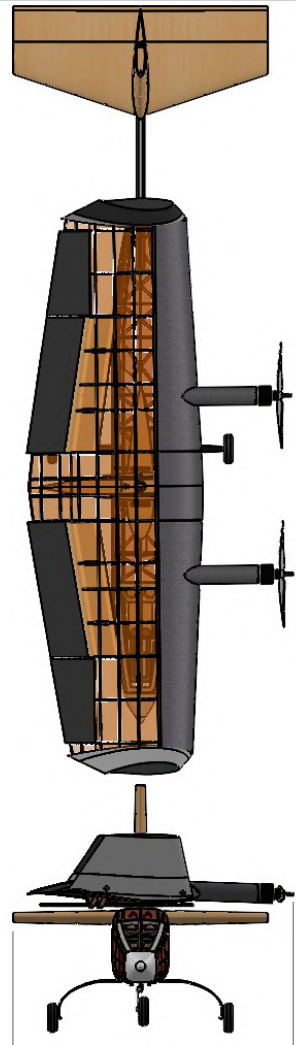
A



ITEM NO.	NAME
7	5 x 2 PASSENGER INSERT
8	4 x 2 PASSENGER INSERT



DETAIL G
SCALE 1 : 8
M3 CONFIGURATION



PARKING CONFIGURATION



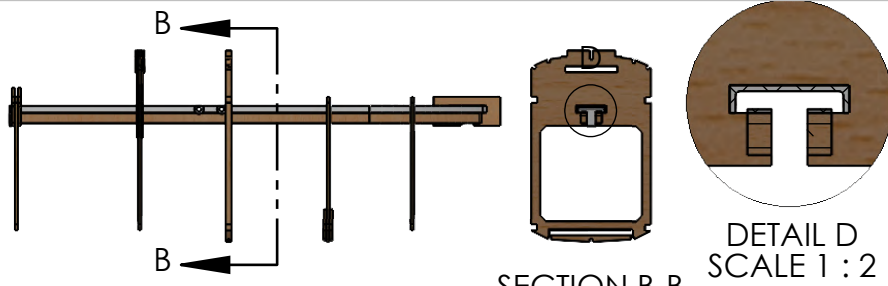
UNLESS OTHERWISE NOTED: ALL DIMENSIONS IN INCHES
2024 UNIVERSITY OF SOUTHERN CALIFORNIA
"EmergenSC"

SIZE	DWG. NO.	REV
A	Systems Overview	3

SCALE: 1:24 Drawing Package SHEET 3 OF 4

1

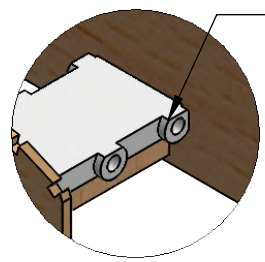
2



SECTION B-B

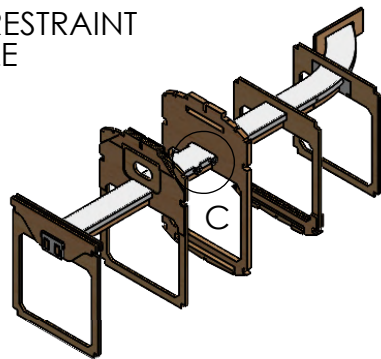
DETAIL D
SCALE 1 : 2

B



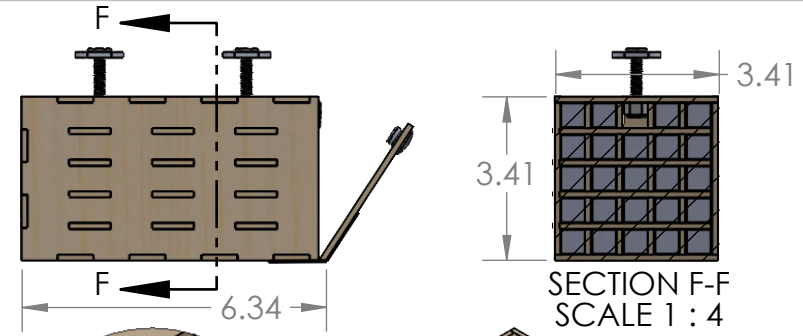
DETAIL C
SCALE 1 : 2

INSERT RESTRAINT
PIN HOLE

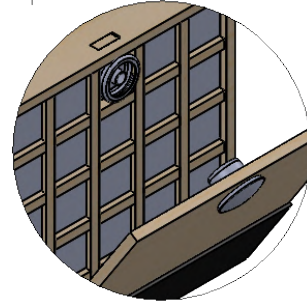


FUSELAGE RAIL SYSTEM

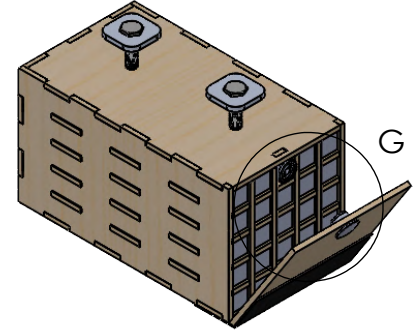
1



SECTION F-F
SCALE 1 : 4



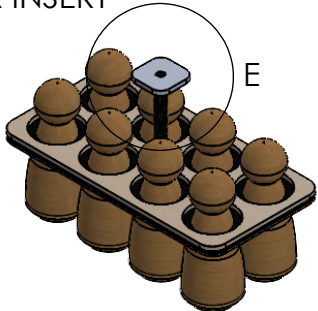
DETAIL G
SCALE 1 : 2



M2 MEDICAL CABINET

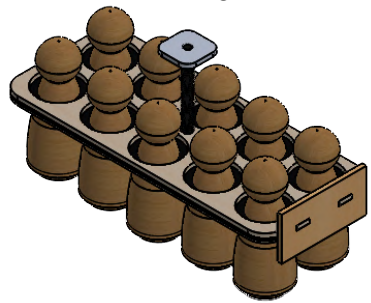
B

4x2 PAX INSERT



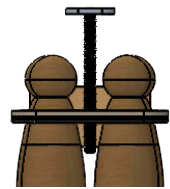
DETAIL E
SCALE 1 : 2

5x2 PAX INSERT



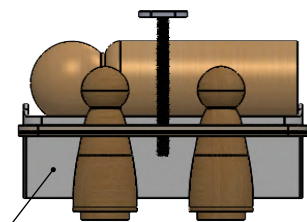
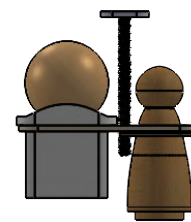
M3 PAX INSERTS

ALUMINUM
INSERT



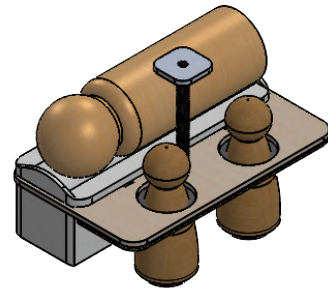
A

NOTE: RUBBER BAND
RESTRAINT NOT SHOWN



MEDICAL GURNEY

EMT + PATIENT INSERT



UNLESS OTHERWISE NOTED: ALL DIMENSIONS IN INCHES

2024 UNIVERSITY OF SOUTHERN CALIFORNIA
"EmergenSC"

SIZE	DWG. NO.	REV
A	PAYLOAD SYSTEMS	3
SCALE: 1:8	Drawing Package	SHEET 4 OF 4

A

2

1

6.0 MANUFACTURING PLAN

Various manufacturing processes were evaluated for each major aircraft component (e.g., wing, spar, fuselage, empennage, etc.) as well as mission-specific elements such as the Mission 2 (M2) Medical Supply Cabinet (MSC) and Mission 3 (M3) Passenger inserts. The processes were selected as described below.

6.1 MANUFACTURING PROCESSES INVESTIGATED

To identify the best manufacturing process for each component, the benefits and drawbacks of each were considered.

6.1.1 FOAM CORE COMPOSITES

Polystyrene foam is a relatively affordable, available, and manufacturable material that can be cut with a hotwire foam bow cutter and laser-cut plywood stencils, allowing for the rapid fabrication of components with complex curvatures. Fiberglass layups on the foam core strengthen the component while creating a smooth finish, despite a lower strength-to-weight ratio compared to built-up methods.

6.1.2 Balsa-Plywood Build Up

Structures built using a combination of balsa and plywood components with cyanoacrylate (CA) adhesive are favorable since well-designed balsa structures are often lighter than equivalent monocoque composite or foam-core components, as demonstrated through the team's prior experience [2]. Plywood components can be used strategically to reinforce structures that require greater strength, optimizing structural weight. The accessibility of Computer-Aided Design (CAD) and laser cutters allows for precise machining of components and, while manufacturing time is a drawback, it can be greatly reduced by using custom jigs.

6.1.3 3D-PRINTING

3D-printing offers a simple method to create complex shapes with precision and replicability. However, 3D-printed components tend to have low strength-to-weight ratios and do not allow for optimization of load paths. Therefore, 3D-printing is preferred for smaller, mission-specific components or other elements.

6.1.4 MOLDED COMPOSITES

The main benefit of composite components, which exhibit semi-isotropic properties, are their high stiffness, high strength-to-weight ratios, and part reproducibility when using molds. Composites can be formed to any mold shape, but have a high material cost, mold preparation complexity, and long manufacturing time.

6.1.5 STEAM BENDING

Steam-bent wood offers a lightweight solution to manufacturing major components that require unique geometry. Combined with a built-up structure, bending structural components allows for a sound structure with minimal weight penalty. Drawbacks of steam-bent wood include slight wood weakening and residual stresses [21]. Due to this, the team used steam-bent wood for structural pieces with shallow bends such as

the longerons. Two steamers, shown in Fig. 44, were built with a commercial wood steaming kit, a PVC pipe “steaming chamber”, and wood support structure.



Figure 44. 7.00 ft (2.13 m) steamer for longerons (left), internals of 2.00 x 0.5 ft (0.61 x 0.15 m) steamer for balsa sheeting (right)

6.2 MANUFACTURING PROCESSES SELECTED

Manufacturing methods were assessed by product quality, required skill, and repeatability. The team found that the best methods for each component utilized a combination of the five processes listed above.

6.2.1 WING STRUCTURE

A built-up structure was selected for the wing due to its lower weight compared to a foam core structure and the ease of integration of other subcomponents. Wing ribs were laser-cut out of 1/8-in plywood, 1/4-in plywood, and 1/8-in balsa based on the strength required for each rib, keeping balsa grains in the chordwise direction. The ribs were epoxied to a commercially purchased carbon fiber reinforced polymer (CFRP) tube after being aligned with a jig that set each rib in twist angle and spanwise location, shown in Fig. 45.



Figure 45. Ribs in jig adhered to spar (left), and wing structure after stringer attachment (right)

The winglets, ailerons, and flaps were cut out of 3 lb/ft³ (48 kg/m³) polystyrene foam. The foam was then reinforced with a fiberglass (FG) and epoxy composite, vacuum-bagged, and cured in mylar-film casing. The winglets were epoxied to the polylactic acid (PLA) winglet adapters. Wing aft spars were laser-cut from 1/8-in plywood attached to the ribs with CA glue. The slotted flap vein plate was laser-cut out of 1/16-in balsa, steamed, pressed to shape, and dried to create the curve for the vein. 1/8-in square stringers were set in pre-cut recesses in the ribs, which provided surfaces for the Solarfilm Lite (Solite) aft skin, a heat shrink plastic wrap, to adhere to the wing assembly. 3 lb/ft³ (48 kg/m³) foam female molds were cut for each carbon-fiber leading edge using a hotwire tool. Molds were prepared by adding a layer of mylar to ensure a smooth surface. The leading-edge skins were manufactured by performing wet layups with a single ply of 6.10 oz/yd² (207 g/m²) twill weave carbon-fiber at a +45°/-45° orientation to the spanwise direction. They

were then vacuum-bagged with a layer of peel-ply on the exposed face for 12 hours. Once the layup was complete, skins were cut to size with holes for the motor mount and epoxied to the ribs.



Figure 46. Solite, CFRP skin, and motor mounts adhered to wing (left), FG reinforced foam flaps, ailerons, winglets (right)

6.2.2 MOTOR MOUNTS

A CFRP layup was selected for the motor mounts since composite fabric is ideal for the loading cases of the motor and can be streamlined to improve aerodynamics. The tube was manufactured using a wet layup on a 3D-printed PLA mandrel. One ply of 6.10 oz/yd² (207 g/m²) twill weave carbon fiber was wrapped twice around the mandrel, which was destructively removed with pliers after curing. The front and aft plates, which connect the motor, CFRP tube, and wing, were laser-cut from plywood and epoxied to the tube.

6.2.3 EMPENNAGE

A balsa built-up structure was selected for the empennage to minimize weight. The tail structural components, including 1/8-in balsa ribs, 1/4-in balsa spars, 1/16-in plywood rib reinforcements, and 1/32-in balsa skin, were manufactured and assembled in a similar process as outlined in Section 6.2.1. The balsa leading edge was steamed, molded to shape, and allowed to dry, as shown in Fig. 47. The balsa skins were then adhered to the rib structure with CA glue. The complete skin was covered with Solite to create a smooth finish.



Figure 47. Steamed balsa sheet formed in mold

6.2.4 FUSELAGE

A built-up structure with balsa and plywood components was selected for the fuselage. It was constructed around a plywood jig, as shown in Fig. 48, to hold the formers during assembly. Structural formers were preassembled with reinforcements and hardpoints. The formers were epoxied together with four spruce-balsa longerons, which were steam-bent to shape before attachment to reduce fracture and stresses within the adhesives. Payload, parking, wiring, and Crew system components were placed, and the truss structure was added once free access to the aircraft interior was no longer required. The tail boom was placed and adhered to the aft three formers. Balsa shapers with stringer cutouts were then adhered to the core structure to create the desired fuselage geometry. Lastly, stringers were added, and the entire structure was covered in Solite film. The Crew and Passenger hatches were assembled separately and hinged last.



Figure 48. Fuselage jig with formers before longeron attachment

6.2.5 LANDING GEAR

The main bow gear was manufactured using 26 plies of unidirectional fiberglass (FG) in a wet layup. Slow-curing epoxy resin was applied after each layer with a 2.4:1 FG-to-epoxy mass ratio, then sealed in a vacuum bag under pressure for 12 hours as seen in Fig. 49, with the final product in Fig. 33.



Figure 49. Bow gear manufacturing with fiberglass weight (left) and vacuum-bagged layup (right)

Holes were drilled through both bow gear tips to fit a 0.25 in (0.64 cm) axle to hold a 3.0 in (7.62 cm) wheel. The wheels and axles were secured in place using collars and set screws. The total weight of the bow was 0.22 lbm (0.1 kg). The FG gear was integrated into the aircraft via a hardpoint beneath the fuselage and sandwiched between 1/4-in plywood. This attachment method prevents unnecessary cracks in high load-bearing areas. The mechanism was fixed by nylon bolts designed to shear off during a landing over 2.5g to protect the fuselage from horizontal loads, seen in Fig. 50.

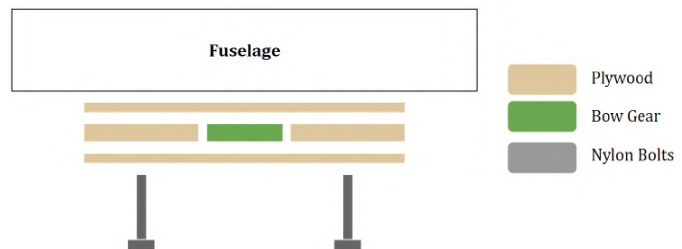


Figure 50. Securing mechanism for main gear

The nose gear wire diameter and angle were sized with an in-house Excel structures spreadsheet, Nose GearSizer. This component was manufactured with a 4.4 in (11.3 cm) long, 1/8-in diameter steel wire. It was attached to the fuselage at a 25° forward angle to match the bow gear height during 1g loading to facilitate payload un/loading. The nose gear was attached to the fuselage on a plywood hardpoint with two 1/8-in mounting saddle straps. A 1 in (2.54 cm) wheel with a foam tire was attached to the strut with collars as seen in Fig. 51.



Figure 51. Nose gear integration

6.2.6 PAYLOAD SYSTEM

The payload rail was constructed out of 3D-printed polylactic acid (PLA) sections and a sized plywood support as shown in Fig. 35 in Section 5.3.6.1. Testing demonstrated that the friction coefficients between the aluminum insert and PLA were lower compared to alternative materials. The 3D-printed PLA section

and the PLA contact areas were cut into sections due to usable volume limitations in the CR-10 3D printer [22]. To support the structural load, the plywood supports were made from a sandwich structure of laser-cut 1/4-in, 1/8-in, 1/16-in panels, and a thin layer of PLA contact area.

6.2.7 MEDICAL SUPPLY CABINET (MSC) AND EMT + GURNEY INSERT (M2)

The M2 MSC, as shown in Fig. 37 in Section 5.3.6.2, was constructed out of laser-cut 1/8-in plywood adhered with CA glue. Laser cutting was chosen to enable accurate manufacturing and tight component fit. Two 18-8 stainless-steel hex-head screws were used to connect the wooden enclosure to the custom waterjet-cut aluminum inserts. These screws were attached to the enclosure with a nylon-insert locknut epoxied on the inside of the wooden enclosure. The waterjet-cut aluminum inserts were sanded to smooth the rough surface created by the cutting process to reduce friction between them and the rail. The 304 stainless-steel bars that can be added to increase the Medical Supply Cabinet mass (m_{MSC}) were purchased in the desired dimensions of 1/2-in x 1/2-in x 6 in (1.3 cm x 1.3 cm x 15.2 cm).

The M2 insert was constructed to hold the two EMTs from their necks. The sandwich structure insert is made from 1/8-in plywood on top, 1/32-in multipurpose neoprene rubber sheet acting as a gasket in the middle, and 1/16-in plywood on the bottom. The plywood components were laser-cut, and the rubber sheet was cut by hand to size. The slits in the rubber that help retain the EMTs were cut with an X-Acto knife, and all three layers were adhered with CA glue. A cutout was made in the M2 insert to recess the 3D-printed PLA gurney and was attached with Velcro to the insert. The gurney was 3D-printed to fabricate a three-dimensional geometry to ensure the upper surface matched the shape of the Patient.

6.2.8 PASSENGER INSERTS (M3)

Like the M2 gurney insert, the M3 Passenger insert comprised of multiple materials: 1/8-in laser-cut plywood to ensure rigidity during the pressing down of inserts over the Passengers, a 1/32-in thick sheet of multipurpose neoprene rubber gasket, and a 1/16-in laser-cut plywood to hold the rubber sheet from the bottom. Like the M2 EMT and gurney insert, the rubber sheet and its slits for the Passengers were cut to size. These were attached using CA glue and rubber cutouts shaped as shown in Fig. 52. Nylon bolts were epoxied onto the insert and onto a custom water-jet aluminum square insert interfacing with the payload rail.



Figure 52. Top-down view of a cutout for EMTs or Passengers (left), and M2 Patient + EMT sandwich structure insert (right)

6.3 MANUFACTURING MILESTONES

A manufacturing milestone chart ensures the team remains on schedule and coordinates build between different sub-teams. Lessons from manufacturing scheduling for each prototype aircraft helped refine the schedule for the competition build. The timeline for full prototypes was three weeks, as can be seen in the full milestone chart in Fig. 3, which shows planned and actual timelines of each iteration. Construction and

assembly of the competition aircraft is expected to take five weeks to ensure the highest quality final aircraft. The competition aircraft schedule, seen in Fig. 53, was created to account for university-scheduled spring break (Week 2). It also includes additional days between scheduled goals to account for potential build delays, ensuring that planned and actual timelines converge.

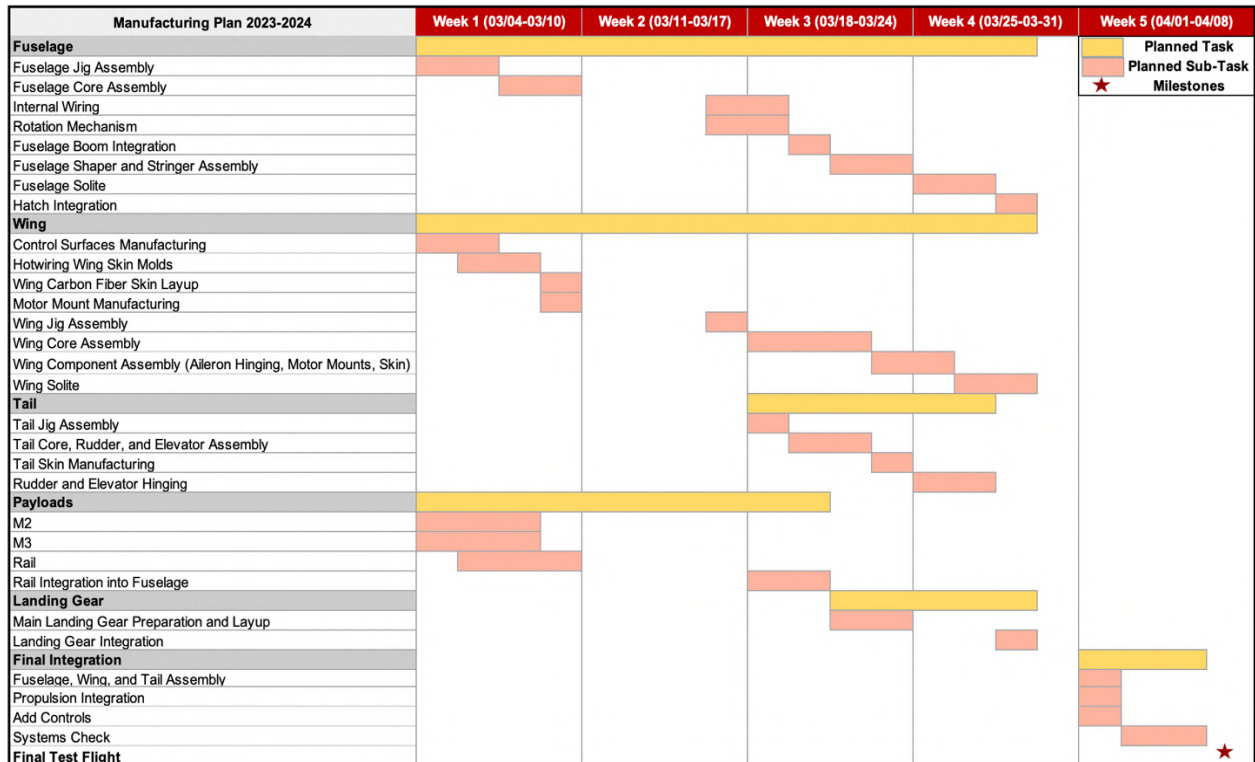


Figure 53. Manufacturing plan for the 2023-2024 competition aircraft

7.0 TESTING PLAN

A test plan verified propulsion, structures, payloads, and flight decisions. Experimental data was gathered by the team both in the laboratory and at test flights. Testing began during the preliminary design phase and continued into the subsequent phases to validate predictions and inform design decisions. The test schedule is presented in Figure 54 and detailed in Sections 7.1 – 7.4.

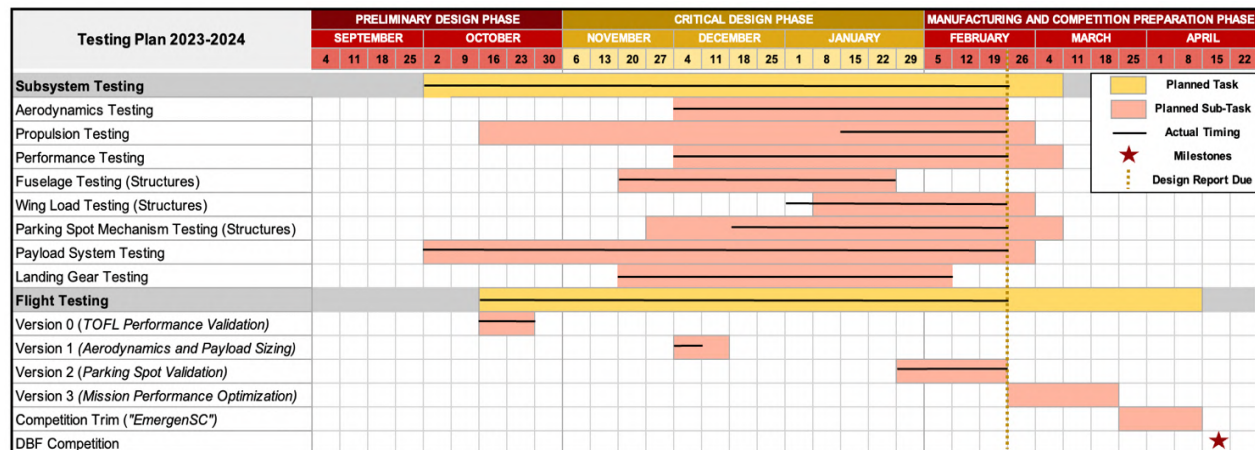


Figure 54. Testing plan for the 2023-2024 competition year

7.1 TEST OBJECTIVES

Sub-component tests were conducted to ensure the aircraft met all competition and design requirements.

Aerodynamics

- Flight tests confirmed XFLR5 and AVL predictions for lift, drag, and stability characteristics [6][7].
- Pilot feedback was used to verify acceptable aircraft stability and maneuverability characteristics.

Propulsion

- Lab testing was conducted using a battery tester to characterize battery capacities and aging.
- Static and dynamic tests were used to compare thrust, torque, and propeller wash to theoretical values.

Performance

- Flight tests were conducted to validate the performance parameters modeled in PlaneTools, including takeoff field length (TOFL), cruise speed (V_{cruise}), lap times, and endurance, discussed in Section 8.

Structures

- Bending tests identified a spar with sufficient stiffness and strength to sustain design loads.
- Motor mounts were tested at the expected thrust, torque, and weight from the motor.
- Fuselage drop-testing was conducted at the maximum expected sink rate and aircraft weight to confirm that the fuselage could withstand energy transferred from the bow gear during landing.
- The parking spot mechanism was prototyped to reduce Ground Mission (GM) time, t_{GM} . The aluminum pipe, which holds the wing and fuselage together, was tested to validate its strength.

Payloads

- The loading and unloading of mission-specific payload inserts were tested to estimate t_{GM} and the functionality of the payload system.
- Payloads were tested in-flight to determine whether Passengers touched during flight.

Landing Gear

- Drop tests with high-speed video were conducted to simulate a sink rate of 4.91 ft/s (1.50 m/s).
- Static load tests simulated a 3g landing load for the landing gear (LG).
- Ground handling tests ensured that the aircraft would track straight for takeoff and landing.

7.2 SUBSYSTEM TESTING

7.2.1 PROPULSION TESTING

Propulsion testing consisted of validating battery performance and theoretical thrust. Battery capacity and energy were examined using the West Mountain Radio Battery Tester. The tester applies a variable load to maintain a constant current and monitors the voltage battery [23]. Thrust testing was performed on the Tyto Robotics Series 1780 Dynamometer, as shown in Fig. 55. The test stand

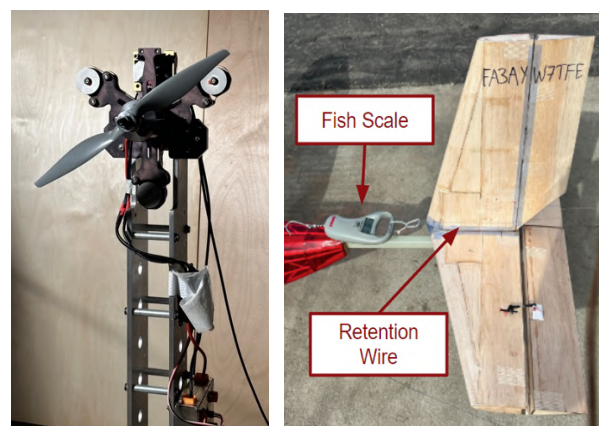


Figure 55. Static thrust test setup using thrust stand (left) and V2 aircraft (right)

is equipped with a load measurement unit for thrust and torque, along with a power module for voltage and current measurements from the electronic speed controller (ESC). The included, open-source RCbenchmark software displayed this data live and recorded measurements as a function of time. Static thrust testing was also conducted directly on the V2 aircraft using a fish scale rated for 25 lbf (111.21 N) of thrust. Redundancy in testing methods allowed for data validation and improvement opportunities to both setups. The results of all tests described above are outlined in Section 8.1.2.

7.2.2 LANDING GEAR (LG) TESTING

Drop, static load, and ground testing was conducted to ensure the LG performed as designed.

7.2.1.1 DYNAMIC DROP TESTING

To verify the LG could withstand the energy upon impact, drop testing was performed at maximum weight. The gear was raised to a height of 8.0 in (20.3 cm) to simulate a 4.91 ft/s (1.50 m/s) sink rate with a factor of safety (FoS) of 1.5, as pictured in Fig. 56. The gear showed no signs of failure.

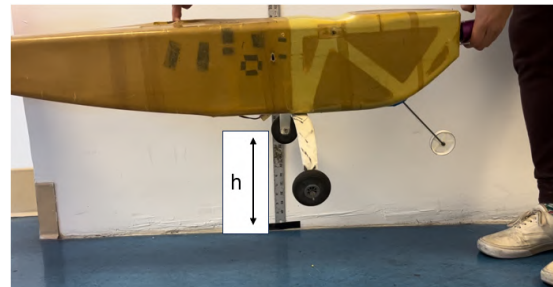


Figure 56. Dynamic drop testing of main fiberglass (FG) gear from an 8 in height

7.2.2.2 STATIC LOAD TESTING

Load tests of the main gear were performed to ensure the gear could withstand the maximum expected loads with an FoS of 1.5 and compare actual to predicted deflections. The bow gear was placed between two skateboards to allow for measurement of vertical deflection, shown in Fig. 57. The aircraft was first loaded to 1g with 11.7 lbm (5.3 kg), resulting in a vertical deflection of 0.5 in (1.3 cm), or 66% of the predicted value. The aircraft was then loaded to 3.2g at 37.4 lbm (17 kg), resulting in a deflection of 2.0 in (5.1 cm), or 71% of the predicted value. Since the gear handled more than the maximum expected load with less than expected deflection, the gear met the necessary loading requirements.



Figure 57. Bow gear load testing set-up

7.2.2.3 GROUND HANDLING TESTING

To ensure the aircraft would track straight, the prototype aircraft was rolled on the ground in all mission configurations. The aircraft did not tip backwards and tracked in a straight line for over 20 ft (6.1 m).

7.2.3 STRUCTURAL TESTING

Spar, motor mount, and drop testing ensured aircraft components could withstand expected loading.

7.2.3.1 SPAR TESTING

A carbon fiber reinforced polymer (CFRP), commercial off-the-shelf (COTS), tube was selected for the spar of *EmergenSC*. Testing was conducted on four RockWest Composites tubes to determine relevant properties used for selecting a final spar. Testing determined the strength and flexural rigidity (EI) of the purchased tubes. The test was performed modelling the tubes as cantilevered beams loaded at the tip, and measurements of deflection were taken.



Figure 58: Spar testing setup

EI was determined using Eq. 25, where y is the beam deflection, P is the load applied, l is the distance at which the load was applied, and x is the measurement location of the deflection. The deflection was measured for several loads and a linear fit determined the value of EI .

$$y = \frac{Px^2}{6EI}(3l - x) \quad \text{Eq. 25}$$

The required spar properties are compared to the experimental values of the selected tube in Table 29. The selected spar must withstand the maximum bending moment in the wing and prevent upward tip deflections of over 2.5 in (6.35 cm), both determined by loading in 6g turns. A 0.33 lbm (0.15 kg) with an inner diameter of 0.75 in (1.9 cm) and an outer diameter of 0.83 in (2.11 cm) tube was selected since it satisfies these criteria while minimizing weight.

Table 29. Properties of selected tube spar

	Allowable Range	Experimental Value
Bending Moment with 1.5 FoS [lb-ft]	> 68.5	71.9*
Flexural Rigidity [psi-in ⁴]	> 50,220	54,750
Tip Deflection in 6g turn [in]	< 2.5	2.3

*Not tested to failure

7.2.3.2 MOTOR MOUNT ASSEMBLY TESTING

A motor mount assembly was manufactured to confirm the design could withstand expected thrust, torque, and weight from the motor. The maximum expected thrust was 11 lbf (48.93 N) per motor, which was simulated by hanging weights below the testing adapter while mounted vertically, as shown in Fig. 59a. The maximum vertical load due to the weight of the motor was 4.44 lbf (19.75 N), which was simulated by securing the motor tube horizontally and hanging weights from the testing adapter as shown in Fig. 59b. The maximum expected torque from the propulsion package was 8.0 lbf-in (0.90 Nm) and was simulated

by hanging weights from the testing adapter at a set distance from the center of the motor mounting location as shown in Fig. 59c. An FoS of 2 was used for testing.

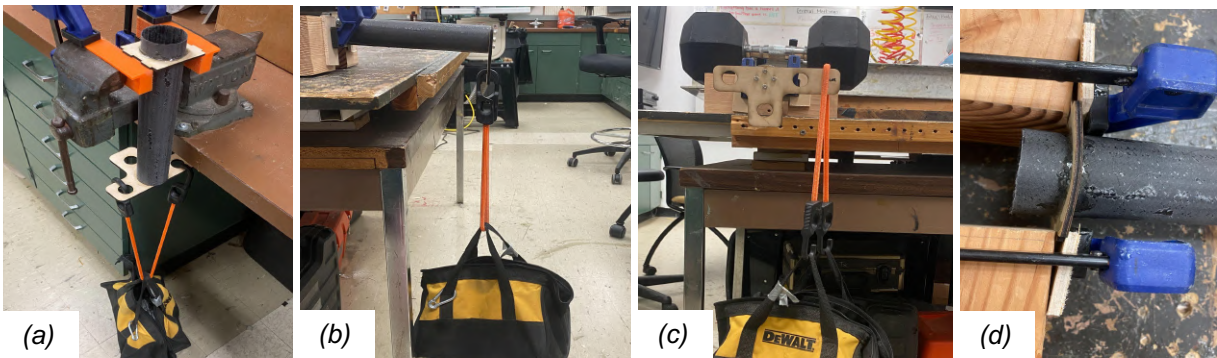


Figure 59. (a) Thrust, (b) motor weight, (c) torque tests and (d) plastic deformation of wing mounting plate

The designed motor tube assembly did not fail under tested loads. There was minimal deflection in the CFRP tube during all tests and no observed issues with the front plate onto which the motor bolts. However, the plate which mounts the CFRP tube to the ribs experienced substantial bending deflection in the weight and thrust test scenarios, seen in Fig. 59d. Because of this deformation, the thickness of the piece was switched from 1/8-in plywood to 1/4-in plywood for subsequent designs.

7.2.3.3 PARKING SPOT WING PIVOT MECHANISM TESTING

The wing rotation mechanism, described in Section 5.3.4, was verified by prototyping, component-level testing, and on the aircraft. Tensile testing was performed on the threaded pipe, nuts, and hardpoints. The test drove the selection of a lighter aluminum pipe over steel and validated the strength of the hardpoints embedded in the fuselage and wing. The assembly was tested to withstand the in a 6g turn at the maximum expected gross weight, excluding the wing and wing mounted components. With a 1.5 FoS, this value was 71 lbm (32 kg). The pipe, nuts, and hardpoints withstood this load when tested. The only observable deformation was in the fuselage hard point, which reversible when unloaded.



Figure 60.
Testing of aluminum pipe

The width of the fully assembled aircraft in the parking configuration was 29 in (74cm) which is under the 30 in (76 cm) rule requirement with some additional leeway. The aircraft could be quickly transferred from parking to flight configuration and flight to parking configuration with consistency.



Figure 61. V2 aircraft in parking configuration

7.2.3.4 FUSELAGE DROP TESTING

After the LG strength and design were validated, the LG was mounted to Version 2 (V2) of the aircraft to confirm that the fuselage could absorb residual energy as designed. This test was also performed at maximum weight and a height of 8.0 in (20.3 cm) to simulate the maximum sink rate with a 1.5 FoS. The test was successful, and no damage was observed in the fuselage or other parts of the aircraft. The fuselage also did not display any tipping tendencies with the designed center of gravity placement.



Figure 62. V2 fuselage drop testing from height of 8 in (20.3 cm)

7.2.4 PAYLOAD TESTING

Testing of the loading and unloading times of mission-specific payloads allowed for a better estimate of the Ground Mission (GM) time, t_{GM} . Testing was conducted on the V2 fuselage in a flight-ready configuration by a single team-member to simulate a competition GM. Both missions are divided into three main tasks: payload loading, payload unloading, and other miscellaneous tasks. Loading consisted of placing the payload (Patient, gurney, EMTs, or Passengers) into the inserts and sliding the inserts onto the payload rail in the fuselage. Unloading involved removing the inserts from the rail inside the fuselage. Finally, miscellaneous times such as inserting/removing the payload restraining pins and opening/closing the payloads hatch were taken. Each task was performed four times with each segment being conducted independently to allow breakdown of t_{GM} into segments.

As shown in Table 30, the average t_{GM} for the payload section was 86.7 s. The results indicate that unloading for both missions seemed to be consistent at approximately 10 s (approximately 5 s per insert). M2 loading times took longer than M3 loading times, with approximately 44% of the entire payload time being the M2 loading time. Inserting the M2 gurney onto the insert and restraining the Patient onto the gurney proved difficult, since the bands that were designed to restrain the Patient interfered with the placing of the gurney on the insert. Times to insert and remove the payload restraining pins were slow as well, as the pins did not align in the rail when inserted. From these results, changes in future iterations include better positioning of the Patient restraint bands on the inserts and improving access to the pins in the fuselage. Table 30 shows the best times recorded for each segment. Total best time describes the best possible loading time for the current payload design.

Table 30. Payload loading time practice

	M2		M3		Misc	Total Best
	Loading	Unloading	Loading	Unloading	Hatch, Pins	
Avg. [s]	38.0	10.1	16.9	9.1	12.7	86.7
Best [s]	37.0	9.1	15.0	7.9	11.3	80.3

7.3 FLIGHT TEST SCHEDULE AND FLIGHT PLAN

Flight tests play a critical role in validating the aircraft design. Aircraft performance data was collected with an integrated sensor package used to measure airspeed, ground speed, altitude, position, g-loading, and heading of the aircraft. Propulsion performance data such as voltage, current, RPM, throttle, and electronic speed controller (ESC)

temperature was collected using data-logging features built into the KDE ESCs. Two cameras, one mounted on the fuselage aft of the wing facing the empennage and another mounted on the tail facing the front of the aircraft, allowed for visual identification of possible modes of flight failure. Pilot feedback for stability and flight performance validation with various throttle settings, control inputs, and payload fractions.

Additionally, pilot feedback was crucial to determining the aircraft response with slotted flaps deployed at high/low throttle settings for takeoff/landing.

Table 31 outlines the flight test schedule and objectives. Incremental validation of aircraft attributes occurred with each flight test. For each prototype, flight testing was conducted weekly until hardware failure.

Each flight test contains multiple flights, each with their own set of unique objectives. A representative flight test plan is shown in Table 32 from a flight test on February 9, 2024.

Table 31. Flight Test Schedule

Date	Location	Aircraft	Objectives
Oct. 18-23, 2023	Whittier Narrows, South El Monte, CA	V0	Validate takeoff field length (TOFL) and test manufacturability over a period of two weeks.
Dec. 5, 2023	Whittier Narrows, South El Monte, CA	V1	Evaluate slotted flaps, winglets, modified wing aspect ratio, and test dual-motor propulsion and blown lift effect on takeoff
Feb. 3-24, 2024	Whittier Narrows, South El Monte, CA	V2	Validate flight performance with rotating wing configuration for parking spot fit.
Mar. 2-23, 2024*	Whittier Narrows, South El Monte, CA	V3	Validate M1, M2, and M3 performance in final configuration.
Mar. 30 – Apr. 13, 2024*	Whittier Narrows, South El Monte, CA	<i>EmergenSC</i>	Test performance of competition aircraft.

*Tests are tentatively scheduled for listed dates.

Table 32. February 9, 2024 test flight plan

Flight	Type	Objectives	Purpose
1	Trim Flight (6S)	1st Lap: Trim 2nd Lap: Trim (as necessary), cruise data 3rd Lap: Glide to low approach (landing gear flaps deployed) 4th Lap: Landing (balked if necessary) 5th Lap: Landing (if balked landing on 4th lap)	Trim Landing practice Glide and cruise data for aerodynamic analysis
2	Trim Flight (8S)	1st Lap: Cruise 2nd & 3rd Lap: 360° turn and glide to low approach (flaps up) 4th Lap: Landing (balked if necessary) 5th Lap: Landing (if balked landing on 4th lap)	Landing practice Glide and cruise data for aerodynamic analysis Turning performance
3	Mission 1 Simulation	1st, 2nd, & 3rd Lap: 360° turn and glide to low approach (flaps up) 4th Lap: slow flight 5th Lap: Landing	Flight mission data (e.g. battery usage, etc.) C _{L,max} estimation
4	TOFL Validation	Takeoff and land for TOFL testing	TOFL data
5	Mission 3 Simulation	Simulate Mission 3 with payload	Flight mission data (e.g. battery usage, etc.) Aircraft handling with payload

7.4 FLIGHT CHECKLISTS

The team adhered to the flight checklists, shown in Table 33, before and during each flight test to ensure team safety, efficiency, and proper data acquisition. These checklists were designed to facilitate a streamlined testing procedure and are intended for use before each flight test and competition. All elements of the flight checklists are performed by the Flight Test Lead, Chief Pilot, and Crew Chief.

Table 33. Flight Checklists

PREFLIGHT	BEFORE TAKEOFF
Aircraft Assembly	Pilot Go/No-Go Pass Wind and Runway Direction Verify/Select Transmitter Verify Charge Throttle Cut On Avionics On Controls Free and Correct Flaps Takeoff Detent Flight Data Recording Throttle Idle Arming Plug Armed Throttle Cut Off Propulsion Run-up Complete Transmitter Data Logging On Video Start Runway Clear Sky Clear Takeoff Intentions Announce Flight Timer Start
Airframe Damage Free Wings Secure Flaps Check Ailerons Check Empennage Secure Elevators Check Rudder Check Landing Gear Secure Servos and Linkages Secure Motors Check Propellor Secure Runcams (if applicable) Secure	
Aircraft Interior	BEFORE LANDING
Crew Secure Mission Payload Secure Payload Hatches Secure	
Avionics	Runway Clear Landing Intentions Announce Flaps Landing Detent
Avionics Battery Verify Charge Propulsion Battery Verify Charge Receiver Secure Receiver Plugs Secure Avionics Battery Secure Propulsion Battery Secure Avionics Hatch Closed Transmitter On Avionics On Controls Trimmed and Centered Failsafe Check Range Check Avionics Off	AFTER LANDING
Final Exterior	Throttle Cut On Flight Timer Stop Arming Plug Disarmed Avionics Off Propulsion Battery Unplugged Avionics Battery Unplugged Transmitter Data Logging Off Video Off Runway Clear
	POSTFLIGHT
Center of Gravity Check Aircraft Weight Check Landing Gear Roll Check Final Walkaround Complete	Aircraft Walkaround Complete Avionics Battery Verify Charge Propulsion Battery Verify Charge Debrief Complete

8.0 PERFORMANCE RESULTS

The following section discusses the results from all ground and flight tests described in the testing plan.

8.1 DEMONSTRATED PERFORMANCE OF KEY SUBSYSTEMS

8.1.1 AERODYNAMICS

Validation of aerodynamic performance was critical during initial test flights. The payload weight was gradually increased up to maximum design capacity to gather takeoff field length (TOFL) data. Handling characteristics and airspeed were observed in cruise, as shown in Table 34.

Table 34. Flight Speed per Flight Segment

Flight Segment	Airspeed		
	Version 0 (V0)	Version 1 (V1)	Version 2 (V2)
Straightaway	77 mph (34 m/s)	72 mph (32 m/s)	67 mph (30 m/s)
180° turn	55 mph (25 m/s)	51 mph (28 m/s)	46 mph (21 m/s)
360° turn	36 mph (16 m/s)	48 mph (21 m/s)	44 mph (20 m/s)

8.1.2 PROPULSION

Battery testing aimed to quantify performance and the impact of aging. Two 6S Thunder Power RC batteries were studied, one newly purchased and the other stressed beyond its maximum C-rate and stored at a non-optimum voltage. Both batteries were drained at 4.7C, the results of which are seen in Fig. 63.

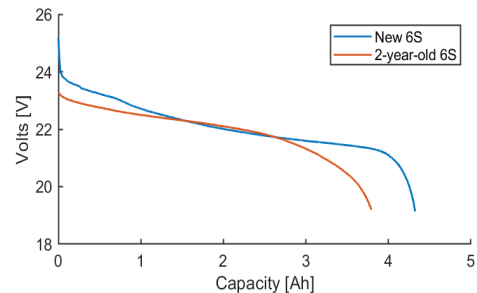


Figure 63. 6S New vs Used Battery Testing

The new battery exhibited 98% of its capacity, while the old battery only reached 85%. These results indicate the importance of using newer batteries for optimal performance to avoid an energy penalty due to age.

Prop wash data was collected during static testing of the M2 propulsion package, as shown in Fig. 64. The propeller wash ranged from 30-50 ft/s above 50% throttle, which coupled with the slotted flap design, proved beneficial in meeting TOFL.

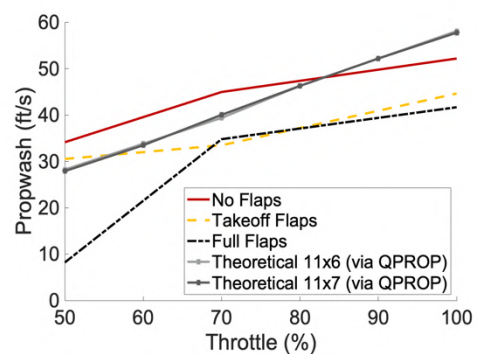


Figure 64. Prop wash data from thrust testing with 11x7 in propellers and 8S battery

Static thrust testing was conducted on the V2 aircraft to validate the thrust model generated by eCalc and QPROP, shown in Fig. 65. QPROP is a software created by Dr. Mark Drela that uses an extended blade element theory formulation to analyze the performance of motor-propeller combinations [24]. Comparing static testing to QPROP and eCalc show the measured thrust was 20% higher than theoretical.

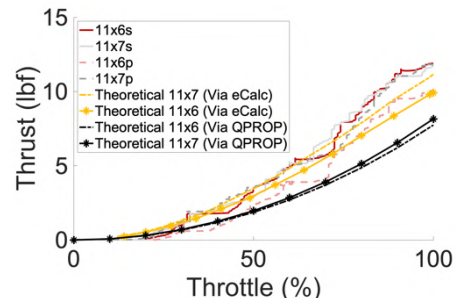


Figure 65. Static Thrust data from varying propellers and 8S 3300 mAh battery

Torque was also investigated for structural sizing of the motor mounts, as shown in Fig. 66, and was calculated by Eq. 26.

$$CQ = \frac{Q}{\rho n^2 D^5} \quad \text{Eq. 26}$$

Q is torque, ρ is air density, n is rotations per second, and D is propeller diameter. An average CQ of 0.01 was found. Although a maximum torque of 4.97 ft-lb (6.7 Nm) was recorded, the propellers counterrotate in the dual motor configuration, negating torque entirely.

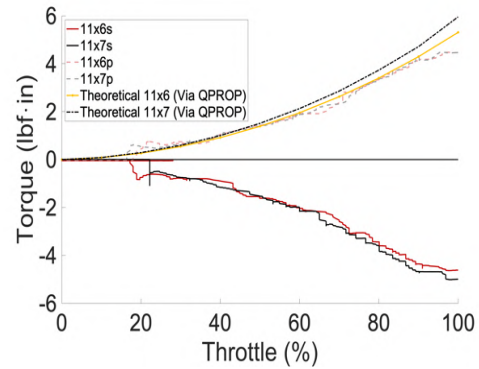


Figure 66. Torque from static thrust testing at a given throttle

8.2 DEMONSTRATED FLIGHT PERFORMANCE OF COMPLETED AIRCRAFT

The first three aircraft prototypes built by the team served as platforms to test and compare primary configuration methods to guide final aircraft design. The first prototype, V0, was configured with a single-motor boom-fuselage with no payloads and served to analyze initial wing and tail sizing. V0 was tested for TOFL performance at several weight increments, with a maximum weight of 14.1 lbm (6.4 kg), representative of a competition aircraft with the target Mission 2 (M2) payload. The second prototype, V1, was a dual-motor aircraft with a fuselage sized to carry 35 Passengers and a 3.1 lbm (1.4 kg) M2 cabinet. V1 validated fuselage design and construction methods and served as a platform to study blown lift effects on TOFL from the wing-mounted dual-motor propulsion package. The third iteration, V2, was the most recent iteration produced and tested at the time of writing. V2 implemented the rotating wing configuration for parking spot validation. Prototypes V0, V1, and V2 are presented in Fig. 67.



Figure 67. From left to right: isometric photos of V0, V1, and V2 at various flight tests.

Table 35 shows the results of the V0 test flights. The V0 prototype validated the selection of the high-thickness airfoil previously mentioned and a low aspect ratio wing as the aircraft was able to meet the TOFL constraint with 1.5 lbm (0.7 kg) of added weight, as shown in Table 36. The significant variation in TOFL performance in calm wind conditions was attributed to inconsistent piloting technique and demonstrated the importance of pilot practice.

Table 35. V0 Flight Test Performance

Flight	Weight	Headwind	Throttle (%)	TOFL	Laps	Observations/Outcomes	
1	12.40 lbm (5.63 kg)	8.5 ft/s (2.6 m/s)	50	20 ft (6.1 m)	6	Slow throttle ramp using a 6S battery, responsive handling	
2	12.40 lbm (5.63 kg)	Calm	75	12 ft (3.7 m)	1	Pilot intentionally used slower throttle ramp.	
3			75	18 ft (5.5 m)		Tailstrike during takeoff, longer takeoff roll due to pilot input.	
4			100	12 ft (3.7 m)		No flaps used during takeoff.	
5			100	8 ft (2.4 m)			
6	13.19 lbm (5.98 kg)		75	12 ft (3.7 m)		Pilot gained experience with aircraft short TOFL handling. P-factor during climb out was controllable. Rotation timing was practiced to prevent tail strikes. Variation in TOFL demonstrates sensitivity to pilot input.	
7			100	13 ft (4.0 m)			
8			100	15 ft (4.6 m)			
9			100	16 ft (4.9 m)			
10	13.89 lbm (6.30 kg)		75	16 ft (4.9 m)			Landing gear sheared during landing.
11	12.40 lbm (5.63 kg)		75	25 ft (7.6 m)			2
12			100	15 ft (4.6 m)	1		
13	13.89 lbm (6.30 kg)		100	25 ft (7.6 m)	2		Longer TOFL attributed to early rotation and tail strike. Stall test performed in landing configuration showed positive stall recovery.
14			100	16 ft (4.9 m)	5		Receiver lost connection, loss of aircraft.

However, due to the absence of a fuselage, V0 could not validate cruise performance of the competition aircraft due to parasite drag from exposed electronics and

Table 36. V0 predicted vs. flight performance characteristics

Parameter	Predicted	Actual	Error [%]
Empty Weight	13 lbm (6.0 kg)	12 lbm (5.6 kg)	-6.72
TOFL (no ballast)	14 ft (4.5 m)	15 ft (4.6 m)	6.14
TOFL (1.8 lb ballast)	18 ft (5.6 m)	19 ft (5.8 m)	3.80

landing gear. Following V0 testing, the team began manufacturing and testing V1. However, due to a build process error, the wing size was unintentionally undersized. As such, during testing, the team was not expecting to meet the TOFL requirement that would be expected of a correctly sized wing, and thus was more interested in testing cruise performance, shown in Tables 37 and 38.

Table 37. V1 Flight Test Performance

Flight	Weight	Wind	Throttle Ramp*	TOFL	Laps	Observations/Outcomes
1	15.11 lbm (6.85 kg)	Calm	3.7 s	100 ft (30 m)	4	Flaps partially retracted during takeoff roll and flight due to blown lift and dynamic pressure. Long TOFL due to intentionally slow throttle ramp.
2			2.5 s	50 ft (15 m)	6	Slow response in pitch, poor 360° turning.
3			1.7 s	30 ft (9 m)	3	Improved pitch control with lower static margin, aircraft lost pitch control due to an elevator servo malfunction, resulting in a crash.

*Idle to full throttle time recorded by the transmitter

The pilot reported overall control sluggishness, and poor TOFL performance was observed. A review of onboard footage showed that both flaps retracted as soon as the motors were throttled up, likely due to the propeller wash of the wing-mounted

Table 38. V1 predicted vs. flight performance characteristics

Parameter	Predicted	Actual	Error [%]
Empty Weight	13.23 lbm (6.00 kg)	15.19 lbm (6.92 kg)	15
TOFL	15 ft (5 m)	30 ft (9 m)	100
Lap Time	25 s	38 s	48
Max Load Factor	-	4.92	-
Flight Endurance	300 s	260 s	-13

motors. During Flight 3, elevator control was lost, resulting in aircraft loss. Post-flight analysis found that receiver connection wasn't lost and control surfaces remained powered. The probable cause was attributed to undersized servos on both flaps and elevator. All control surface servo torque ratings were increased for further versions to account for increased propeller wash. Furthermore, the aircraft flew slower in cruise than predicted, seen in Table 38. This was partially due to increased drag from the large gap between the retracted slotted flap and the wing during cruise, so flap geometry was adjusted to minimize this gap in future prototypes.

While V1 did not meet TOFL predictions and experienced significant control problems, flight test results showed promise for a dual-motor blown-lift configuration. V2 was test flown for all mission profiles to analyze performance with integrated payloads. Results are in Tables 39 and 40, and V2 is shown in Fig. 68.

Table 39. V2 Flight Test Performance

Flight	Weight	Headwind	Throttle Ramp*	TOFL	Laps	Observations/Outcomes
1	12.42 lbm (5.65 kg)	2 mph (1 m/s)	6 s	45 ft (14 m)	5	Throttle ramp was intentionally slow to determine pilot handling on takeoff.
2	12.42 lbm (5.65 kg)	3 mph (1 m/s)	0 s	11 ft (3 m)	4	No major wing bending or skin rippling. No structural damage to aircraft during flight.
3	14.00 lbm (6.32 kg)	1 mph (0.5 m/s)	1 s	14 ft (4 m)	1	Loaded 18 Passengers and achieved TOFL. Passenger loading changes static margin by 2%.
4	15.6 lbm (7.1 kg)	0.4 mph (0.2 m/s)	1 s	19 ft (6 m)	4	Glide testing demonstrated a fast sink rate of 4 m/s when throttle was cut. M2 payload was loaded, and placement had flexibility for CG adjustment to attain desired static margin.

*Idle to full throttle time recorded by the transmitter

Table 40. V2 predicted vs. flight performance characteristics

Parameter	Predicted	Actual	Error [%]
Empty Weight	14.0 lbm (6.4 kg)	15.4 lbm (7.0 kg)	9.1
TOFL	15.5 ft (4.7 m)	11 ft (3 m)	3.3
ROC	-	28 ft/s (8.5 m/s)	-
Max Load Factor	-	5.2	-
Cruise Airspeed	75 mph	62 mph	17



Figure 68. Completed V2 aircraft

V2 was designed to validate the pivoting-wing configuration and M2 payload. The V2 servos withstood the force generated by blown lift over the wings and maintained the desired deflection throughout takeoff and cruise. With functioning flaps, the aircraft was able to takeoff in 11 ft (3.35 m) without payload, and 19 ft (5.79 m) in an M2 configuration. This prototype was lost due to a loss of receiver connection attributed to the fact that the carbon-fiber D-box of the wing was positioned between the receiver and the transmitter at approximately 700 ft (213 m), causing a receiver signal strength critical warning and a loss of transmitter connection. For future iterations, telemetry configuration will be improved to prevent loss of signal during flight.

9.0 BIBLIOGRAPHY

- [1] AIAA, "2023-2024 DBF Rules," Reston, VA, 2023.
- [2] USC AeroDesign Team, "Aircraft Design Report, 2023 AIAA DBF Competition," 2023.
- [3] "Matlab," Mathworks. [Online]. Available: <https://www.mathworks.com/products/matlab.html>.
- [4] Gudmundsson, S., *General Aviation Aircraft Design: Applied Methods and procedures*, Oxford: Butterworth-Heinemann, 2022
- [5] D. Raymer, in *Aircraft Design: A Conceptual Approach*, Reston, Virginia, AIAA, 1999.
- [6] "XFLR5," 2019. [Online]. Available: <http://www.xflr5.tech/xflr5.html>.
- [7] M. Drela and H. Youngren, "AVL," 2017. [Online]. Available: <https://web.mit.edu/drela/Public/web/avl/>.
- [8] M. Drela, "XFOIL," MIT, 2013. [Online]. Available: <http://web.mit.edu/drela/Public/web/xfoil>.
- [9] Python. [Online]. Available: <https://www.python.org/>
- [10] B. Rawdon, "Plane Geometry",
https://envisiondesignusa.com/evdusa/Plane_Geometry_Overview.html
- [11] MIL-F-8785C, *Flying Qualities of Piloted Planes, Military Specification*, 1980.
- [12] J. B. Brandt, R. W. Deters, G. K. Ananda, D. Dantsker, M. S. Selig, "UIUC Propeller Data Site," University of Illinois at Urbana-Champaign, Department of Aerospace Engineering. [Online]. Available: <https://m-selig.ae.illinois.edu/props/propDB.html>.
- [13] C. Zhang, J. Jiang, L. Zhang, S. Liu, L. Wang, P. C. Loh, "A Generalized SOC-OCV Model for Lithium-Ion Batteries and the SOC Estimation for LNMCO Battery," *Energies*, 2016. Available: <https://doi.org/10.3390/en9110900>.
- [14] "Wichita, KS," Weather Underground, The Weather Company. [Online]. Available: <https://www.wunderground.com/history/daily/us/ks/wichita>.
- [15] M. Müller, "eCalc," [Online]. Available: <https://www.eCalc.ch/>.
- [16] "Whats the difference between Nickel Cadmium (Nicaid), Nickel-metal hydride (NiMH), and Lithium Ion (Li-Ion)," Battery Universe. [Online]. Available: <https://www.batteryuniverse.com/help/battery-chemistries>
- [17] B. Rawdon, *Wing Upwash Calculator*, 2024.
- [18] B. Rawdon, *Landing Gear Design*, 2009.
- [19] M. H. Sadraey, *Aircraft Design: A Systems Engineering Approach*, Chichester, U.K., 2013.
- [20] Dassault Systems, "Solidworks," [Online]. Available: <http://www.solidworks.com/>.
- [21] W. A. Keyser, *Steam Bending: Heat and moisture plasticize wood in Fine woodworking on Bending Wood*. Taunton Press. pp. 2–119.
- [22] "Creality CR Series," [Online]. Available: <https://www.creality.com/pages/products?collection=CR+Series>.
- [23] West Mountain Radio, "CBA IV - Computerized Battery Analyzer," 2017. [Online]. Available: http://www.westmountainradio.com/product_info.php?products_id=cba4.
- [24] Drela, Dr. M., "QPROP," *QPROP Propeller/Windmill Analysis and Design*, Mar. 2007

AIAA 33F 2023/24

ADRIA



EDVARD RUSJAN TEAM

UNIVERSITY OF LJUBLJANA

Contents

1	Executive Summary	1
2	Management Summary	2
2.1	Team Organization	2
2.2	Milestone Chart	3
3	Conceptual Design	4
3.1	Mission Requirements and Scoring	4
3.1.1	Mission Flight Rules	5
3.1.2	Mission 1: Delivery Flight	5
3.1.3	Mission 2: Medical Transport Flight	5
3.1.4	Mission 3: Urban Taxi Flight	6
3.1.5	Ground Mission: Configuration Demonstration	6
3.2	Aircraft Constraints	6
3.3	Sensitivity Study of Design Parameters	7
3.4	Design Selection Process	9
3.4.1	Wing Placement	10
3.4.2	Parking Mechanism	10
3.4.3	Empennage and Landing Gear Design	11
3.4.4	Passenger accomodation	12
3.5	Final Conceptual Design	12
4	Preliminary Design	13
4.1	Design and Analysis Methodology	13
4.2	Mission Model	14
4.2.1	Flight Model	14
4.3	Design Trade Studies	15
4.3.1	Medical Cabinet Weight	15
4.3.2	Number of Passengers	16
4.3.3	Propulsion	16
4.3.4	Wing Area and Aspect Ratio	17
4.3.5	Takeoff Requirements	18
4.4	Optimal Aircraft Parameters and Total Mission Score	18
4.5	Aerodynamic Characteristics	19
4.5.1	Wing Airfoil Analysis	19
4.5.2	Wing Analysis	20



4.5.3	Tail Analysis	21
4.5.4	Airplane Fuselage Analysis	22
4.5.5	Lift And Drag Analysis	23
4.6	Dynamic stability	24
4.7	Estimated Mission Performance	25
5	Detail design	26
5.1	Dimensional parameters	26
5.2	Systems and Sub-Systems Integration	27
5.2.1	Fuselage	27
5.2.2	Empennage	28
5.2.3	Wing	29
5.2.4	Parking Mechanism	29
5.2.5	Passenger Compartment	30
5.2.6	Landing gear	31
5.2.7	Propulsion	31
5.2.8	Avionics	31
5.2.9	Structural Characteristics	32
5.2.10	Wight and Balance	34
5.2.11	Flight and Mission Performance	34
5.2.12	Drawing package	35
6	Manufacturing	40
6.1	Manufacturing Milestones	40
6.2	Manufacturing Processes Investigated	40
6.2.1	CNC Milling	40
6.2.2	Composite Material Construction	40
6.2.3	Foam Core Modeling	41
6.2.4	Balsa and Plywood	41
6.2.5	Additive Manufacturing	41
6.2.6	Forged Carbon Fiber	41
6.3	Selection Process	41
6.4	Composite Manufacturing of Fuselage, Empennage and Wings	43
6.4.1	Preparation of Molds for Wet Lamination	43
6.4.2	Composite Manufacturing of Fuselage	43
6.4.3	Composite Manufacturing of Wings, Fowler flaps and Empennage	43
6.5	Composite Manufacturing of Floor Inserts and Landing Gear	44



6.5.1	Composite Manufacturing of Landing gear	44
6.5.2	Composite Manufacturing of Floor Inserts	45
7	Testing Plan	45
7.1	Proof of Concept Testing	46
7.2	Propulsion Testing	46
7.3	Aerodynamics Testing	47
7.4	Ground Mission Testing	47
7.5	Flight Testing	48
7.6	Checklists	48
7.6.1	Propulsion and Aerodynamics Test Checklist	48
7.6.2	Flight checklist	48
8	Performance Results	49
8.1	Proof of Concept	49
8.2	Propulsion	50
8.3	Aerodynamics	50
8.4	Ground Mission Test	51
8.5	Test Flights	51
9	References	52



Acronyms and Nomenclature

α	-	Angle of Attack	D	-	Drag Force
β	-	Sideslip Angle	DBF	-	Design Build Fly
η	-	Efficiency	DoE	-	Design of Experiments
μ	-	Friction Coefficient	d	-	Diameter
φ	-	Thrust Angle	E_{cell}	-	Energy of Cell
ϕ	-	Speed Angle	$E_{required}$	-	Energy Required
$\dot{\phi}$	-	Derivative of Speed Angle	ESC	-	Electronic Speed Control
$\ddot{\phi}$	-	Second Derivative of Speed Angle	FEA	-	Finite Element Analysis
ρ	-	Air Density	FEM	-	Finite Element Method
ρ_{wing}	-	Wing Area Density	FF	-	Form Factor
A	-	Surface Area	FoM	-	Figure of Merits
AoA	-	Angle of Attack	GM	-	Ground Mission
AIAA	-	American Institute of Aeronautics and Astronautics	g	-	Gravitational Acceleration
APC	-	APC Propeller Company	J	-	Mass Moment of Inertia
AR	-	Wing Aspect Ratio	K	-	Turn Damping Factor
AVL	-	Athena Vortex Lattice	k_{m1}	-	Constant for Weight Calculation 1
A_{wing}	-	Wing Surface Area	k_{m2}	-	Constant for Weight Calculation 2
b	-	Wing Span	l	-	Fuselage Length
C_{Df}	-	Drag Coefficient of the Fuselage	L	-	Lift Force
C_d	-	Drag Coefficient	L'	-	Plane Lift Component
C_f	-	Flat Plate Coefficient	L_a	-	Antenna length in Mission 3
C_L	-	Lift Coefficient	L/D_{cruise}	-	Lift to Drag Ratio at Cruise Speed
$C_{d_{cruise}}$	-	Cruise Drag Coefficient	LiPo	-	Lithium Polymer
$C_{l_{cruise}}$	-	Cruise Lift Coefficient	L_H	-	Distance from Tail Aerodynamic Center
$C_{l_{max}}$	-	Max Lift Coefficient	L_K	-	Loading Efficiency Factor
cs_1	-	Form Factor Equation Coefficient 1	L_V	-	Distance from Rudder Aerodynamic Center
cs_2	-	Form Factor Equation Coefficient 2	M'	-	In Plane Component of Pitching Moment
cs_3	-	Form Factor Equation Coefficient 3	M1	-	Flight Mission 1
CAD	-	Computer Aided Design	M2	-	Flight Mission 2
CAM	-	Computer Aided Manufacturing	M3	-	Flight Mission 3
CFD	-	Computational Fluid Dynamics	MAC	-	Mean Aerodynamic Chord
CG	-	Center of Gravity	MTOW	-	Maximum Takeoff Weight
CNC	-	Computer Numerical Control	m	-	Mass
			NiCd	-	Nickel Cadmium
			NiMh	-	Nickel Metal Hydride



N_L	-	Number of Laps in Mission 2	v_{cruise}	-	Cruise Speed
N_P	-	Passenger Capacity	v_{stall}	-	Stall Speed
P	-	Electric Power Input	$V_{fuselage}$	-	Fuselage Volume
PLA	-	Polylactic Acid	V_{tail}	-	Tail Volume
PTFE	-	Polytetrafluoroethylene	$Vk_{antenna}$	-	Antenna Volume Coefficient
PU	-	Polyurethane	Vk_{safety}	-	Volume Safety Coefficient
PVA	-	Polyvinyl Alcohol	V_{TO}	-	Takeoff Speed
P	-	Power of Motor	w	-	Fuselage Corner Radius
QFD	-	Quality Function Deployment	$W_{aircraft}$	-	Weight of Aircraft
RPM	-	Revolutions Per Minute	W_{base}	-	Weight of Base
Re	-	Reynolds Number	$W_{battery\ pack}$	-	Weight of Battery Pack
r	-	Radius	W_C	-	Cabinet Weight
s	-	Straight Segment Length	W_{cell}	-	Weight of Cell
SAS	-	Score Analysis Simulation	$W_{fuselage}$	-	Weight of Fuselage
S_{ref}	-	Reference Surface	W_{motor}	-	Weight of Motor
S_{wet}	-	Wet Surface	W_{rudder}	-	Weight of Rudder
S_{TO}	-	Takeoff Distance	$W_{stabilizer}$	-	Weight of Stabilizer
STOL	-	Short Takeoff or Landing	W_{wing}	-	Weight of Wings
t	-	Time	WRS	-	Written Report Score
T	-	Thrust	\dot{x}	-	Velocity in x Direction
t_{config}	-	Aircraft Configuration Time	\ddot{x}	-	Acceleration in x Direction
t_{GM}	-	Ground Mission Time	\ddot{y}	-	Acceleration in y Direction
t_{m2}	-	Mission 2 Payload Loading Time			
$t_{M2,lap}$	-	Mission 2 Lap Time			
$t_{M3,lap}$	-	Mission 3 Lap Time			
$t_{passenger}$	-	Single Passenger Loading Time			
t_{5min}	-	5 Minute Time Span			
TMS	-	Total Mission Score			
TPU	-	Thermoplastic Polyurethane			
UD	-	Unidirectional			
V_H	-	Horizontal Tail Volume Coefficient			
V_V	-	Vertical Tail Volume Coefficient			
v	-	Velocity			
v_{M2}	-	Velocity in Mission 2			
v_{M3}	-	Velocity in Mission 3			



1. Executive Summary

This report details the design, manufacturing and testing of the University of Ljubljana's aircraft for entry in the 2024 American Institute of Aeronautics and Astronautics (AIAA) Design, Build, Fly (DBF) competition. Edvard Rusjan Team devised Adria, a radio-controlled (RC) aircraft, designed to successfully perform three flight missions and one ground mission following the AIAA requirements.

Adria strives to complete the following tasks: demonstration flight, rapid medical transport, efficient passenger transport, fast loading and unloading, as well as meeting takeoff and parking space limitations.

The aircraft's high-wing configuration and T-tail contribute to great flight characteristics and offer sufficient space for the mission payloads. With a wingspan of 59.11 in and a fuselage length of 68.80 in, Adria's design provides sufficient space for a total of 48 passengers. The aircraft is powered by a single electric motor and has a maximum takeoff weight (MTOW) of 14.02 lbs. A thrust of 13 lbs enables takeoff in the required 20 ft and a cruising speed of 95.46 mph. The team designed Adria's wing to be able to rotate by 74° and thus fit into the parking spot.

Adria was devised, designed, fabricated, and tested by a team of 20 students from the University of Ljubljana. The team is divided into 5 sub-teams: Design, Aerodynamics, Testing & Electronics, Manufacturing, and Finances & PR. A comprehensive sensitivity analysis was carried out to better understand the parameters affecting the mission scores. We used Quality Function Deployment (QFD) matrices and conducted Finite Element Method (FEM) analysis to determine the conceptual design of the aircraft. Based on the outcome, the team decided to design Adria mainly for M3 and GM requirements. During the preliminary design phase, two prototypes were developed and improved in an iterative process. Addressing all of the shortcomings and implementing improvements throughout the detail design phase, the team completed Adria. Manufacturing included CNC milling, 3D printing, composite molding, laminating, and vacuum bagging. The majority of Adria's skin consists of a carbon fiber structure paired with foam or honeycomb cores, ensuring a lightweight sandwich design with maximum structural strength. Ground and flight tests were crucial to continuously improve on the design. During flight testing, the final design of Adria proved to have outstanding stability characteristics.

Using a proprietary Score Analysis Simulation (SAS), the team seeks to achieve optimal flight performance and maximize the final score. Based on performance simulations, the aircraft is expected to be able to take off in under 20 ft. We predict the GM to be completed in 84 seconds, earning a score of 0.84, and M2 in 70.4 seconds, finishing well within the time limit and earning a score of 1.83. For M3, the aircraft is anticipated to fly for a total of 4 minutes and 50 seconds while completing 13 scoring laps, reaching an approximate score of 2.76. Adria is estimated to achieve a competitive score of 6.43 points in total.



2. Management Summary

2.1 Team Organization

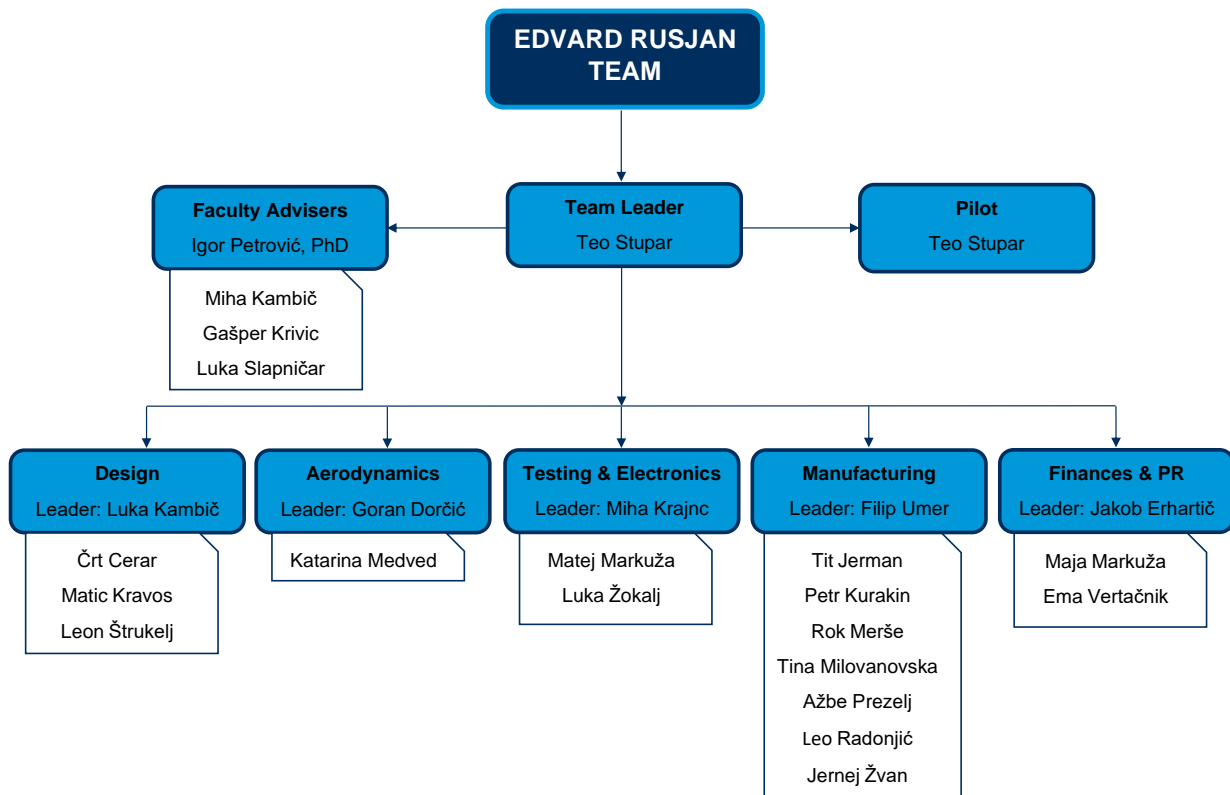


Figure 1: Team structure

Edvard Rusjan Team consists of 20 student members of different faculties from the University of Ljubljana, along with advisors from the Faculty of Mechanical Engineering. 50% of the team members are freshmen, sophomore, or junior students. The team is divided into 5 separate groups: Aerodynamics, Design, Testing & Electronics, Manufacturing, and Finances & PR (Figure 1), each of which play a crucial role in its own aspect of the aircraft development process. Members are not limited to just one group but can participate in multiple groups at once depending on their interests and fields of expertise. This dynamic approach fosters a collaborative environment where each team member is encouraged to adapt their work based on other groups' findings and progress. By allowing individuals to contribute across different domains, we not only encourage skill diversification, but at the same time improve the overall productivity of each group with regular feedback between the members. Table 1 outlines the tasks of each group and the specific skills expected of its respective members. Each group has a leader, an experienced team



member who delegates and supervises work, ensures completion of tasks on time, and passes down experience and knowledge from previous years to newer team members. Group leaders encourage cross-team communication and provide feedback to each other as well as report to the team leader who oversees the entire project. The team holds weekly meetings where various solutions are presented and discussed, and progress is evaluated. These meetings also serve a decision-making purpose, where all team members can suggest and decide on different ideas and concepts. Faculty advisers monitor the progress of the project and advise the team on more complex problems.

Table 1: Tasks and requirements by group

Group	Tasks	Required skills and knowledge
Design	Definition of aircraft's characteristics, conceptual design, CAD modelling, numerical simulations.	Computer programming, FEM, CAD, numerical simulations.
Aerodynamics	Conducting CFD analysis in collaboration with Design team.	CFD, fluid dynamics, aerodynamics.
Testing & Electronics	Electronic components selection and validation, configuration of propulsion and control systems, validation of entire aircraft.	DoE, data acquisition and processing.
Manufacturing	Selection of manufacturing processes, production of aircraft parts, assembly of the prototypes and final model.	CNC, CAM, experience with composite materials, manual dexterity.
Finances & PR	Media and social networks coverage, budget management, advertising, sponsorship acquisition and liaison.	Communication and negotiation skills, financial literacy, marketing strategies.

2.2 Milestone Chart

In the early stages of the project, a Gantt chart was devised to ensure efficient time management and, most importantly, that all deadlines are met. Time frames for various tasks were determined in advance based on prior experience in Design, Build, Fly competitions. The team met weekly to track the progress of the tasks and update the Gantt chart. Monitoring by group leaders was recorded on the chart to offer the team leader with real-time project status updates. The Gantt chart shown in Figure 2 shows project status at the time of writing this report.



3.1.1 Mission Flight Rules

Every flight mission involves completing the specified number of laps within the designated flight time window on the flight course, shown in Figure 3. The procedure for each mission commences with the following steps: The aircraft must enter the staging box in its parking configuration with the gurney, Medical Supply Cabinet, floor insert, and propulsion battery packs removed. During the 5 minute staging window the ground crew has to reconfigure the airplane from parking into flight configuration, install the batteries, and place the crew and any mission-specific payload. A successful flight mission necessitates the aircraft taking off within 20 ft and executing a successful landing at the end.

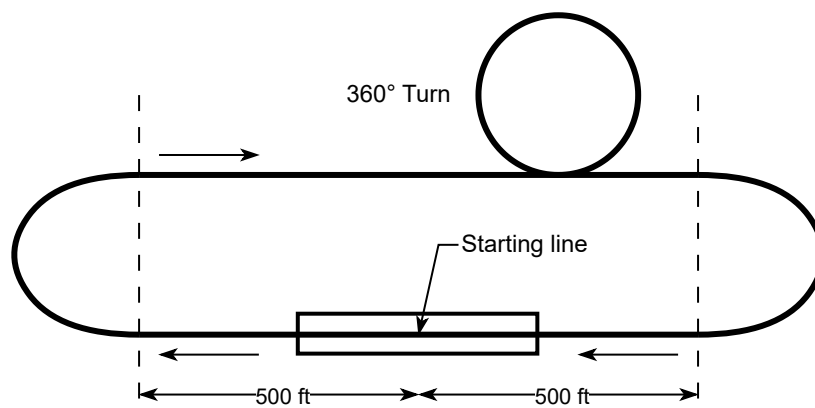


Figure 3: Official flight course

3.1.2 Mission 1: Delivery Flight

Mission 1 is considered completed if the aircraft finishes the three laps within the 5 minute window while adhering to the specified flight mission rules outlined in Section 3.1.1. The team will receive one point for successfully completing the mission:

$$M1 = 1.0. \quad (3)$$

3.1.3 Mission 2: Medical Transport Flight

Mission 2 is accomplished when the aircraft transports the Emergency Medical Technicians (EMTs), patient on a gurney, and the Medical Supply Cabinet while flying three laps within the 5 minute limit, adhering to the mission flight rules. The score is determined by the ratio of the Medical Supply Cabinet weight W_c to the mission time t_{M2} , normalized by the performance of the best-performing team:

$$M2 = 1 + \frac{W_c / t_{M2}}{\max[W_c / t_{M2}]} \quad (4)$$



3.1.4 Mission 3: Urban Taxi Flight

Mission 3 is completed when the aircraft transports the passengers within the 5 minute window and adhering to the mission flight rules. The score is calculated as the product of the number of laps flown N_L and the number of passengers N_P , divided by the rated battery capacity C , and then normalized based on the performance of the best-performing team:

$$M3 = 2 + \frac{N_L \cdot N_P / C}{\max[N_L \cdot N_P / C]} \quad (5)$$

3.1.5 Ground Mission: Configuration Demonstration

Ground Mission involves measuring the time required to transition the aircraft through each mission configuration. The timing commences with the aircraft in the parking configuration. Subsequently, it must be put into the flight configuration with Mission 2 payloads loaded. Following this, the payloads are unloaded and the Mission 3 payload is loaded. Finally, the payloads need to be removed and the aircraft returned to the parking configuration where the timing is stopped. During each transition between mission configurations, the timing halts as the pilot ensures the proper functioning of flight control surfaces. Mission score is determined solely by the elapsed time for the entire attempt t_{GM} in comparison to the best team:

$$GM = \frac{\min[t_{GM}]}{t_{GM}} \quad (6)$$

3.2 Aircraft Constraints

The design of the aircraft should adhere to the following fundamental constraints:

- **Design:** Any design is permissible except for rotary wing or aircraft lighter than air.
- **Propulsion:** Electrical power must be supplied by a NiCd, NiMh, or LiPo battery pack. Total propulsion battery capacity must not exceed 100 Wh. Each battery pack must be independently connected to its own propulsion system. Batteries cannot be connected in series or parallel. Both the propeller and electric motor must be commercially available.
- **Takeoff:** The aircraft must be capable of taking off within 20 ft without any external assistance.
- **Medical Supply Cabinet:** The cabinet weight can be varied. However, the minimum dimensions must be 3 x 3 x 3.5 in.
- **Configuration:** The wingspan of the aircraft may not exceed 5 ft. In addition, the aircraft must fit into a 2.5 ft wide slot in the parking configuration.
- **Passengers:** Represented by a wooden peg doll with a height of 3.5 in with a 1.5 in radius.
- **Crew:** The crew, sized the same as passengers, must be in a cockpit with their heads positioned above the fuselage. The crew should be separated from the passenger compartment by a solid bulkhead.
- **EMTs:** Sized the same as passengers, EMTs need to be situated next to the gurney.



- **Patient:** A wooden cylinder with a height of 5.5 in and a radius of 1.69 in.
- **Gurney:** Must be at least the same width and length as the patient, with a minimum height of 1.5 in.
- **Passenger Compartment:** It should have a single-plane horizontal floor. Separate inserts are allowed for each mission. Access to the compartment should be via hinged hatches on the side. The hatch opening cannot extend past the fuselage's vertical centerline, with a maximum width of 6 in.

The requirements for individual missions, scoring equations, and guidelines were examined and translated into basic problem statements, further breaking down key design parameters for each specific mission, as illustrated in Table 2.

Table 2: Translation of problem statements into key design parameters

Mission	Problem Statement	Key Design Parameters
Mission 1	Basic flight maneuvering, takeoff within limit.	Power, low stall speed.
Mission 2	Fast lap times, takeoff within limit.	Power, cabinet weight, low stall speed.
Mission 3	Endurance flight, optimal passenger capacity, speed, flight stability, takeoff within limit.	Power, passenger capacity, low stall speed, battery capacity.
Ground Mission	Fast payload loading mechanism.	Loading efficiency.

3.3 Sensitivity Study of Design Parameters

Optimal aircraft design selection requires some basic guidelines regarding design parameters. Based on the team's previous experience, the crucial relationships between design parameters, found in Table 2, can all be mathematically described with respect to six parameters: electric power input P , weight of the cabinet W_c , passenger capacity N_p , wing surface area A , and wing aspect ratio AR . Aircraft gross weight mainly influences energy consumption and takeoff distance. Empty weight was estimated by considering the weight of the wing, fuselage, empennage and propulsion. The propulsion weight was approximated by estimating the weight of a battery pack and motor with coefficients k_{m1} and k_{m2} described by Equations (7) and (8). The fuselage weight was approximated with the Equation (9). Wing, stabilizer, and rudder weights were estimated based on wing surface area, tail volume coefficients, average area, and longitudinal densities considering manufacturing experience. Equations (10), (11) and (12) mathematically describe the mentioned relationships, whereas Equation (13) represents total aircraft weight. When the aircraft weight was being calculated for M2 or M3, the weight of the payload was also included in the total aircraft weight.

$$W_{motor} = P^2 \cdot k_{m1} + k_{m2} \quad (7)$$

$$W_{battery} = \frac{E_{required}}{E_{cell}} \cdot W_{cell} \quad (8)$$

$$W_{fuselage} = W_{base} + W_c \quad (9)$$

$$W_{wing} = A_{wing} \cdot \rho_{wing} + L_a \quad (10)$$

$$W_{stabilizer} = \frac{V_H \cdot A_{wing} \cdot MAC}{L_H} \cdot \rho_{wing} \quad (11)$$

$$W_{rudder} = \frac{V_V \cdot A_{wing} \cdot b}{L_V} \cdot \rho_{wing} \quad (12)$$



$$W_{aircraft} = W_{motor} + W_{battery} + W_{fuselage} + W_{wing} + W_{stabilizer} + W_{rudder} \quad (13)$$

Using design parameters P , AR and A , the average cruise speeds of the aircraft were calculated for M2 and M3. The aircraft drag coefficient C_d , used in Equation (14), was based on experience from previous competitions. With known speeds, M2 and M3 lap times were estimated using Equations (15) and (16). Distance flown in each lap was summed using the length of the straight segments s that equals to 1000 ft and turn radius r that is kept constant at 131 ft based on the teams' experiences in past competitions. With lap times known, performance in M2 can be estimated using Equation (15), as well as the total number of completed laps in M3 using Equation (17).

$$v_{M2} = v_{M3} = \sqrt[3]{\frac{2 \cdot P}{\rho \cdot A \cdot C_d}} \quad (14) \quad t_{M3,lap} = \frac{2 \cdot s + 4 \cdot \pi \cdot r}{v_{M3}} \quad (16)$$

$$t_{M2,lap} = \frac{2 \cdot s + 4 \cdot \pi \cdot r}{v_{M2}} \quad (15) \quad N_L = \left\lfloor \frac{t_{5min}}{t_{M3,lap}} \right\rfloor \quad (17)$$

The time required to execute GM was approximated using Equation (18). The equation uses various constants and a coefficient to estimate the time for configuring the aircraft and loading different payload types. The constants t_{config} , t_{m2} and $t_{passenger}$ denote the time to configure the aircraft, load the M2 payload, and load a single passenger in M3, respectively. Additionally, a loading efficiency factor L_K has been introduced to approximate the time saved by loading multiple passengers with the floor inserts. Assuming that the times to load and unload payloads are very similar, we can simply multiply the equation by a factor of 2.

$$t_{GM} = 2 \cdot \left(t_{config} + t_{m2} + \frac{t_{passenger} \cdot N_P}{L_K} \right) \quad (18)$$

It was presumed that the aircraft could consistently rotate the main wing to fulfill the 2.5 ft parking configuration constraint. The necessary takeoff speed was estimated using Equation (19), incorporating parameters such as aircraft weight $W_{aircraft}$, wing surface area A , and an estimated lift coefficient C_L . Subsequently, the takeoff distance was deduced using a straightforward equation that considered the aircraft weight $W_{aircraft}$, motor power P , and the estimated takeoff speed v_{TO} as per Equation (20).

$$v_{TO} = \sqrt{\frac{2 \cdot W_{aircraft}}{\rho \cdot A \cdot C_L}} \quad (19) \quad S_{TO} = \frac{v_{TO}^3}{2 \cdot P \cdot W_{aircraft}} \quad (20)$$

With all quantities known, TMS can be computed. It was found that maximizing W_C and N_P to a certain point results in higher TMS, as seen in Figure 4, where EDA denotes the optimal score. The limiting factors being the takeoff distance in M2 and the 5 minute flight window. This simple model assumes that the battery capacity is high enough to sustain 5 minutes of flight time in M3. At this stage of the design, the team was only concerned with the conceptual design guidelines and not the actual values of design parameters. This assumption was later deemed valid through detailed design and experimental validation. Figure 5 shows how each crucial design parameter impacts TMS for aircraft with average expected design parameters. From there it can be concluded that choosing the right number of passengers and medical cabinet weight will be crucial factors in maximizing the total mission score. Furthermore, the team should focus on finding the optimal propulsion combination and wing area for take off, fast performance in M2, and flight endurance in M3.



Based on the presented sensitivity study, the aircraft concept design should focus on maximum payload capacity with efficient floor inserts to excel in GM as illustrated in Figure 4.

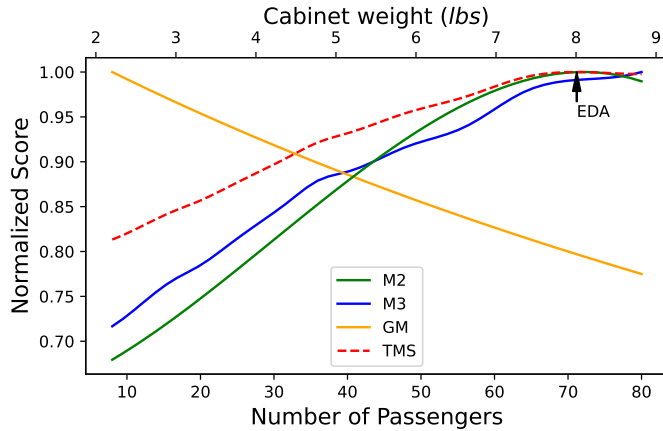


Figure 4: Mission scores as a function of W_C and N_P

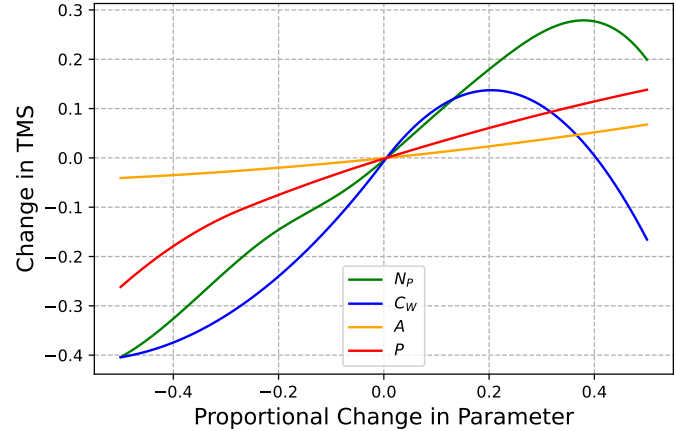


Figure 5: Sensitivity study of crucial design parameters

3.4 Design Selection Process

To comprehensively evaluate the various design configurations, we employed a series of Quality Function Deployment (QFD) matrices, derived from the critical configuration factors identified in Section 3.3. These matrices assigned importance ratings ranging from 0 to 5 to each design function, with 5 indicating utmost significance and 0 denoting negligible impact on the overall design. Team members meticulously analyzed each design iteration, ultimately selecting the most optimal design based on the comprehensive assessment outlined in Tables 3, 4, and 5. Each function is further broken down as follows:

Payload Capacity: The payload capacity was decided to be one of the most important characteristics. The number of passengers has a significant impact on TMS and must be minimized to achieve the highest TMS.

Weight: The weight is crucial in M3 and takeoff. A heavier aircraft will impact the number of passengers it can carry. Furthermore, it is also important to consider the weight in regard to takeoff limitations.

Speed & Drag: The speed of the airplane contributes to faster completion of missions and thus higher scoring in M2 and M3. Less drag allows the aircraft to fly faster with less required power which results in the completion of more M3 scoring laps.

Rigidity: The aircraft has to be rigid in order to withstand heavy payload. Rigidity is also important when the aircraft is experiencing high G forces. Aircraft rigidity should be considered crucial.

Simplicity: Simplicity is important for faster and more consistent aircraft manufacture. It is especially important for the manufacturing of fuselage and wings, however, it may still be outweighed by the increase in performance.

Stability: Mid-flight stability does not have to be prioritized. An unstable plane will have trouble carrying the payload and completing M2 and M3, but stability can be maintained by an experienced pilot to a certain degree.



Reliability: Reliable performance of the aircraft and its mechanisms should be prioritized to a certain degree. The mechanisms must not fail for the entire duration of the competition and withstand unfavorable weather condition.

Takeoff & Landing: In case of unsuccessful takeoff or landing no mission scores are granted, giving them high importance.

Parking Configuration: Parking configuration is a critical aspect that directly influences both GM capabilities and the structural integrity of the aircraft.

3.4.1 Wing Placement

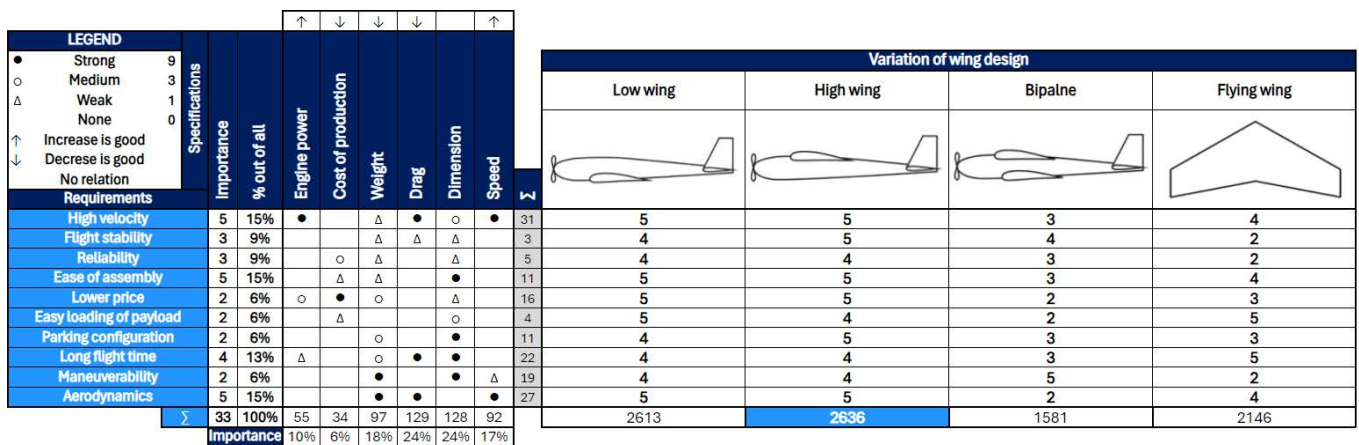


Figure 6: QFD matrix for the wing

In considering wing placement for the aircraft design, critical factors such as speed, aerodynamics, and parking feasibility are essential. Flying wing and biplane configurations were swiftly eliminated because of their limitations in passenger capacity and potential drawbacks to ground operations. Even though both low and high wing designs offer comparable advantages in assembly and aerodynamics, the high wing configuration proved to be the optimal choice for its facilitation of smoother ground mission execution.

3.4.2 Parking Mechanism

In the evaluation of parking mechanisms for our aircraft design, emphasis was placed on firmness and simplicity. We prioritized robust connections to prevent potential in-flight structural failures due to weak attachment points, necessary for parking configurations. Moreover, maintaining the integrity of the aircraft's fuselage and wing structure was a primary concern, leading us to reject the idea of separating these components into multiple parts. Instead, we opted for a design where the fuselage and wing remain integrated for enhanced rigidity.

Furthermore, the implementation of a rotating wing system addresses both durability and simplicity requirements. This system ensures a secure connection between the fuselage and main wing during flight, bolstering the overall strength of the aircraft. Additionally, the rotating wing design offers a straightforward locking mechanism, contributing



LEGEND									Variation of Parking Mechanism				
●	Strong	9											
○	Medium	3											
△	Weak	1											
	None	0											
↑	Increase is good												
↓	Decrease is good												
	No relation												
Requirements		Specifications											
Importance	% out of all	Engine power	Cost of production	Weight	Drag	Dimension	Speed	Σ	Folding wings	Rotating empennage	Rotating wing		
High velocity	5	15%	●		△	●	○	●	31				
Flight stability	3	9%			△	△	△		3	3	4	5	
Reliability	3	9%		○	△		△		5	3	3	4	
Ease of assembly	5	15%		△	△		●		11	4	3	3	
Lower price	2	6%	○	●	○		△		16	4	3	4	
Easy loading of payload	2	6%		△			○		4	4	5	4	
Parking configuration	2	6%			○		●		11	4	3	3	
Long flight time	4	13%	△		○	●	●		22	4	4	5	
Maneuverability	2	6%			●		●	△	19	2	4	5	
Aerodynamics	5	15%			●	●	●		27	4	4	4	
Σ	33	100%								1973	2112	2286	
	Importance		10%	6%	18%	24%	24%	17%					

Figure 7: QFD matrix for parking configuration

to ease of operation and maintenance.

Following the selection of the parking mechanism, rapid experimentation with numerous locking mechanisms was undertaken. These mechanisms were 3D printed and subsequently assessed for their ease of construction, stiffness, and unlocking efficiency. After thorough evaluation, we selected the most robust mechanism, while also prioritizing simplicity in manufacturing (Figure 8, right picture).

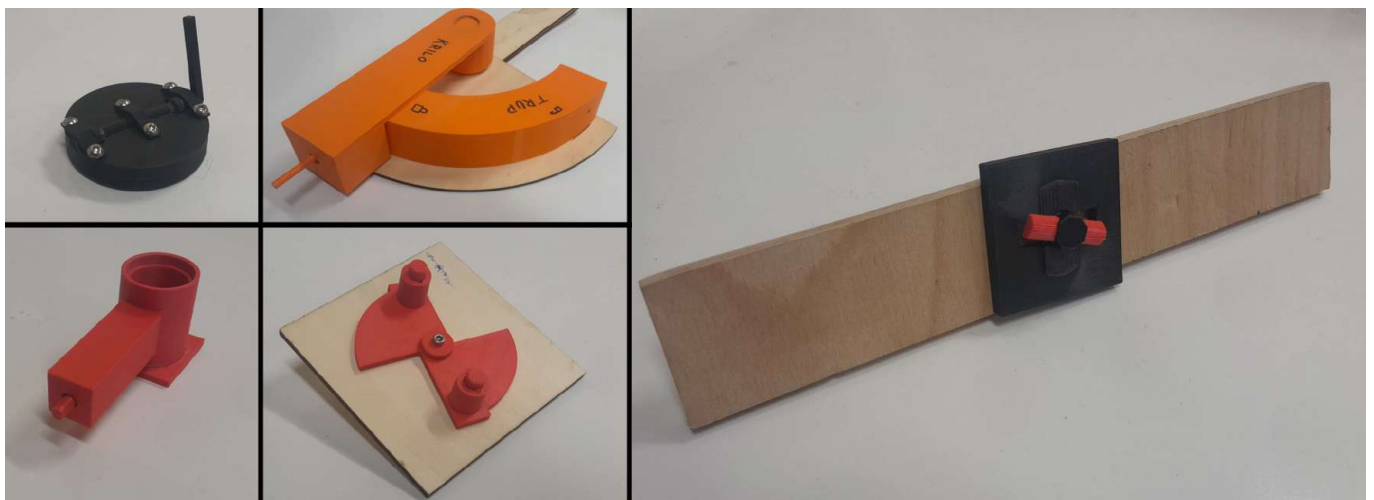


Figure 8: Rotation mechanism concepts

3.4.3 Empennage and Landing Gear Design

The driving factor in selecting the T-tail configuration for the empennage design was our focus on facilitating efficient passenger loading while minimizing interference from the wing's wake on the horizontal stabilizer. Additionally, the

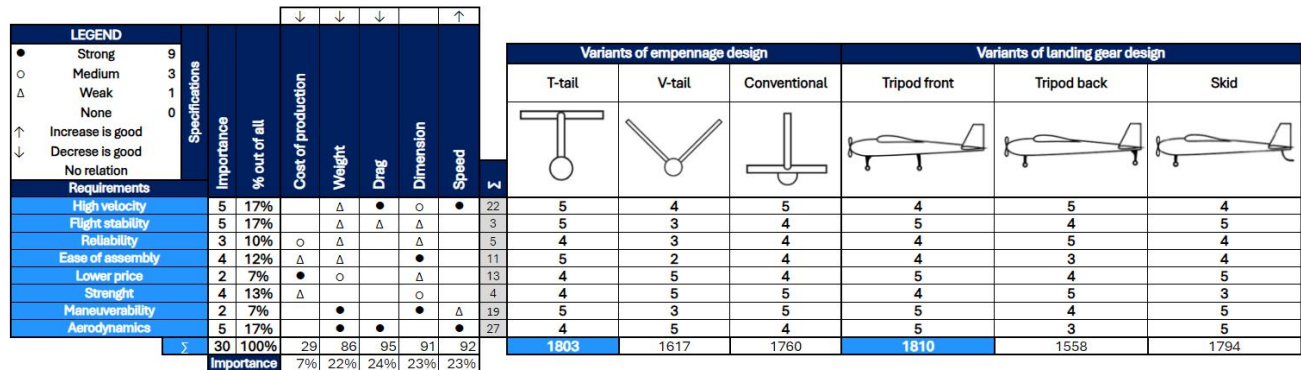


Figure 9: QFD matrix for empennage and landing gear design

T-tail setup mitigates the risk of the horizontal stabilizer contacting the ground during tilting maneuvers at takeoff and landing.

For the landing gear design, our analysis led us to endorse the front tricycle undercarriage configuration as superior. This choice optimizes both takeoff and ground mission operations by streamlining the passenger loading sequence without obstruction. Consequently, the tricycle undercarriage design outperforms alternative options, aligning effectively with our aircraft's operational requirements.

3.4.4 Passenger accommodation

No QFD matrix was created for the passenger compartment design. It was decided the best design features the least possible number of hatches, to reduce complexity and maintain structural integrity of the fuselage. Consequently, the chosen design consists of a separate side hatch for the medical cabinet and another hatch at the rear of the airplane, through which the passengers are inserted in bulk. The exact configuration for the passenger compartment was determined in preliminary design, together with fuselage sizing.

3.5 Final Conceptual Design

Figure 10 shows the final conceptual design. It has a wing span of 59.10 in and an aspect ratio of 4. The tail size is estimated with the use of tail volume coefficients. The fuselage is shaped so it can accommodate 50 passengers in 4 rows or a 3 x 3 x 3.5 in, medical cabinet, and the patient with EMTs. The passenger compartment is accessible from a side hatch at the rear of the aircraft. A carbon fiber tube connects the T-tail to the fuselage. The wing can rotate around the vertical axis to enter the parking configuration. We also implemented a classic tricycle landing gear to maximize takeoff distance because of the shorter distance between the front and the back wheels.

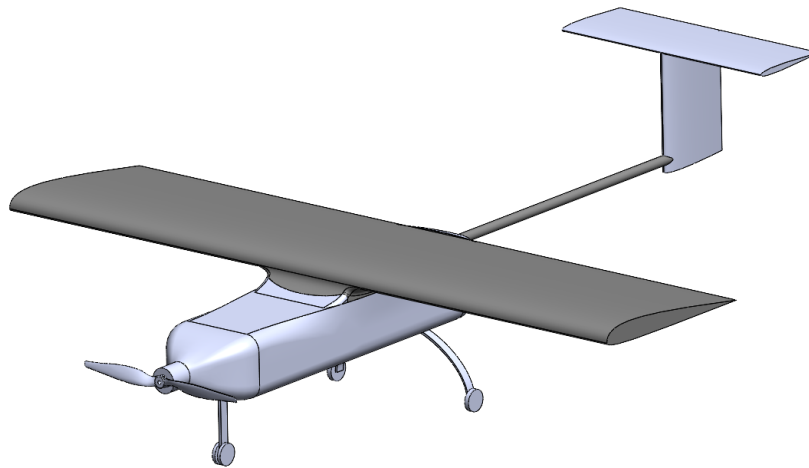


Figure 10: Conceptual aircraft design

4. Preliminary Design

The primary goal of the preliminary design phase was to identify and refine the parameters of the conceptual design to maximize the final score. Using the aircraft's geometry, design considerations, aerodynamics, propulsion system, and mission model, a SAS was developed in the Python programming language [1]. The optimized aircraft parameters, along with estimated mission performance, are detailed in Table 7 at the conclusion of this section.

4.1 Design and Analysis Methodology

Based on previous experience and competition rules, it was deduced that the aircraft characteristics can be defined using the following input parameters to SAS: cabinet weight, number of passengers, wing area, wing aspect ratio, and propulsion configuration. The propulsion system model is created from the provided propeller, motor, and battery. Basic thrust-speed and electric current-speed relationships, weight, and dimensions of the propulsion system are evaluated based on manufacturer data and team measurements (Sections 7 and 8). Lifting surfaces are created based on specified wing area and aspect ratio. In the next step, propulsion system and lifting surfaces are added to the fuselage and its dimensions are iteratively modified to achieve optimal center of gravity (CG) position in the mission with the heaviest payload. The generated design is then evaluated whether it can adhere to designated constraints. Final aircraft geometry is further used to estimate mass, mass moment of inertia, and drag and lift characteristics. Estimated aerodynamic, propulsion, and mass properties are then used as input into the mission model that calculates performance in GM, M1, M2 and M3. As a result, TMS of any aircraft configuration can be calculated, as represented in Figure 11.

The SAS served as the cost function in the optimization problem, aiming to determine the optimal aircraft parameters. For each input parameter in the SAS, a practical range of discrete values was assigned, generating a comprehensive list of all potential input combinations that adhere to the competition constraints. Subsequently, the performance in all missions was computed for each conceivable aircraft configuration. Based on the outcomes, the

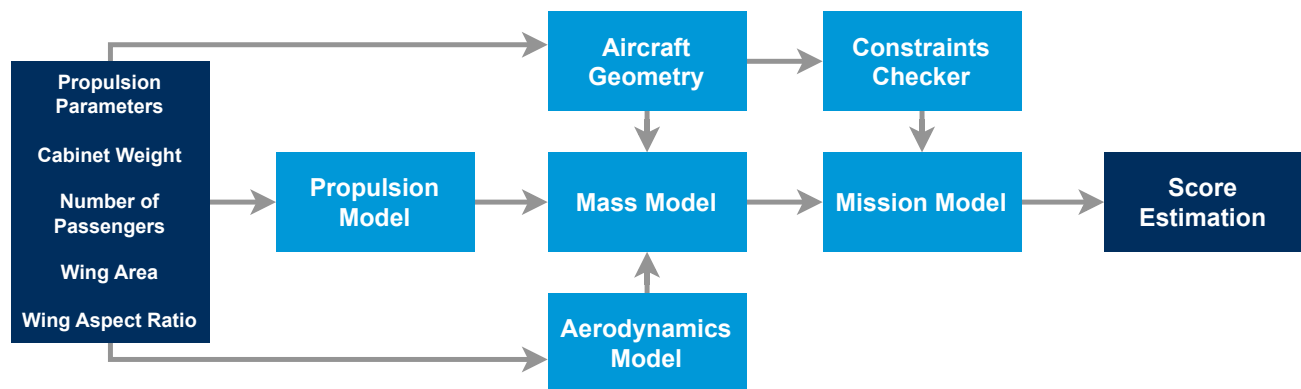


Figure 11: Score analysis simulation diagram

most favorable aircraft configuration for each mission was identified, leading to the decision on the best-performing mission-specific aircraft. The mission scores obtained were then used as inputs in the TMS calculation, ultimately yielding the overall optimal aircraft parameters.

Based on propulsion tests, structural integrity tests, and prototype flight tests, SAS was corrected multiple times to achieve more realistic results. Subsequently, the optimization problem was solved ten times in total, until the final set of aircraft input parameters were determined.

The iteration process unfolded in several stages. Initially, various combinations of input parameters were computed to gain an initial understanding of the optimal strategy. From that, it was deduced that the optimal aircraft should carry a substantial payload for a high score in M2 and accommodate a large number of passengers to excel in M3. Additionally, an insert design for faster times in GM was deemed necessary. Achieving the right balance between payload weight and takeoff distance proved to be a crucial factor for success in this year's DBF competition, emphasizing its prioritization in the design process. Following this, the SAS was employed to identify the winning aircraft for M2 and M3 independently. The optimal aircraft input parameters for M2 and M3 were then used to assess their influence on other missions. In the end, the overall best-performing aircraft, considering GM as well, was selected as the most optimal choice for this year's DBF competition.

4.2 Mission Model

The team designed and implemented different mission models to approximate the mission results for different design parameters.

4.2.1 Flight Model

The flight mission model consisted of straight and turn lap segments. Straight segments were simulated using Equation (21), whereas turn maneuvers were simulated using Equations (22), (23) and (24). Equations were integrated over time using the 4th order Runge-Kutta method written in Python. Thrust T was defined as a function of speed that was obtained from the SAS propulsion module and testing. In-plane lift component L' , drag D , and in-plane pitching



moment component M' were defined as functions of speed and angle of attack. Turn damping factor K , mass m , and mass moment of inertia J were defined as functions of dimensional parameters of the aircraft. L' and M' also greatly depend on the bank angle of the aircraft, which is a function of the maximum load factor. Figure 12 presents further clarification of symbols used in calculations of the turn maneuver. The flight mission model also accounted for wind speed. Its direction was assumed to align with straight segments of the lap.

$$\ddot{x} = \frac{1}{m}(T - D) \quad (21)$$

$$\ddot{y} = \frac{1}{m}(T \sin \varphi + L' \cos \varphi - D \sin \phi) \quad (23)$$

$$\ddot{x} = \frac{1}{m}(T \cos \varphi - L' \sin \varphi - D \cos \phi) \quad (22)$$

$$\ddot{\varphi} = \frac{1}{J}(M' - K\dot{\varphi}^2) \quad (24)$$

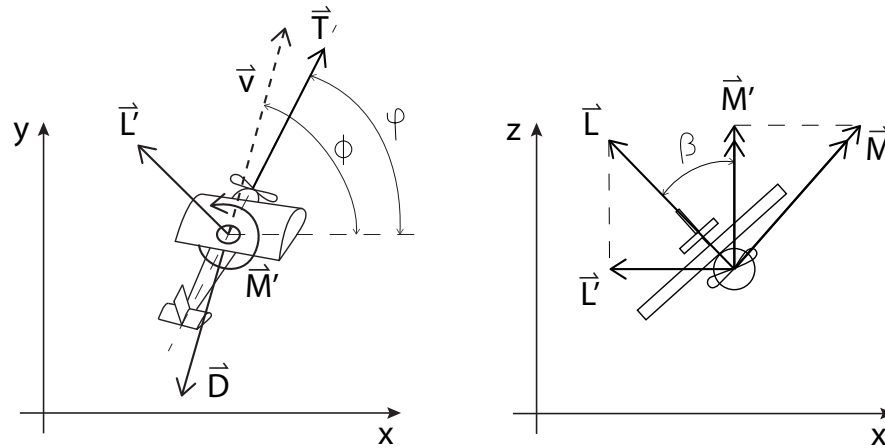


Figure 12: Free body diagram of forces induced on the aircraft during simulated turn maneuver

The approach described above also contains some uncertainties and limitations. While forces are modeled in three dimensions, the movement of the aircraft itself is strictly two-dimensional and does not account for the vertical dimension. Loss of time and energy due to aircraft climb is therefore neglected. Furthermore, straight cruise flights are exactly 1000 ft long, followed by instantaneous aircraft roll. With this assumption, the pilot's reaction time and transient of the aircraft roll are ignored. Lastly, uncertainties and errors in drag and thrust prediction in addition to pitching moment could further affect the mission model. The biggest uncertainty being the lift and drag prediction during takeoff, as well as the subsequent effects of flaps. To address these challenges, the team undertook a comprehensive study of aerodynamic effects, complemented by real-world testing and validation efforts.

4.3 Design Trade Studies

4.3.1 Medical Cabinet Weight

Based on the mission model described in Section 4.2, M2 performance concerning medical cabinet weight was obtained. Figure 13 presents the result of M2 optimization iteration. M2 scoring is presented as a function of the cabinet weight for the highest possible M2 score of an aircraft with a chosen propulsion combination that shows



maximum power. M2 score is directly proportional to the cabinet weight. With an increased payload, the stall speed increases, which in turn dictates the takeoff speed and subsequently takeoff length. Higher propulsion power enables the aircraft to take off within the required distance but consumes more power during the flight, which negatively impacts scoring in M3. The winning combination for M2 is a propulsion configuration with a maximum power of 2400 W and a medical cabinet weight of 6.6 lbs, thus being the combination chosen by the team.

4.3.2 Number of Passengers

Passenger capacity affects scores in M3 and GM almost equally, with an inverse relationship. Aircrafts with a lower passenger capacity generally score better in GM, as the crew member does not need to load as many passengers, thus reducing time and increasing mission score. On the other hand, aircrafts with higher passenger capacity score higher for M3. The trade-off between GM and M3 score as a function of number of passengers and required battery capacity is shown in Figure 14. Even though increasing the passenger count also requires higher battery capacity, the rate of change is minimal compared to the benefits of additional passengers and higher speeds in M3. As seen from TMS, gains from both missions are at their highest in the middle point. 48 passengers are chosen as the winning strategy for our aircraft. M3 mission score is also affected by the battery capacity, which is detailed in Section 4.3.3.

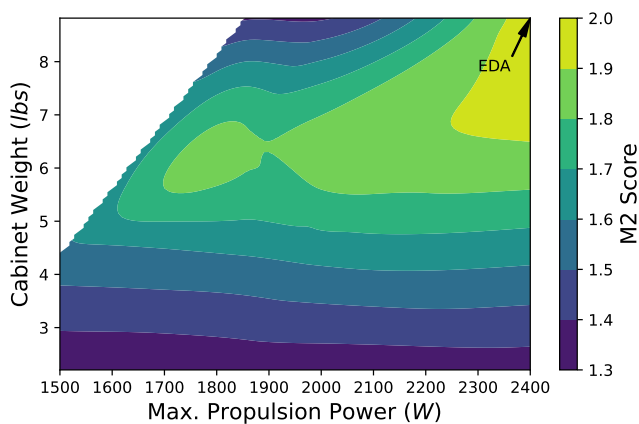


Figure 13: Medical Cabinet Weight and propulsion power effect on M2

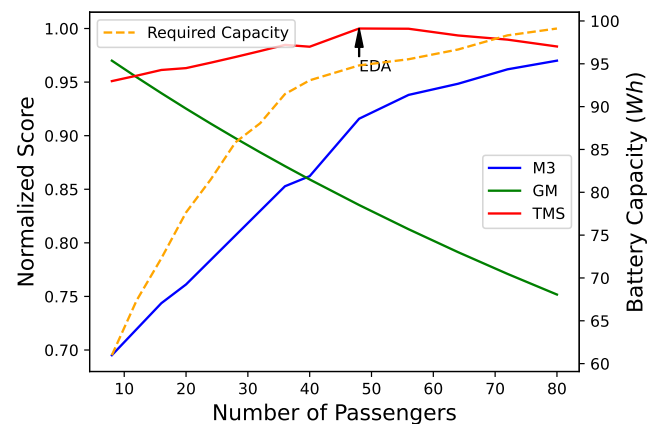


Figure 14: Number of Passengers and Battery Capacity effect on M3, GM and TMS score

4.3.3 Propulsion

The propulsion configuration was chosen through iterating 102 brushless direct current (BLDC) motors, 132 propellers, 10 electronic speed controllers (ESC), and 12 different batteries of various voltages and capacities. In each iteration, the components were passed down to the propulsion module, which produced the proper thrust curve for desired throttle settings. The obtained thrust curve was used by the mission model for flight simulation. The best combinations for flight missions can be seen in Figure 15.



The challenge in M2 was to maximize power output to enable the aircraft to take off with a heavy payload and fly a fast lap, while still conforming to the battery capacity limit. Alternative evaluated propulsion combinations had a similar score in M2, with the combination of Scorpion SII-4035-330KV motor and an APC 15x6E propeller being the highest scoring combination and was therefore chosen as the best combination in M2.

M3 requires a propulsion with the best efficiency to fly the highest number of laps within the 5 minute flight window, while still providing enough static thrust for a successful takeoff. A Scorpion SII-4035-330KV motor in pair with an APC 14x6E propeller was chosen as the most optimal propulsion combination in M3, seen as the largest M3 bar in Figure 15.

Figure 15 contains the best scores from M1 and GM, therefore the best overall propulsion configuration can also be determined. The apparent optimal combination is the Scorpion SII-4035-330KV motor with the APC 15x6E propeller for M2 and the APC 14x6E propeller for M3.

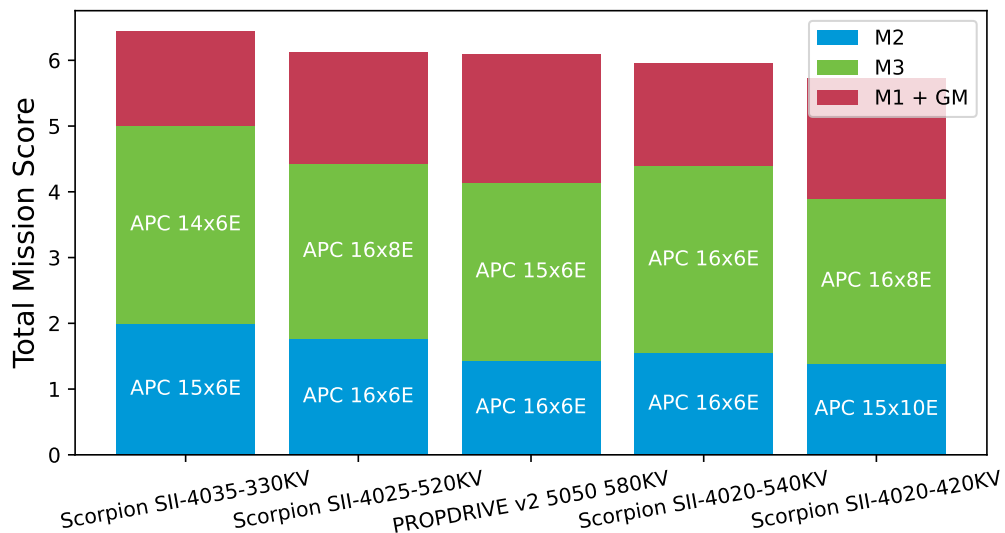


Figure 15: Optimal propulsion configurations for M2 and M3

4.3.4 Wing Area and Aspect Ratio

The optimal wing area and wing aspect ratio were calculated during the optimization process. Optimal wingspan offers the least amount of total drag in a wide range of speeds while still providing enough lift for the aircraft to take off safely within the constraint. Decreasing the wing aspect ratio also increases the speed of the aircraft and is key for a high TMS, as shown in Figure 16. The missing areas in Figure 16 are the effects of the imposed wingspan limitation at the top right and failed takeoff simulations at the bottom left. With a higher aspect ratio and wing area, the overall efficiency of the aircraft increases at the cost of speed. The optimal wing area of 6.56 ft² and a wing aspect ratio of 3.81 were chosen since they contribute the most towards a high TMS.

4.3.5 Takeoff Requirements

The aircraft must be able to take off within 20 ft. The team calculated the stall speed by considering aircraft mass Cl_{max} , lift increase by flaps, wing area, drag coefficient, and static thrust. Stall speed as a function of distance was calculated by integrating the differential equation presented by Equation (25). The drag coefficient in aircraft's drag force D was calculated using SAS at 0 degrees angle of attack. Same for lift coefficient and lift force L . Thrust T as a function of speed was obtained from the SAS propulsion module. Friction drag was approximated using factor μ . Functions L , D , and T were later adjusted to fit the data gathered from testing described in Section 7. Figure 17 shows that aircraft with optimal SAS parameters will successfully take off in every flight mission.

$$T(\dot{x}) - D(\dot{x}) - \mu(mg - L(\dot{x})) = m\ddot{x} \quad (25)$$

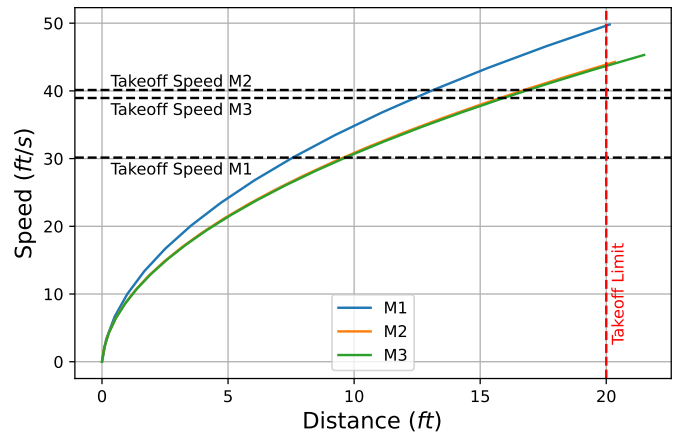
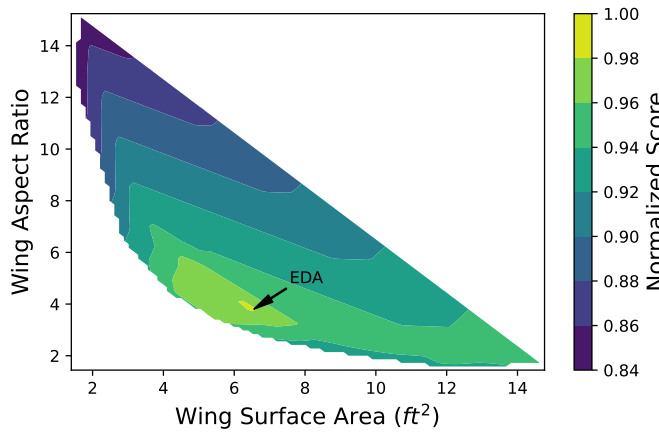


Figure 16: Effect of wing area and wing aspect ratio on TMS

Figure 17: Takeoff analysis for each flight mission

4.4 Optimal Aircraft Parameters and Total Mission Score

Table 3 includes SAS input parameters that yield the optimal aircraft configuration with the highest total mission score. As previously mentioned, it was discovered that the optimal aircraft must carry 48 passengers with the optimal medical cabinet weight of 6.6 lbs, as seen in Figure 18. With the use of SAS, it was therefore found that the optimal aircraft should achieve a score of 1.83 in M2, 2.76 in M3, and 0.84 in GM. A maximum TMS of 6.43 was calculated.



Table 3: Optimal aircraft input parameters calculated with SAS

Parameter	Cabinet Weight	Number of Passengers	Wing Area	Wing Aspect Ratio
Value	6.6 lbs	48	6.56 ft ²	3.81
Parameter	Propulsion Configuration			
M2	SII-4035-330KV, APC 15x6E, LiPo 2000mAh 12S 44.4v Battery Pack			
M3	SII-4035-330KV, APC 14x6E, LiPo 2000mAh 12S 44.4v Battery Pack			

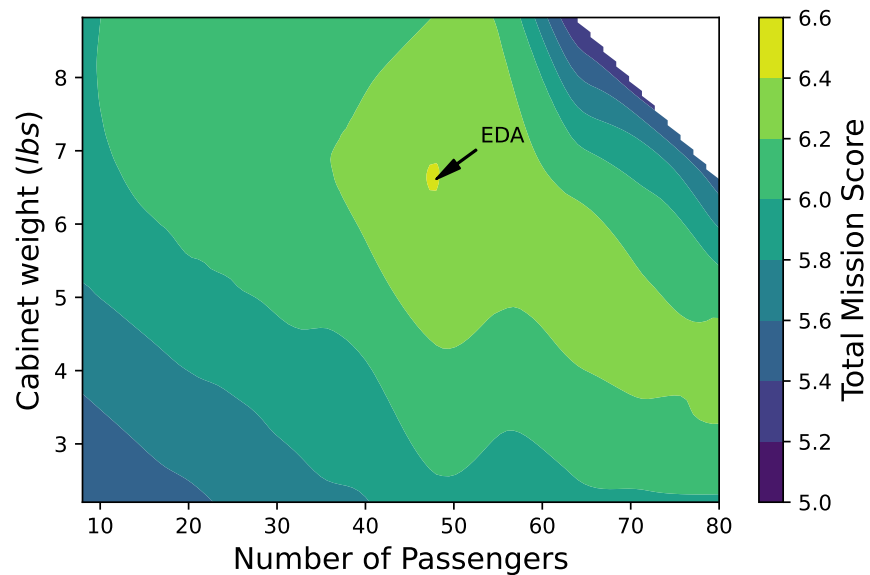


Figure 18: Heatmap representing TMS in relation to cabinet weight and number of passengers

4.5 Aerodynamic Characteristics

4.5.1 Wing Airfoil Analysis

Selecting the most optimal wing airfoil is one of the more crucial aspects of wing design. Analysis was conducted on all available airfoils between 11% and 15% thickness. We established the lower limit to accommodate servo motors and the upper limit to minimize empty space. Aerodynamic analysis was performed in program XFLR5 [2] because of its ability to conduct batch analysis of different airfoils at once. Analysis was conducted at Reynolds numbers Re 300000, 400000, 500000, 600000, 800000, 1000000, and 1200000. A value of Re 300000 was selected since aircraft takeoff occurs at roughly that value. At an approximate value of Re 1200000, chosen as the upper limit, the aircraft reaches its top speed. The dataset of the best airfoils and their data is shown in Figure 19. Most optimal airfoil would require having the highest possible $C_{l_{max}}$ at takeoff and the lowest possible C_d while cruising. Because of a tail strike possibility during takeoff, $C_{l_{max}}$ was limited to an AoA of 15° . The angle of incidence changes between airfoils because they have a different zero AoA. The incidence angle was selected so that the aircraft would produce the lowest drag possible during cruise speed. Airfoils with the biggest averaged ratio between $C_{l_{max}}$ and C_d at Re



values of 6000000, 8000000, and 1000000 were selected. By these criteria, the best airfoil for our aircraft was dfvlrr4. However, because it is a transonic airfoil and has a too difficult shape to manufacture, we rejected it. Martin Hepperle 70 airfoil was chosen by the team, because it achieved highest score and has an easy shape to manufacture. Basic information about the airfoil is shown in table 4.

airfoil name	max thickness	cl max	Re 400000	Re 500000	Re 600000	Re 800000	Re 1000000	Re 1200000	incidence angle
dfvlrr4.dat	13.38	1.50	1.49E-02	8.42E-03	7.40E-03	6.22E-03	5.61E-03	5.34E-03	-2.25
ms313.dat	13.13	1.50	1.28E-02	8.04E-03	7.33E-03	6.26E-03	5.73E-03	5.55E-03	-1.68
mh80.dat	12.7	1.50	1.15E-02	9.10E-03	8.24E-03	6.78E-03	6.08E-03	6.19E-03	0.88
mh70.dat	11.07	1.44	8.62E-03	6.57E-03	5.94E-03	6.25E-03	6.55E-03	6.63E-03	-1.04
oa213.dat	12.56	1.45	1.14E-02	8.14E-03	7.00E-03	6.07E-03	7.29E-03	7.84E-03	0.25
mh81.dat	12.98	1.56	1.12E-02	8.68E-03	7.78E-03	6.66E-03	7.69E-03	8.05E-03	0.15
naca2113.dat	13	1.45	1.27E-02	8.91E-03	7.38E-03	6.59E-03	6.94E-03	7.54E-03	-0.08
naca2114.dat	14	1.42	1.28E-02	9.13E-03	7.53E-03	6.79E-03	6.77E-03	6.94E-03	-0.08
s102b.dat	14.98	1.45	1.07E-02	1.04E-02	9.58E-03	8.23E-03	7.16E-03	6.31E-03	-1.42
naca3214.dat	14	1.51	1.13E-02	8.63E-03	7.32E-03	7.77E-03	8.32E-03	8.07E-03	-1.19

Figure 19: Dataset of best airfoils

Table 4: Basic MH 70 airfoil information

Airfoil	Max thickness	max camber	$C_{l_{max}}$	$C_d @ Re 800000$
MH70	11.1%	3%	1.44	0.0062

4.5.2 Wing Analysis

In our pursuit of optimal aerodynamics, we carefully studied both tapered and rectangular wing configurations, taking into account critical parameters such as lift generation, drag, and moments around the three principal axes (pitch, yaw, and roll) to analyze the aircraft's stability. The goal was to select the most appropriate wing configuration for our aircraft within the 5 ft length constraint as mentioned in Section 3.2 .

Rectangular Wing Analysis: Optimization of the rectangular wing included a focus on chord and span of wing. Analysis from OpenVSP [3] showed that varying the chord of the wing affected pitch moment and the lift-to-drag ratio. The results showed that a shorter chord wing had increased pitch moment, indicating less stable aerodynamics. Conversely, the shorter chord airfoil achieved more efficient aerodynamic performance in terms of lift-to-drag ratio. Based on this analysis, we chose a 1.32 ft chord to balance stability and efficient aerodynamics.

Tapered Wing Analysis: For the tapered wing, a taper value of 0.5 was chosen to address challenges such as tip stall [4] [5]. Results from OpenVSP [3], indicated that a smaller tip chord improved aerodynamic efficiency, whereas a larger tip chord resulted in a higher pitching moment coefficient. After evaluating the lift distribution in MATLAB [6], we chose a tapered wing with a root chord of 1.32 ft, a tip chord of 0.65 ft, and a taper ratio of 0.5 to avoid tip stall concerns.

While the tapered wing showed superior aerodynamic characteristics such as lower pitch moment and higher



lift coefficient as shown in Figure 20, practical constraints, as detailed in section 3.2, such as wingspan, parking space, takeoff distance, and rotating mechanics of wings, favored the rectangular wing. To strike a balance between performance and these constraints, we chose a design with a rectangular shape and tapered towards the wingtips (Figure 29).

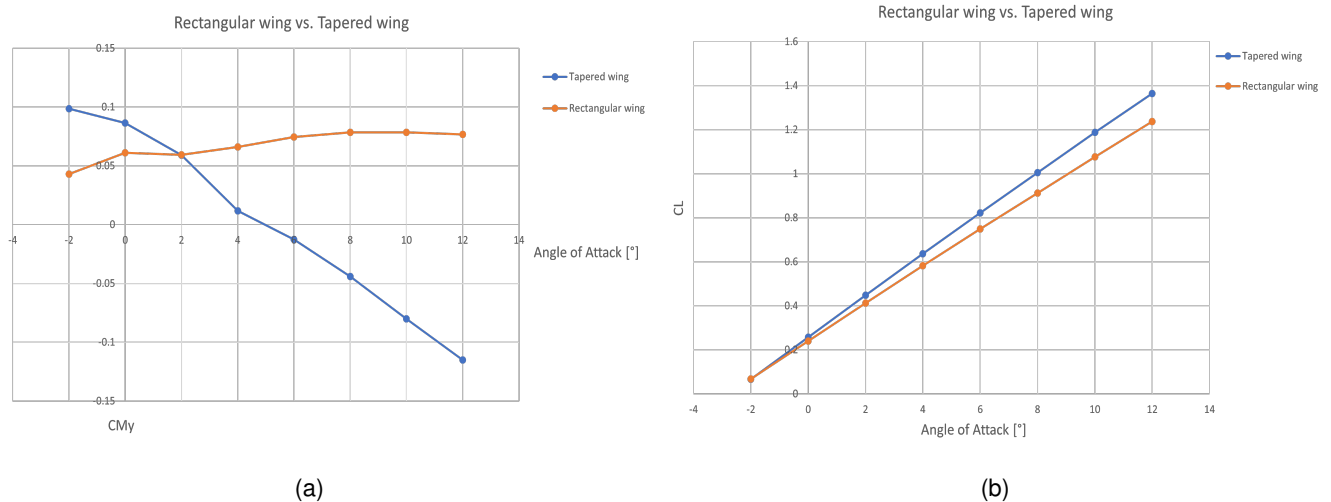


Figure 20: Comparison of Pitch Moment Coefficient at different Angle of Attack (a) and Lift Coefficient at different Angle of Attack (b) for Rectangular and Tapered shape of Wings.

4.5.3 Tail Analysis

The study of the aircraft's tail configuration focused on the horizontal and vertical tail components as we conducted extensive testing on various dimensions and shapes to optimize performance.

Horizontal Stabilizer Analysis: Consideration of dimensions, drawing insights from various sources [5] [7] [8], involved tail span of 1.47 ft, 1.64 ft, and 1.70 ft, each paired with a consistent tail chord of 0.65 ft to meet area requirements. The assessment of roll and yaw moments, obtained through OpenVSP [3], guided the decision-making process, emphasizing longitudinal stability and ultimately favoring a 1.70 ft tail length for enhanced longitudinal stability. In the pursuit of minimizing induced drag, an examination of reducing the tip chord to 0.40 ft, resulting in a taper of 0.6, revealed that such adjustments did not significantly impact performance or stability (Figure 21b). This strategic choice contributes to reduced induced drag without compromising functionality.

Vertical Stabilizer Analysis: We analyzed different vertical tail configurations, including rectangular and tapered shapes, with consideration for a dorsal fin. For the rectangular shape, the dimensions were set at a span of 0.83 ft and a chord of 0.58 ft. For the tapered shape, the same length, the root chord was set at 0.58 ft and the tip chord was set at 0.50 ft, based on literature [5] [7] [8] [9]. Exploring the addition of a dorsal fin, tests revealed minimal changes in pitch and roll, but a notable increase in yaw stability. Considering the results in Figure 21a, the tapered vertical tail with a tip chord of 0.50 ft was chosen to meet the area requirements specified in the literature. In addition,

the dorsal fin was implemented to increase stability and connectivity. This configuration provides the best balance between stability and performance.

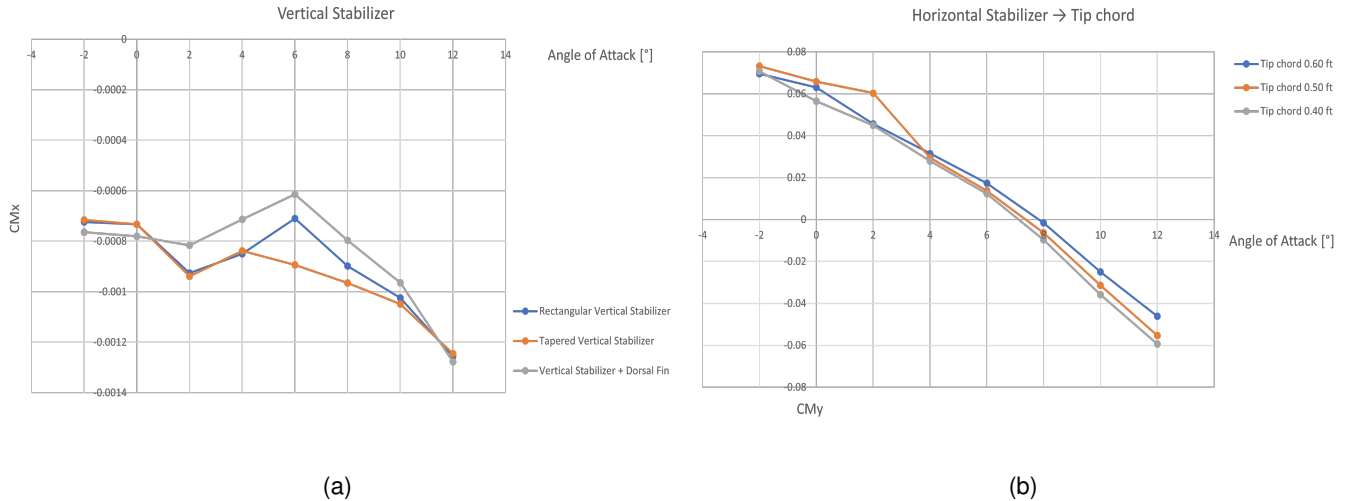


Figure 21: Tail Analysis: Influence of different Vertical Tail configurations on aerodynamic characteristic (a) and different tip chord values on pitch moment of the Horizontal Tail (b)

4.5.4 Airplane Fuselage Analysis

Guided by the AIAA competition guidelines and considering factors such as passenger load, total weight, and mission-specific components, two distinct fuselage designs were created. The first accommodates four rows in a wider, shorter fuselage, while the second accommodates two rows in a narrower, longer design. Notably, the number of passengers and total weight remain the same between the two. Simulations using Fluent 2D [10] with Spalart-Allmaras turbulence modeling were performed to analyze these configurations.

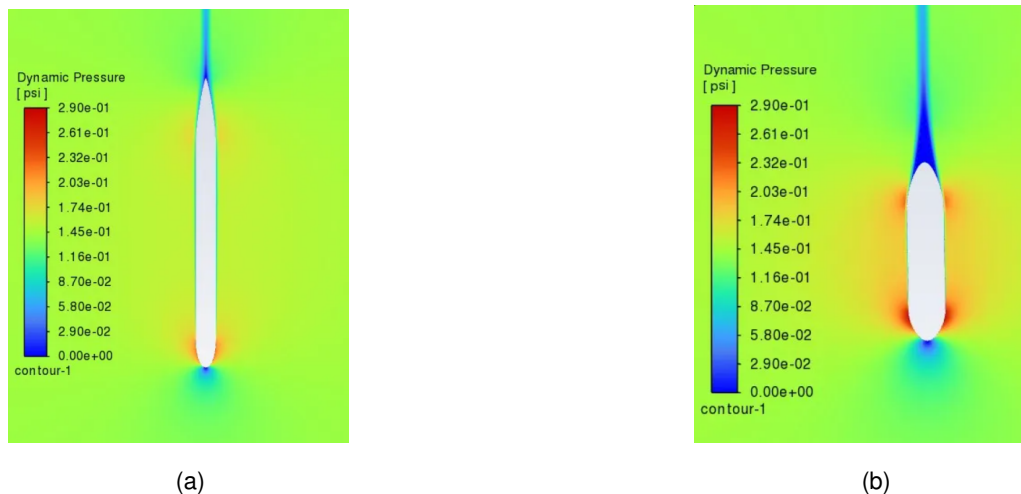


Figure 22: Comparison of the Dynamic Pressure on the wide type (a) and narrow type (b) of Fuselage



The analysis showed that the fuselage design that is narrower and longer has superior aerodynamic characteristics specifically considering dynamic pressure shown and its influence on drag as shown in . The calculated drag force for the narrower fuselage was found to be significantly lower than the wider alternative. Specifically a wider fuselage produces 3.71 lbf of air drag force and a narrower fuselage produces 1.87 lbf, suggesting that the wider fuselage is experiencing higher parasitic drag. Based on a comprehensive evaluation of these factors, we have determined that the narrower and longer fuselage design is the most optimal choice.

4.5.5 Lift And Drag Analysis

Three methods were used to evaluate the fuselage drag: Roskam/Raymer methodology [11], Torenbeek approach [9], and Improved Form Factor for Drag Estimation of Fuselages with Various Cross Sections [12]. The main drag coefficient calculation equation is shown in Eq. (26), including skin friction C_f , form factor FF , wet surface S_{wet} , and reference surface S_{ref} . The skin friction coefficient equation is given in Eq. (27), with C_f and Reynolds number Re .

$$C_D = \frac{C_f \cdot FF \cdot S_{wet}}{S_{ref}} \quad (26) \quad C_f = \left(\frac{1}{3.46 \cdot \log(Re) - 5.6} \right) \quad (27)$$

In the Equations (28) to (33), l is the length of the fuselage, d is the diameter of the fuselage, and w is the radius of the corners of the fuselage, cs_1 , cs_2 , cs_3 are coefficients in form factor equation (Eq. 30)

$$FF = 1 + \frac{0.0025 \cdot l}{d} + \frac{60}{\left(\frac{l}{d}\right)^3} \quad (28) \quad cs_1 = -0.825885 \cdot \left(\frac{2r}{w}\right)^{0.4117995} + 4.0001 \quad (31)$$

$$FF = 1 + \frac{2.2}{\left(\frac{l}{d}\right)^{1.5}} + \frac{3.8}{\left(\frac{l}{d}\right)^3} \quad (29) \quad cs_2 = -0.340977 \cdot \left(\frac{2r}{w}\right)^{7.54327} - 2.27920 \quad (32)$$

$$FF = cs_1 \cdot \left(\frac{l}{w}\right)^{cs_2} + cs_3 \quad (30) \quad cs_3 = -0.013846 \cdot \left(\frac{2r}{w}\right)^{1.34253} + 1.11029 \quad (33)$$

The results of the calculated drag coefficient using different equations for Form Factor are shown in the Table 5

Table 5: Calculated drag for fuselage using different methods

Roskam/Raymer old [Eq. 28]	Torenbeek [Eq. 29]	Improved Form Factor Method [Eq. 30]
$C_D = 0.0040$	$C_D = 0.00369$	$C_D = 0.0043$

For the final phase of calculating the drag on all aircraft components, we chose to use the Torenbeek method to determine the form factor for calculating the drag coefficient. Our decision was influenced by the detailed definition of all aircraft components in the OpenVSP [3] software with integrated Torenbeek method. This detailed definition allowed accurate calculations of volume, area and related parameters that affect the drag calculation. Drag contributions during cruise flight at a speed of 98.40 ft/s are shown in Figure 23.

For the lift analysis, we used MATLAB [6] to evaluate the lift coefficient distribution across the wing based on a segmentwise approach. The analysis, which was tailored to our specific wing parameters, calculated the lift coefficients for each segment, taking into account factors such as aspect ratio, taper ratio, and wing area. The resulting

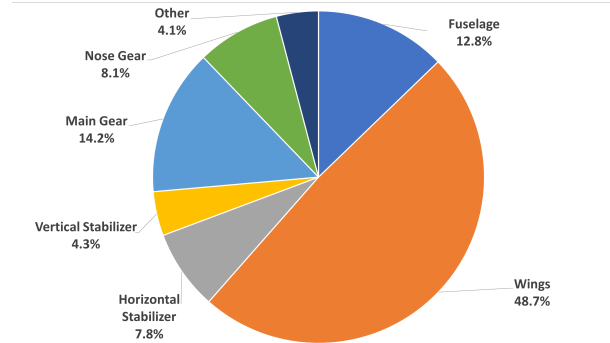


Figure 23: Drag Contributions

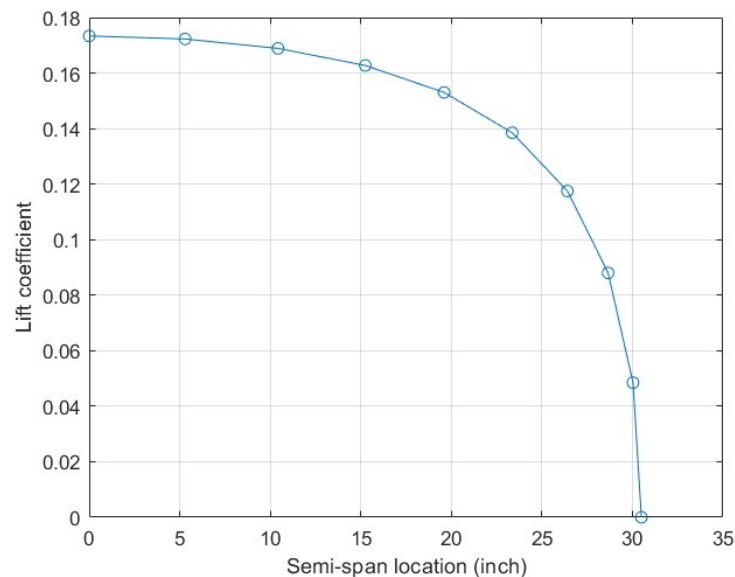


Figure 24: Lift coefficient distribution across wing

distribution plot vividly illustrates how the lift coefficients vary along the half-span positions. This analysis allowed us to visualize and understand the lift coefficient distributions across the span. In the Figure 24, the blue curve represents the lift distributions across the wing during cruise flight at a speed of 98.40 ft/s.

4.6 Dynamic stability

Dynamic stability of the aircraft was performed in AVL [13] program. Analysis was conducted for M2 at cruise speed. M2 was selected for the analysis because this mission has longest endurance and aircraft will weight the most. All dynamic stability data is shown in table 6. Data for three oscillating modes show that all of them have damping factors smaller than 1 meaning they are under damped. The most critical is Dutch Roll which has the lowest damping factor. While all oscillating modes are under damped, they are still stable. Both non-oscillating modes which are roll and spiral modes are both stable. This is very important for flying in Wichita since strong wind gusts are expected.



Table 6: Dynamic stability of the aircraft in M2 at cruise speed

Mode	Longitudinal Modes		Lateral Modes		
	Short Period	Phugoid	Dutch Roll	Roll	Spiral
Eigenvalue	$-9.62 \pm i13.23$	$-0.048 \pm i0.28$	$-1.01 \pm i8.81$	-40.87	-0.044
Damping factor [/]	0.588	0.165	0.114	/	/
Natural Frequency [Hz]	2.1	0.046	1.4	/	/

4.7 Estimated Mission Performance

All performance characteristics were calculated within the SAS optimization process, described in Sections 4.2 and 4.3, and then further corrected using the findings from Section 4.5. Table 7 contains the predicted aircraft performance in each mission. Optimal M2 score can be achieved with a 6.60 lbs medical cabinet on board with an average lap time of 23.47 s. It is estimated that the aircraft can fly 13 laps in M3 while loaded with 48 passengers. Using the propulsion configuration listed in Table 3, speed profiles regarding the time of the first three laps in M2 and M3 were obtained. Every decrease in speed, visible in Figures 25 and 26, corresponds to the turn maneuver.

Table 7: Preliminary design mission performance characteristics

Performance Parameter	M1	M2	M3	GM
$C_{l_{max}}$	1.61	1.61	1.61	/
$C_{l_{cruise}}$	0.37	0.37	0.35	/
$C_{d_{cruise}}$	0.02	0.02	0.03	/
L/D_{cruise}	13.17	13.30	12.66	/
Wing Loading [lbs/ft ²]	1.08	2.13	1.80	/
v_{cruise} [ft/s]	143.1	143.6	140.02	/
v_{stall} [ft/s]	28	38.77	36.28	/
Aircraft MTOW [lbs]	7.13	14.02	11.85	Varied
Carried Payload	/	2 EMTs, Gurney, Patient, Medical Cabinet	48 Passengers	Varied
Number of Laps	3	3	13	/
Mission Time [s]	65	70.4	290.3	84
Mission Score	1	1.83	2.76	0.84

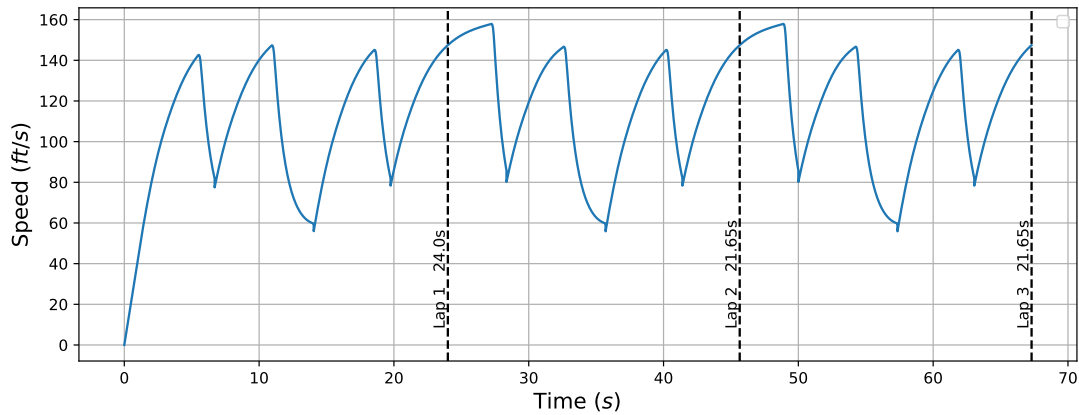


Figure 25: M2 speed profile

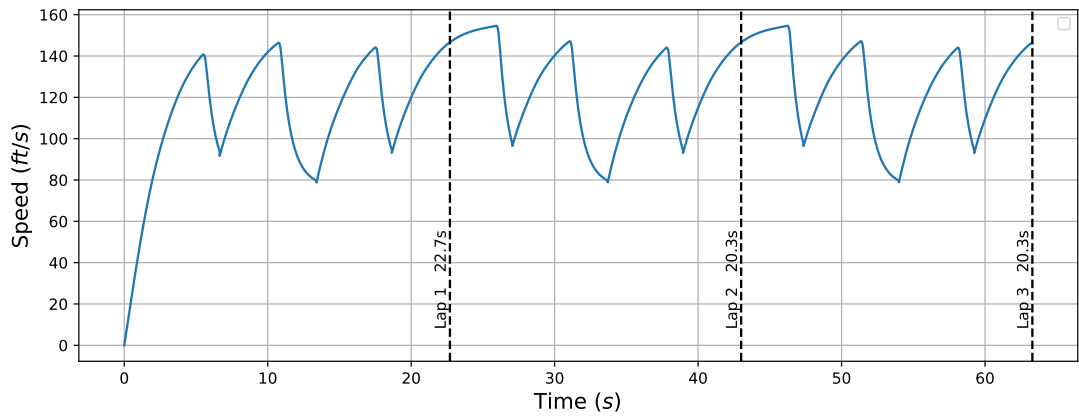


Figure 26: M3 speed profile for the first three laps

5. Detail design

5.1 Dimensional parameters

Table 8 shows the main aircraft dimensions and characteristics the team deemed ideal for the 2024 AIAA Design, Build, Fly competition.



Table 8: Aircraft dimensions

Fuselage		Vertical Tail	
Total length [in]	60.91	Airfoil	NACA0010
Cockpit length [in]	12.5	Span [in]	10
Tail Length [in]	6.9	Chord-base [in]	7
Width [in]	5.35	Chord-tip [in]	6.1
Height [in]	4.22	Wing Area [in ²]	60
Wing		Aspect Ratio	1.7
Airfoil	MH70	Angle of Incidence [°]	0
Span [in]	59.11	Horizontal Tail	
Chord-base [in]	15.82	Airfoil	NACA0010
Chord tip [in]	11.86	Span [in]	20.44
Wing Area [ft ²]	6.56	Chord-base [in]	7.89
Aspect Ratio	3.81	Chord-tip [in]	4.72
Angle of Incidence [°]	2	Wing Area [in ²]	130
Dihedral Angle [°]	2	Aspect Ratio	3.2
Twist [°]	0	Angle of Incidence [°]	0

5.2 Systems and Sub-Systems Integration

5.2.1 Fuselage

The fuselage design is based on conventional norms of aircraft fuselage design (Figure 27). A very narrow, streamlined shape was chosen to minimize drag (4.5.4). The fuselage slowly widens from the frontal section, where the cockpit and the electronics are placed, to the passenger compartment. The electronics are placed in such a way as to provide a clear view for the pilots. Each pilot is secured to the aircraft with a TPU ring that grips the lower part of the pilot. The passenger compartment extends from the bulkhead almost to the back of the aircraft, where it quickly tapers to the empennage. The cross-sectional shape of the fuselage is square with filleted edges to accommodate passengers efficiently.

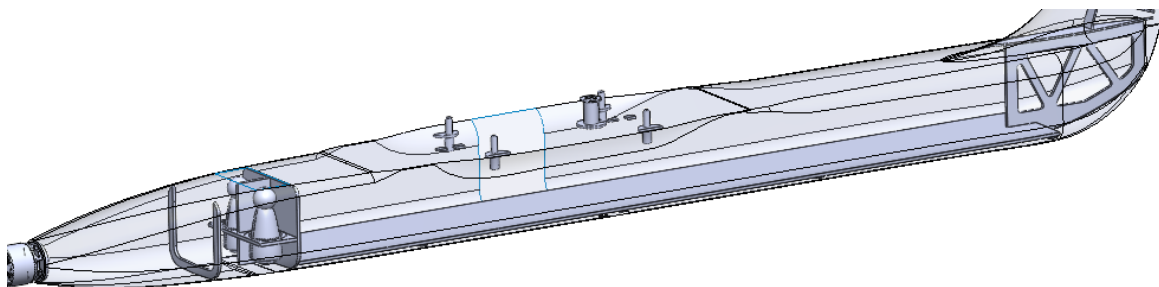


Figure 27: Detail fuselage design

From previous competition experience it was deemed best to construct the fuselage from carbon fiber and hon-



eycomb composite material, as this combination offers the best strength-to-weight ratio. Fiberglass-foam composite frames and carbon fiber or aramid reinforcements are placed in the fuselage to help transfer loads from critical locations. Because of space limitations, the passenger compartment contains almost no frames which is compensated for with additional carbon fiber reinforcements that increase the rigidity of the monocoque. The passenger compartment floor is a fiberglass-foam composite that also acts as a structural element.

The side hatch for the Medical Cabinet is located below the wing to prevent the cabinet from affecting the CG too much. Another side hatch is located at the rear of the aircraft where the fuselage transitions to the empennage. At the front of the aircraft, two additional hatches are located at the top; one to provide access for the crew and another for electronics. All hatches are secured with velcro strips.

5.2.2 Empennage

The empennage consists of a vertical and horizontal stabilizer in a T-tail configuration, which enables easier access to the rear passenger compartment hatch (Figure 28). The horizontal stabilizer is moved aft of the vertical to allow for better elevator control and is attached to the aircraft with two bolts. The vertical stabilizer is merged with the fuselage.

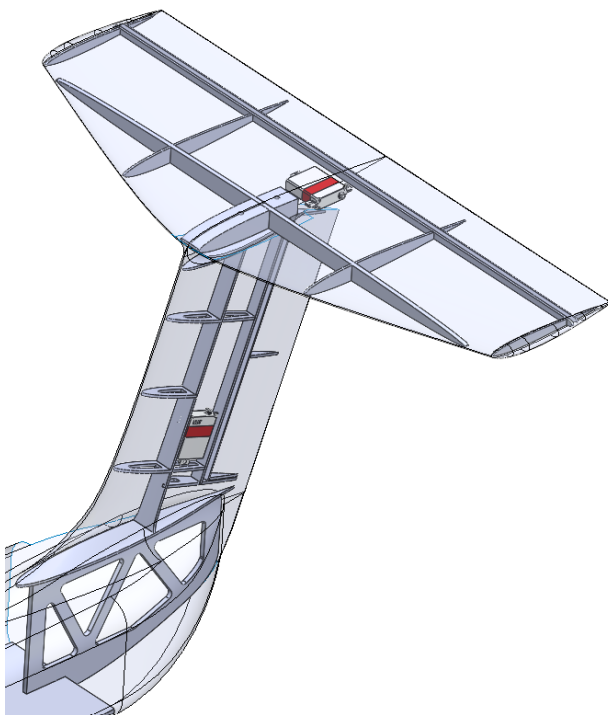


Figure 28: Empennage design

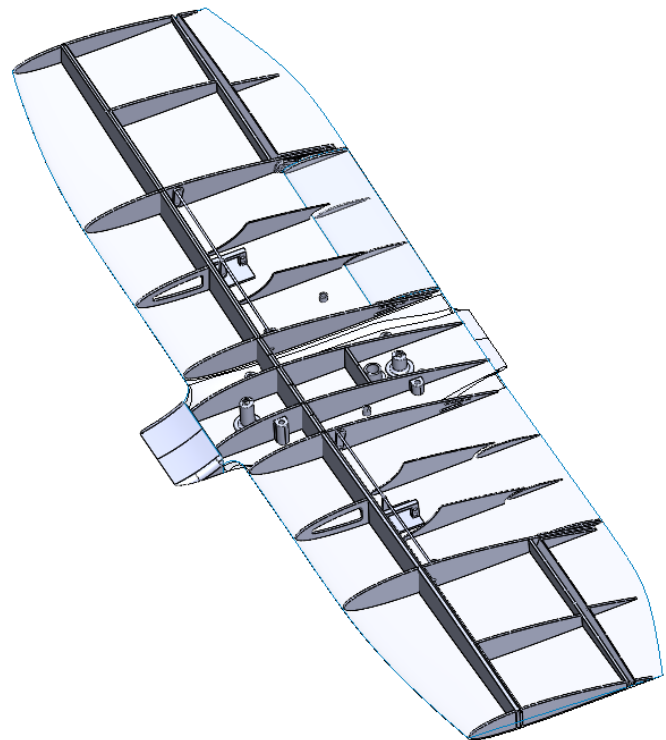


Figure 29: Wing design



5.2.3 Wing

The wing is of a roughly rectangular shape and tapered towards the wingtips (Figure 29). It has a dihedral angle of 2° for increased stability. The skin of the wing is a carbon fiber and honeycomb composite, whereas the wing spar is a carbon fiber and foam composite. UD carbon fiber is placed above and below the spar, to provide flexural stiffness. Fiberglass-foam composite ribs are spaced equally along the span of the wing to prevent buckling and indentation.

Because of STOL requirements, we used Fowler flaps in our design (Figure 30). They consist of a separate flap airfoil that is connected to the wing via guides in carbon fiber ribs at both sides. The servo motor is also connected to both sides and actuates the flap, whereas the guides ensure the flap moves with the required kinematics.

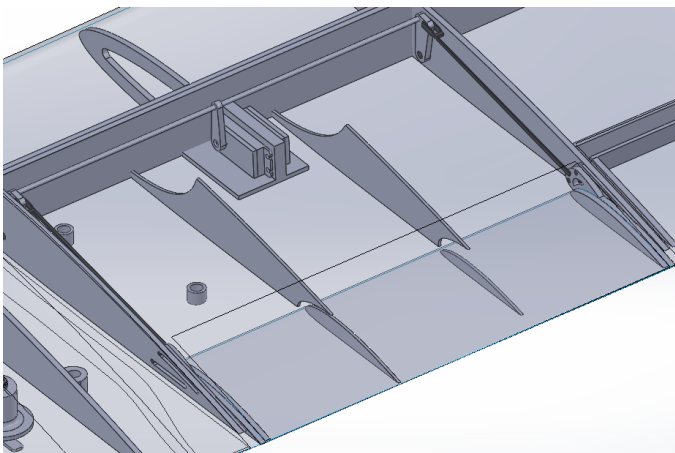


Figure 30: Fowler flap design

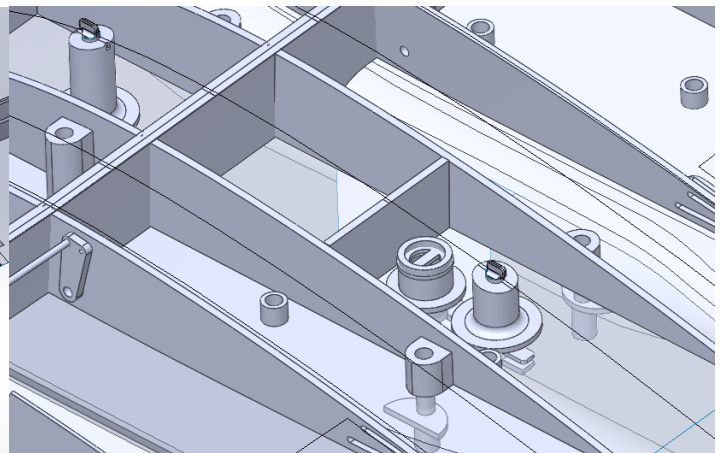


Figure 31: Rotation mechanism design

5.2.4 Parking Mechanism

To comply with the parking limitation, the wing and the fuselage feature a mechanism that allows the wing to rotate above the fuselage (Figure 31). The wing is held in place with 4 pins and 2 latches. The pins are located at the side of the fuselage and position the wing while also transmitting moments along the vertical axis. The two latches are placed at the centerline. They consist of a rod with a flat plate at the end. When the rod is rotated 90° , the plate is wedged below a protrusion in the fuselage and prevents the wing from moving vertically, while friction prevents the plate from unlatching. Two latches are implemented for additional safety. A hollow tube provides the axis around which the wing is rotated. It also enables the cables to pass from the fuselage to the wing. A spring-loaded cap on top of the tube prevents the wing from separating from the aircraft, while enabling enough vertical movement to lift the wing above the pins and put it into the parking configuration. Extra pin holes are placed in the wing to hold it when parked.



5.2.5 Passenger Compartment

The passenger compartment occupies most of the fuselage. It consists of a plane, horizontal floor constructed out of fiberglass-foam composite. Two side hatches - one under the wing and one at the rear of the aircraft, allow the payload to be inserted.

For mission 3, the passengers are placed into the 2 inserts before loading. The insert is a carbon fiber C-shaped profile. Each passenger is placed in its own hole in the insert. Flexible TPU "inserts" ensure the passengers are completely restrained. The inserts are then loaded through the rear hatch. The first insert is loaded into the airplane and slid laterally. It is held in place by a protrusion at the bulkhead, which restricts vertical and longitudinal movement. A similar protrusion holds the insert on the rear side. Velcro prevents the insert from sliding laterally. The second insert is loaded parallel to the first one. It uses the same restraint system at the bulkhead, but uses a pin at the rear. The pin is pushed through a hole in the floor. Guides are placed along the passenger compartment to additionally restrain the inserts. (Figure 32).

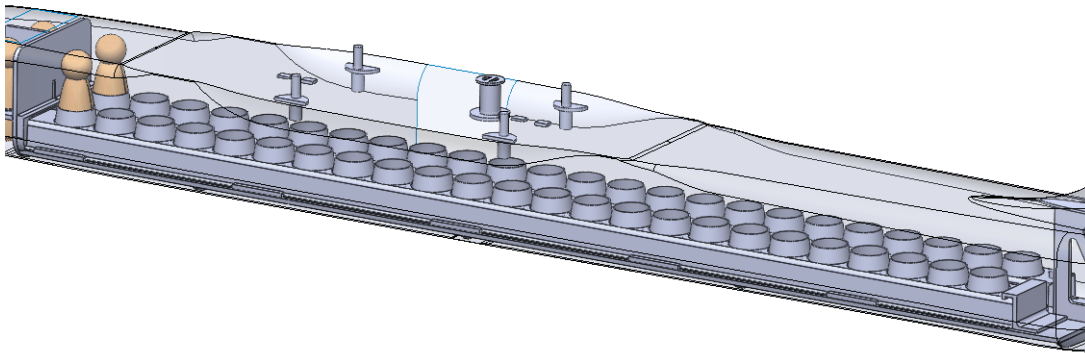


Figure 32: M3 passenger compartment layout

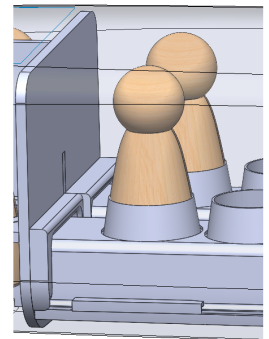


Figure 33: Front closeup

For mission 2, the Medical Cabinet is inserted through the hatch under the wing. Guides on both sides restrain longitudinal movement. Vertical movement is restrained by the floor and the ceiling, while velcro strips prevent the package from moving sideways. The EMTs are placed into an insert and then loaded into the airplane the same way as the passengers in Mission 3. The patient with the gurney is loaded in a similar way to the first insert in Mission 3 - the same protrusion is used at the rear to hold the gurney while a frame and velcro hold the gurney on the other side. The patient is secured to the gurney with two plastic clips. (Figure 34).

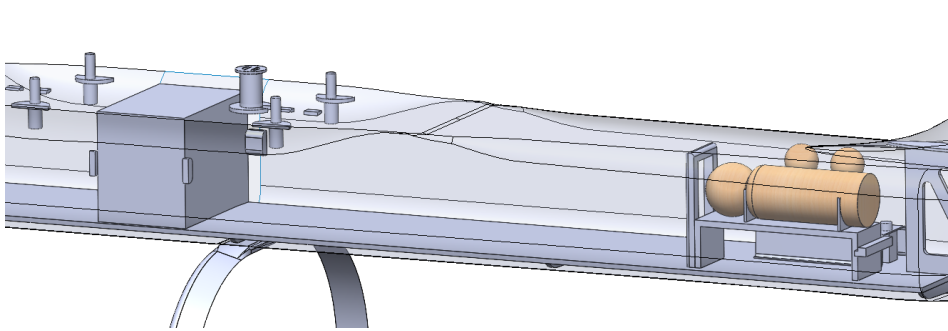


Figure 34: M2 passenger compartment layout

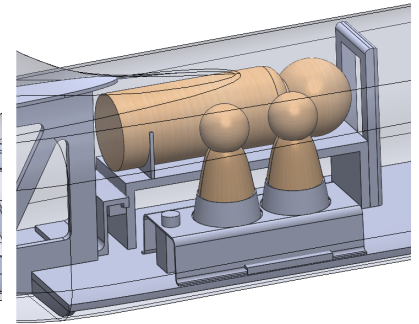


Figure 35: Rear closeup

5.2.6 Landing gear

The front landing gear is fork-shaped and the rear landing gear is U-shaped. (Figure 36) Both are made out of forged carbon fiber and are 7.10 in tall to give enough ground clearance for the propeller. Additionally, the rear landing gear is 15 in wide to ensure stability during takeoff and landing. To reduce drag, all wheels are covered by fairings.

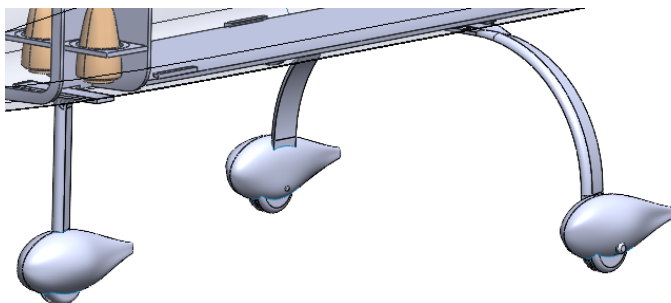


Figure 36: Landing gear design

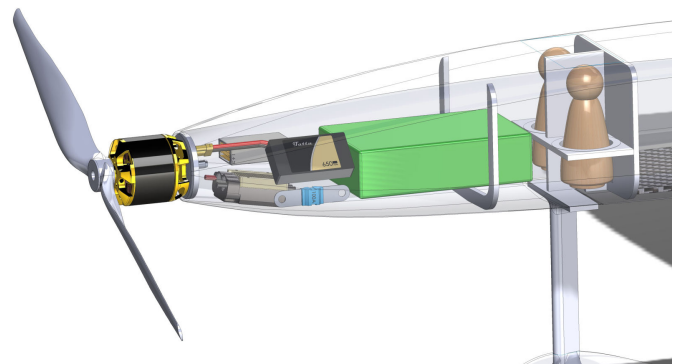


Figure 37: Propulsion design

5.2.7 Propulsion

The motor is mounted outside at the nose of the aircraft through a composite firewall for CG and cooling purposes (Figure 37). The ESC is located in the nose and is pressed to the skin of the fuselage, where holes provide sufficient cooling. The battery pack, which is connected to the ESC, is placed as forward as it fits to move the CG toward the front. Arming plug is located under the fuselage, below the battery and consists of two 0.31 in gold plated connectors accessible from the outside with a 100 A automotive fuse in between.

5.2.8 Avionics

To ensure safe flight and provide the pilot with the best possible control of the aircraft, a dual-band FrSky Tandem TD SR10 receiver was used. The receiver works simultaneously at both 2.4 GHz and 900 MHz frequencies, offering



low latency and reliable signal integrity. It also offers precise in-flight stabilization which will help the pilot mitigate the high winds in Wichita. No additional sensors were included in the final design, as the ESC offers voltage, current, and motor RPM data, which is sufficient to further adjust our SAS model during the competition and adjust our strategies to ensure optimal performance. Lastly, a 650 mAh 2S lithium polymer battery was used to power the receiver and servo motors.

5.2.9 Structural Characteristics

The aircraft structure is designed to direct loads from each subsystem to the major load-bearing components of the aircraft. (Figure 38). The motor thrust and torque are directed through a composite motor mount into the fuselage. Ground loads from the landing gears are directed to the fuselage through carbon fiber reinforcements and frames. Aerodynamic loads on the wing are transmitted through ribs to the spar, and then to the pins and the latches, which are connected to the fuselage. Aramid fiber reinforcements are placed under the latches, to prevent the skin from failing suddenly and catastrophically. The loads from the horizontal stabilizer are directed to the fuselage through the vertical stabilizer. Because of that, the vertical stabilizer structure is reinforced, and a dorsal fin is added to increase shell rigidity.

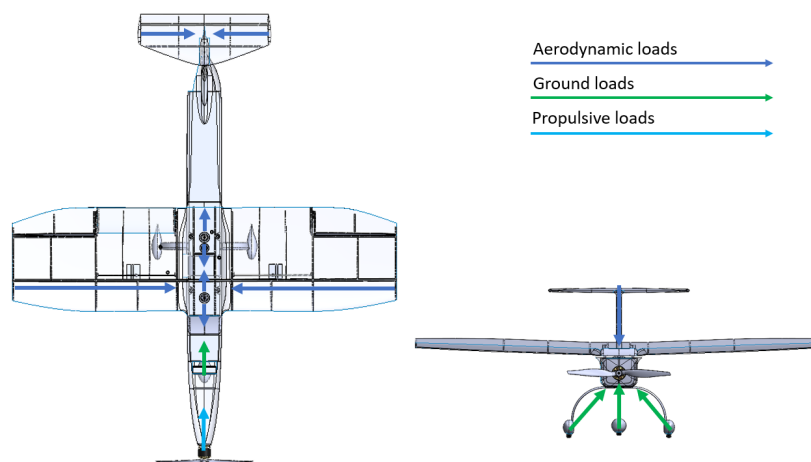


Figure 38: Load path diagram

A numerical analysis was conducted to size the wing structure. The goal of the conducted analysis was to obtain data on the load distribution of the aircraft wing and individual components, to calculate the structural strength of the aircraft wing. We decided on a static analysis of the model under loads that occur during sharp turns, which will be prevalent in the competition, to achieve the best results in the third mission. The analysis was performed in the Ansys software environment [10], using a previously prepared simplified planar model of one half of the wing. The meshed body consists of cells sized at 0.315 in. In the analysis, the model was statically fixed at the cut half of the wing, and the lower and upper surfaces of the wing were divided into 3 spanwise segments for more precise determination of loads on each part. Pressure distribution on the wing resulting from the airflow was computed with Xfoil and transferred as a boundary condition to Ansys. We found that the lift coefficient of the airfoil steeply



increases up to an angle of 15° where the airfoil stalls. Therefore, we decided to analyze the wing at an AoA of 12° . The obtained pressure distribution was used to calculate the force on each selected wing surface and then converted into the surface pressure of each segment. During sharp turns, piloted aircraft experience loads of up to 5 G [1]. A RC aircraft can greatly exceed these values because of their high agility, thus we decided to use an assumed load value of 10 G. Since we observed half of the wing model, we considered half the value of the total load that amounts to 5 G, at MTOW.

The deformation of the aircraft wing (total deformation), measured in millimeters is presented in Figure 39. The maximum wing deflection of 0.4368 in occurs in the lower right part, which is an acceptable deflection.

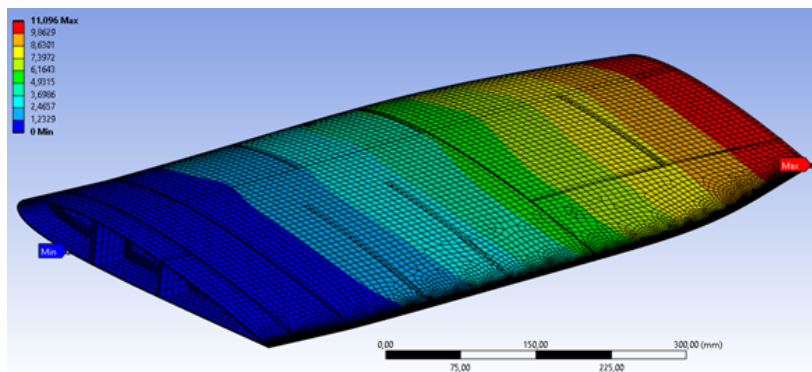


Figure 39: Total deflection of the wing

Figure 39 represents the deformation of individual elements in the assembly. The most noticeable compression and expansion of cells occur inboard, on the surfaces of the spar and the wing skin in vicinity - additional reinforcements are placed in this location. Figure 41 illustrates the stresses on the spar, which are highest at the initial section of the spar, where the wing is constrained. The maximum stress value is 12489 psi, which is well below the compressive strength of carbon fiber composites [14].

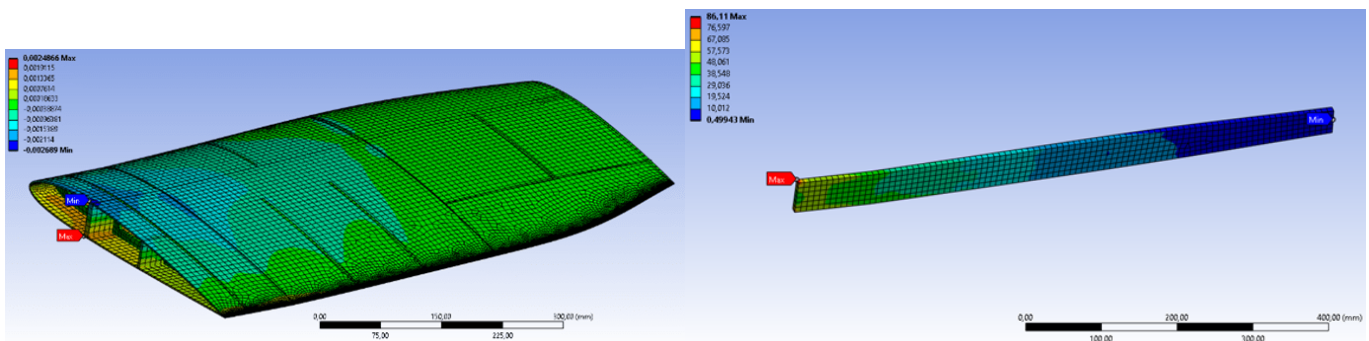


Figure 40: Display of normal elastic deformation of the wing

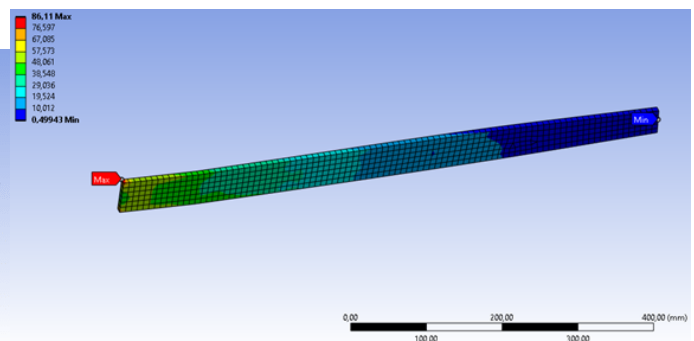


Figure 41: Stress loading of the spar

We also conducted a failure analysis of the aircraft's wing over the entire model surface with the inbuilt Ansys composite failure tool, focusing mainly on critical areas. The obtained results showed that the static load on critical



areas accounts for 33% of the failure strength load, confirming the wing's static strength. The difference between the current magnitude of the load and the failure value represents a safety factor, as the obtained results are from static analysis and values during flight can vary significantly due to additional environmental influences.

5.2.10 Wight and Balance

Weight and balance are crucial steps for good flight stability in aircraft design. The planned CG is set to be at around 25% MAC of the wing. The aircraft was designed with Mission 3 in mind, as that payload is the greatest restriction in terms of CG – a large insert filled with passengers. Mission 2 payloads were then positioned in a way to not affect the CG too much; the cabinet under the wing, and the passengers at the back. In Mission 1, a ballast weight is placed in the aircraft to compensate for a lack of payload, so no special design considerations are required. The weight of all components was calculated from CAD models and weighting of the manufactured components. Table 9 contains complete weight and balance data for all flight missions.

Table 9: Weight & Balance

Aircraft Component	Weight [lb]	Z [in]	Y [in]	Aircraft Component	Weight [lb]	Z [in]	Y [in]
M1							
Propeller	0.099	-1.96	0	Wing	2.20	27.56	3.54
Motor	0.99	-0.98	0	Servo battery	0.15	5.51	0.59
Fuselage	0.92	31.50	-0.20	Transmitter	0.03	7.09	0.79
ESC	0.26	4.72	0.39	Vertical stabiliser	0.18	58.27	7.28
Propulsion battery	1.43	5.90	0	Horizontal stabiliser	0.26	62.00	12.01
Front landing gear	0.18	11.61	-4.52	M1 balast weight	1.10	55.12	0
Rear landing gear	0.26	30.51	-4.13				
Total M1	8.09	24.36	1.29				
M2							
Medical cabinet	6.61	27.56	0				
EMT and patient	0.55	51.18	0.47				
Total M2	14.15	24.50	0.76				
M3							
Passengers with inserts	4.85	31.50	-0.39				
Total M3	11.84	24.42	0.72				

5.2.11 Flight and Mission Performance

Flight performance characteristics as well as mission results of the final aircraft were determined and are shown in Table 10.



Table 10: Mission performance characteristics

Performance Parameter	M1	M2	M3	GM
$C_{l_{max}}$	1.6	1.6	1.6	/
$C_{l_{cruise}}$	0.33	0.33	0.31	/
$C_{d_{cruise}}$	0.02	0.02	0.03	/
L/D_{cruise}	16.5	16.5	10.33	/
Wing Loading [lbs/ft ²]	1.08	2.13	1.80	/
v_{cruise} [ft/s]	140.4	140.4	134.1	/
v_{stall} [ft/s]	27	35.5	33.3	/
Aircraft MTOW [lbs]	8.09	14.15	11.84	Varied
Carried Payload	/	2 EMTs, Gurney, Patient, Medical Cabinet	48 Passengers	Varied
Number of Laps	3	3	13	/
Mission Time [s]	72.5	75.1	297	86

5.2.12 Drawing package

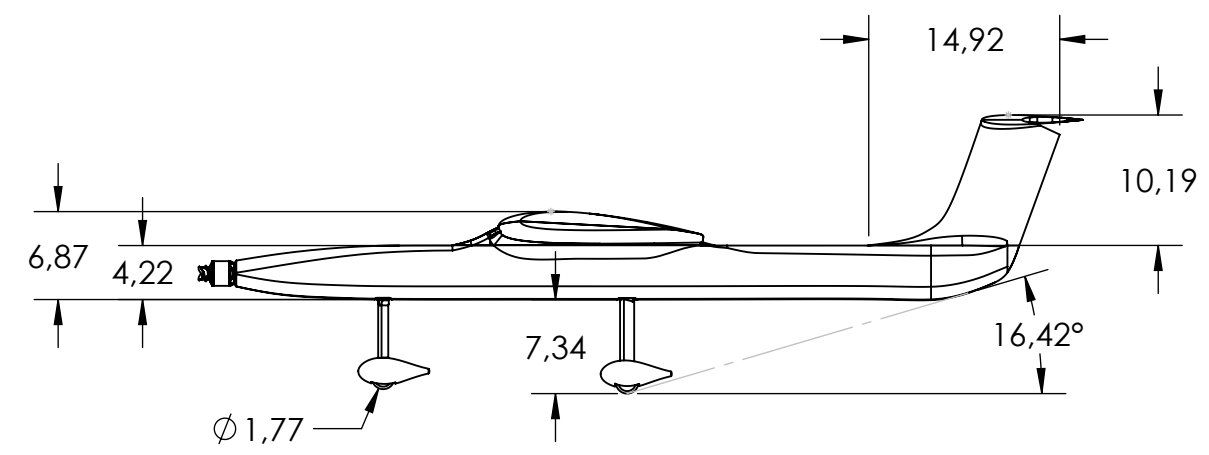
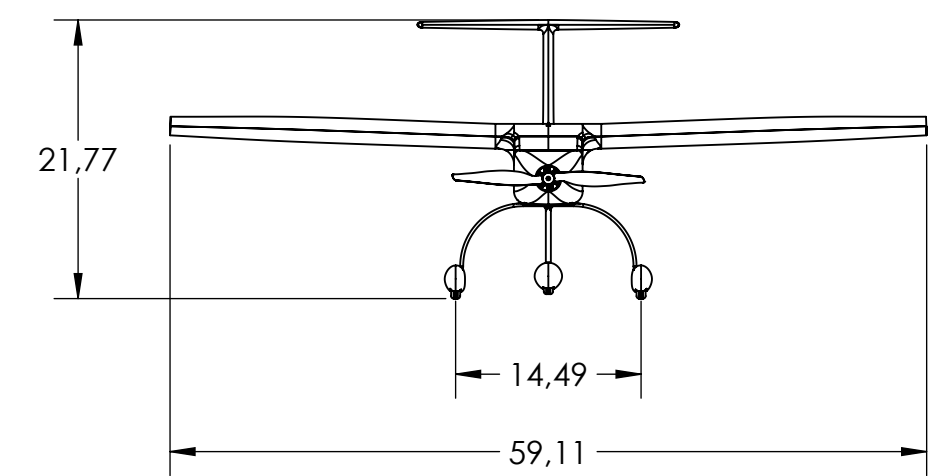
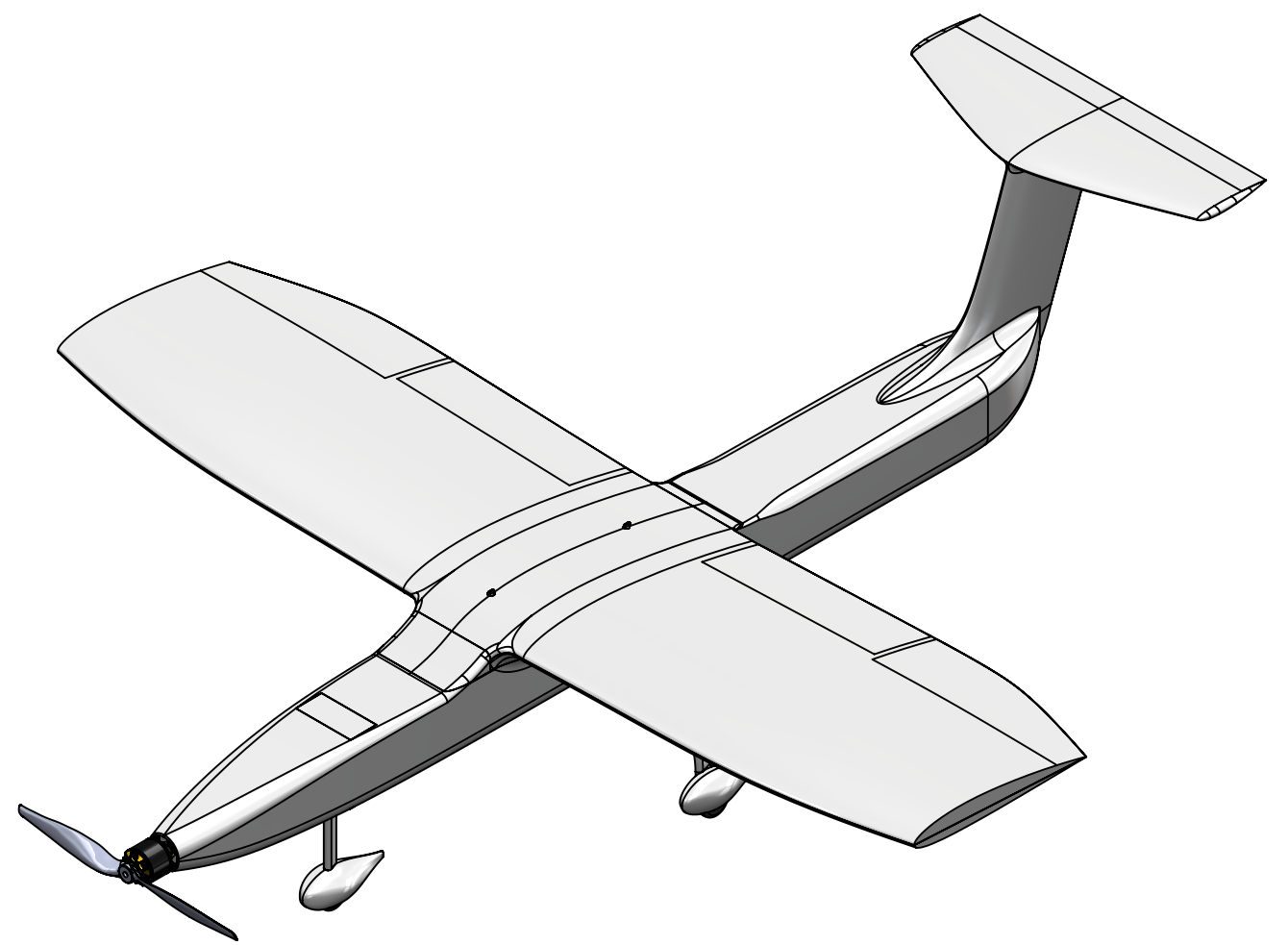
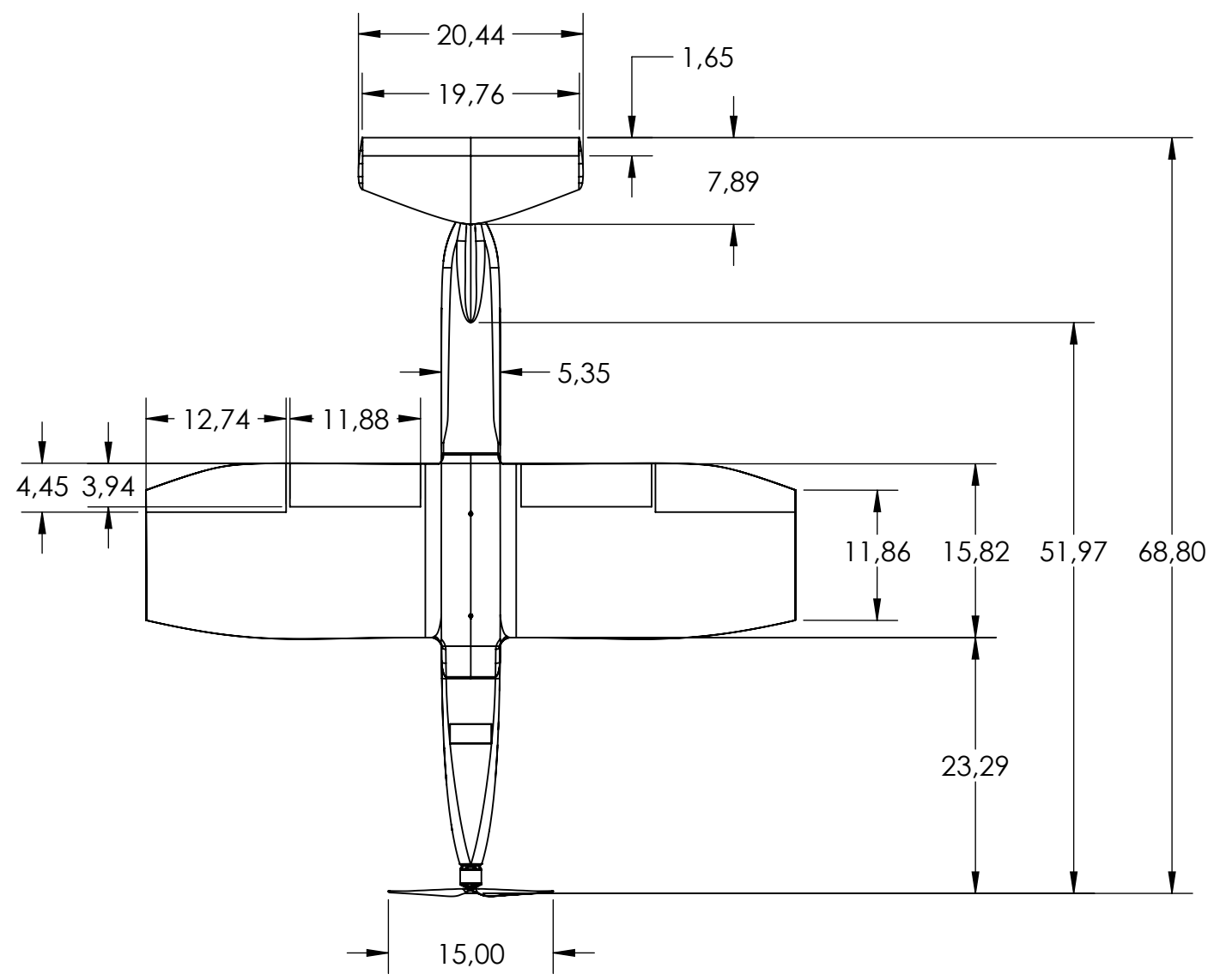
The following section contains the 3-view drawing, the structural arrangement drawing, the systems layout drawing and the payload accommodation drawing. The first sheet shows the 3-view drawing with dimensions of all configurations, the following two sheets show structural arrangement and systems layout. The last page in this section shows the payload accommodation and the wing rotation mechanism.

4

3

2

1



	NAME	DATE	UNIVERSITY OF LJUBLJANA TEAM EDVARD RUSJAN	
DRAWN	Krivos M.	19. 2. 24	TITLE:	
CHECKED	Kambic L.	21. 2. 24	3 POINT VIEW	
ENG APPR.			SIZE	DWG. NO.
MFG APPR.			B	ER2024-1
Q.A.			SCALE: 1:15	WEIGHT: /
COMMENTS:				SHEET 1 OF 4
				REV

3

2

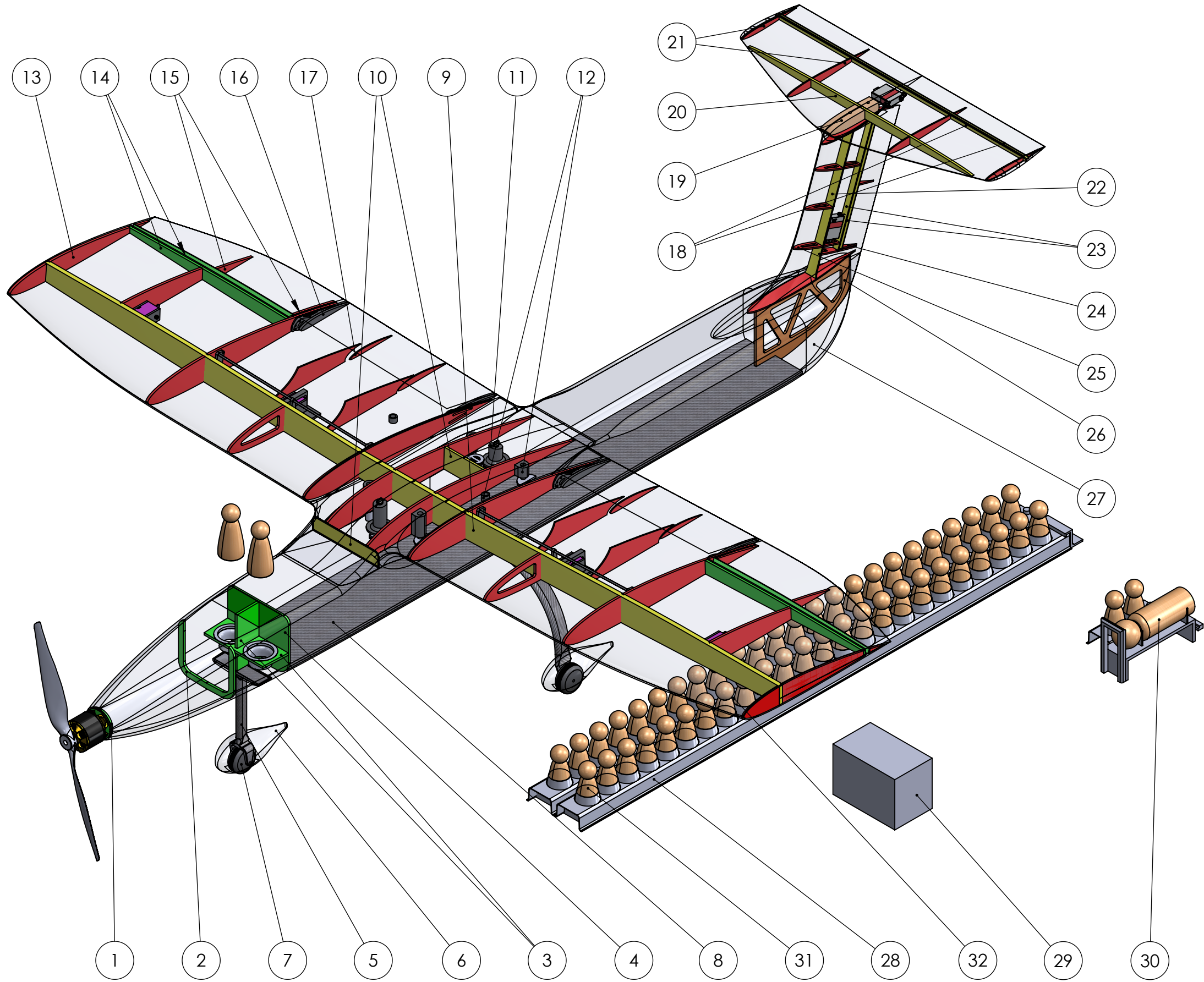
1

4

3

2

1



ITEM	QTY.	DESCRIPTION	MATERIAL
1	1	Firewall	Aramid
2	1	Fuselage rib	GF + foam
3	2	Cockpit structure	GF, foam, TPU
4	1	Bulkhead	GF + foam
5	1	Front strut	CF
6	3	Wheel fairing	GF
7	3	Wheel	Rubber
8	1	Floor	CF
9	1	Wing spar	CF + foam
10	2	Wing secondary spar	GF + foam
11	3	Rotation mechanism	PAHT
12	8	Wing Alignment pin	PAHT
13	14	Wing rib	GF + foam
14	4	Aileron spar	GF + foam
15	6	Aileron rib	GF + foam
16	8	Fowler flap rail	PAHT
17	4	Fowler flap rib	GF + foam
18	2	Elevator spar	GF + foam
19	1	Horizontal tail mount	Balsa
20	1	Horizontal tail spar	GF + foam
21	4	Horizontal tail rib	GF + foam
22	1	Vertical tail spar	GF + foam
23	2	Rudder spar	GF + foam
24	3	Rudder rib	GF + foam
25	3	Vertical tail rib	GF + foam
26	1	Hatch rib	GF + foam
27	1	Rear hatch	CF
28	1	Passenger insert	CF, TPU
29	1	Medical cabinet	Plywood
30	1	Patient, EMTs	CF, LW-PLA
31	1	Passenger	Birch
32	/	Aircraft skin	CF

	NAME	DATE	UNIVERSITY OF LJUBLJANA EDVARD RUSJAN TEAM		
DRAWN	Kravos M.	20. 2. 24	TITLE: Structural arrangement		
CHECKED	Kambic L.	21. 2. 24			
ENG APPR.					
MFG APPR.					
Q.A.					
COMMENTS:			SIZE	DWG. NO.	REV
			B	ER2024-2	
	SCALE: 1:6	WEIGHT:	SHEET 2 OF 4		

4

3

2

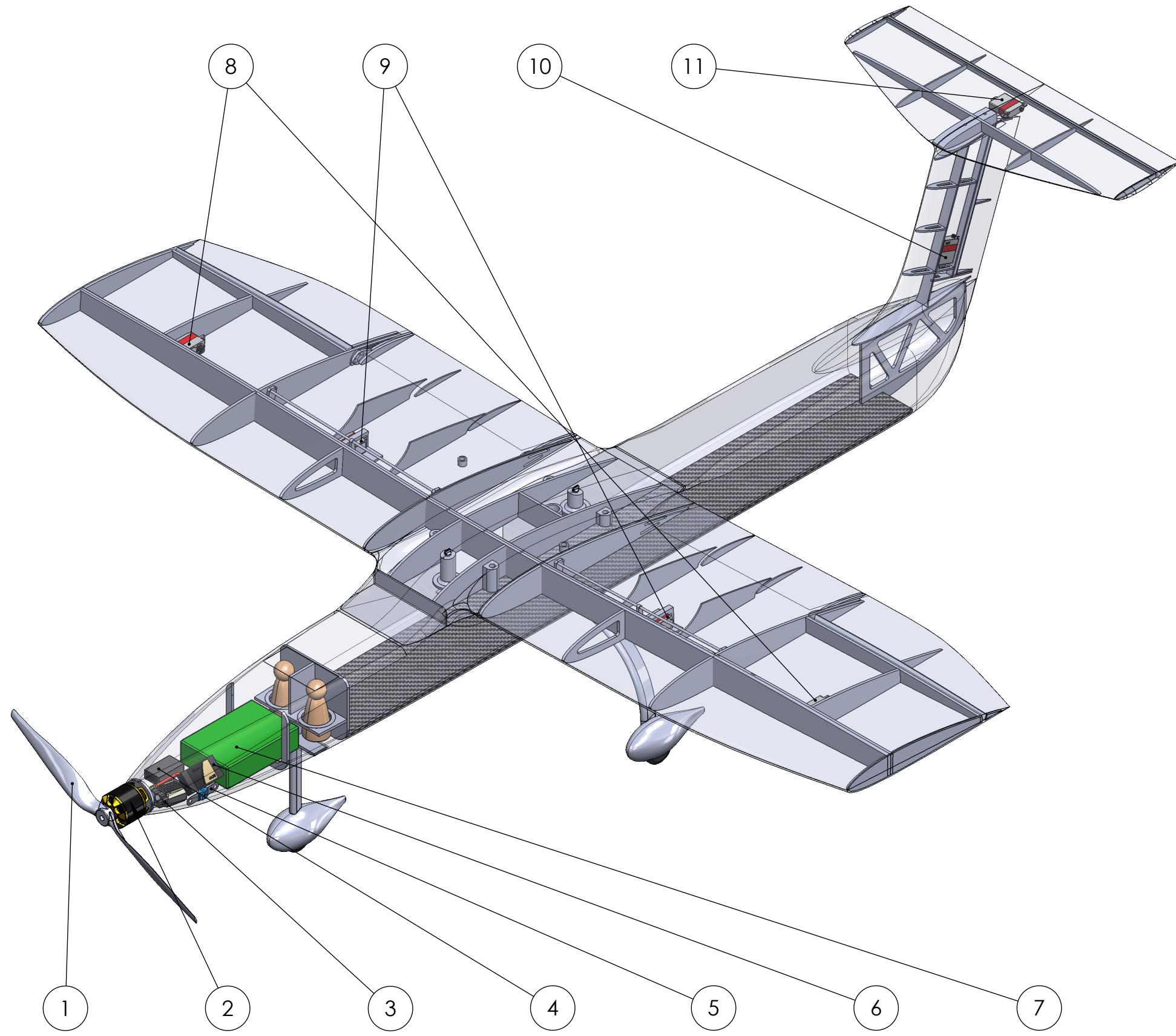
1

4

3

2

1



ITEM	QTY.	SYSTEM	DESCRIPTION
1	1	Propeller	APC 14x6E / 15X6E
2	1	Electric motor	Scorpion SII-4035 330KV
3	1	ESC	AeroStar Advance 150A HV
4	1	Receiver	FrSky TD SR10
5	1	Fuse	Littlefuse 142.5631.6102
6	1	Receiver battery	Tattu 650mAh 2S1P 75C 7.4V
7	1	Propulsion battery	LiPo 2000mAh 12S1P 44.4V
8	2	Aileron servo	KST DS1509MG HV
9	2	Fowler flap servo	KST DS1509MG HV
10	1	Rudder servo	KST X10
11	1	Elevator servo	KST X10

	NAME	DATE	UNIVERSITY OF LJUBLJANA EDVARD RUSJAN TEAM		
DRAWN	Krivos M.	21. 2. 24	TITLE: Systems arrangement		
CHECKED	Kambic L.	22. 2. 24			
ENG APPR.					
MFG APPR.					
Q.A.					
COMMENTS:			SIZE	DWG. NO.	REV
			B	ER2024-3	
			SCALE: 1:6	WEIGHT: /	SHEET 3 OF 4

4

3

2

1

4

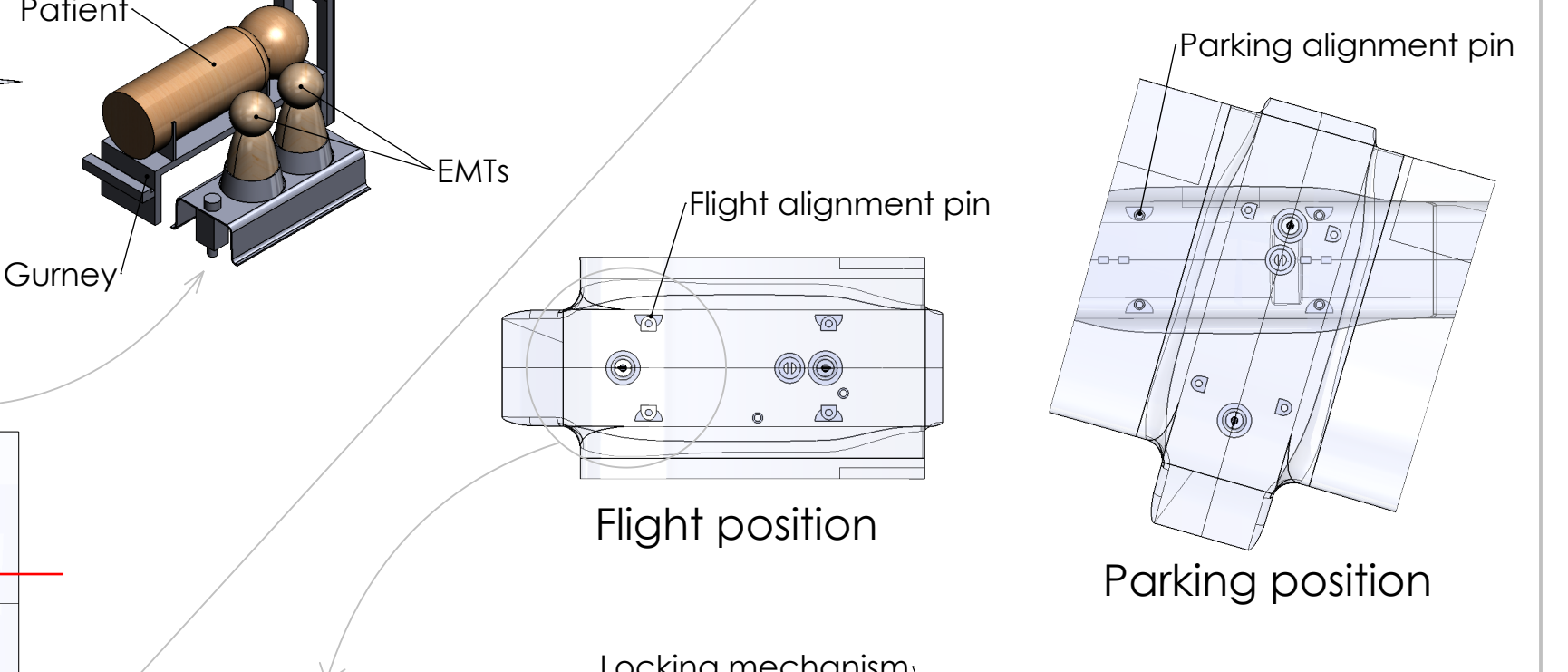
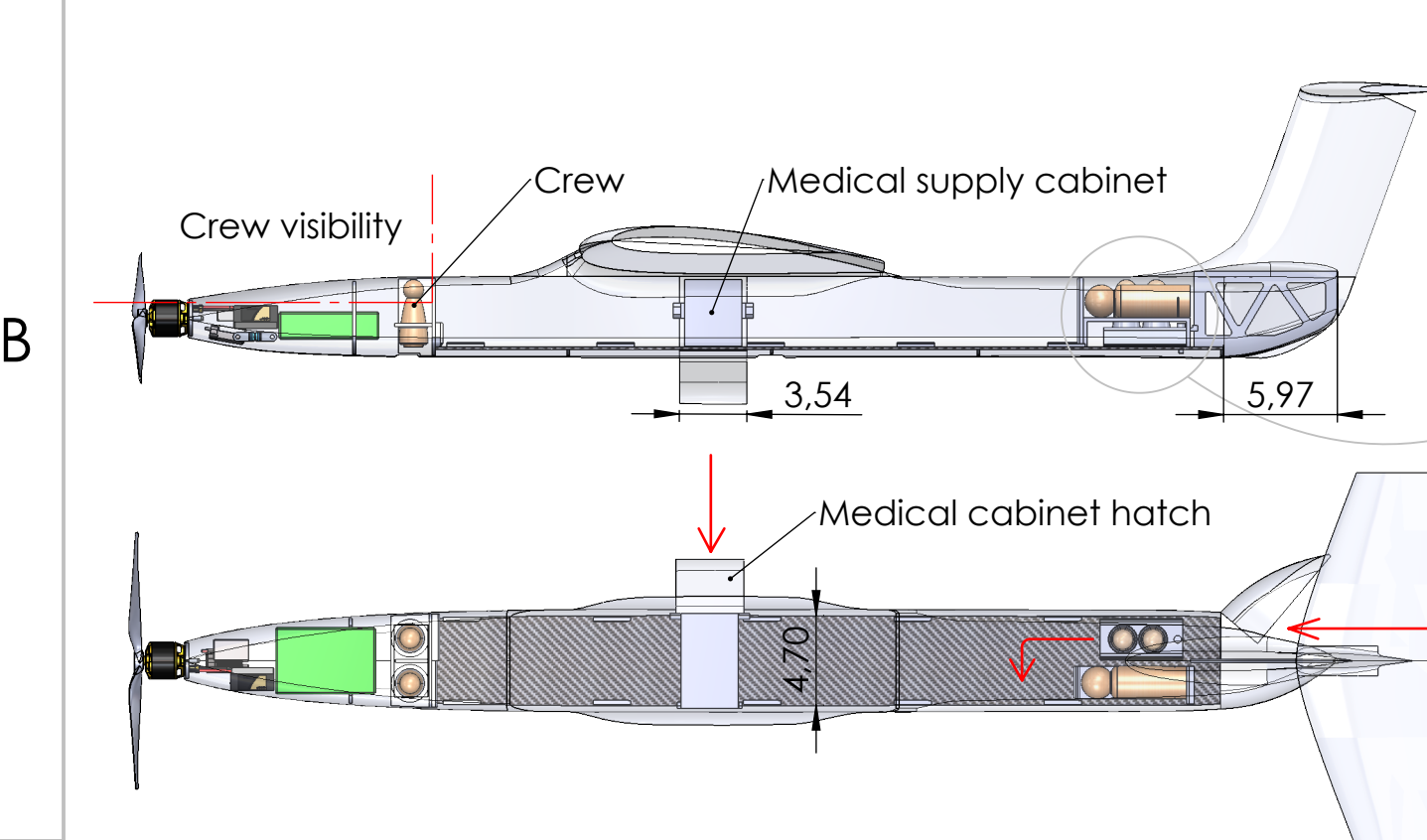
3

2

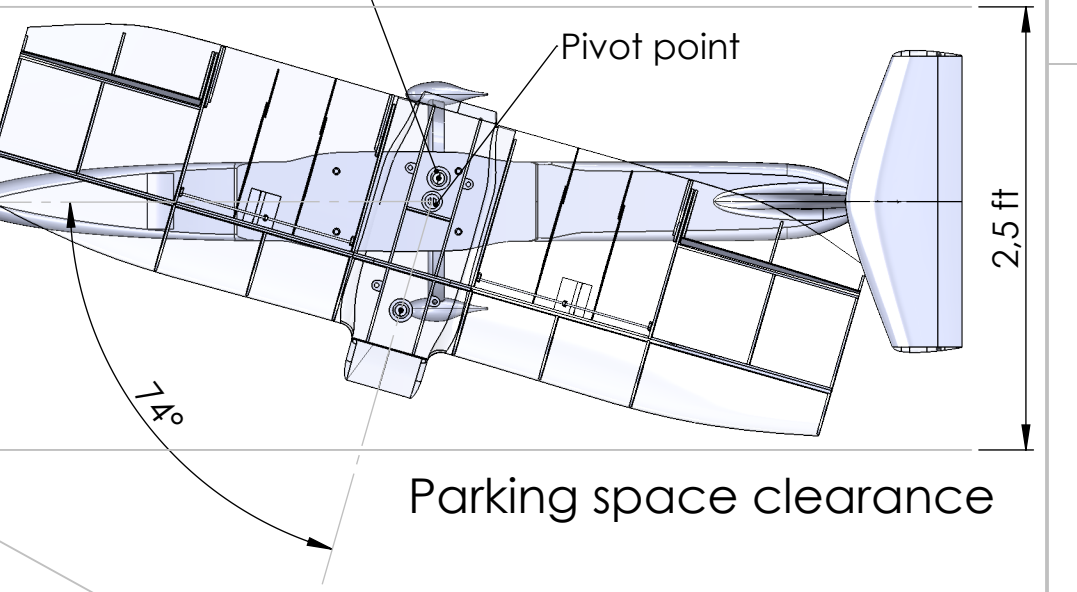
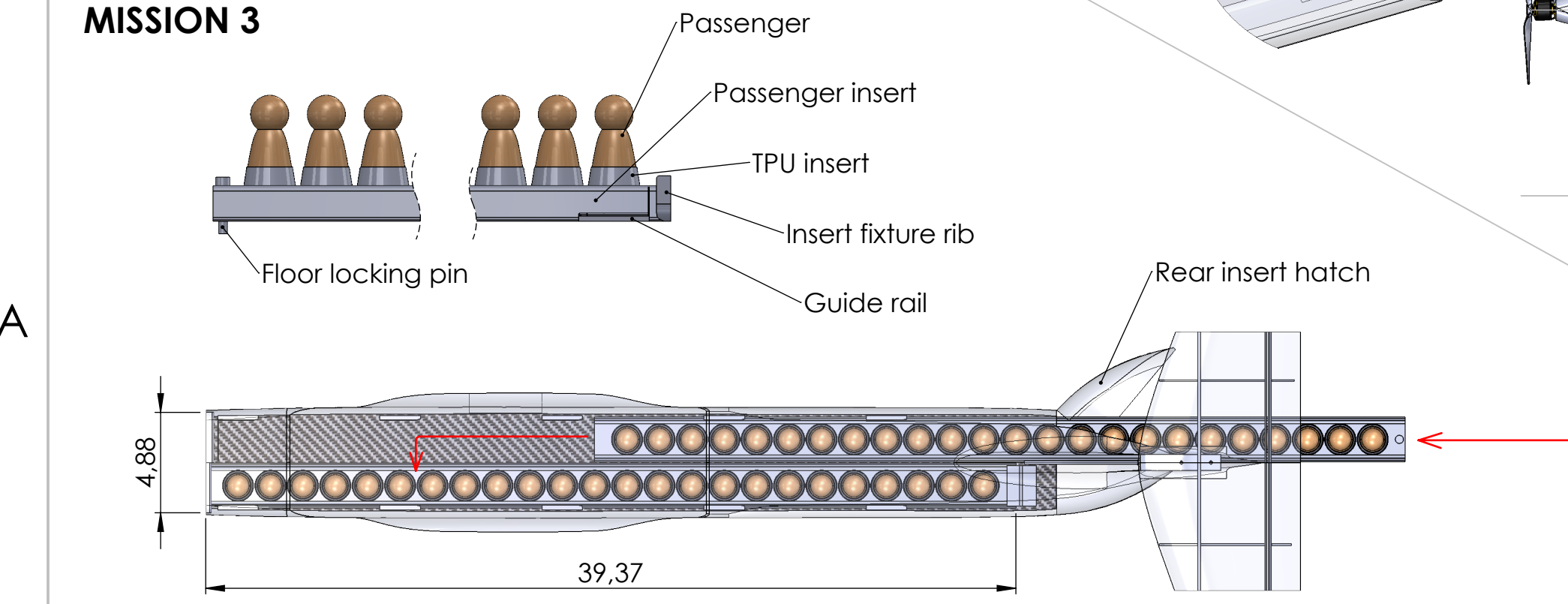
1

MISSION 2

ROTATION



MISSION 3



	NAME	DATE	UNIVERSITY OF LJUBLJANA EDVARD RUSJAN TEAM	
DRAWN	Krivos M.	21. 2. 24	TITLE: Payload acomodation	
CHECKED	Kambic L.	22. 2. 24	SIZE	DWG. NO.
ENG APPR.			B	ER2024-4
MFG APPR.			SCALE: /	WEIGHT: /
Q.A.			REV	
COMMENTS:			SHEET 4 OF 4	

4

3

2

1



6. Manufacturing

6.1 Manufacturing Milestones

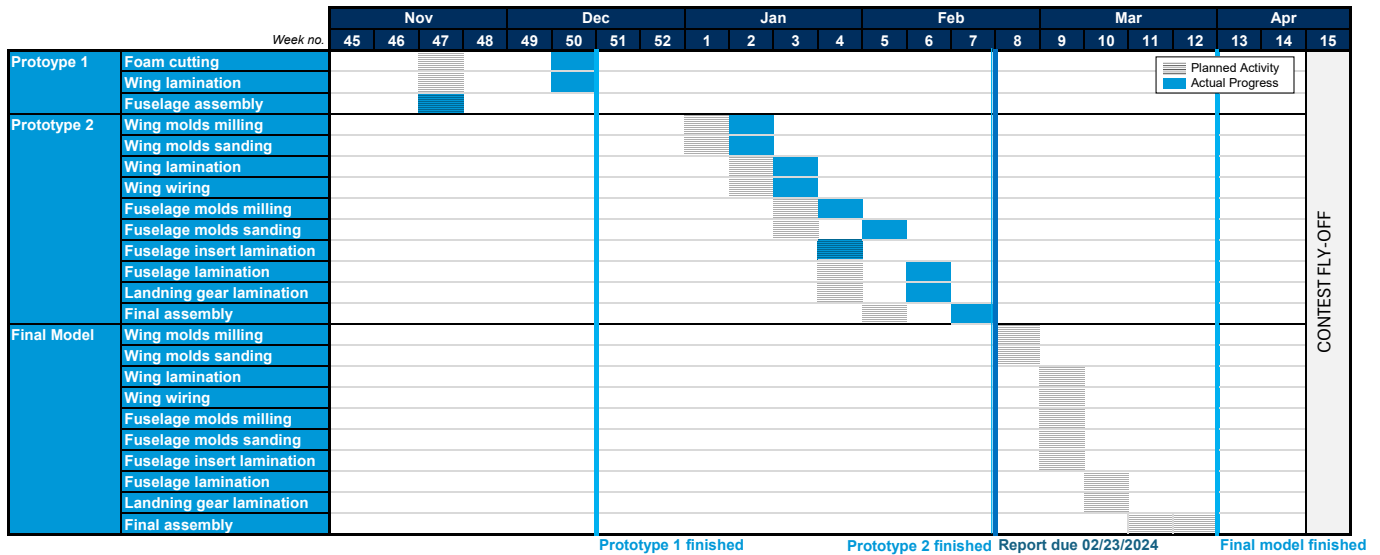


Figure 42: Manufacturing schedule

6.2 Manufacturing Processes Investigated

Different manufacturing processes were considered with the plane's design to find optimal building techniques for each part of the aircraft, yielding optimal performance. Taken into account were also the team's experience, financial and technological resources. An overview of techniques is given below.

6.2.1 CNC Milling

CNC milling is a widely used and versatile cutting process. The main advantages it offers are high accuracy, efficiency, consistency and reliability. On the downside, CNC mills are complex tools that require skilled operators, are costly to acquire and maintain, and can be unsuitable for production of larger parts due to their size limitations. With CNC milling, we were able to produce parts with complex geometries, such as wing and fuselage molds.

6.2.2 Composite Material Construction

Composite materials combine high strength and low weight which makes them ideal for aircraft construction. The main disadvantages – hand lay-up process being time-consuming and materials such as carbon fibers and epoxy resin being expensive – are offset by excellent properties of composites (namely great strength-to-weight ratio) compared to conventional materials. In addition, with proper preparation of the molds, a very low surface roughness of finished parts can be achieved, lowering the skin drag of the aircraft.



6.2.3 Foam Core Modeling

Foam core modeling is an undemanding and inexpensive way of producing different aircraft parts. Foam can be quickly and accurately cut with a CNC hot wire cutter and is thus especially suitable for producing airfoils. Unfortunately, even though the foam core technique is simple, the final products are still heavier, less strong, and less durable than those made from composite materials. For these reasons, foam core modeling is acceptable for production of early prototypes.

6.2.4 Balsa and Plywood

Balsa, being the lowest density wood, can be used to produce very lightweight model aircraft. Because of its low strength, it cannot always be used for load-bearing structures and requires special attention in design stages. For improved strength, it can be used in combination with plywood at the expense of greater weight. The main advantage of wood is that sheets can be cut easily and accurately with a CNC laser, making it a viable option for building early prototypes.

6.2.5 Additive Manufacturing

One of the more recent technologies is 3D printing, more specifically fused deposition modeling (FDM), which is very well suited for rapid prototyping, and production of complex and lightweight structures. However, the bonds between layers can fail easily and catastrophically, therefore this technique is suitable mostly for non-load-bearing parts (e.g. connectors or adapters) and smaller molds.

6.2.6 Forged Carbon Fiber

Forged carbon fiber involves compressing carbon fiber components. With its unique properties, forged carbon provides a lightweight and strong alternative to traditional composite manufacturing. It allows for the creation of parts with varied geometries, making it particularly well-suited for manufacturing smaller parts that require stiffness in all directions, such as front and rear landing gear.

6.3 Selection Process

The team evaluated the processes and methods described in the previous section to select the most suitable ones for production of prototypes and the final model. Taken into account were the requirements and design of the aircraft as well as the team's resources and experience.

Figure of Merits (FoM) was used to rate the processes, factoring in the following criteria using weights from 1 (lowest priority) to 5 (highest priority). **Financial cost:** As a result of a higher budget this year, the team could consider more expensive and lighter composite reinforcements to construct the lightest plane possible. **Technical resources:** Having a CNC milling machine, CNC laser, and a CNC hot-wire cutter of our own construction at disposal,



we could ensure the production of all necessary components in a timely matter at no cost. **Experience:** As the team has an adequate number of experienced senior members to teach and guide new ones, we could opt for more complex techniques resulting in higher quality of finished parts. **Strength:** As the airframe does not have to withstand excessive forces, strength has a lower priority factor. **Weight:** Given the takeoff distance of only 20 ft, low weight has been assigned high priority to ensure that the plane is capable of complying with this limitation. **Surface finish:** Because the plane will be using a low-capacity battery, it is vital to maximize the efficiency of the airplane. For that reason, surface roughness has a high weight factor in the selection process.

Table 11: Manufacturing Figure of Merits

	Weight Factor	Material			Process		
		Balsa & Plywood	Foam Core	Composite Materials	Molds	Laser Cutting	Additive Manufacturing
Financial cost	3	2	3	1	2	5	4
Technical resources	2	1	3	3	4	5	2
Experience	2	4	3	5	5	4	2
Strength	4	3	3	5	5	3	2
Weight	5	5	3	4	5	4	4
Surface finish	5	2	1	5	5	2	4
Total		63	53	84	94	75	68

We have established that the use of composite materials and molds would produce an aircraft that fulfills the criteria to most extent. However, foam core and laser-cut balsa/plywood were used for the first prototype, where ease of manufacture, low cost, and short build time were of higher importance. The final choice of materials and manufacturing techniques for each of the main components is shown in Table 12.

Table 12: Materials and building techniques by component

Component	Material and Technique
Fuselage	CNC milled Necuron 620 molds, carbon fiber + aramid honeycomb laminate
Fuselage Insert	Carbon fibre + Airex foam laminate
Wing	CNC milled Necuron 620 molds, carbon fiber + aramid honeycomb laminate
Empennage	CNC milled Necuron 620 molds, carbon fiber + Airex laminate
Ribs and Internal Reinforcements	Fiberglass reinforced Airex foam laminate
Front Landing Gear	Forged carbon fiber
Main Landing Gear	Forged carbon fiber
Passenger Insert	Carbon fiber laminate



6.4 Composite Manufacturing of Fuselage, Empennage and Wings

6.4.1 Preparation of Molds for Wet Lamination

Preparation of molds for wet lamination involved fabricating the fuselage, wings and empennage using the wet layup process. Negative molds for each part were CNC machined from Necuron 620. Material selection was based on both the manufacturer's guidelines and the team's previous experience. After CNC cutting, the molds were initially sanded to grit 400, then cleaned and coated with epoxy sealant. Once the epoxy was cured, the surface was finely sanded and polished to a mirror finish. Owing to the refinement of our team's mold preparation process, only one coat of wax was required before composite laying took place.

6.4.2 Composite Manufacturing of Fuselage

Lamination began with the placement of two layers of 1.78 oz/sq yard spread tow carbon fiber on the mold in a +45°/-45° orientation and the other in a 0°/90° orientation. The carbon fiber fabric was precisely trimmed to match the mold's required shape and subsequently saturated with epoxy resin. Additional strengthening for the fuselage was achieved by using thin strips of 4.72 oz/sq yard plain weave carbon in various areas. Hinges for hatches and the rudder were crafted using 5.01 oz/sq yard plain weave aramid cloth. Once all auxiliary strips were positioned, the outer shell was vacuum-bagged at 75% vacuum and left to cure for 3 hours to initiate epoxy gelling. This step is critical for eliminating any indentations caused by the honeycomb sandwich structure. After three hours, the mold was removed, and an aramid honeycomb was inserted, covered with an additional layer of 1.18 oz/sq yard biaxial carbon fiber cloth in a +45°/-45° orientation. The finished laminate underwent a 24-hour curing process under 85% vacuum, followed by an 18-hour post-cure at 130°F under 20% vacuum to ensure maximum rigidity. To ensure optimal adhesion between the two mold parts, an overhang was created on one half of the laminate using thin glass fiber cloth, as illustrated in the Figure 44. Upon completion of both fuselage parts, the internal structure was glued in place, including reinforcement ribs, cables, the passenger floor, and servo motors. The halves were then joined together and the two mold halves were pressed together using clamps. After 24 hours of curing, post-processing involved cutting out access holes for electronics, and creating a hatch for passengers, EMTs, and the medical cabinet. Fowler flaps were also fixed onto the wing in this stage.

6.4.3 Composite Manufacturing of Wings, Fowler flaps and Empennage

Initially, the molds were coated with a thin layer of epoxy resin. For the outer layer, dry carbon fiber fabric was placed into the mold and thoroughly saturated with epoxy. Employing dry cloth for the outer layer allowed for precise placement and easier lamination. The wings and empennage were laminated using two layers of 1.18 oz/sq yard biaxial carbon fiber. We constructed Fowler flaps using two layers of 1.78 oz/sq yard spread tow. Aramid honeycomb was chosen for the fuselage because it facilitated lamination, whereas Airex foam was used for constructing the wings and empennage. However, we did not use Airex for the Fowler flaps because it could not fit into the smaller mold. Hinges were reinforced with 5.01 oz/sq yard plain weave aramid cloth and each half of the wing was further



Figure 43: Fuselage decoupling

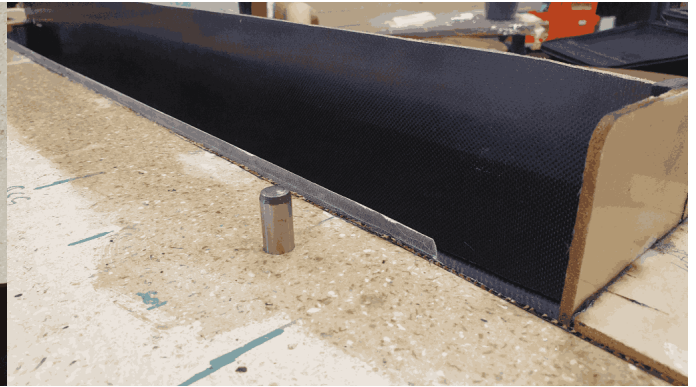


Figure 44: Fuselage overhang

strengthened with 5 strips of 1.48 oz/yard UD carbon fiber under the spar, ensuring adequate longitudinal stiffness as calculated in the FEM analysis in Section 5.2.9. Airex foam was then placed over and covered with properly saturated carbon fiber fabric. The second layer of fabric had to be saturated with epoxy before being placed into the mold, as laminating it in the mold would cause much of the epoxy to soak into the Airex foam. The parts were vacuum-bagged and cured for 24 hours under 85% vacuum, followed by an 18-hour post-cure at 130°F.



Figure 45: Extended Fowler flaps in the main wing



Figure 46: Main wing lamination

6.5 Composite Manufacturing of Floor Inserts and Landing Gear

6.5.1 Composite Manufacturing of Landing gear

The front and rear landing gear were manufactured using the carbon forging technique. The molds were 3D printed as CNCing is too time-consuming and cannot produce smaller molds with adequate detail needed as in the case of landing gear. After printing, the molds were finely sanded, then covered with 3 layers of wax and polished. Before lamination, an additional layer of PVA was added to allow for easier decoupling.

For lamination, we prepared the necessary amount of chopped carbon fiber by using the volume of the part derived from the CAD model. For example, the volume of front landing gear is 2.14 in³ which was then multiplied by



the density of epoxy (0.81 oz/in³). Forged carbon parts are constructed from an optimum mix of 60% carbon and 40% epoxy. We have calculated the required amount of epoxy, allowing us to determine the needed amount of chopped carbon fiber.

We began laminating by spreading a thin layer of epoxy onto the mold and covering it with chopped carbon which was then carefully saturated. This process was repeated until all the epoxy and carbon fiber were used. The parts were then squeezed together and left to cure for 36 hours at room temperature. Lastly, we removed the parts from the mold and post-processed them by fine sanding and cutting the necessary holes for the wheels.



Figure 47: Forged carbon front landing gear

6.5.2 Composite Manufacturing of Floor Inserts

To fabricate the floor inserts, we used two aluminum spars as molds, an efficient method for producing lengthy, straight composite panels and inserts with minimal preparation. The spars underwent polishing and waxing before use. The floor insert was crafted by laminating two layers of 80 g/m² plain weave carbon fiber cloth and positioning them onto the aluminum mold with a 5 mm Airex foam layer placed in between. Clamps were used to compress the spars together and the part was allowed to cure for 36 hours at room temperature.

7. Testing Plan

Testing plan was implemented to validate numerical simulation results regarding aerodynamic performance, propulsion, stability and load-bearing capabilities. Additional tests were performed to check the functionality of the aircraft. Testing was divided into three categories according to the stage of the design. A detailed schedule, seen in Figure 48, was proposed to track errors before they negatively impacted later steps.

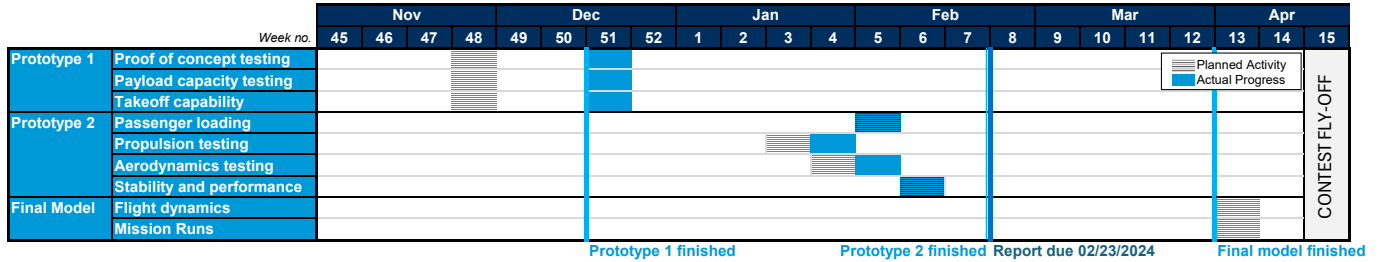


Figure 48: Testing schedule

7.1 Proof of Concept Testing

The first prototype was designed to be simple and easy to build, but it did not have the full functionality required for the competition. The goals of the initial tests were to determine the general conceptual design of the airplane, takeoff capabilities, and flight dynamics with the different payload configurations. The maximum takeoff weight and electric current draw were determined through these initial tests, as well as the effect of the payload weight on the top speed. To test the maximum current draw during takeoff and during flight, the aircraft was equipped with our custom-made onboard measuring system, where all significant data was tracked: air speed, accelerations, GPS positioning, height, current and voltage. Basic aerodynamic characteristics and propulsion system requirements calculated via SAS were validated and corrected if necessary.

7.2 Propulsion Testing

The aim was to determine the optimal combination of motors, propellers, and batteries for the aircraft. Cross comparison of propellers and motors at different air speeds and throttle settings was made to obtain complete propulsion characteristics.

A propulsion testing rig that could be mounted high above the roof of a car in clean air, shown in Figure 49, was used to test different combinations of batteries, motors and propellers at different speeds. The motor was mounted onto a circular beam and run at different throttle settings while measuring the input current and voltage as well as the produced force of the motor with a strain gauge sensor. The airflow was measured using an anemometer, positioned at the front of the rig to mitigate the aerodynamic effects of the vehicle. Dynamic thrust was measured for airflow rates ranging from 0 ft/s to 130 ft/s, resulting in thrust/speed and current/speed characteristics that were used to improve numerical simulation accuracy in the SAS mission model.

Tests were performed using the Scorpion SII-4035-330KV and Scorpion SII-4020-420KV motors in combination with APC 15x10E, APC 14x6E, APC 17x6E and APC 16x4E propellers. The batteries used for the tests was TATTU R-LINE 4500mah 6S1P 95C 22.2V battery and LiPo 2000mAh 12S 44.4v Battery Pack.



7.3 Aerodynamics Testing

The aerodynamic surface testing consisted of measuring the lift produced by various main wing designs at varying air speeds.

The propulsion testing rig, described in Section 7.2, was retrofitted to support the mounting of main wings, as shown in Figure 50. The wing itself had to be positioned further in front to minimize the aerodynamic interference of the vehicle. The wing mounting system was directly attached to the circular beam, similar to the motor, which enabled the team to measure lift. The airflow was again measured with an anemometer at the front of the rig. Lift was measured for airflow rates ranging from 0 ft/s to 130 ft/s, as well as at different flap deployment settings which produced characteristics that helped us determine the optimal wing design and configuration for takeoff and mission performance.



Figure 49: Propulsion testing rig

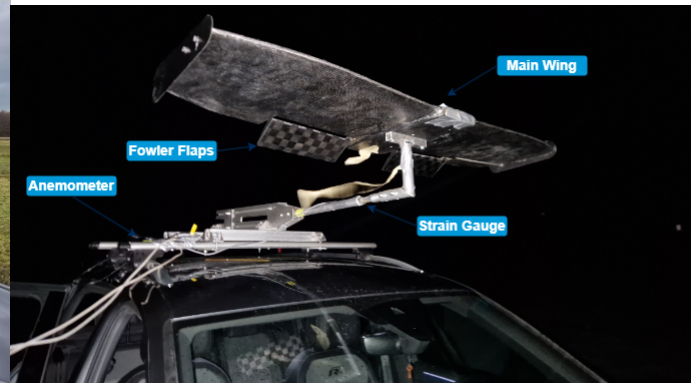


Figure 50: Aerodynamics testing rig

7.4 Ground Mission Testing

The Ground Mission tests provided crucial insight into the times needed to reconfigure the aircraft and load different payload configurations. The initial goal was to determine if it is possible to configure the aircraft for flight, install the batteries and load the crew in less than 5 minutes, as required by the rules.

Further testing consisted of multiple simulated runs of the GM procedure. The assembly crew member would set up the aircraft in the flying configuration, load and unload every mission payload and finally reconfigure the aircraft into the parking configuration. Another crew member of the team would note the time required to perform the whole GM procedure. During the process, notes were taken and checkpoints created to determine whether the individual assembly and loading mechanisms were time efficient. The results were then averaged and used to further improve the SAS model.



7.5 Flight Testing

The objective of test flights with the second prototype was to validate the simulated M2 and M3 performance and provide additional feedback for the fine-tuning of the design. The flight tests also offered an opportunity for the pilot to get accustomed to the aircraft's behavior. Data was gathered using the same acquisition system detailed in Section 7.1. Additionally, tests such as the dive test and inverted flight, were conducted to check the aircraft's trim.

7.6 Checklists

Checklists are an essential part of every design process, which is why we incorporated them into our flight test process. This was done to minimize the possibility of human errors and ensure proper data acquisition and test efficiency.

7.6.1 Propulsion and Aerodynamics Test Checklist

The following checklist in Table 13 was carried out before every test that involved the car-mounted test rig. Because of the high speeds needed for data collection, we had to ensure the safety of everyone involved.

Table 13: Propulsion and Aerodynamics test checklist

General			
Test rig fastened		Sensors calibrated	
Spotters ready		DAQ system ready	
Propulsion Test		Aerodynamics Test	
Check battery voltage		Wing secured	
Connection secured		Flaps fixed	
Propeller secured		Sufficient ground clearance	
Transmitter check		AoA fixed	
Final Inspection			
Roads clear		Driver ready	
DAQ system storing		Operator ready	

7.6.2 Flight checklist

The preflight checklist, seen in Table 14, was used before each test flight. It has been modified to meet the specific requirements of every mission. The following checklist will also serve as the last check-up before each fly-off in the upcoming DBF competition.



Table 14: Pre Flight checklist

Overview			
Date & Time		Aircraft	
Location		Battery	
Wind speed & Direction		Additional Info	
Before Power Up			
Check battery voltage		Battery packs secured	
Connection secured		Prop & motor secured	
Check CG		Visual inspection	
Crew secured		Payload secured	
After Power Up			
Control surfaces check		Transmitter check	
Fail-safe		Fuse	
Final Inspection			
Ground surface movement		Pilot and Spotter check	

8. Performance Results

8.1 Proof of Concept

While performing test flights of prototype 1 (Figure 51), the airplane took off within 26 ft while weighing 13.4 lbs. It was found that with moderate pilot correction, the prototype's 0.050 vertical and 0.61 horizontal tail volume coefficients provide sufficient stability. Even though the T-tail proved effective, it caused noticeable torsion on the carbon fiber tube used for the empennage. At that point, the pilot noted how the wide fuselage affected the aerodynamic performance. During takeoff and flight, data on the aircraft's speed, position, electric current, and voltage was collected. The performance results showed that the team was progressing well.



Figure 51: First prototype during takeoff testing



8.2 Propulsion

The propulsion data in Figure 52 clearly showed us the best setup for efficiency while maintaining thrust. Updating our SAS mission models with this info made them much more accurate. Surprisingly, we found that the best wing size and passenger count are now only half of what we thought before. After thorough evaluation, we reached the decision to proceed with designing the aircraft according to the original plan. This choice was made because there was only a minor 2% difference in TMS between the new and current configuration and altering the design at this stage would introduce more design problems rather than significantly improve the performance. We are confident that by refining and optimizing the current design, we can more than just compensate for the 2% difference.

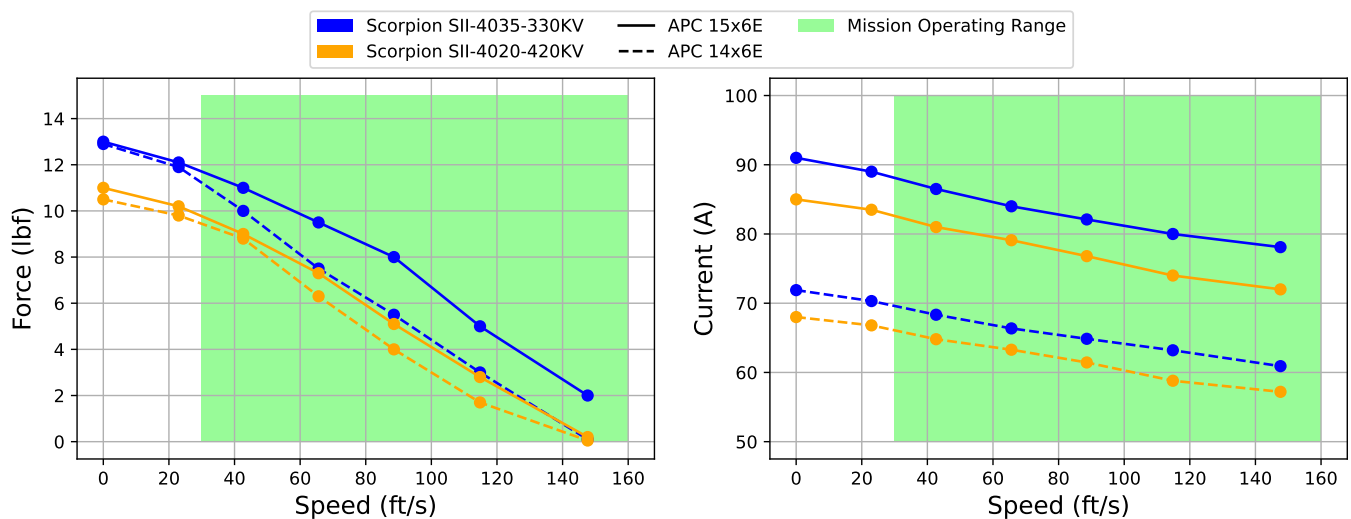


Figure 52: Propulsion force / speed characteristic (left) and current / speed characteristic (right) for all missions

8.3 Aerodynamics

The results of main wing aerodynamics testing, shown in Figure 53, confirmed the expected lift characteristics. Furthermore, Fowler flaps proved effective, providing additional 95% of lift compared to the configuration without them. Results insured that the aircraft would take off within the assigned limit. For Fowler flap testing, the operating speed range was based on the expected takeoff speed.

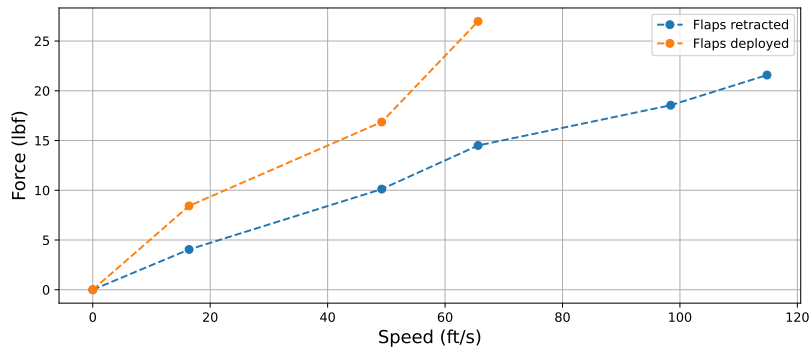


Figure 53: Lift force / speed characteristic

8.4 Ground Mission Test

The goal was to assess whether an aircraft could be configured for flight, with batteries installed and crew loaded, within a 5 minute time frame, as mandated by competition rules. The team conducted repeated Ground Mission tests, timing the complete procedure of configuring the aircraft for flight, handling payloads, and reverting to parking configuration. These efforts aimed to identify, and optimize time-efficient assembly and loading mechanisms. The gathered data, shown in Table 15 revealed that strategic workflow optimization and the aircraft's design for rapid reconfiguration significantly reduced preparation times.

Table 15: Ground mission testing results

Attempt #	1	2	3	4	5	Avg.
Flight configuration [s]	20	21	20	24	22	21
M2 payload [s]	15	20	17	15	16	17
M3 payload [s]	30	32	36	32	29	32
Parking configuration [s]	15	12	17	10	15	14
Σ	80	85	90	81	82	84

8.5 Test Flights

Prototype 2 excelled in test flights, with comprehensive data collected by FrSky telemetry sensors that were tracking speed, position, electric current, and voltage. It exceeded speeds of 160 ft/s in M1, displaying exceptional maneuverability and stability.

The second mission lap times averaged 24 seconds, validating our simulations. Successful Mission 3 flights with 48 passengers required only minor trim-up adjustments to accommodate the added weight. Further analysis of M1 and M2 tests supported our decision to include Fowler flaps, effectively reducing takeoff distance without adding significant weight.



The primary objective of the second prototype was to evaluate the impact of added weight on overall flight dynamics. Detailed analysis of simulated and tested M2 runs, shown in Figure 54 uncovered minor deviations from simulations, due to potential inaccuracies in the designated flight model described in Section 4.2. In the majority of laps flown, the pilot reported no severe impacts on flight performance.

An identified risk involves aggressive turns, exacerbated by passenger weight, crucial for competition success. Mitigation strategies include comprehensive pilot training to limit bank angles within 75° and ensure speed remains above the stall threshold. Cumulatively, the pilot logged 3 hours of flight time, achieving an average M3 lap time of 23 seconds.

The team is proud to present our final manufactured aircraft called Adria to the world and judges at Wichita airfield.

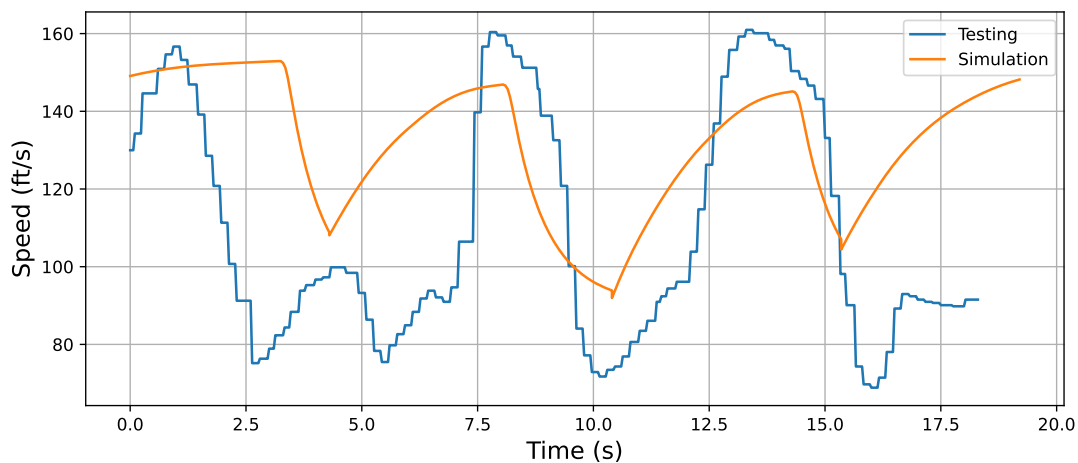


Figure 54: Speed profile of simulated and tested M2 lap.

9. References

- [1] PythonCoreTeam, *Python: A dynamic open source programming*, Python Software Foundation [online], <https://www.python.org>.
- [2] XFLR5, <http://www.xflr5.tech/xflr5.htm/>.
- [3] NASA, *OpenVSP: Open Vehicle Sketch Pad, open source parametric aircraft geometry tool*, OpenVSP software [online], <https://openvsp.org/>.
- [4] *Wing Taper Considerations*, <https://api.semanticscholar.org/CorpusID:1650546>, 2006.
- [5] Sadraey, M. H., *Aircraft Design: A Systems Engineering Approach*, 2013.
- [6] *MATLAB: programming and numeric computing platform*, <https://www.mathworks.com/products/matlab.html>.
- [7] *RCPlanes Online*, <https://rcplanes.online/index2.htm>.



- [8] Howe, D., *Aircraft Conceptual Design Synthesis*, Professional Engineering Publishing, 2000.
- [9] Torenbeek, E., *Synthesis of Subsonic Airplane Design*, Delft University Press, Delft, 1982.
- [10] *Ansys® Academic Research Mechanical 2021*, ANSYS, Inc., <https://www.ansys.com/>.
- [11] Roskam, J., *Airplane Design*, No. VI part in *Airplane Design*, DARcorporation, 1985.
- [12] Götten, F., Havermann, M., Braun, C., Marino, M., and Bil, C., "Improved Form Factor for Drag Estimation of Fuselages with Various Cross Sections," *Journal of Aircraft*, Vol. 58, 12 2020. 10.2514/1.C036032.
- [13] AVL, <https://web.mit.edu/drela/Public/web/avl/>.
- [14] *MatWeb*, https://www.matweb.com/search/datasheet_print.aspx?matguid=39e40851fc164b6c9bda29d798bf3726.

Design, Build, Fly Virginia Tech "The Hokie Express"



Brady Bourgoyne, Owen Cain, Will Durham, David Eweka,
Joseph Gould, Ally Hai, Evan Kelly, Zach Moore,
Pranay Patel, Pramil Patel, Michael Sciacca, Nathan Shune,
Calvin Siemers, Dante Stellar, Kate Taipale, Emma Whitney





TABLE OF CONTENTS

1 EXECUTIVE SUMMARY	4
2 MANAGEMENT SUMMARY	5
2.1 Team Organization	5
2.2 Milestone Chart	6
3 CONCEPTUAL DESIGN	6
3.1 Mission Requirements and Constraints	6
3.2 Scoring Summary	10
3.3 Translating Mission Requirements to Sub System Design Requirements	10
3.4 Competition Score Sensitivity Analysis	12
3.5 Airplane Configuration Selection	13
3.6 Final Conceptual Design Configuration	19
4 PRELIMINARY DESIGN	20
4.1 Design Methodology	20
4.2 Aerodynamics	20
4.3 Stability and Control	24
4.4 Propulsion System Sizing	30
4.5 Payload Sizing	31
4.6 Mission Performance	32
4.7 Uncertainties	32
5 DETAILED DESIGN	32
5.1 Dimensional Parameters	32
5.2 Structural Characteristics and Capabilities	33
5.3 System and Sub-System Design/Selection/Integration	37
5.4 Drawing Package	41
6 MANUFACTURING PLAN	46
6.1 Manufacturing Processes Investigated	46
6.2 Manufacturing Processes Selected	47
6.3 Summary	50
6.4 Manufacturing Milestones	51
7 TESTING PLAN	52
7.1 Testing Objectives	52
7.2 Sub-System Testing	52
7.3 Flight Test Schedule and Flight Plan	54
7.4 Flight Checklist	55
8 PERFORMANCE RESULTS	56
8.1 Demonstrated Performance of Key Sub-Systems	56
8.2 Demonstrated Flight Performance of Completed Airplane	57
References	60



Acronyms, Abbreviations, and Symbols

AIAA	American Institute of Aeronautics and Astronautics	GPS	Global Positioning System
AoA	Angle of Attack	LiPo	Lithium Polymer
AR	Aspect Ratio	MTOW	Maximum Takeoff Weight
AV1	Air Vehicle 1	mAh	Milli-Amp Hours
AV2	Air Vehicle 2	M_T	Moment from Thrust
b	Wing Span	M_W	Moment from Weight
CG	Center of Gravity	M_{wt}	Moment from Wing
CA	Cyanoacrylate	M_1	Mission 1
CAD	Computer Aided Design	M_2	Mission 2
CAM	Computer Aided Manufacturing	M_3	Mission 3
CFD	Computational Fluid Dynamics	MSC	Medical Supply Cabinet
$C_{D,i}$	Induced Drag Coefficient	NiCd	Nickel-Cadmium
CG	Center of Gravity	NiMH	Nickel-Metal Hydride
C_L	3D Lift Coefficient	RC	Remote Control
c_l	2D Lift Coefficient	RFP	Request for Proposal
$C_{L,max}$	Maximum 3D Lift Coefficient	RPM	Revolutions per Minute
CNC	Computer Numerical Controlled	S_{ref}	Reference Area
d	Takeoff Distance	S_{M1}	Mission 1 Score
DBF	Design, Build, Fly	S_{GM}	Ground Mission Score
e	Oswald Efficiency Factor	S_{M2}	Mission 2 Score
ESC	Electronic Speed Controller	S_{M3}	Mission 3 Score
FEA	Finite Element Analysis	T	Thrust
FS	Factor of Safety	T/W	Thrust to Weight Ratio
FoM	Figures of Merit	THE	The Hokie Express
EMT	Emergency Medical Technician	TOGW	Takeoff Gross Weight
g	Load Factor	UAM	Urban Air Mobility
g	Acceleration Due to Gravity	VT	Virginia Tech
GM	Ground Mission Score	W-h	Watt-hours
		XPS	Extruded Polystyrene



1 EXECUTIVE SUMMARY

The purpose of this report is to detail the Design, Build, Fly (DBF) at Virginia Tech (VT) team's entry, *The Hokie Express* (THE), into the 2023-24 American Institute of Aeronautics and Astronautics (AIAA) DBF competition. The competition objective is to design, build, and test a radio-controlled Urban Air Mobility (UAM) airplane capable of completing three flight missions and one ground mission. Mission 1 (M_1) serves as a design validation flight of three laps around the flight course. In Mission 2 (M_2) the airplane must fly three laps carrying a Patient, medical crew, and medical supply cabinet as fast as possible. In Mission 3 (M_3) the airplane must fly as many laps as possible in five minutes carrying passengers while minimizing battery pack Watt-hours. During Ground Mission (GM), the airplane must start in a 2.50 ft (0.762 m) wide parking space, be configured for M_2 , then M_3 , then back to the parked configuration as quickly as possible.

Aircraft Design and Configuration

The Hokie Express is a high-wing monoplane with a conventional tail and tricycle landing gear powered by twin counter-rotating propellers. THE's wing generates sufficient lift to account for high payload weight in M_2 . The conventional tail provides a balance between maneuverability and size. The twin-motor configuration was sized to maximize speed while meeting endurance and takeoff distance goals in all flight missions. The wing structure was sized to withstand a competitive payload and aerodynamic loading during flight. The team conducted scoring and sensitivity analysis to determine starting points for the following design parameters: airplane dimensions, lift generated, speed, battery capacity, weight of the medical supply cabinet (MSC), and number of passengers. It was determined that a medical supply cabinet weighing 6.00 lb (2.72 kg) payload for M_2 and carrying 52 passengers for M_3 led to competitive scores in all missions.

THE Performance Capabilities

- Empty Weight: 10.0 lb
- Maximum Takeoff Weight: 16.0 lb (71.2 N)
- Mission 2 Top Speed: 120 ft/s (36.7 m/s)
- Mission 3 Top Speed: 90.6 ft/s (27.7 m/s)
- MSC Weight: 6.00 lb (26.7 N)
- Number of Passengers: 52
- Ground Mission Configuration Time: 300 s
- Takeoff Distance: 17.0 feet



Figure 1: The Hokie Express

THE's rectangular wing has a span of 60.0 in (152 cm) and chord of 13.0 in (33.0 cm). The wing produces 20.7 lb (9.4 kg) of lift at cruise and 20.2 lb (9.2 kg) at take-off. The tail has a moment arm of 41.5 in (105.4 cm), and the horizontal and vertical stabilizers have areas of 182 in² (1175 cm²) and 112 in² (724 cm²) respectively. The tail boom is a square tube extending from the tail to the wing spar. The wing spar is a square carbon fiber spar and spans the entire wing. The leading edge of THE's wing is foam-core covered with carbon-composite while the trailing edge is a traditional balsa wood structure covered with Monokote. All tail surfaces are made of foam-core covered with carbon-fiber. The team developed a testing plan and schedule for all major components of the airplane. Static thrust testing indicated a thrust-to-weight ratio (T/W) of 1.39 for M_2 and 1.63 for M_3 . Flight testing was conducted using three air vehicles throughout the preliminary and detailed design process to verify predicted performance parameters of THE.



2 MANAGEMENT SUMMARY

The 2023-24 AIAA DBF @ VT team is entirely student-led and consists of 12 leads and a pilot, primarily composed of juniors and seniors. The team has 85 additional underclassmen members and a faculty advisor from the Department of Aerospace and Ocean Engineering. The team receives additional support from other faculty members, team alumni, and industry consultants at design reviews.

2.1 Team Organization

The team uses a co-lead structure with specialized sub-teams, as seen in Figure 2. The team leads (**dark orange**) consist of the Chief Engineer and the Project Manager. The Chief Engineer is responsible for key technical decisions and overall systems and component integration on the airplane. The Project Manager is responsible for team administration including planning, outreach, schedule maintenance, and finances. The remainder of the team is divided into ten distinct sub-teams led by one or two sub-team leads (**orange**).

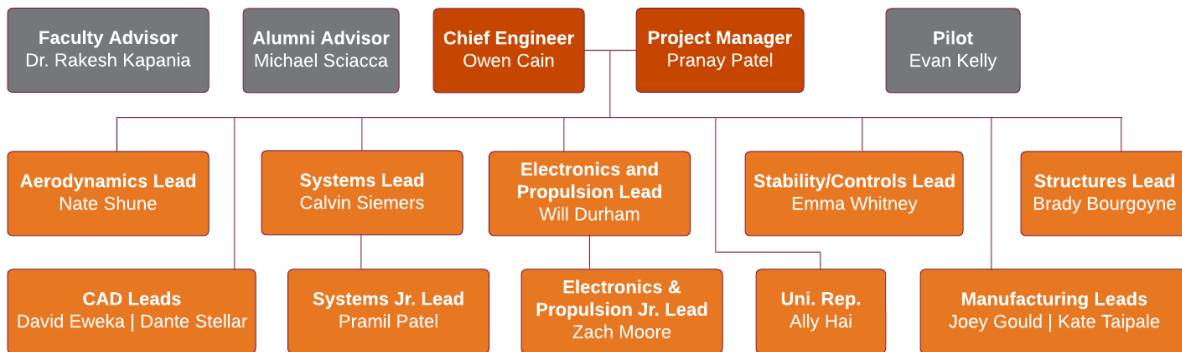


Figure 2: 2023-24 DBF @ VT Team Organization

The Aerodynamics team sizes the wing and analyzes airplane performance. The Electronics and Propulsion team selects the airplane's propeller, motor, battery, and Electronic Speed Controller (ESC). The Stability and Controls team sizes the tail and control surfaces to ensure stable flight and maneuverability. The Structures team designs the internal structure of the airplane and conducts Finite Element Analysis (FEA) to guarantee overall structural integrity during flight. The Computer Aided Design (CAD) team produces digital models to be sent to the Manufacturing team who determines proper build methods to produce each airplane. The Systems team designs the fuselage, landing gear, and implements the competition components into the airplane. The team also has a University Representative for the Virginia Tech Student Engineers' Council to acquire university funding.



2.2 Milestone Chart

The Project Manager maintains a Gantt Chart with milestones as shown in Figure 3. The schedule shows a full-scale timeline for the project.

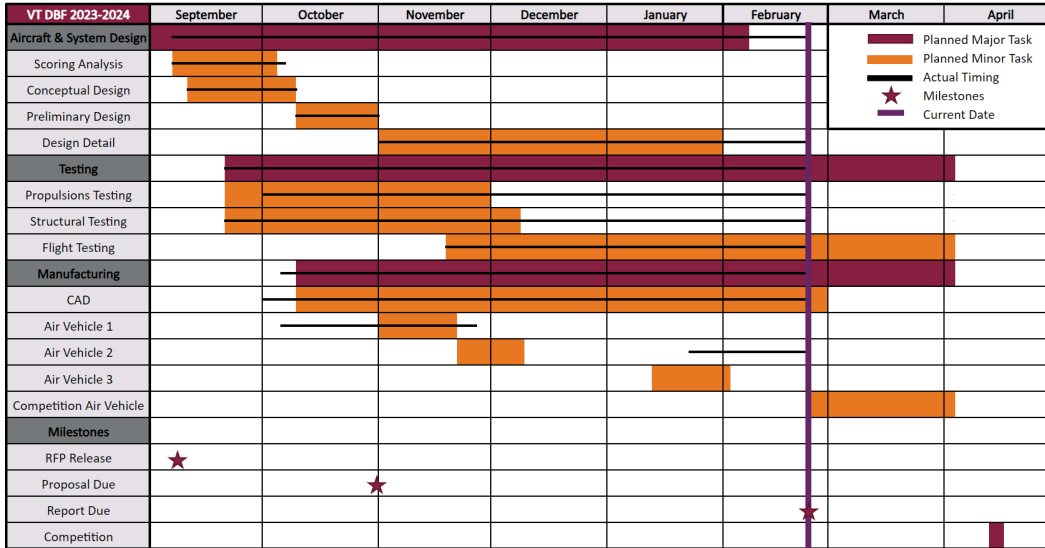


Figure 3: 2023-24 DBF @ VT Gantt Chart

3 CONCEPTUAL DESIGN

The team began the conceptual design phase with an analysis of the 2023-24 DBF rules [1] to generate a list of requirements and Figures of Merit (FoMs). The FoMs were used to down-select to the design which satisfied the competition requirements and maximized mission scoring. The preferred system concept was a high wing, twin-motor airplane with tricycle gear and a conventional tail.

3.1 Mission Requirements and Constraints

The mission requirements and constraints for this year are outlined in the 2023-24 DBF competition rules [1]. The objective of the 2023-24 DBF competition is to design, build, and test an airplane to demonstrate UAM missions. These missions are characterized by the transportation of people and/or cargo over congested areas. UAM missions are also typically shorter range, and require the airplane to takeoff and land in tight spaces. For each mission, the takeoff ground roll cannot exceed 20.0 ft (6.10 m), and the airplane must carry a crew of two pilots. Each member of the crew is a 3.50 in (8.89 cm) jumbo angel doll as seen in Figure 4.



Figure 4: 3.50 in (8.89 cm) Jumbo Angel Doll [1]

The crew must be carried in a cockpit separated from the cargo compartment with a bulkhead. This bulkhead must allow the pilots to sit with their heads above the fuselage forward of the cockpit, and must allow the pilots to be loaded through hatches forward of the required bulkhead. The crew placement can be seen in Figure 5.

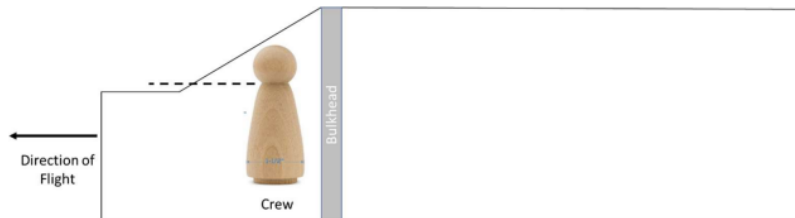


Figure 5: Placement of Crew Members with Respect to the Fuselage [1]

All cargo must be loaded through hatches on the side of the airplane with a width less than 6.00 in (15.2 cm). The hatch hinge(s) and the opening(s) opposite the hinge(s) cannot pass beyond the fuselage vertical center line. The cargo and cockpit openings must be separate from one another.

The competition lap is shown in Figure 6. The lap begins with a 20.0 ft (6.10 m) takeoff followed by a climb to a safe altitude. The plane flies 500 ft (152 m) upwind of the starting line, then turns around and flies a 1000 ft (305 m) downwind leg which includes a 360° turn. The plane then turns around and flies 500 ft (152 m) upwind and completes one lap as it passes the starting line in the air. The landing at the end of a mission is not included in the lap time.



Figure 6: Competition Lap

Each mission is scored separately. Three of the mission scoring equations contain a normalization to the highest score achieved at competition.



3.1.1 Staging

Prior to each mission, the airplane is brought to the staging box in the parked configuration. The parked airplane is stowed in a 2.50 ft (0.762 m) wide parking spot with all cargo, floor insert(s), and propulsion battery pack(s) removed. The assembly crew member is the only person allowed to touch the airplane while it is being prepared for flight. During GM and inside the staging box, the airplane cannot be put into any configuration other than upright on its landing gear while mission systems are loaded and the airplane is configured for flight. Assembly and payload installation must not exceed 5 minutes.

3.1.2 Mission 1: Delivery Flight

M_1 is a proof of flight. The airplane is brought to the flight line and staged. The only payload for this mission is the two pilots, and the airplane must complete 3 laps in 5 minutes. Teams are required to demonstrate their airplane's airworthiness to score 1 point for M_1 .

$$S_{M_1} = 1 \text{ For Completion} \quad (1)$$

3.1.3 Mission 2: Medical Transport Flight

M_2 is a demonstration of the airplanes's medical emergency response capabilities. The M_2 payload is the crew, 2 EMTs, the Patient on the gurney and the Medical Supply Cabinet (MSC). The EMTs must be next to the Patient while the MSC can be in front of or aft of the EMTs and the Patient. The EMTs are the same angel doll seen in Figure 4, the Patient is shown in Figure 7, and an example M_2 layout is shown in Figure 8.



Figure 7: 5.5 in (14.0 cm) Jumbo Man Doll [1]

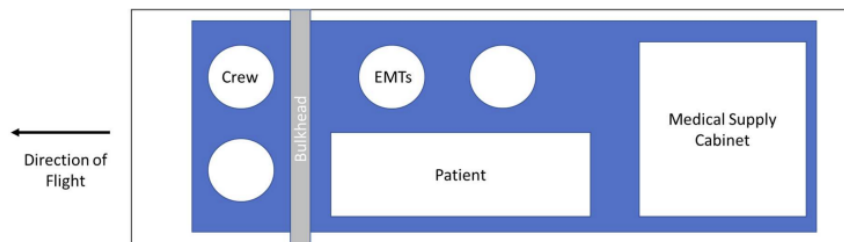


Figure 8: Medical Transport Flight Mission Layout [1]



The M_2 score is a function of the MSC weight and time to fly 3 laps as shown in Equation 2. Teams are rewarded if they maximize the MSC weight and minimize the time to fly 3 laps in M_2 .

$$S_{M2} = 1 + \left[\frac{N_{(\text{MSC Weight} / \text{time})}}{\text{Max}_{(\text{MSC Weight} / \text{time})}} \right] \quad (2)$$

3.1.4 Mission 3: Urban Taxi Flight

M_3 is a demonstration of the airplane's passenger transportation capabilities. The M_3 payload is the crew and angel doll passengers which are carried in the cargo compartment. An example M_3 layout is shown in Figure 9.

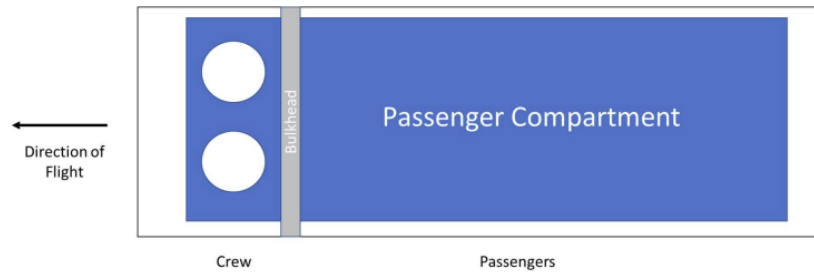


Figure 9: Urban Taxi Flight Mission Layout [1]

The M_3 score is a function of the number of passengers carried, the number of laps flown in 5 minutes, and the propulsion battery pack Watt-hours as shown in Equation 3. Teams are rewarded for maximizing the laps flown in 5 minutes, maximizing the number of passengers carried, and for minimizing the propulsion battery pack Watt-hours.

$$S_{M3} = 2 + \left[\frac{N_{(\# \text{ laps} * \# \text{ passengers} / \text{battery capacity})}}{\text{Max}_{(\# \text{ laps} * \# \text{ passengers} / \text{battery capacity})}} \right] \quad (3)$$

3.1.5 Ground Mission: Configuration Demonstration

GM is a demonstration of how quickly the airplane can be configured for different missions. The airplane is brought to the GM staging area in the parking configuration with no payloads or components installed. The assembly crew member is then timed for the following tasks:

1. Airplane is removed from the parking spot and configured for flight
2. M_2 payload installation
3. M_2 payload removal
4. M_3 payload installation
5. M_3 payload removal
6. Airplane is returned to the parking spot in the parked configuration



The GM score is a function of the time required to complete these tasks. Equation 4 indicates that teams are rewarded for minimizing airplane configuration time.

$$S_{GM} = \left[\frac{\text{Min}_{(\text{mission time})}}{N_{(\text{mission time})}} \right] \quad (4)$$

3.2 Scoring Summary

A team's competition score is a function of a their Design Report Score, Total Mission Score, and Participation Score as shown in Equation 5. A team's Total Mission Score is the sum of their individual mission scores shown in Equation 6, and their Participation Score P as shown in Table 1.

$$\text{Competition Score} = \text{Design Report Score} \bullet \text{Total Mission Score} + P \quad (5)$$

$$\text{Total Mission Score} = S_{M1} + S_{M2} + S_{M3} + S_{GM} \quad (6)$$

Table 1: Participation Score

P	Participation Score
1	Attending the Fly-off
2	Completing Tech Inspection
3	Attempting a Flight Mission

3.3 Translating Mission Requirements to Sub System Design Requirements

A list of all requirements and constraints from the 2023-24 DBF Rules was created to derive subsystem design requirements. These requirements and constraints are shown in Table 2.



Table 2: Mission Requirements and Constraints

Type	Label	Requirement
General	G.1	The airplane must be remotely controlled
	G.2	The wingspan cannot exceed 5 feet (1.52 m)
	G.3	The airplane must fit within a 2.5 ft (0.762 m) wide parking spot while upright on its gear in the parked configuration
	G.4	The airplane must takeoff within 20 feet (6.10 m) for all missions
	G.5	The airplane must have a single plane, horizontal floor to carry payloads
	G.6	All payloads must be mounted upright and perpendicular to the floor (excluding the patient)
	G.7	All payloads must have a restraint system to keep them from moving during all phases of flight
	G.8	All payloads cannot touch any part of the airplane except for the floor, restraint system, and insert(s)
	G.9	The Crew shall be in a cockpit such that their heads are above the fuselage forward of the cockpit
	G.10	The hatches must comply with constraints set out in the rules
	G.11	The airplane must complete a successful landing after each mission to receive a score
	G.12	The Crew must be loaded through hatches forward of the required bulkhead
	G.13	The radio control system and propulsion system(s) must have an externally accessible switch and arming plug(s), respectively
	G.14	Propulsion power total energy stored cannot exceed 100 watt-hours
	G.15	Maximum of one battery connected to each propulsion system
Staging	S.1	The time to assemble the airplane and install the Crew, propulsion battery packs, and mission payload must be less than 5 minutes
	S.2	The airplane must remain upright on its gear
	S.3	The airplane must be put into the flight configuration prior to installing any payload components or propulsion batteries
Mission 1	M1.1	Stage the airplane for M1
	M1.2	Carry no payload
	M1.3	Fly 3 laps within 5 minutes
Mission 2	M2.1	Stage the airplane for M2
	M2.2	Carry the Crew, EMTs, Patient on gurney, and Medical Supply Cabinet
	M2.3	Fly 3 laps within 5 minutes
	M2.4	Maximize Medical Supply Cabinet weight and minimize time to fly 3 laps
Mission 3	M3.1	Stage the airplane for M3
	M3.2	Carry the Crew and passengers
	M3.3	Maximize passengers carried and laps flown in 5 minutes, minimize propulsion battery pack watt-hours
Ground Mission	GM.1	Configure the airplane for M2, then M3, beginning and ending with the airplane in the parked configuration with no payload installed
	GM.2	Minimize airplane configuration time

The list of subsystem design requirements derived from Table 2 is shown in Table 3. Each item in Table 3 lists the mission requirement(s) and constraint(s) from which it was derived.



Table 3: Derived Sub System Design Requirements

Category	Label	Parent Requirement(s)	Sub-System Requirement
Aircraft Performance	A.1	M2.3, M3.3	Minimize drag to maximize top speed and minimize propulsion energy required
	A.2	M2.3, M3.3	Maximize lift generated to carry more payload
	A.3	G.4	Achieve high static thrust and sufficient lift for a short ground roll
	A.4	M1.2, M2.2, M3.2	Ensure the airplane remains balanced under different loading configurations
	A.5	G.2, G.3	If the wing(s) have a span exceeding 2.5 ft, they must be stowable to fit within a 2.5 ft wide parking space
	A.6	G.14, M2.3, M3.3	Ensure the airplane can achieve endurance and range targets
	A.7	G.1	Have good stability and control characteristics
Payload Accommodations	P.1	S.1, GM.1	The hatches and fuselage compartments must permit mission payloads to be loaded in minimum time
	P.2	S.1	Stowable wing (if used) must be quickly configurable
	P.3	G.7	Include restraint systems for all payloads
	P.4	G.8	Provide sufficient space in cockpit and payload compartments
	P.5	G.10	Payload insert(s) must fit through 6 in wide hatches
Electronics	E.1	G.13	Holes in fuselage to accommodate an arming fuse for each propulsion system and a switch for radio system
	E.2	G.3	Wire organization to prevent tangling when manipulating the stowed wing(s) (if used)
	E.3	G.15	Use more than one propulsion battery if more than one motor is used

3.4 Competition Score Sensitivity Analysis

Scoring Analysis

To obtain the highest competition score, a MATLAB [2] script was written to analyze airplane performance. The team chose ranges of airplane design parameters expected to be seen at the competition fly off. Values of thrust, propulsion battery Watt-hours, wing area, Take Off Gross Weight (TOGW), and flight speed were discretized over these ranges; combinations of these parameters were then translated to mission scores using the scoring equations listed in Section 3.1. Wing areas between 3.00-6.50 ft² (0.279-0.557 m²), MTOWs between 10.0-35.0 lb (44.5-156 N), thrusts between 10-35 lb (44.5-156 N), and flight speeds between 73.0-147 ft/s (22.2-44.8 m/s) were considered. The airplane design parameters were selected to maximize the M_2 and M_3 scores. Designs not satisfying all competition requirements and constraints were removed. The ideal airplane design parameters selected as a result of this analysis are shown in Table 4.

Sensitivity Analysis

After finding airplane design parameters which maximized the M_2 and M_3 scores, a sensitivity analysis was performed on the overall score to identify which design parameters should be prioritized over others. Design parameters were varied around their predicted optimal values, and the resulting percent change in the score was calculated. The results of the sensitivity analysis are shown in Figure 10. This analysis shows that M_3 has the most potential to increase the overall score. Decreasing M_3 laptime and Watt-hours are of equal importance, while increasing the number of passengers carried has a relatively smaller effect on the overall score. For M_2 , decreasing laptime offers more gains than increasing the MSC weight. Decreasing the ground mission loading time increases the overall score more than any other parameter.



Table 4: Scoring Analysis Results

Parameter	Value	
	M2	M3
Speed (mph)	70.0	60.0
Watt-hours	100	90.0
Weight (lb)	16.0	16.0
Wing Area (ft ²)	5.00	

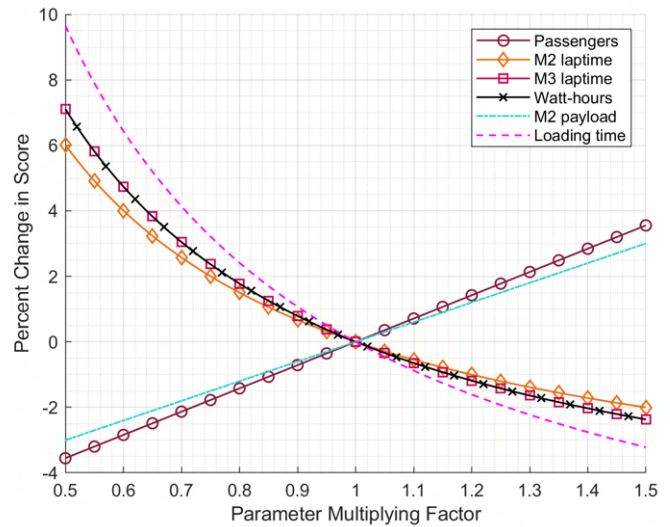


Figure 10: Competition Score Sensitivity

3.5 Airplane Configuration Selection

Using the results of the sensitivity analysis discussed in Section 3.4, the team produced FoM to down select the aircraft configuration, wing placement, tail configuration, propulsion system placement, and landing gear configuration. The FoM are listed in Table 5. These criteria were placed through an analytical hierarchy process to obtain weights to be used in decision matrices. The configurations were then scored on the relevant criteria with a higher value corresponding to a more desirable choice.

Table 5: Figures of Merit

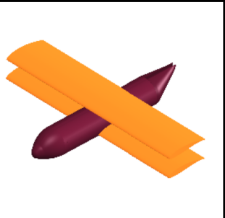
FoM Criteria	Reasoning
Cargo Space	High cargo capacity maximizes M3 score
Drag	Low drag allows for higher top speed and lower power draw
Lift	High lift maximizes payload and reduces takeoff distance
Efficiency	Increased propulsive efficiency maximizes endurance
Ground Effect	Increased L/D near the ground reduces takeoff ground roll
Loading Ergonomics	Ergonomic design maximizes GM score
Maneuverability	Faster turns minimize lap time
Manufacturability	Low manufacturing time keeps the project on schedule
Simplicity	Design must be feasible
Size	Wing span and hatch sizing constraints
Stability	High stability reduces pilot workload
Structural Integrity	Robust structure minimizes the chance of failure
Takeoff Performance	Good takeoff performance minimizes takeoff ground roll
Velocity	High velocity maximizes mission scoring
Weight	Low weight improves flight performance



3.5.1 Wing Configuration

The team compared monoplane, biplane, and flying wing configurations for THE. The FoM corresponding to these configurations are lift, drag, maneuverability, weight and manufacturability. These FoM are shown in the decision matrix in Table 6.

Table 6: Aircraft Configuration Decision Matrix

				
Figures of Merit	Weight (%)	Biplane	Monoplane	Flying Wing
Lift	30	5	3	4
Drag	25	1	4	5
Maneuverability	20	5	3	4
Weight	15	1	3	2
Manufacturability	10	1	5	2
Total Score	100	1.9	3.2	2.9

Lift and drag were weighed first and second when choosing the wing configuration as they have the highest bearing on airplane performance and mission scoring. However, lift is weighted higher than drag due to the 20.0 ft (6.10 m) takeoff requirement. Maneuverability and weight were weighted third and fourth as they decrease lap time and increase payload capacity to maximize the M_2 and M_3 scores. Manufacturability was weighed the least since the team determined that manufacturing complexity was an acceptable cost to increase airplane performance.

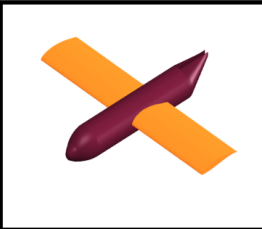
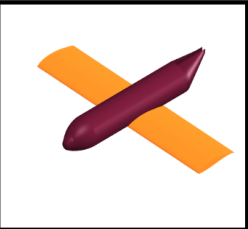
The monoplane configuration is simple and stable, but does not have as much lift as the biplane and generates more drag than the flying wing. The biplane configuration provides the most lift but also comes with much more drag and weight than monoplane and flying wing configurations due to the additional wing. The flying wing configuration is the smallest and generates the least drag, but it also comes with a high degree of design complexity and low stability as it has no tail or fuselage. The team chose a monoplane configuration as it provides the best balance between size, drag, and predicted performance.

3.5.2 Wing Placement

The team compared low-, mid-, and high-wing configurations for THE. The FoM corresponding to these configurations are cargo space, ground effect, manufacturability, simplicity, and maneuverability. These FoM are shown in the decision matrix in Table 7.



Table 7: Wing Placement Decision Matrix

				
Figures of Merit	Weight (%)	High Wing	Mid Wing	Low Wing
Cargo Space	25	5	1	2
Ground Effect	25	2	3	5
Manufacturability	20	5	2	3
Simplicity	15	5	1	3
Maneuverability	15	3	4	5
Total Score	100	3.5	1.4	2.3

When choosing the wing placement, the team weighted cargo space and ground effect the highest. Cargo space allows the airplane to carry a high payload, while ground effect allows the airplane to takeoff in a shorter distance. Manufacturability was weighed lower than these two FoM since the team determined that airplane performance should take precedence over manufacturability. Simplicity and maneuverability were weighted the least since all wing placements do not significantly affect these two FoM.

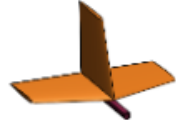
A high-wing configuration is not able to benefit from ground effect as much as the low- and mid-wing configurations, but it does not affect cargo space and is simple to manufacture. A mid-wing configuration benefits more from ground effect but would require the spar of the wing to cut through the fuselage which decreases cargo space and increases GM time. Low-wing designs allow for more efficient use of ground effect to increase lift at low altitudes and are structurally sound, but they have less stability than the high- and mid-wing configurations and still cut through the fuselage decreasing cargo space. The team chose a high-wing configuration for THE because it is simple, structurally sound and does not decrease cargo space.

3.5.3 Tail Configuration

The team compared the T-Tail, V-Tail, and conventional tail configurations for THE. The FoM used to compare these contenders were stability, manufacturability, control, weight, drag, and ground clearance. The weighted rating of each tail configuration to these criteria are quantified in Table 8.



Table 8: Tail Configuration Decision Matrix

				
Figures of Merit	Weight (%)	T-Tail	V-Tail	Conventional Tail
Stability	25	3	5	4
Manufacturability	20	3	2	5
Control	20	5	3	5
Weight	15	3	5	4
Drag	15	4	5	4
Ground Clearance	5	5	5	4
Total Score	100	3.7	4.0	4.4

Stability was given the highest weight as this is the primary function of the tail and reduces pilot workload. Manufacturability was given the second greatest importance as this allows the empennage to be built quickly and consistently. Controllability was rated as the third most important feature, as the airplane must be easily controlled in all missions to minimize lap time. The weight contributed by the tail in each configuration was considered, as a lower weight will allow greater payload capacity in M_2 and M_3 . Lower drag helps increase the overall speed in M_2 and M_3 , but the low overall contribution compared to the wing and fuselage gave this category a low weighting. The design's ability to avoid a tail strike had to be considered due to the Angle of Attack AoA required for the 20.0 ft (6.10 m) take-off in all flight missions.

Utilizing the above criteria and weighting, it became clear that while the T-Tail configuration provides ample ground clearance and offers strong longitudinal control, the complexity of the design makes manufacturing difficult and combined with the risk of deep stall, this configuration is not the strongest option. The V-Tail configuration would allow for decreased weight and drag from the combined stabilizer surfaces. However, this configuration would add design complexity. The conventional tail was selected due to its consistent performance in all categories. The manufacturing of this configuration is well known by the team, allowing efficient and accurate builds with more than sufficient stability and control.

3.5.4 Wing Stowing Mechanism

DBF @ VT considered folding wingtips, a rotating wing, and a 2.50 ft (0.762 m) wing span to fit the airplane in the parking spot described in the 2023-24 DBF rules.



Table 9: Wing Stow Mechanism Decision Matrix

				
Figures of Merit	Weight (%)	Folding Wingtips	Rotating Wing	2.5 ft Span Wing
Structural Integrity	25	4	4	5
Weight	20	4	5	2
Manufacturability	15	3	4	5
Loading Ergonomics	15	3	3	5
Lift	15	3	5	1
Simplicity	10	3	4	1
Total Score	100	3.5	4.2	3.4

Structural integrity was weighed the highest as stowable wings carry a high risk for sustaining structural damage, and a structural failure of the wing is an unacceptable outcome. The weight (as in mass) of the wing stow mechanism was weighed second as each of these concepts would add a significant amount of mass to the design. Manufacturability, loading ergonomics, and lift were tied for third. Manufacturability allows for a quick build time and reduces the risk of schedule overruns. Loading ergonomics and lift maximize the GM and flight mission scores by reducing the airplane configuration time and maximizing THE's payload.

The 2.50 ft (0.762 m) wing was quickly ruled out due to the very low lift it was capable of producing. Folding wingtips allow the midwing to be permanently fixed to the fuselage allowing for good structural integrity. However, this configuration increases the loading time by forcing the ground crew member to unfold two wingtips, and adds mass by having to reinforce the wing at the two folding locations. The rotating wing allows for a quick configuration time, has the lowest mass, has a high degree of structural integrity, and has no discontinuities in the wing lifting surface. The rotating wing concept was rated the highest and was selected for THE.

3.5.5 Propulsion

The conceptual design of the propulsion system examined the tractor, twin, and pusher configurations. The FoM corresponding to these configurations were takeoff performance, velocity, efficiency, weight, and simplicity. These FoM are depicted in the decision matrix in Table 10.



Table 10: Propulsion Decision Matrix

				
Figures of Merit	Weight (%)	Tractor	Twin	Pusher
Takeoff Performance	30	1	5	3
Velocity	25	4	3	2
Efficiency	20	3	1	5
Weight	15	4	3	2
Simplicity	10	5	4	1
Total Score	100	3.0	3.3	2.8

Takeoff performance was weighed the highest due to the restrictive 20.0 ft (6.10 m) takeoff distance. Velocity, efficiency, and mass were weighed second, third, and fourth, respectively. These three FoM maximize flight mission scoring and are weighed according to the team’s deliberation on their importance. Simplicity is weighed the least as the team valued flight performance more.

A twin-motor configuration produces the most thrust and can take advantage of blown lift. This phenomenon increases the lift generated by accelerating air over the wing using the propellers. However, a twin-motor configuration produces more induced drag, limiting the top speed and endurance of the configuration. The tractor configuration could achieve the highest velocity and is the least complex, but does not have the added benefit of blown lift. The pusher configuration has the highest efficiency, but this method of mounting the motor increases the design complexity. The team chose the twin-motor configuration as it provides the best takeoff performance with balanced velocity and simplicity.

3.5.6 Landing Gear

The team compared taildragger, tricycle, and retractable tricycle gear configurations for THE. The FoM corresponding to these configurations are takeoff performance, weight, complexity, drag, and shock absorption. These FoM are shown in the decision matrix in Table 11.

Table 11: Landing Gear Decision Matrix

				
Figures of Merit	Weight (%)	Taildragger	Tricycle	Retractable Tricycle
Takeoff Performance	25	3	4	4
Weight	20	4	3	2
Drag	20	3	3	5
Simplicity	20	3	5	1
Structural Integrity	15	3	4	2
Total Score	100	2.6	2.8	2.7



The landing gear configuration has a large effect on THE's takeoff ground roll, and takeoff performance was rated as the highest FoM for the landing gear. Weight, drag and simplicity are tied for second after takeoff performance. Reducing the weight and drag from the gear increases mission scoring.

The highest consideration was given to landing gear configurations which minimized takeoff ground roll to meet the 20.0 ft (6.10 m) takeoff requirement. The gear placement affects the takeoff ground roll of the airplane as all ground contact points must be ahead of the starting line. The tricycle gear was rated higher than the taildragger in this category as a tail wheel would require the empennage to begin ahead of the starting line, whereas a tricycle gear permits the empennage to hang behind the starting line.

3.6 Final Conceptual Design Configuration

The final airplane configuration features a high wing, conventional tail, twin motors and tricycle gear. The twin motors allow for maximum thrust to takeoff within 20 ft (6.10 m) while the high wing and conventional tail aid airplane stability and manufacturability. This airplane configuration is shown in Figure 11.

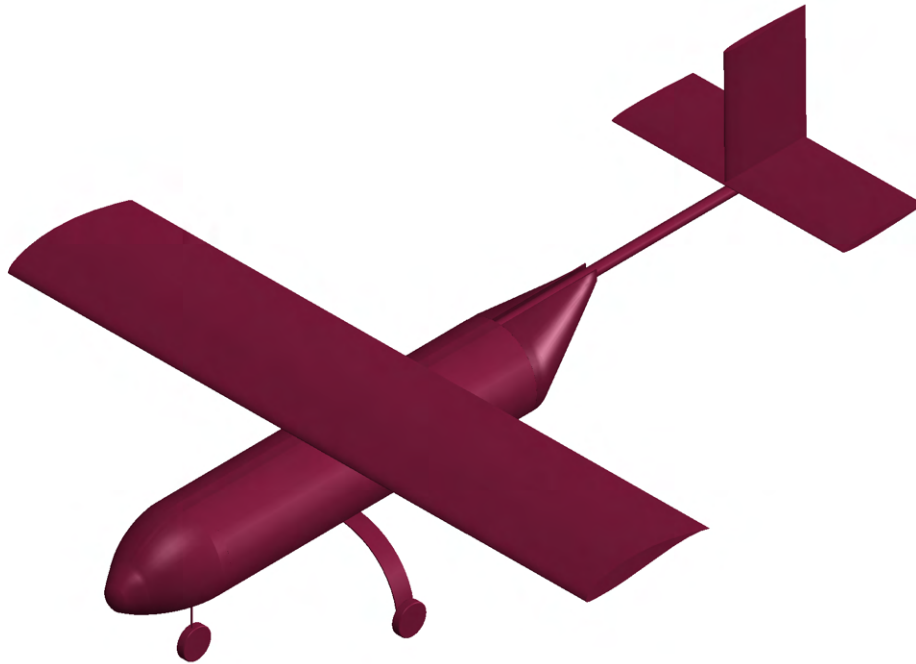


Figure 11: THE Final Airplane Configuration



4 PRELIMINARY DESIGN

The preliminary design phase of THE generated a design which complied with all mission requirements and maximized mission scoring. Testing of two prototypes allowed the team to validate predicted performance and refine the design to satisfy all dimensional and performance-related constraints.

4.1 Design Methodology

The team's design methodology is based on experience from prior years and input from team alumni. The scoring analysis performed in Section 3.4 provided starting points for the design. Each sub team used computer simulations, hand calculations, and historical data to perform trade studies for their respective component(s). Software including SOLIDWORKS, Fusion 360, XFLR5, AVL, and MATLAB were used to model and iterate upon the design until the team converged on a competitive airplane [2, 3, 4, 5, 6]. The models generated in these software helped predict the mission performance parameters that THE could achieve. Performance models generated in Section 3.4 were used to select designs which maximized the competition score. Flight and ground testing was performed to evaluate the airplane's actual performance after the design was judged to meet all the requirements in Section 3.1. The team iterated on the design to converge on an airplane which maximized performance. This design process is shown in Figure 12.

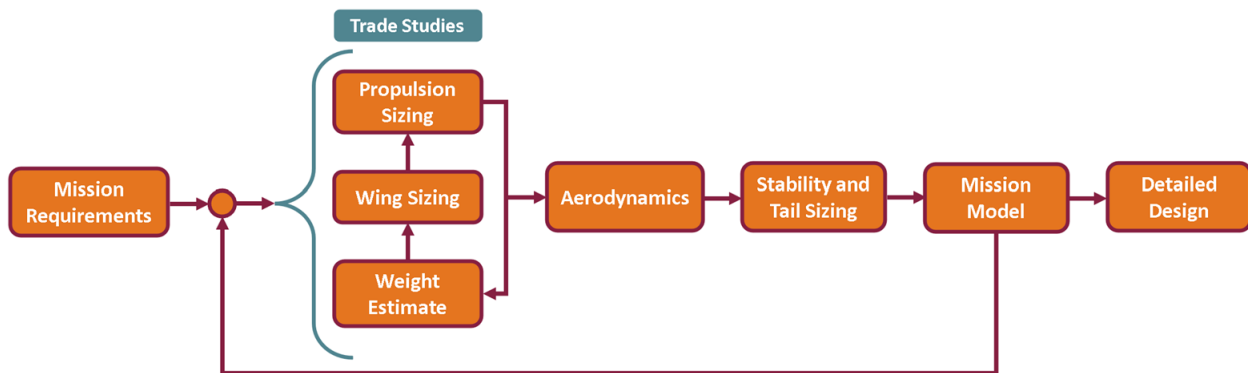


Figure 12: Design Process

4.2 Aerodynamics

4.2.1 Weight Estimation

Initial weight estimates were determined using the results of the sensitivity analysis performed in Section 3.4. This analysis set a preliminary target MTOW of 16.0 lbs (7.26 kg) for each mission. Using historical DBF data, weights of each airplane subsystem were approximated to maximize payload and performance capabilities in each mission.

4.2.2 Wing Sizing and Geometry

With the given geometry restrictions in Section 3.3, the wing was designed to maximize efficiency and produce the low-speed lift necessary to meet the 20.0 ft (6.10 m) takeoff requirement. The lift generated by a wing is directly proportional to the reference area (S_{ref}), dynamic pressure ($\frac{1}{2}\rho V^2$), and lift coefficient (C_L) as shown in Equation 7.

$$L = \frac{1}{2}\rho V^2 S_{ref} C_L \quad (7)$$



The RFPs dimensional constraint on wing span (b) of 5.00 ft (1.54 m) was the primary challenge when designing a wing to maximize payload with high aerodynamic efficiency. Equation 8 calculates the MTOW based on maximum lift coefficient ($C_{L,max}$), static thrust (T), takeoff distance (d), and gravitational acceleration (g).

$$MTOW = \frac{\sqrt{SC_{L,max}Tdg\rho}}{1.2} \quad (8)$$

Increasing the wing's area and $C_{L,max}$ will increase the MTOW of THE. $C_{L,max}$ is dictated by the airfoil selection, covered in Section 4.2.3. A longer wingspan, given a constant wing area would increase the Aspect Ratio (AR) of the wing, as seen in Equation 9. A higher AR decreases the Induced Drag ($C_{D,i}$) of the wing as seen in Equation 10, calculated using the Oswald Efficiency Factor (e), which is typically about 0.8.

$$AR = \frac{b^2}{S} \quad (9) \quad C_{D,i} = \frac{C_L^2}{\pi e AR} \quad (10)$$

High Lift Devices

To take-off in under 20.0 ft (6.10 m) while lifting 16.0 lb (7.26 kg), the use of high lift devices was necessary. For ease of manufacturing, simple flaps were chosen that occupied 64.0% of the wing span that deflect to 30°. These flaps allow THE to generate the required lift necessary to lift 120% of the expected MTOW. During take-off, THE's ailerons deflect to 15° down when flaps are deployed to ensure take-off in less than 20.0 ft (6.10 m). A visual geometry of the airplane's wing planform is shown in Figure 13.

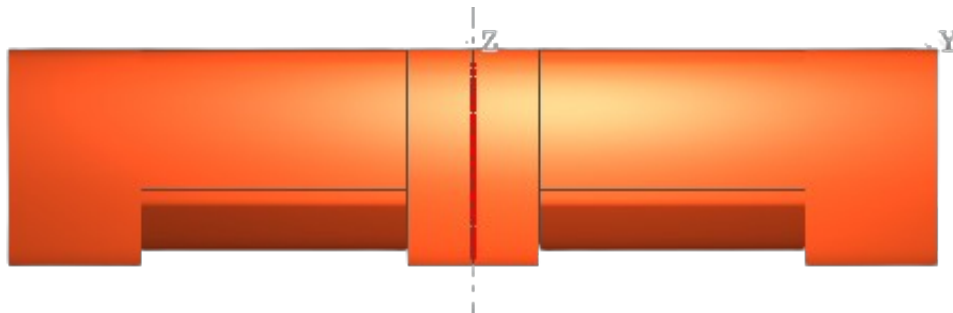


Figure 13: THE Wing Planform

The full details of THE's wing are listed in Table 12.

Table 12: THE Wing Characteristics

Wing Characteristics	
Span	60.0 in (1.52 m)
Root Chord	13.0 in (0.33 m)
Tip Chord	13.0 in (0.33 m)
Flap type	Simple
Flap Span Percentage	64.0%
Flap Chord Percentage	35.0%
Maximum Flap Deflection	30.0°
Aileron Takeoff Deflection	15.0°



4.2.3 Airfoil Selection

The goal of the airfoil selection process was to find a high-lift airfoil that minimized drag between Reynolds numbers of 200,000 to 750,000. These Reynolds numbers encompass the expected flight regime of THE. The desired foil would exceed the $C_{L,max}$ necessary to achieve THE's MTOW. The chosen airfoil was down-selected from a list of over twenty high lift airfoils. The top three airfoils and a benchmark NACA 2412 are compared in Table 13 and Figure 14.

Table 13: Airfoil Key Characteristics

Airfoil	Max C_l/C_d	$C_{l,Max}$	$C_l (\alpha = 0^\circ)$	$C_m (\alpha = 0^\circ)$	$C_{d,\alpha} (\alpha = 0^\circ)$	
NACA 2412	79.8 @ 5.5 deg	1.34 @ 14 deg	0.233	-0.050	0.007	
SD 8040	83.4 @ 5 deg	1.39 @ 13 deg	0.310	-0.061	0.007	
FX 60-126	95.9 @ 5.5 deg	1.62 @ 14.5 deg	0.507	-0.116	0.009	
FX 63-137	103.0 @ 3.0 deg	1.68 @ 11.5 deg	0.910	-0.204	0.010	

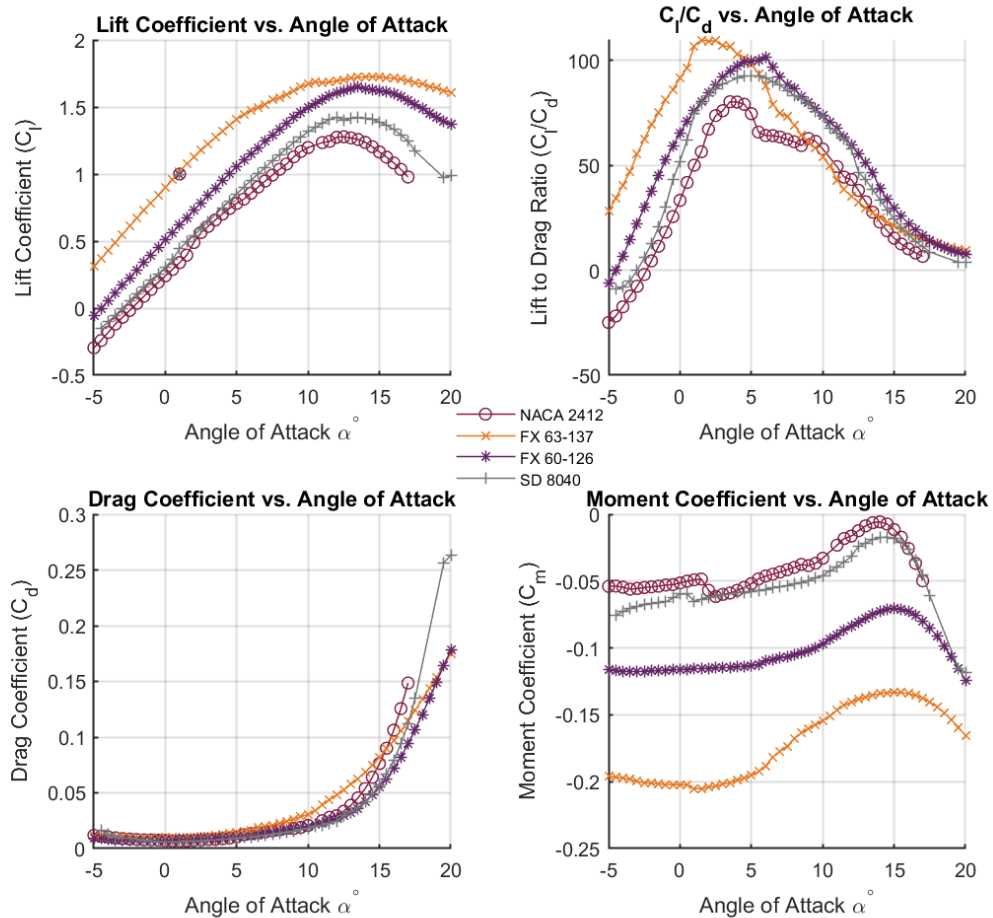


Figure 14: Airfoil Comparison between: NACA 2412, SD8040, FX 60-126, FX 63-137



The Wortmann FX 63-137 was chosen as the airplane's airfoil due to its high aerodynamic efficiency and c_{l_i} . The high $c_{l_{max}}$ combined with the geometry of the wing described in Table 12 allows THE to exceed the desired MTOW of 16.0 lbs (7.25 kg).

4.2.4 Component Analysis

The team performed analysis on the lift and drag of the aircraft using SOLIDWORKS Flow Simulation to validate the results from preliminary sizing. The flow conditions used in the simulation were set to match the predicted take-off and cruise conditions for M_2 and M_3 . The team analyzed the aircraft at an AoA between -5° and 30° and airspeeds between 30.0 ft/s (9.00 m/s) and 110 ft/s (34.0 m/s) with a standard ambient pressure of 14 psi (965 hPa) and temperature of 65°F (18.3°C). The simulation indicated that THE produces a lifting force of 20.6 lb (9.34 kg) and a drag force of 3.31 lb (1.50 kg) on take-off. At maximum speed, the lifting force of THE approached a maximum 28.3 lb (12.8 kg) with a drag of 1.68 lb (0.76 kg). Table 14 shows the parameters DBF @ VT used in its CFD analyses and Figures 15,16, and 17 show example simulations run. These values validate that the preliminary design of THE produces sufficient lift to meet the MTOW targets defined in Section 3.4.

Table 14: Initial Simulation Parameters

Simulation Parameter	Value
Turbulence Model	Kappa-Omega
Fluid Cells	1.80 Million cells
Fluid Cells Contacting Solids	650,000 cells
Reynolds Number	500,000
Airspeed Range	30.0-110 ft/s (9.00-34.0 m/s)
Angle of Attack Range	-5.00 to 30.0°
Temperature	65.0°F (18.3°C)
Pressure	28.5 inHg (965 hPa)

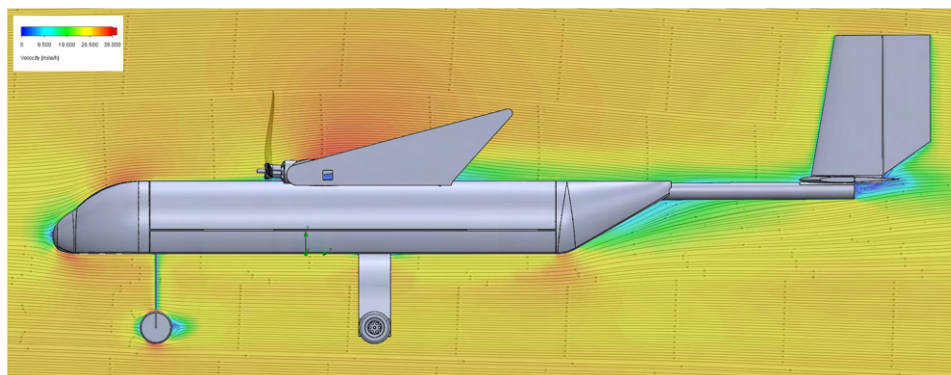


Figure 15: Flow Simulation over THE fuselage

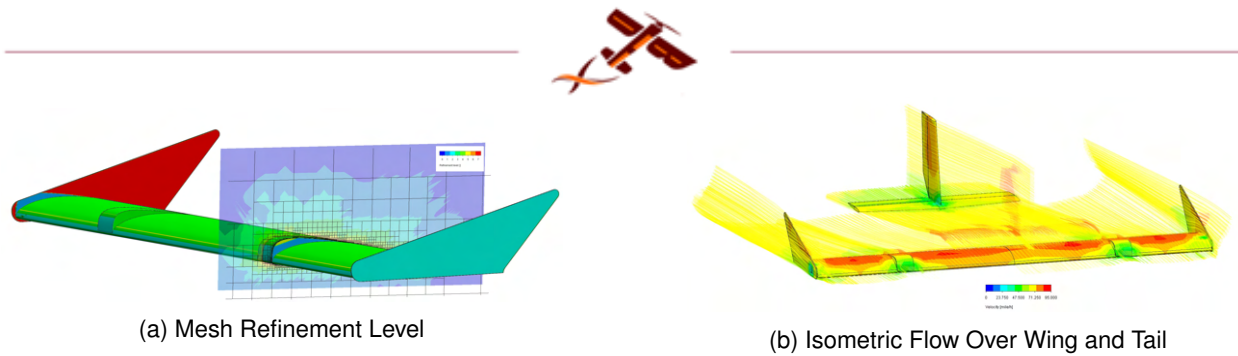


Figure 16: THE Mesh and Flow Simulation

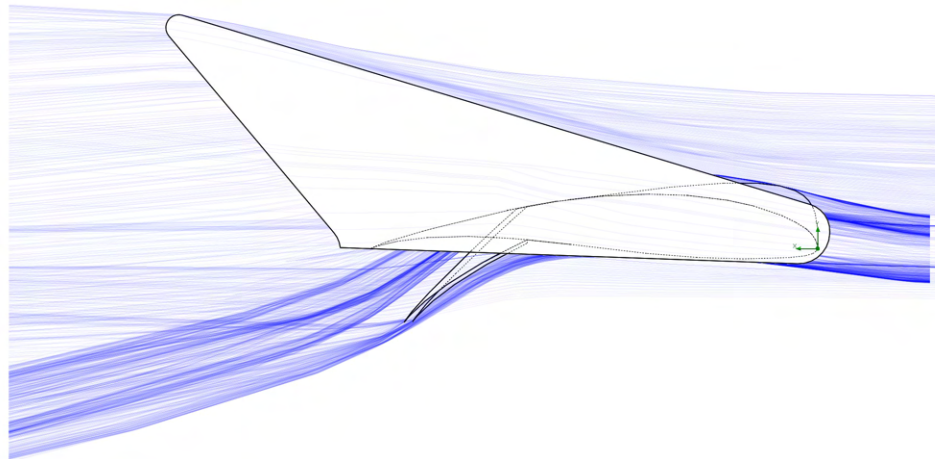


Figure 17: Flow In Takeoff Conditions

4.3 Stability and Control

4.3.1 Tail Sizing and Placement

Tail Sizing

The airplane tail must be designed to maintain static and dynamic stability throughout all flight modes and conditions. To provide sufficient stability, the vertical and horizontal tail coefficients were chosen to be $V_H = 0.750$ and $V_V = 0.100$. These coefficients quantify the size of the tail stabilizers relative to the wing and were selected based on historical DBF @ VT designs. These coefficients are defined in Equations 11 and 12 and were used in all tail sizing calculations.

$$V_H = \frac{S_H l_H}{S \bar{c}} \quad (11)$$

$$V_V = \frac{S_V l_V}{S b} \quad (12)$$

Tail Placement

As a second priority, the tail should minimize its weight and the drag it produces. In order to achieve minimum drag and weight from the tail, the wetted area of the horizontal tail must be minimized. This optimal tail arm can be found through a minimization problem resulting in Equation 13. The tail geometry for THE is shown in Table 15.

$$l_{opt} = K_c \sqrt{\frac{4 \bar{c} S V_H}{\pi D_f}} \quad (13)$$



Table 15: Tail Geometry Values

Surface	Tail Arm	Span	Chord	Tip Chord	Area	Angle	Airfoil
Horizontal Stabilizer	41.5 in (105 cm)	23.7 in (60.1 cm)	8.55 in (21.7 cm)	6.85 in (17.4 cm)	182 in ² (1180 cm ²)	-0.14°	NACA 0007
Vertical Stabilizer	43.0 in (109 cm)	12.1 in (30.7 cm)	10.3 in (26.2 cm)	8.24 in (20.9 cm)	112 in ² (724 cm ²)	0°	NACA 0007

Using Equation 13, the optimal tail arm for the horizontal stabilizer was found. The tail arm for the vertical stabilizer was chosen to maximize directional and lateral stability in cross wind conditions. The team selected tapered stabilizer surfaces to maximize efficiency. A NACA 0007 was chosen to minimize drag while leaving enough volume to fit the tail servos entirely within the tail surfaces. A negative horizontal tail incidence angle was used to balance all moments from the wing. An AVL [6] model of the tail and wing design is displayed in Figure 18.

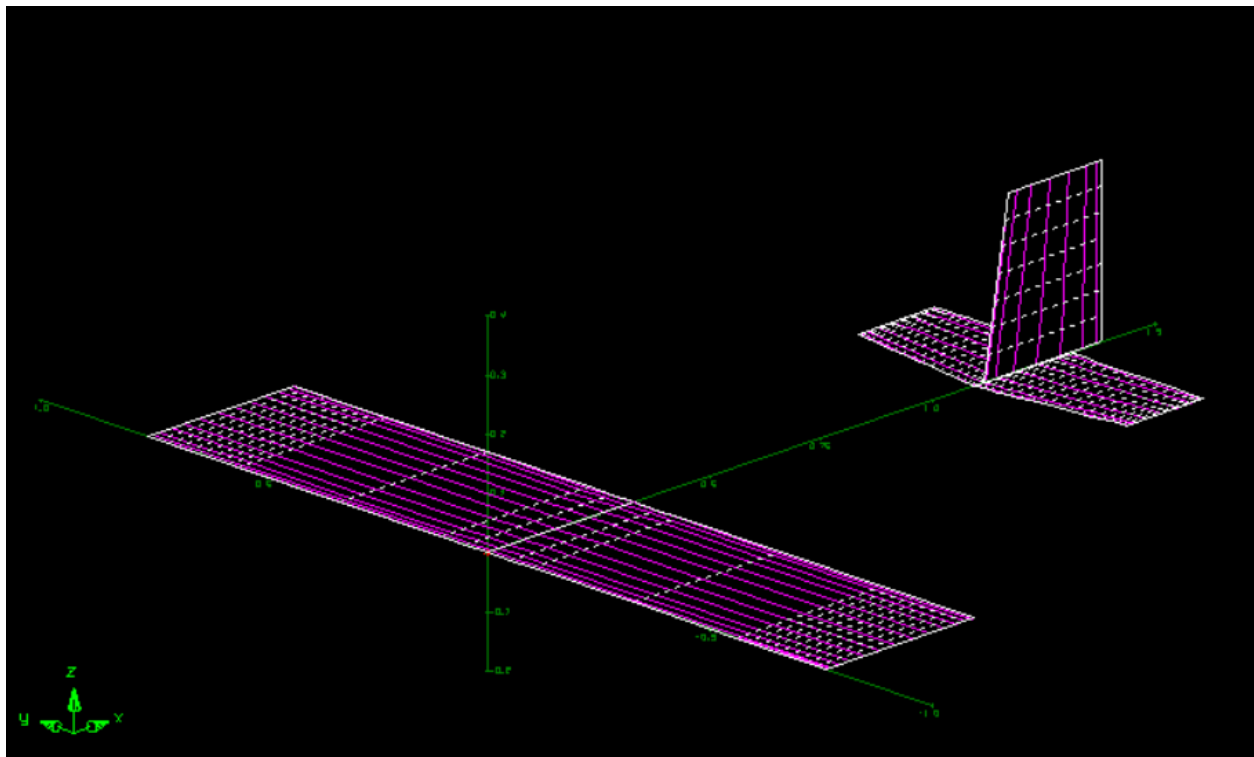


Figure 18: AVL Wing and Tail Model

4.3.2 Control Surface Sizing

Elevator

The primary functions of the elevator are to maintain longitudinal stability, produce adequate take-off rotation, and provide consistent and effective pitch control. Historical DBF @ VT values were used to produce an initial elevator design. The elevator was sized such that a sufficient longitudinal moment was produced to pitch the airplane up at low speeds due to the 20.0 ft (6.10 m) takeoff requirement. Ensuring adequate takeoff rotation also ensured sufficient pitch authority in cruise.



To estimate the take-off rotation, the forces producing a moment about the wheel axle were simplified. This allows the sum of moments to be calculated using Equation 14. The take-off rotation can then be calculated using Equation 15.

$$\Sigma M_{yy} = M_{wt} + M_W + M_t \quad (14)$$

$$\Sigma M_{yy} = \ddot{\theta} I_{yy} \quad (15)$$

The moment of inertia about the lateral axis was estimated using a SOLIDWORKS [3] model of the airplane. In Equation 14, M_T is the moment about the wheel axle produced by thrust, M_W is the moment produced by weight, and M_{wt} is the moment produced by the wing with flaps fully deployed and elevator in the maximum up deflection. Utilizing Equation 14 results in a sum of moments about the wheel axle of 16.9 lb-ft (22.9 N-m). Using SOLIDWORKS, the estimated moment of inertia about the y axis is 1970 lb-in² (222 N-m²). Using the relation in Equation 15 the resulting angular acceleration about the longitudinal axis is 9.62°/s².

The team used the criteria dictated by Jan Roskam in Airplane Flight Dynamics and Automatic Flight Controls, in which he states that a small transport aircraft should have a take-off rotation design point of 8-10°/s² [11]. The takeoff rotation commanded by the elevator when used with the flaps is on the high end of this range and therefore the elevator allows sufficient rotation on take-off and throughout flight. A 50.0% margin of safety was used when sizing the elevator for takeoff rotation. An elevator area of 50.0% of the horizontal stabilizer area was selected based on the results of the takeoff rotation analysis shown in Figure 19.

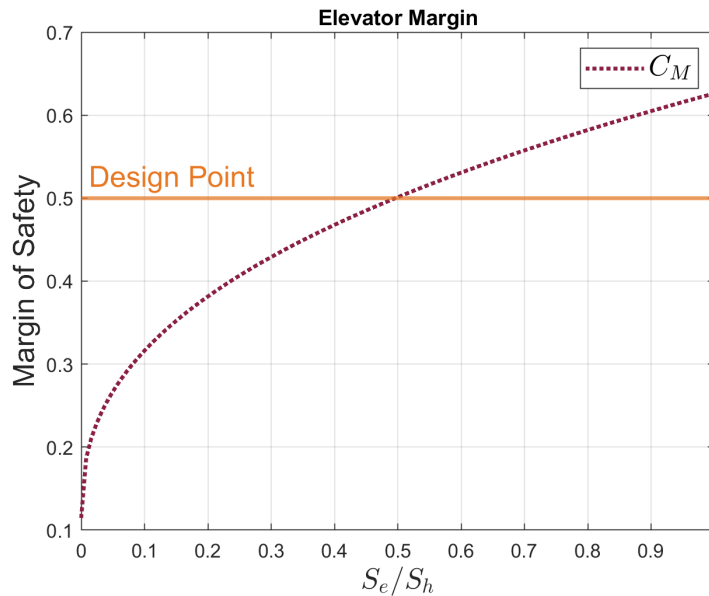


Figure 19: Elevator Control Margin

Rudder

The rudder must be able to effectively coordinate turns with the ailerons and oppose the moments produced by crosswinds. These conditions were a challenge for many teams at past DBF competitions. Because of this, the rudder is designed primarily to maintain the airplane's course under high wind conditions. Based on past DBF @ VT rudder dimensions, the rudder span was selected to be 100% of the vertical stabilizer span and the chord was selected to be 40.0% of the mean vertical stabilizer chord. These choices result in a rectangular rudder with a small cut-out section at the bottom to allow for full elevator deflection.



The test case was selected to be a 20.0 mph (8.94 m/s) crosswind perpendicular to the fuselage on landing, as this was decided by the team to be the maximum allowable crosswind for the airplane. The airplane is designed to maintain a forward heading through crabbing with the rudder alone. Sadraey provides equations which can be solved for the rudder deflection necessary to keep the airplane longitudinal axis aligned with the runway [7]. The required rudder deflection in a 20.0 mph crosswind was found to be 26.5° , which is 3.50° less than the maximum.

Ailerons

The ailerons serve to roll the plane and work with the rudder to coordinate turns. The ailerons span the outer 8.00 in (20.3 cm) of the wing with a constant chord of 3.90 in (9.91 cm). The ailerons will perform sufficiently to induce roll during any flight condition if they produce an adequate roll rate during takeoff. MIL-STD-1797A Class IV requirements state a necessary minimum roll rate of $90^\circ/s$ [8]. This roll rate, P can be calculated using Equation 16.

$$P = \frac{-2VC_{l_{\delta_A}}\delta_A}{bC_{l_p}} \quad (16)$$

AVL was used to estimate the aileron control derivatives used in Equation 16 [6]. The control surface sizing and placement results in a roll rate of 305° per second, more than satisfying the MIL-STD-1797A requirement, and producing a Factor of Safety (FS) on the roll rate of 3.39. In addition to roll control during flight, the ailerons will be drooped on takeoff to produce additional lift by acting as an extension of the flaps.

4.3.3 Control Surface Hinge Moment Identification

Each control surface is actuated by a single servo. These servos must be properly sized to overcome the hinge moments produced by the loads on the control surfaces. AVL was used to calculate the hinge moment coefficient for each surface at its maximum deflection and maximum flight speed. The required torque for each servo can be found using these coefficients and Equation 17 [6]. The required servo torque and servo selections are listed in Table 16.

$$H_m = 1/2\rho V^2 S_{ref} C_{ref} C_{H_m} \quad (17)$$

Surface	Maximum Deflection ($^\circ$)	Hinge Moment	Servo	Maximum Servo Output
Flap	30	68.0 oz-in (4.89 kg-cm)	HITEC HS-5645MG	168 oz-in (12.1 kg-cm)
Aileron	20	10.9 oz-in (0.786 kg-cm)	HITEC D145SW	84.0 oz-in (6.05 kg-cm)
Elevator	25	29.3 oz-in (2.11 kg-cm)	HITEC D145SW	84.0 oz-in (6.05 kg-cm)
Rudder	30	20.4 oz-in (1.47 kg-cm)	HITEC HS-5125MG	48.6 oz-in (3.50 kg-cm)

Table 16: Hinge Moments and Resulting Servo Selections

4.3.4 Static Stability Analysis

Static stability is the immediate tendency of a system to return toward the nominal state when perturbed. The airplane must be statically stable in all axes of motion to minimize pilot workload. The recommended ranges of stability derivatives suggested by Sadraey [7] and those calculated for THE are displayed in Table 17. All values fall within the suggested ranges which indicate the plane has sufficient static stability in all axes of motion.



Table 17: Static Stability Values

	C_{m_α}	C_{m_q}	C_{l_β}	C_{n_β}	C_{n_r}	Static Margin
Recommended	-0.3 to -1.5	-5 to -40	<0	0.05 to 0.4	-0.1 to -1	10% to 30%
Calculated	-1.24	-17.0	-0.10	0.216	-0.366	26.8%

Static stability is heavily influenced by the static margin. The team calculated the static margin of the airplane by taking the distance between the CG and neutral point and normalizing this distance to the wing chord. The neutral point of THE was calculated using AVL and is located at 6.99 in (17.8 cm) of the wing chord. The CG location for the airplane is located at the quarter chord for all airplane configurations. Based on this, the nominal static margin for THE was calculated as 26.8%. To keep the static margin within the limits shown in Table 17, forward and aft CG locations of -2.40 in (-6.10 cm) and 6.99 in (17.8 cm) respectively, were set. These distances were measured aft from the leading edge of the wing.

4.3.5 Dynamic Stability Analysis

Dynamic stability is the tendency of a system to return to equilibrium over time. This is characterized by oscillating motion about a nominal state and exponential decay of this oscillation. THE must have adequate dynamic stability to reduce pilot workload; underdamped modes result in the need for constant input from the pilot to correct the motion. The team considered the Dutch-Roll, Phugoid, Roll, Short Period, and Spiral modes when designing for dynamic stability. The response of the airplane to each mode can be quantified through complex eigenvalues that characterize the equation of motion specific to that mode. Imaginary eigenvalue components characterize oscillation while real eigenvalue components characterize exponential growth or decay. AVL was used to calculate these eigenvalues, and they can be seen on the root locus plot in Figure 20a. A flight mode is considered damped if the corresponding eigenvalues lay in the left half of the plane.

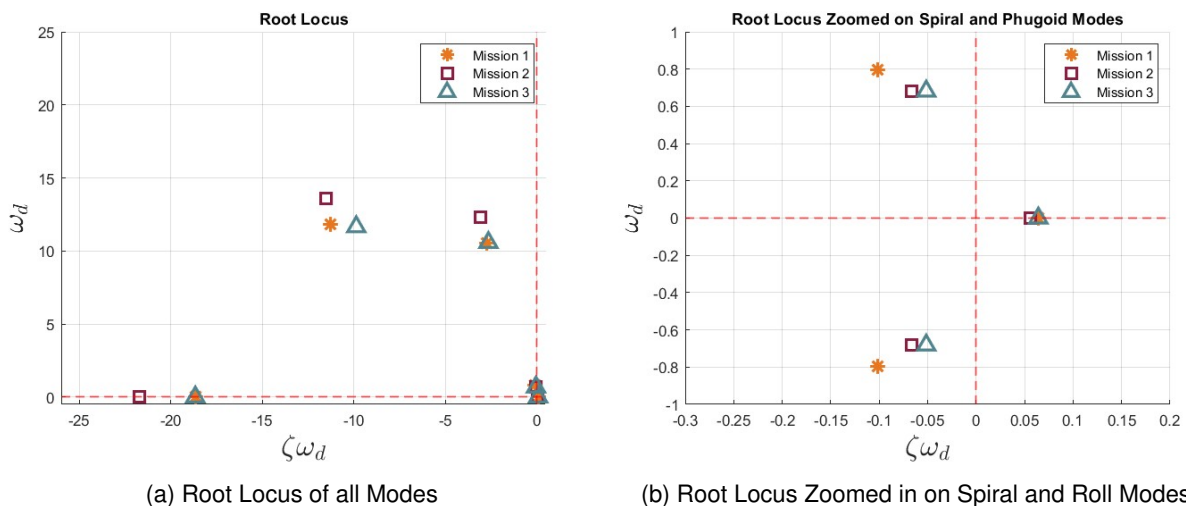


Figure 20: Root Locus Plots

MIL-F-8785C defines three mission categories: A, B, and C. Category A encompasses flight phases such as reconnaissance and ground attack, Category B encompasses sub-terminal flight phases including climb



and descent, and Category C encompasses terminal flight phases such as takeoff and landing. In addition to these three categories, MIL-F-8785C defines 3 flying quality levels, these levels and associated pilot workloads are described in Table 18

Table 18: Flying Quality Levels

State	Description	Pilot Workload
Level 1	More than sufficient flight characteristics to complete the mission in a safe manner	Minimal
Level 2	Sufficient flight characteristics to complete the mission in a safe manner	Slightly increased
Level 3	Flight characteristics that cause excessive pilot workload, plane is still considered flyable	High

Tables 19 and 20 show the requirements for an airplane to achieve different flight qualities. Category B is not investigated further due to its similarity to Category C. In these tables, t_2 is the time to double amplitude of any mode, and s is the time constant of the roll mode.

Table 19: Category A Dynamic Mode Requirements

	Category A Dynamic Modes Requirements							
	Short Period		Phugoid	Dutch Roll		Spiral	Roll	
Level 1	$\omega_{sp} \geq 1$	$0.35 < \zeta < 1.3$	$\zeta > 0.04$	$\zeta > 0.4$	$\zeta \omega_n > 0.4$	$\omega_n > 1$	$t_2 > 12s$	$s < 1.0$
Level 2	$\omega_{sp} \geq 0.6$	$0.25 < \zeta < 2.0$	$\zeta > 0$	$\zeta > 0.02$	$\zeta \omega_n > 0.05$	$\omega_n > 0.4$	$t_2 > 8s$	$s < 1.4$
Level 3	-----	$0.15 < \zeta$	$t_2 \geq 55s$	$\zeta > 0$	-----	$\omega_n > 0.4$	$t_2 > 4s$	$s < 10$

Table 20: Category C Dynamic Mode Requirements

	Category C Dynamic Modes Requirements							
	Short Period		Phugoid	Dutch Roll		Spiral	Roll	
Level 1	$\omega_{sp} \geq 1$	$0.35 < \zeta < 1.3$	$\zeta > 0.04$	$\zeta > 0.08$	$\zeta \omega_n > 0.1$	$\omega_n > 0.4$	$t_2 > 12s$	$s < 1.0$
Level 2	$\omega_{sp} \geq 0.6$	$0.25 < \zeta < 2.0$	$\zeta > 0$	$\zeta > 0.02$	$\zeta \omega_n > 0.05$	$\omega_n > 0.4$	$t_2 > 8s$	$s < 1.4$
Level 3	-----	$0.15 < \zeta$	$t_2 \geq 55s$	$\zeta > 0$	-----	$\omega_n > 0.4$	$t_2 > 4s$	$s < 10$

From the root loci in Figures 20a and 20b, the damping coefficient ζ and damped natural frequency ω_d can be determined for each mode. From these values, the stability of all modes can be evaluated. The characteristic values of each mode are identified in Table 21.

Table 21: Calculated Characteristics of Dynamic Modes

Mission	Mode					
	Short Period		Phugoid		Dutch Roll	
	Value	Flying Quality	Value	Flying Quality	Value	Flying Quality
M1	$\zeta = 0.96$ $\omega = 11.8$	L1	$\zeta = 0.127$	L1	$\zeta = 0.26$ $\zeta \omega = 2.77$ $\omega = 10.5$	L2
M2	$\zeta = 0.85$ $\omega = 13.6$	L1	$\zeta = 0.097$	L1	$\zeta = 0.25$ $\zeta \omega = 3.11$ $\omega = 12.3$	L2
M3	$\zeta = 0.85$ $\omega = 11.7$	L1	$\zeta = 0.076$	L1	$\zeta = 0.25$ $\zeta \omega = 2.65$ $\omega = 10.6$	L2

Mission	Mode			
	Spiral		Roll	
	Value	Flying Quality	Value	Flying Quality
M1	$t_2 = 10.8$ s	L2	$s = 0.0536$	L1
M2	$t_2 = 12.5$ s	L1	$s = 0.0460$	L1
M3	$t_2 = 10.8$ s	L2	$s = 0.0536$	L1



For all missions, THE had Level 1 flying qualities in the Short Period, Phugoid, and Roll modes. For all missions, the Dutch Roll Mode has Level 2 flying qualities, which are not exemplary but pose no issue to the pilot during flight. The M1 spiral mode also exhibits Level 2 performance, but careful pilot input should alleviate any risk of spiral.

4.4 Propulsion System Sizing

4.4.1 Power Pack Sizing

The RFP specified that NiCd, NiMH or Lithium-based power packs could be used. Lithium polymer (LiPo) batteries were chosen for analysis as they have the highest energy density, discharge rate, and nominal voltage of the available battery types. The RFP also states the total stored energy of the power packs must not exceed 100 Watt-hours W-h. Equation was used to determine maximum capacity for each power pack. This was found to be 50 W-h as each propulsion system requires a separate battery.

$$E_{\text{total}} = \text{Capacity (Ah)} \cdot \text{Voltage (V)} \times \text{Number of Batteries} \leq 100 \text{ (Wh)} \quad (18)$$

For M₂, two 6-cell 2250 mAh batteries were selected. These totaled to 100 W-h, this maximized the total allowable stored energy. For M₃, two 5-cell, 2250 mAh batteries were selected, these totaled to 82.2 W-h. The total battery capacity was not maximized for M₃ as a decreased battery capacity has an exponential impact on the M₃ score.

Table 22: Selected Battery Configuration

	Mission 1	Mission 2	Mission 3
Battery	Thunder Power Rampage 5s 2700 mAh 70C	Thunder Power Rampage 6s 2250 mAh 70C	Thunder Power Rampage 5s 2250 mAh 70C
Max Continuous Discharge (A)	189	157.5	189
Energy Stored (Watt-Hours)	100	100	82.2

4.4.2 Motor Sizing

THE's propulsion system was sized to maximize thrust, speed, and endurance while minimizing weight. The primary constraint on the propulsion system was static thrust as this was key to achieve the 20.0 ft (6.10 m) takeoff. It was determined that a 1.45 T/W is required to meet the takeoff constraint with the heaviest configuration. Based on scoring analysis, M₂ must reach a minimum cruising speed of 117 ft/s (35.6 m/s) to achieve a competitive score. For M₃, the airplane must reach a minimum cruising speed of 88.0 ft/s (26.8 m/s) and fly for the entire 5-minute flight window. MotoCalc and Ecalc were used for the analysis along with data charts from the manufacturers [?]. Only Scorpion brushless outrunner motors were considered for analysis due to a team partnership with the company. The analysis showed the Scorpion A-4220-540kV to be the highest performing motor as it produced the highest static thrusts and velocities.

4.4.3 Propeller Sizing

Using the motor's kV of 540 and the missions' respective battery voltages, Equation 19 determined efficient RPM ranges for propeller sizing.

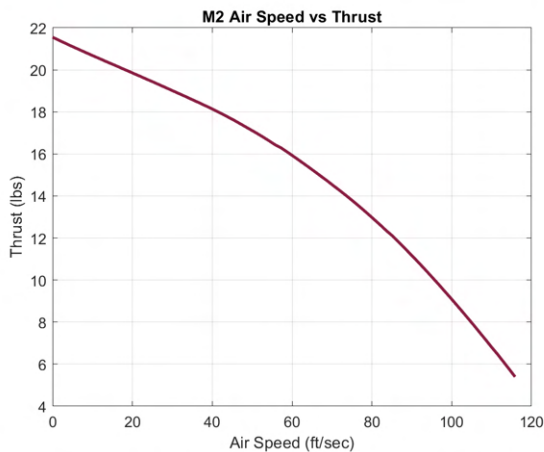
$$kV = \frac{\text{RPM}}{\text{Volts}} \quad (19)$$



With this equation it was found that to perform at maximum efficiency with a 6S battery, 12,000 RPM are needed and with a 5S battery, 10,000 RPM are needed. The APC and the Aeronaut propeller databases [9] were reviewed to find propellers that operate in this range of RPM and could meet the target thrust of 22.0 lbs (97.9 N). The selected propellers were the 14"x9" and 17"x9" Aeronaut folding propellers. These propellers were chosen because of their high pitch-to-diameter ratio, which allows for a higher top speed. Additionally, their smaller size increases efficiency and would not over-stress the motors. The performance predictions for THE are listed in Table 23. Predicted Thrust vs. Airspeed of THE's M₂ and M₃ configurations are shown in Figure 30.

Table 23: Final Propulsion System Configuration

Component	Mission 1	Mission 2	Mission 3
Motor	Scorpion A-4220-540kV		
ESC	Cobra 100A ESC with Switching 6A BEC		
Wire AWG	12		
Battery	Thunder Power Rampage 5s 2700 mAh 70C	Thunder Power Rampage 6s 2250 mAh 70C	Thunder Power Rampage 5s 2250 mAh 70C
Propeller (in x in)	17x9	14x9	17x9
Total System Weight lbs (kg)	3.32 (1.51)	3.32 (1.51)	3.32 (1.51)
Energy Stored (Watt-Hours)	100	100	82.2
Max Continuous Current (A)	90	90	90
Maximum Cruise Speed ft/s (m/s)	90.9 ft/s (27.72 m/s)	120.3 ft/s (36.66 m/s)	90.9 ft/s (27.72 m/s)
Peak Static Thrust lbf (N)	22.8 (101.42 N)	21.6 (96.08 N)	22.8 (101.42 N)
Lap time (s)	33.0	23.9	33.0
Expected Total Mission Time (mm:ss)	1:20	1:12	5:00



(a) M2 Airspeed vs Thrust



(b) M3 Airspeed vs Thrust

Figure 21: THE Thrust vs. Airspeed

4.5 Payload Sizing

4.5.1 Mission Systems Sizing

THE's mission systems were sized to fit in the fuselage, maximize payload density, and allow the systems to adjust the airplane's CG. For M₂, the team designed inserts which complied with the sizing constraints set out in the 2023-24 DBF Rules [1]. The maximum weight for the MSC was determined to be the difference



between THE's MTOW and empty weight to maximize the M_2 score. The rules dictate that the MSC have minimum width and length of 3.00 in (7.62 cm) and a minimum height of 3.50 in (8.89 cm). DBF @ VT has sized the MSC to comply with these rules. Based on the design value of 52 passengers for M_3 , the team determined that 4 passenger inserts each with a length of 5.90 in (15.0 cm) and width of 7.00 in (17.8 cm) would maximize passenger density while still allowing the inserts to fit through 6.00 in (15.2 cm) wide hatches. Each insert carries the passengers in a staggered pattern to carry a maximum of 14 passengers.

4.5.2 Fuselage Sizing

The fuselage was sized to fit the M_2 and M_3 payloads; 1.50 in (3.81 cm) was left between the fuselage ceiling and the top of the MSC to allow ample room to fit wing hardware and wiring. This results in a total fuselage height of 6.25 in (15.9 cm). THE's fuselage width was set at 8.69 in (22.1 cm) to fit all mission inserts; all inserts have a width of 7.00 in (17.8 cm). The team considered the time it would take the ground crew member to open and close the hatches during loading when choosing the number of hatches. The team selected 2 hatches because this was determined to minimize the airplane loading time.

4.6 Mission Performance

The team used MotoCalc, XFLR5, and AVL to predict the performance of THE. These predicted performance parameters were corroborated with the team's historical data to improve their accuracy. THE's mission performance predictions are shown in Table 24.

Table 24: THE Mission Performance

Parameter	Mission 1	Mission 2	Mission 3
Takeoff Weight	11.31 lbs (5.13 kg)	16.0 lb (7.26 kg)	16.0 lbs (7.26 kg)
Takeoff Distance	17.0 ft (5.18 m)	19.5 ft (5.94 m)	19.5 ft (5.94 m)
Stall Speed	33.2 ft/s (10.1 m/s)	39.5 ft/s (12.0 m/s)	39.5 ft/s (12.0 m/s)
Maximum Speed	90.9 ft/s (27.72 m/s)	120.3 ft/s (36.66 m/s)	90.9 ft/s (27.72 m/s)
Cruise Speed	88.0 ft/s (26.82 m/s)	117.7 ft/s (35.76 m/s)	88.0 ft/s (26.82 m/s)
Mission Lap Time	33.0 s	23.9 s	33.0 s

4.7 Uncertainties

Uncertainties associated with each phase of the design process must be acknowledged. Simplifying assumptions and estimations were made during preliminary design to predict airplane performance. Analysis error came from discrepancies between computer models and the manufactured airplane. For example, software such as AVL and XFLR5 cannot model adverse aerodynamic effects due to surface imperfections. Other analysis software suffer from user input error or the inability to account for real-life complexities. The team established margins of safety to prevent any uncertainty from causing a failure in the design.

5 DETAILED DESIGN

5.1 Dimensional Parameters

The team compiled THE's preliminary dimensional parameters into Table 25 for use throughout the detailed design process.



Table 25: THE's Dimensional Parameters

	Wing	Horizontal Tail	Vertical Tail
Airfoil	Wortmann FX 63-137	NACA 0007	NACA 0007
Span	60.0 in (243 cm)	23.7 in (60.1 cm)	12.1 in (30.6 cm)
MAC	13.0 in (33.0 cm)	7.70 in (19.6 cm)	9.27 in (23.5 cm)
AR	4.61	3.08	1.30
Area	728 in ² (7432 cm ²)	181 in ² (1,171 cm ²)	112 in ² (725 cm ²)
Incidence Angle	2.00°	-0.14°	0.00°
Volume Ratio	--	0.75	0.1
Fuselage		Propeller	
Total Length	53.4 in (135 cm)	Manufacturer	Aeronaut
Storage Length	24.0 in (60.9 cm)	Mission 1	17" x 9"
Width	8.40 in (21.3 cm)	Mission 2	14" x 9"
Height	6.22 in (15.8 cm)	Mission 3	17" x 9"
Electronics		Motor (2x)	
Receiver	Spektrum AR14400T	Manufacturer	Scorpion
Servos	HS-5125MG	Model	Scorpion A-4220-540KV
	HS-5065MG		
	D89MW		
Mission 1 Battery	Thunder Power 5S 2700 mAh	Electronic Speed Controller (2x)	
Mission 2 Battery	Thunder Power 6S 2250 mAh	Manufacturer	Cobra
Mission 3 Battery	Thunder Power 5S 2250 mAh	Model	100A ESC with Switching 6A BEC

5.2 Structural Characteristics and Capabilities

The airplane weight and expected flight loads were the main considerations that went into the design of the structure. An MTOW of 16.0 lb (7.25 kg), was used. Of that MTOW, 37.5 percent is the payload weight which equates to 6.00 lb (2.72 kg) in the maximum loading configuration. The remaining 62.5% is the structure of the airplane along with all electronic components.

5.2.1 Wing Structure

The team used carbon fiber tubing for the main structural components because of the material's low weight and high rigidity. A detailed calculator was created and used to choose a spar using a maximum allowable deflection of 0.500 in (1.27 cm) and an FS of 1.50. The final spar configuration consisted of a square tube to prevent components from twisting and to allow for easier implementation of the wing's rotation mechanism. The chosen spar had an outer diameter of 0.875 in (2.22 cm) and a length of 60.0 in (152 cm).

Performing FEA was crucial to the spar's selection process as it predicted performance prior to physical testing. The aforementioned spar was modelled in SOLIDWORKS [3] as a cantilevered beam to simulate half span loading. FEA was run on this model using a tip load of 24.0 lb (106.7 N) to approximate a 2.4 G loading case for the wing spar with a 1.50 FS. The simulation showed a maximum deflection of 0.240 in and is shown in Figure 22. Results of the physical load testing are discussed in Section 8.1.2.

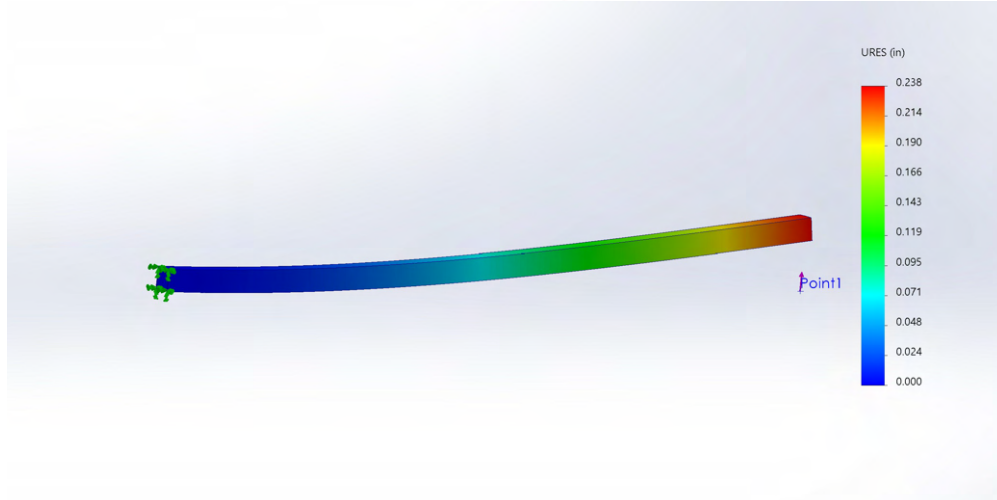


Figure 22: THE Spar FEA

5.2.2 Tail Structure

DBF @ VT chose a single square tube with an outer diameter of 1.00 in (2.54 cm) as the airplane's boom. The boom is attached to bottom of the wing spar at the quarter chord location of the wing using one channel bracket and M5 bolts. To simulate the boom, a 1.00 in (2.54 cm) diameter square tube with a length of 45.0 in (1.14 m) was modeled in SOLIDWORKS [3] in a similar manner to that mentioned in Section 5.2.1. In this case, however, there are two fixed points: one at the end and one 17.0 in (43.2 cm) away from this point to simulate a second boom support at the aft end of the fuselage. A downward force of 17.0 lbs (75.6 N) was applied to the tip to simulate maximum tail down force. The boom displayed a maximum deflection of 0.113 in (.287 cm). The FEA result is shown in 23, and the results of physical load testing are discussed in Section 8.1.2.

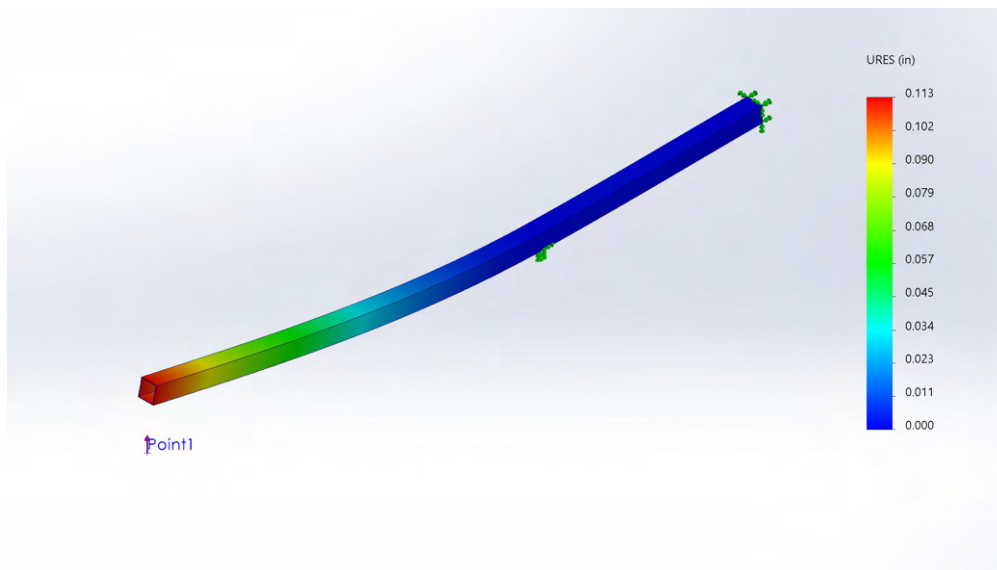


Figure 23: THE Boom FEA



5.2.3 Landing Gear Structure

DBF @ VT designed THE's landing gear to have a height of 7.00 inches, span of in 18.0 in, width of 7.50 in , and wall thickness of 0.130 inches. To confirm that the landing gear configuration would work, the team performed FEA to verify that the gear could handle the expected landing loads. To simulate these forces, the gear was modeled in SOLIDWORKS with a fixed region where the gear would attach to the fuselage. 48.0 lb (21.7 N) loads were placed at the wheel axles, resulting in a maximum deflection of 0.55 in (1.40 cm).

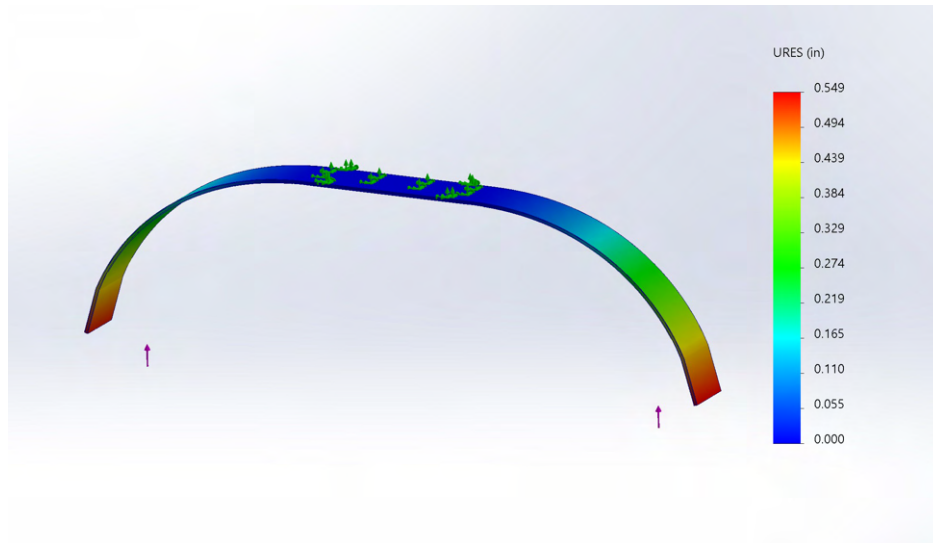


Figure 24: THE Gear FEA

5.2.4 Airplane Weight Breakdown

The team produced a table to evaluate the mass properties of the airplane. Weights predicted by CAD software were compared to those of the manufactured components. For all parts, the coordinate system origin is set at the tip of the nose, with the positive x direction pointing aft along the fuselage, the positive y direction pointing outboard along the right wing, and the z direction pointing down. The mass properties of THE's sub components are shown in Table 26. This information helped the team to place the CG at the quarter-chord of the wing.



Table 26: THE's Weight Breakdown by Mission

Aircraft Component	Mass (CAD)		Mass (Actual)		X Location		Y Location		Z Location	
	oz	g	oz	g	in	cm	in	cm	in	cm
Fuselage	22.4	635.0	22.4	635.0	26.6	67.5	0.4	0.9	1.3	3.2
Boom	8.0	226.8	8.0	226.8	52.7	133.9	0.0	0.0	3.7	9.4
Nose Cone	8.6	244.9	8.6	244.9	6.3	16.1	0.0	0.0	0.9	2.3
Left Motor Mount	0.6	18.1	0.6	18.1	26.6	67.6	-16.6	-42.1	5.4	13.6
Right Motor Mount	0.6	18.1	0.6	18.1	26.6	67.6	16.6	42.1	5.4	13.6
Left Wing	7.4	208.7	8.2	233.1	29.1	73.9	-15.3	-38.7	5.0	12.8
Auxiliary Spar	0.5	13.6	0.5	13.6	31.1	78.9	0.0	0.0	5.0	12.8
Right Wing	7.4	208.7	8.2	233.1	29.1	73.9	15.3	38.7	5.0	12.8
Right Aileron	0.2	4.5	0.7	20.9	33.5	85.0	19.2	48.7	5.1	13.0
Left Aileron	0.2	4.5	0.7	20.9	33.5	85.0	-19.2	-48.7	5.1	13.0
Right Flap	0.2	4.5	1.4	39.0	35.1	89.1	12.1	30.7	5.0	12.6
Left Flap	0.2	4.5	1.4	39.0	35.1	89.1	-12.1	-30.7	5.0	12.6
Wing Spar	9.4	267.6	9.4	267.6	28.8	73.1	0.0	0.0	5.3	13.4
Right Winglet	0.8	22.7	0.8	22.7	31.3	79.4	30.0	76.2	5.0	12.8
Left Winglet	0.8	22.7	0.8	22.7	31.3	79.4	-30.0	-76.2	5.0	12.8
Tail Cone	3.4	95.3	3.4	95.3	46.6	118.4	0.0	0.0	1.8	4.5
Left Horizontal Stabilizer	1.0	27.2	1.0	27.2	72.4	183.8	-5.6	-14.3	4.7	12.0
Right Horizontal Stabilizer	1.0	27.2	1.0	27.2	72.4	183.8	5.6	14.3	4.7	12.0
Left Elevator	1.1	31.8	1.1	31.8	75.6	192.0	-6.3	-15.9	4.8	12.1
Right Elevator	1.1	31.8	1.1	31.8	75.6	192.0	6.3	15.9	4.8	12.1
Vertical Stabilizer	2.9	81.6	2.9	81.6	74.2	188.4	0.0	0.0	10.5	26.6
Rudder	1.3	36.3	1.3	36.3	78.1	198.3	0.0	0.0	11.6	29.5
Tail Mount	1.8	49.9	1.8	49.9	73.1	185.5	0.0	0.0	4.8	12.1
Main Landing Gear	14.7	417.3	7.0	199.6	32.8	83.3	0.0	0.0	-7.9	-20.0
Nose Gear	3.2	91.6	3.2	91.6	8.5	21.5	0.0	0.0	-1.0	-2.5
Left Motor	11.5	324.8	11.5	324.8	24.8	-42.1	-16.6	-42.1	5.4	13.7
Right Motor	11.5	324.8	11.5	324.8	24.8	63.0	16.6	42.1	5.4	13.7
Avionics										
Spektrum Receiver	3.2	90.7	3.2	90.7	44.8	113.8	1.6	4.0	1.0	2.6
Brake Battery Pack	1.4	40.8	1.4	40.8	45.8	116.3	1.6	4.1	1.0	2.5
Receiver Battery Pack	1.4	40.8	1.4	40.8	45.8	116.3	1.6	4.1	1.0	2.5
ESC	6.4	181.4	6.4	181.4	26.2	66.5	0.0	0.0	4.7	12.0
Wire Harness	20.8	589.7	20.8	589.7	32.1	81.5	0.0	0.0	0.0	0.1
Mission 1										
M1 Propellers	1.3	38.1	1.3	38.1	23.7	60.1	0.0	0.0	5.5	14.1
M1 Batteries	24.8	702.2	24.8	702.2	10.8	27.3	0.0	0.0	0.7	1.7
Total Mass	180.9	5128.3	178.5	5061.2	----	----	----	----	----	----
Center of Gravity	----	----	----	----	29.2	74.1	0.1	0.2	2.5	6.3
Mission 2										
Medical Supply Cabinet	50.0	1417.5	102.0	2891.6	22.0	55.9	0.0	0.0	0.0	0.0
Cabinet Insert Tray	3.4	95.3	2.4	66.9	22.0	55.9	0.0	0.0	-1.3	-3.2
EMTs/Patient Insert	23.7	671.3	28.7	813.1	52.8	134.0	0.0	0.0	-0.2	-0.5
M2 Propellers	2.1	59.9	2.1	59.9	23.7	60.1	0.0	0.0	5.5	14.0
M2 Batteries	24.8	702.2	24.8	702.2	10.8	27.3	0.0	0.0	0.7	1.8
Total Mass	258.7	7334.1	312.3	8854.6	----	----	----	----	----	----
Center of Gravity	----	----	----	----	28.9	73.5	0.1	0.1	1.4	3.6
Mission 3										
4 Passenger Racks	96.0	2721.6	96.0	2721.6	17.5	44.5	0.0	0.0	-0.1	-0.2
M3 Propellers	1.3	38.1	1.3	38.1	23.7	60.1	0.0	0.0	5.5	14.1
M3 Batteries	24.8	702.2	24.8	702.2	5.0	12.7	0.0	0.0	0.7	1.7
Total Mass	237.9	6743.1	235.5	6676.0	----	----	----	----	----	----
Center of Gravity	----	----	----	----	28.6	72.8	0.1	0.2	1.8	4.7



5.3 System and Sub-System Design/Selection/Integration

5.3.1 Fuselage

The main part of THE's fuselage is untapered and made of hexagonal Lantor Soric core material sandwiched between two layers of carbon fiber spread tow. The tapered nose and tail sections are made with 3 layers of fiberglass reinforced with plywood bulkheads. Fiberglass is transparent to radio waves and THE's avionics are placed in the tail section of the fuselage to minimize the carbon fiber's interference with transmitter communication. The fuselage wall is approximately 0.125 in (0.318 cm) thick. The tapered nose section is 8.44 in (21.4 cm) in length, and the tapered tail section is 10.0 in (25.4 cm) in length. These tapered sections reduce drag from the fuselage. The non-tapered section of the fuselage has a length of 35.0 in (88.9 cm) and houses THE's payload. A cross section of the fuselage is shown in Figure 25.

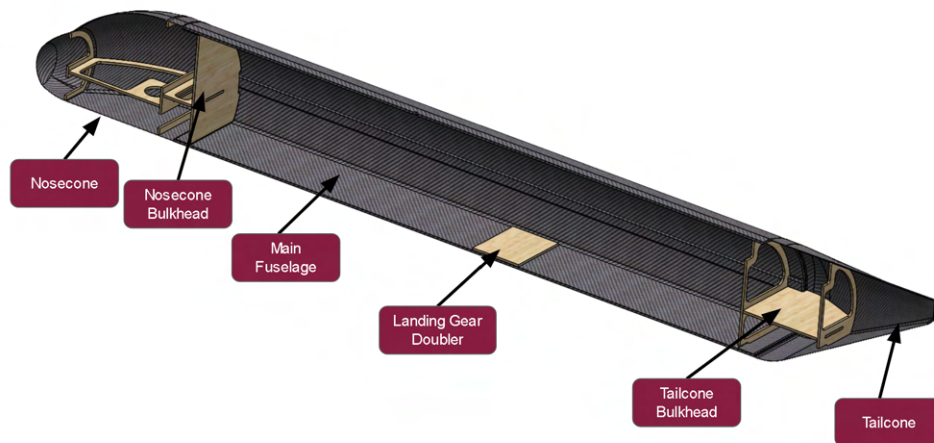


Figure 25: Fuselage Cross Section

5.3.2 Wing

THE's wing is rectangular with a span of 60.0 in (152.4 cm) and a chord of 13.0 in (33.02 cm) resulting in an aspect ratio of 4.61. The wing is assembled on one continuous carbon fiber spar with a square cross section. The spar's width is 0.875 in (2.22 cm) and is made of standard modulus carbon fiber. The outer surface of the wing consists of Monokote wrapped over wooden ribs and a carbon fiber foam core leading edge. The motor mount structures are made of 0.125 in (0.318 cm) thick plywood to transfer the thrust loads to the spar. An auxiliary spar is attached to the middle of the main wing spar with steel corner and mounting braces. The wing is bolted to the fuselage with 3 M6 bolts which transfer wing loads to a plywood doubler inside of the fuselage.

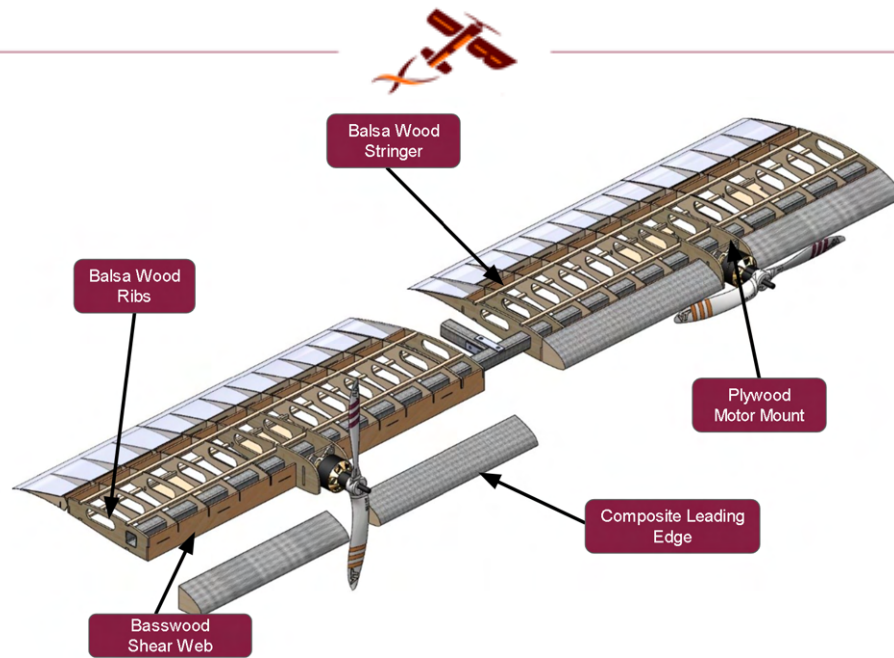


Figure 26: Wing Structural Arrangement

Wing Rotate Mechanism

Shown in Figure 27 is the Wing Rotate Mechanism. Of the three bolts that mount the wing to the fuselage, one of these bolts is on the wing spar while the other two are on the auxiliary spar. The bolt on the wing spar transfers wing loads to the fuselage while the 2 bolts on the auxiliary spar supplement this bolt and prevent wing vibration. These bolts are partially tensioned while the airplane is in the parked configuration, and the wing pivots about the bolt on the main spar.

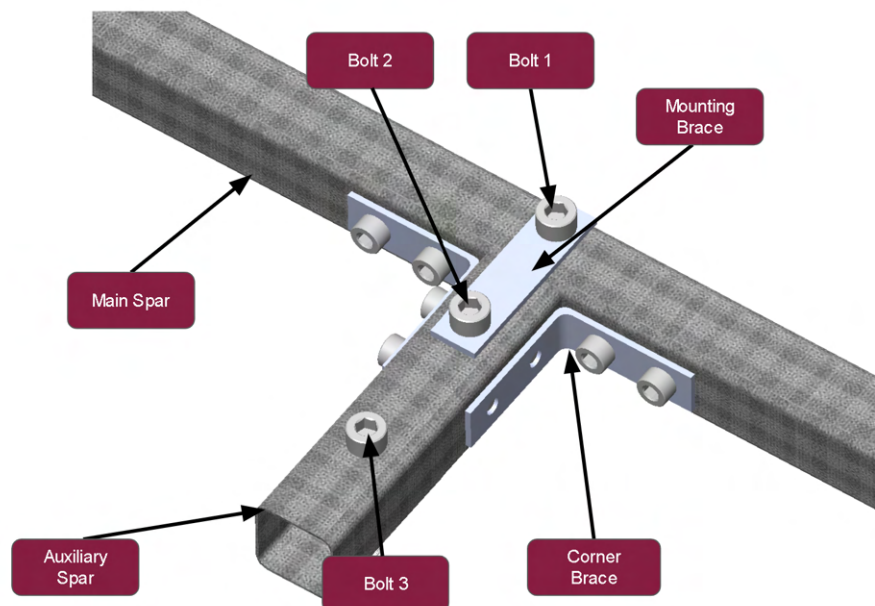


Figure 27: CAD of the Wing Rotate Mechanism



5.3.3 Empennage and Tail Boom

THE's empennage is a conventional tail supported by a 43.0 in (109 cm) long carbon fiber boom. A 3D-printed tail mount is fixed to the boom with epoxy and carbon fiber lashing. The 3D-printed tail mount is designed with holes for pultruded carbon spars which support the tail surfaces and allow for a horizontal stabilizer setting angle of -0.50° . The tail surfaces are made of carbon fiber spread tow laid up over XPS foam core, and are capped with basswood to conceal the foam core. The elevator and rudder are attached to the stabilizer surfaces with nylon hinges and epoxy. The tail structure is shown in Figure 28.

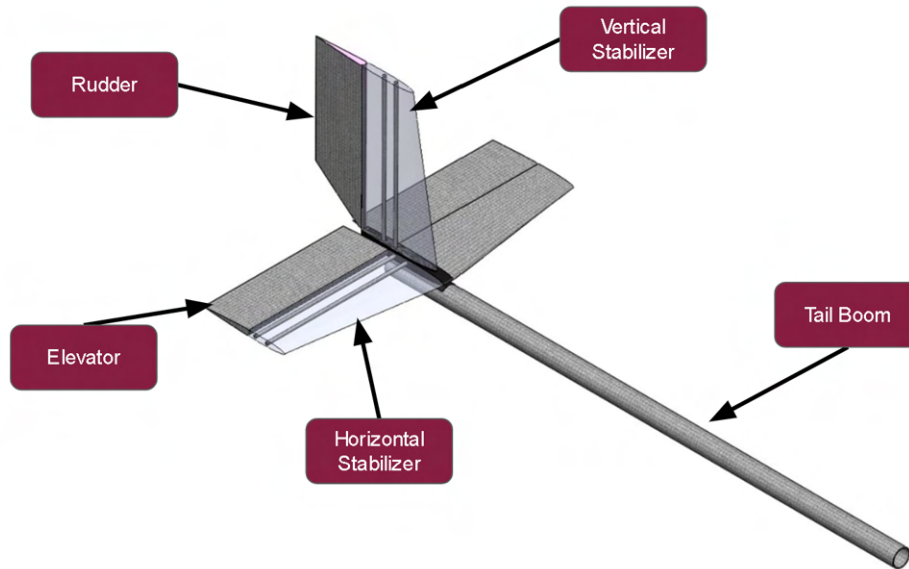


Figure 28: Empennage Structural Arrangement

5.3.4 Landing Gear

The team manufactured the landing gear in-house rather than purchasing a commercial product. The main gear and nose gear are designed to hold approximately 80.0% and 20.0% of the MTOW respectively during taxi and takeoff. During landing, the team expected the landing gear load to reach no more than 2.50 times taxi and takeoff load. As a result, the main gear is designed to hold 200% MTOW or 32.0 lbs (14.5 kg). The team designed the main gear to be 0.167 in (0.424 cm) thick. Carbon fiber was laid up around a 0.0625 in (0.160 cm) thick balsa wood core for added stiffness. A layer of aramid plain weave fabric is added to the layup to prevent the gear from shattering in the event of a failure. THE's nose gear can withstand 40% MTOW or 6.40 lbs (2.90 kg). The nose gear's load path was designed to go through a 0.157 in (0.400 cm) thick vertical steel rod sufficient for hard landings without deformation. The landing gear configuration is shown Figure 29. The landing gear FEA simulation is shown in Figure 29.

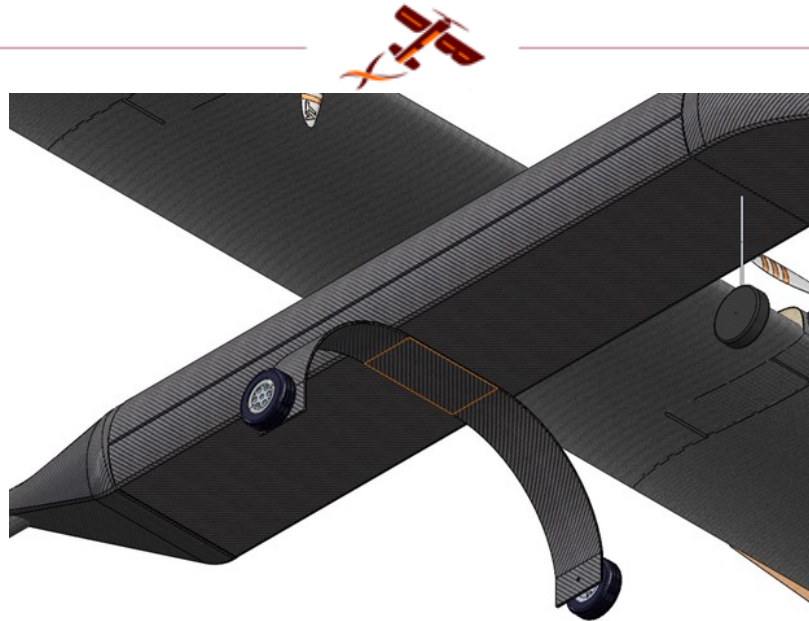
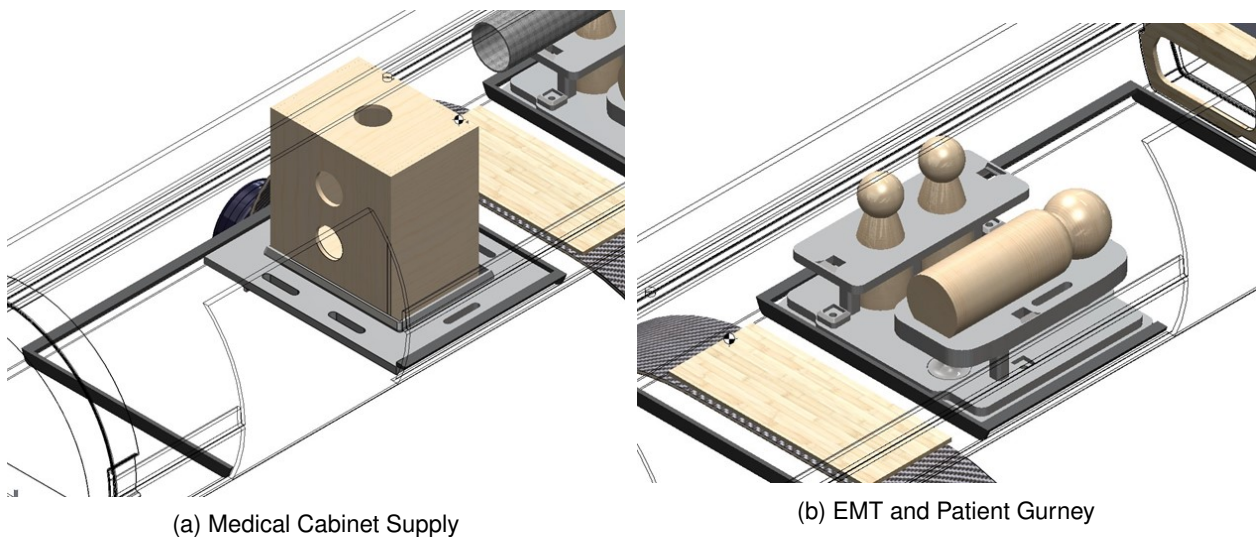


Figure 29: Landing Gear

5.3.5 Mission Systems

The M_2 systems consist of the MSC, gurney and EMT tray. This tray was 7.00 in x 5.90 in (17.8 cm x 15.0 cm) and had two 1.20 in (3.05 cm) diameter cutouts for the EMTs. The restraint for the EMTs utilizes magnets and clips to align and secure the EMTs during flight. The bed of the gurney was held up by two supports with clips that prevent the bed from shifting during flight. The Patient is placed into a groove on the bed and secured using a Velcro strap permanently fixed to the tray. The medical supply cabinet insert has dimensions of 7.00 in x 5.75 in (17.78 cm x 14.61 cm). Raised sections in the middle of the insert allow the MSC to be placed inside. Velcro runs through slots which surround the center of the insert and strap the MSC securely to the tray. The MSC box was designed in Fusion360 and laser cut with 0.125 in (0.318 cm) thick plywood. The box is made up of 5 walls that are joined with epoxy and a removable lid[4].



(a) Medical Cabinet Supply

(b) EMT and Patient Gurney

Figure 30: THE M_2 and M_3 Mission Systems



THE's passenger insert trays and passenger restraints for M₃ are both 3D-printed. The parts contain cutouts to attach magnets and clips which connect the two components of the passenger restraint. The passenger tray is 7.00 in x 5.96 in (17.78 cm x 15.14 cm) with four 1.53 in (3.86 cm) high supports with space for 14 passengers and magnets to aid with alignment. The holes at the bottom of the passenger tray are 0.125 in (0.318 cm) in diameter to constrain the bottom of the passengers while the restraint is placed over the top to fix passengers to the tray.

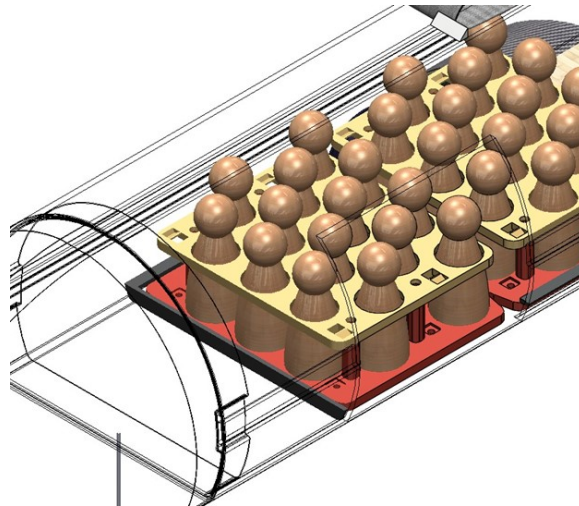


Figure 31: Passenger System Assembly

5.3.6 Flight and Mission Performance

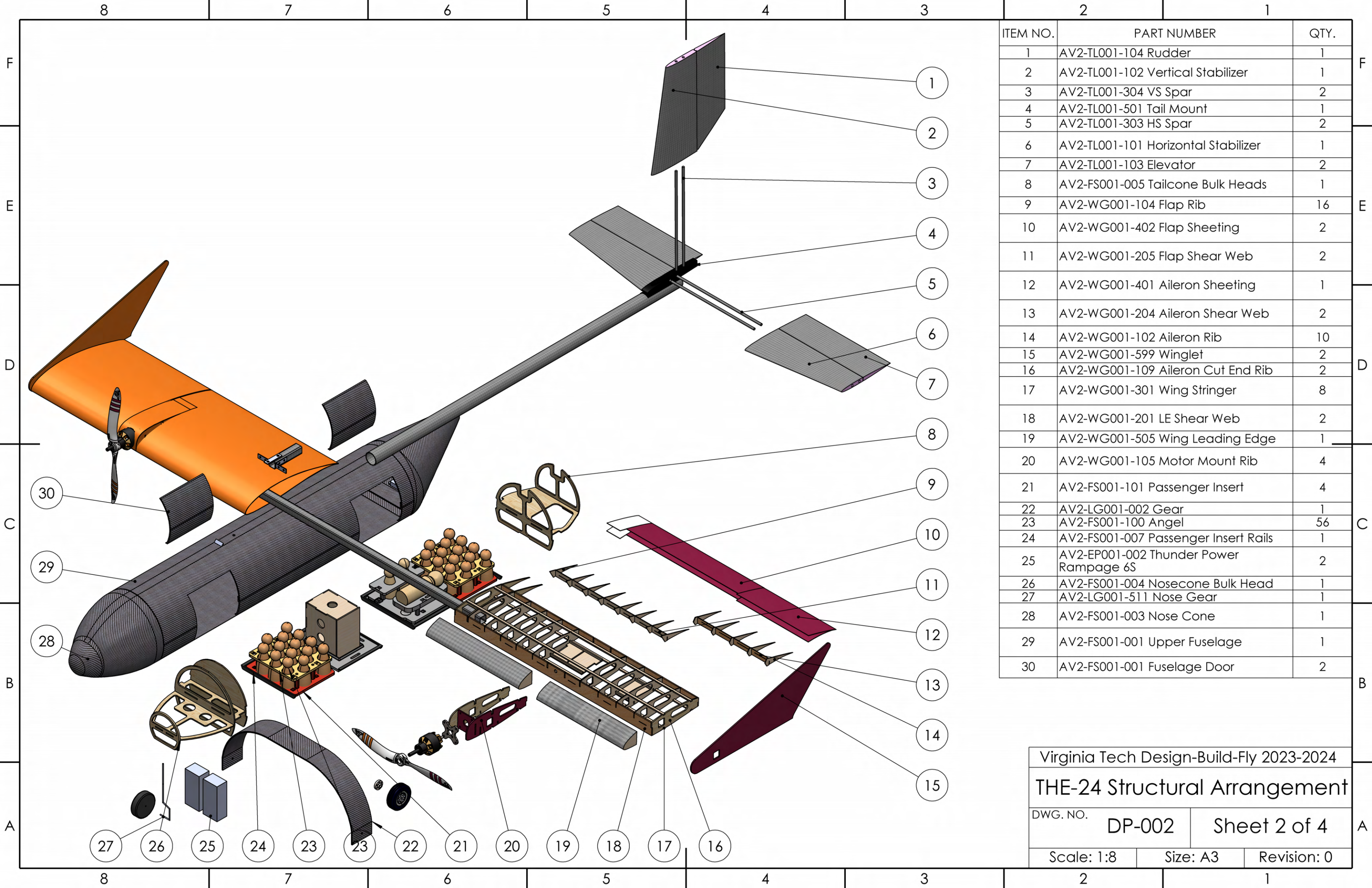
The team used the analysis tools MotoCalc, XFLR5, and AVL to refine the performance predictions of THE. The results of this analysis were compared with team historical data to better predict true performance, summarized in Table 27.

Table 27: THE Mission Performance

Parameter	Mission 1	Mission 2	Mission 3
Takeoff Weight	11.31 lbs (5.13 kg)	16.0 lb (7.26 kg)	16.0 lbs (7.26 kg)
Takeoff Distance	17.0 ft (5.18 m)	19.5 ft (5.94 m)	19.5 ft (5.94 m)
Stall Speed	33.2 ft/s (10.1 m/s)	39.5 ft/s (12.0 m/s)	39.5 ft/s (12.0 m/s)
Maximum Speed	90.9 ft/s (27.72 m/s)	120.3 ft/s (36.66 m/s)	90.9 ft/s (27.72 m/s)
Cruise Speed	88.0 ft/s (26.82 m/s)	117.7 ft/s (35.76 m/s)	88.0 ft/s (26.82 m/s)
Mission Lap Time	33.0 s	23.9 s	33.0 s

5.4 Drawing Package

The team employed the CAD modeling tools SolidWorks and Fusion360 to facilitate detailed design and CAM of THE.



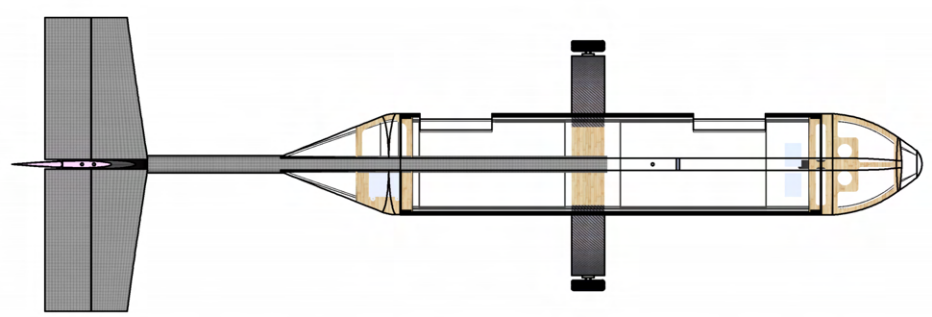
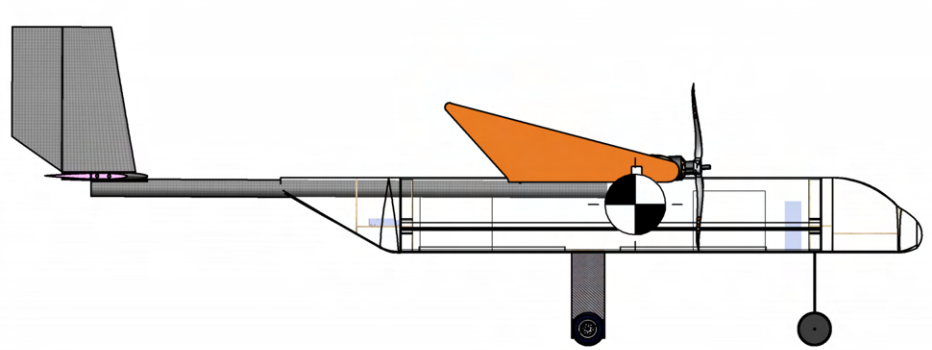
ITEM NO.	PART NUMBER	QTY.
1	AV2-TL001-104 Rudder	1
2	AV2-TL001-102 Vertical Stabilizer	1
3	AV2-TL001-304 VS Spar	2
4	AV2-TL001-501 Tail Mount	1
5	AV2-TL001-303 HS Spar	2
6	AV2-TL001-101 Horizontal Stabilizer	1
7	AV2-TL001-103 Elevator	2
8	AV2-FS001-005 Tailcone Bulk Heads	1
9	AV2-WG001-104 Flap Rib	16
10	AV2-WG001-402 Flap Sheeting	2
11	AV2-WG001-205 Flap Shear Web	2
12	AV2-WG001-401 Aileron Sheeting	1
13	AV2-WG001-204 Aileron Shear Web	2
14	AV2-WG001-102 Aileron Rib	10
15	AV2-WG001-599 Winglet	2
16	AV2-WG001-109 Aileron Cut End Rib	2
17	AV2-WG001-301 Wing Stringer	8
18	AV2-WG001-201 LE Shear Web	2
19	AV2-WG001-505 Wing Leading Edge	1
20	AV2-WG001-105 Motor Mount Rib	4
21	AV2-FS001-101 Passenger Insert	4
22	AV2-LG001-002 Gear	1
23	AV2-FS001-100 Angel	56
24	AV2-FS001-007 Passenger Insert Rails	1
25	AV2-EP001-002 Thunder Power Rampage 6S	2
26	AV2-FS001-004 Nosecone Bulk Head	1
27	AV2-LG001-511 Nose Gear	1
28	AV2-FS001-003 Nose Cone	1
29	AV2-FS001-001 Upper Fuselage	1
30	AV2-FS001-001 Fuselage Door	2

Virginia Tech Design-Build-Fly 2023-2024

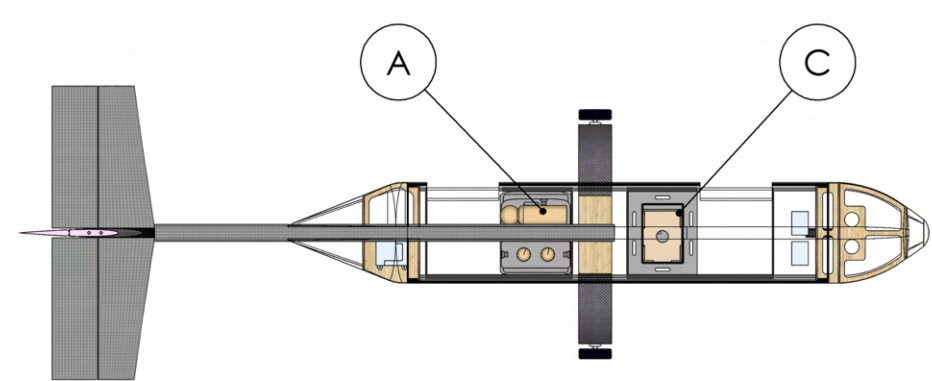
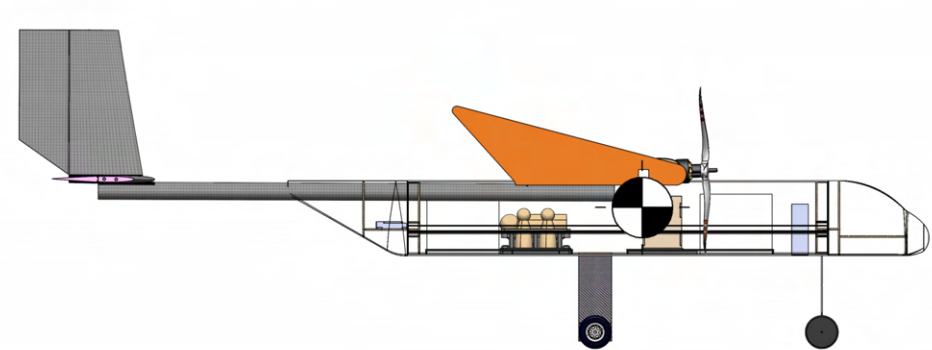
THE-24 Structural Arrangement

DWG. NO. **DP-002** Sheet 2 of 4

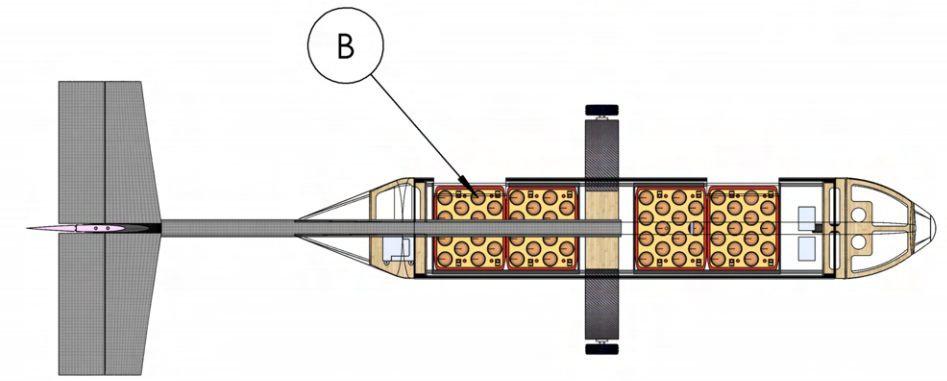
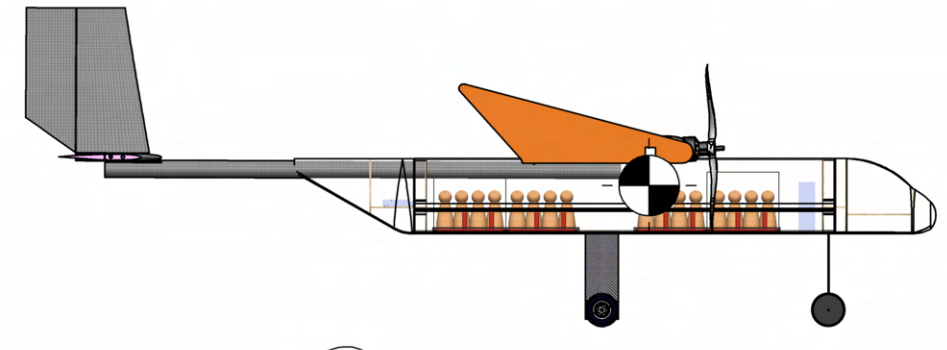
Scale: 1:8 Size: A3 Revision: 0



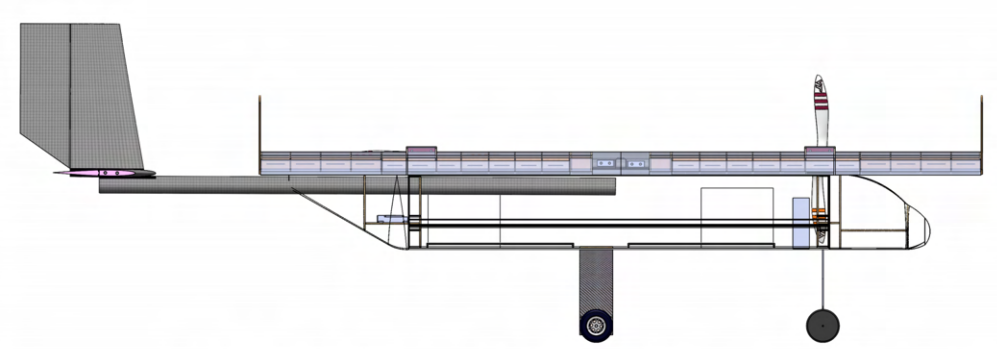
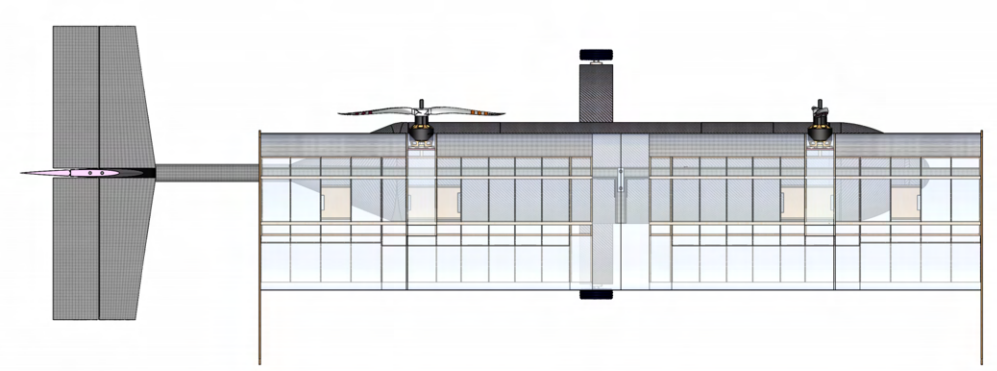
Mission 1 Configuration



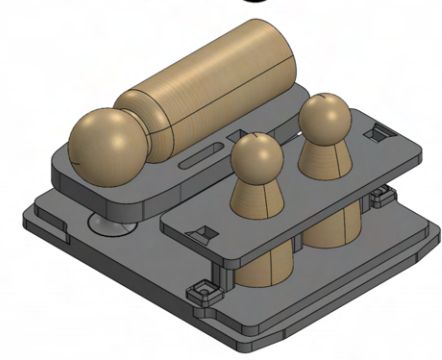
Mission 2 Configuration



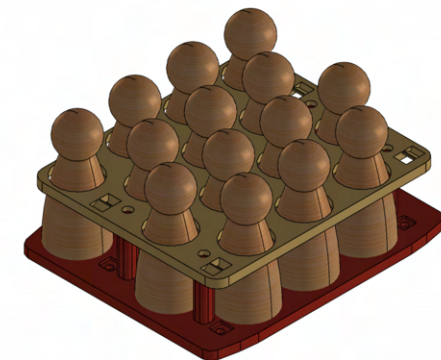
Mission 3 Configuration



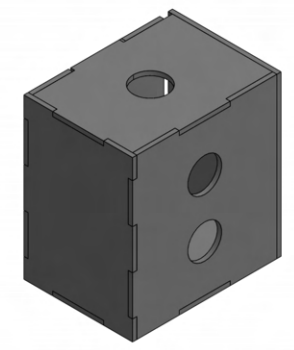
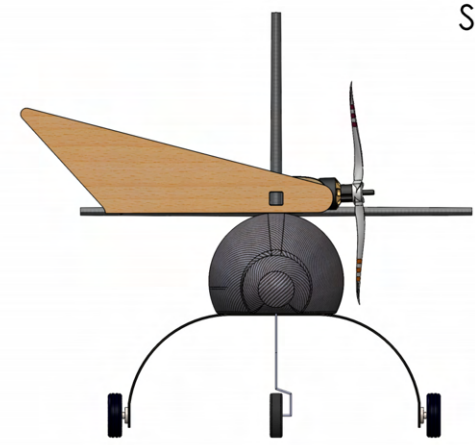
Parking Configuration



DETAIL A
SCALE 1 : 4



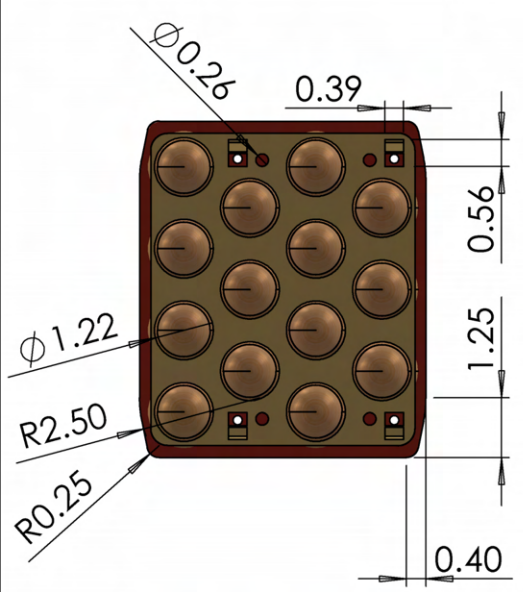
DETAIL B
SCALE 1 : 4



DETAIL C
SCALE 1 : 4

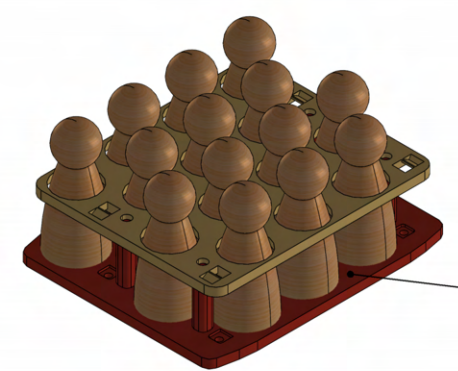
Detail	Description	Mission Number
A	EMT and Gurney	2
B	Passenger System	3
C	Medical Cabinet	2

Virginia Tech Design-Build-Fly 2023-2024		
THE-24 Systems		
DWG. NO.	DP-003	Sheet 3 of 4
Scale: 1:16	Size: A3	Revision: 0

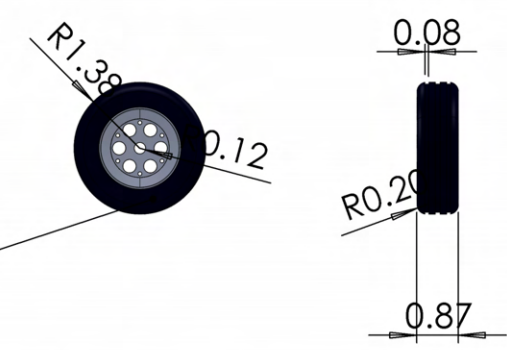


Passenger System

SCALE 1 : 4

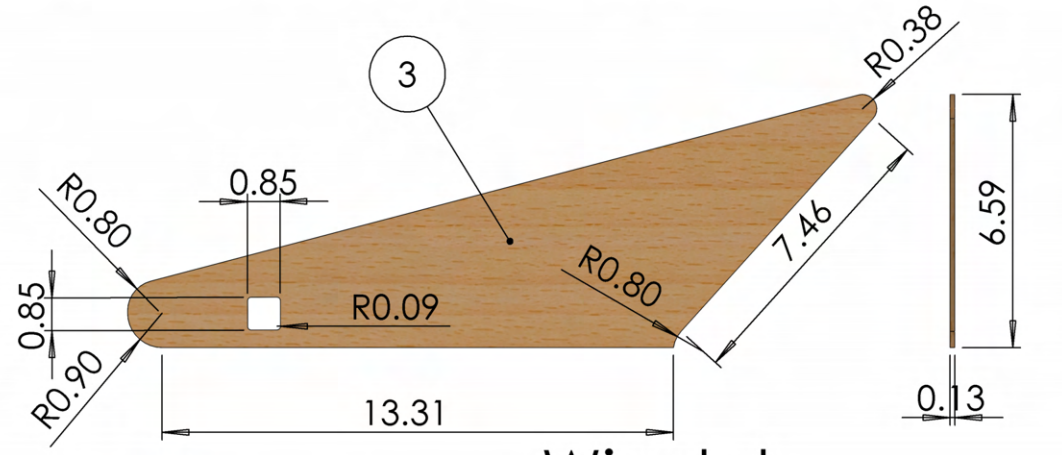


1



Main Gear Tire

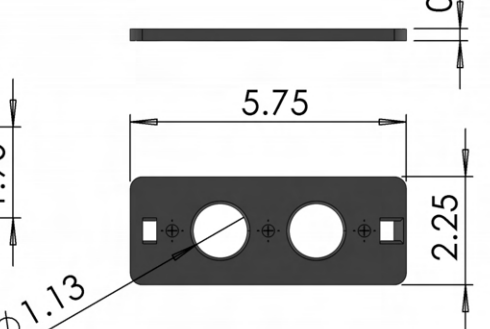
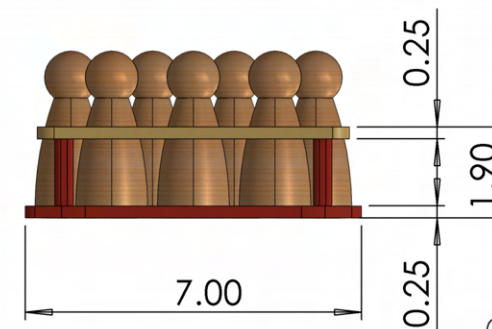
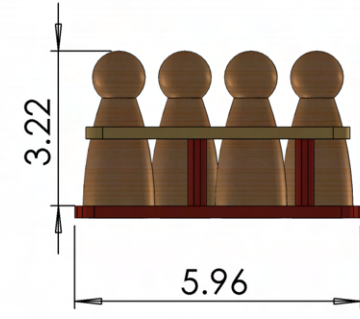
2



Winglet

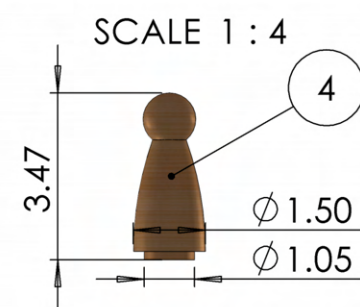
SCALE 1 : 5

3



Gurney Restraint

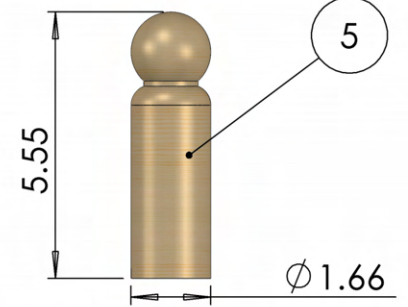
SCALE 1 : 4



Passenger

SCALE 1 : 4

4



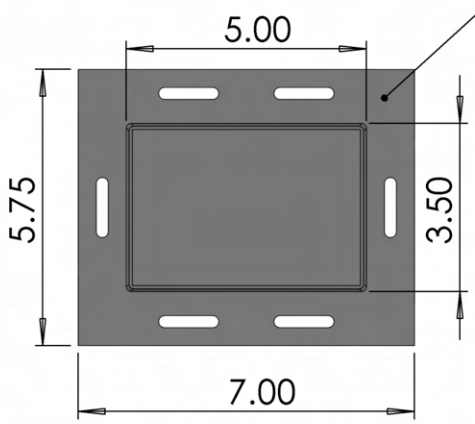
Patient

SCALE 1 : 4

5

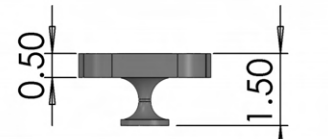


7



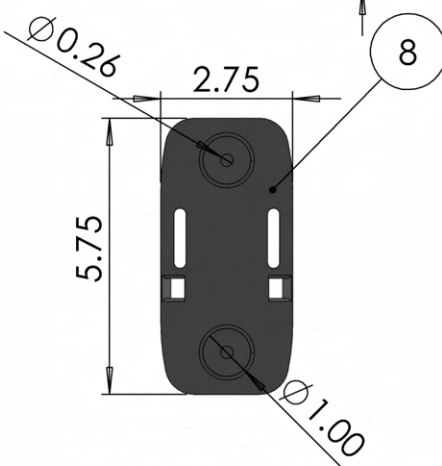
Cabinet Base

SCALE 1 : 4

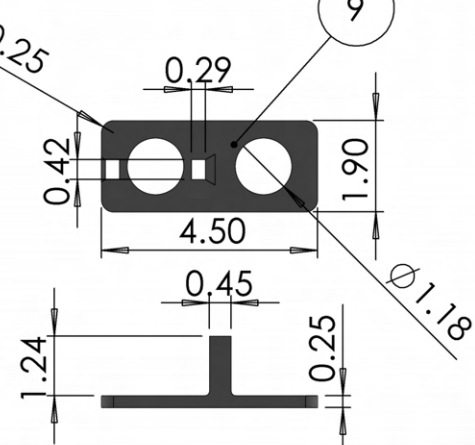


Gurney

SCALE 1 : 4



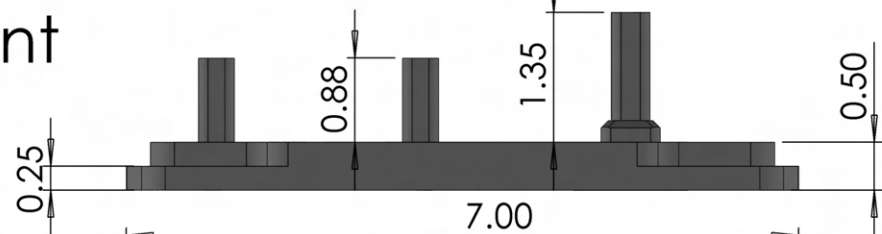
8



Pilot Restraint

SCALE 1 : 4

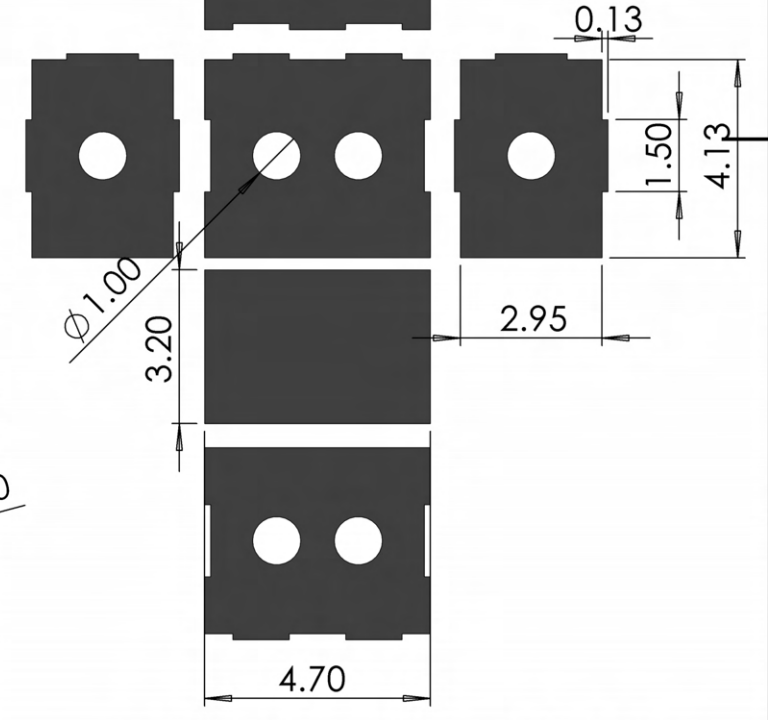
9



Gurney Base

SCALE 1 : 2

10



Medical Cabinet

SCALE 1 : 4

6

Description	Mission
Gurney	2
Gurney Restraint	2
Main Gear Tire	
Medical Cabinet	2
Medical Cabinet Base	2
Passenger System	3
Patient	2
Pilot Restraint	
Pilot/Pax/EMT	
Winglet	

Virginia Tech Design-Build-Fly 2023-2024		
THE-24 Systems Details		
DWG. NO.	DP-004	Sheet 4 of 4
Scale: 1:4	Size: A3	Revision: 0



6 MANUFACTURING PLAN

Many materials and manufacturing processes were evaluated to build the airplane. The following materials and fabrication processes were selected for each specific airplane component after consideration and deliberation of their specific materialistic properties.

6.1 Manufacturing Processes Investigated

6.1.1 Wood

Balsa, basswood, and plywood are common materials used in RC airplane manufacturing due to their lightweight nature and ease of use. Balsa is the most lightweight and was primarily used in rib construction. Basswood is stronger but heavier than balsa and was used to construct parts undergoing more load such as shear webs. Plywood is the heaviest of the woods, but is the strongest and was used for the most load bearing components such as motor mounts. Unlike balsa or basswood, plywood also mitigates failures due to grain direction as it is comprised of multiple layers of wood normal to each other. Wooden components are made using a laser cutter as it enables quick and precise cuts. Tolerances were built in to all laser cut components to account for the width of the laser.

6.1.2 Foam

Extruded Polystyrene (XPS) Foam is a low-cost and lightweight material used to build non-structural components and composite molds for the airplane. The team uses a hot-wire foam Computer Numerical Controlled CNC cutter that enables the precise manufacturing of complex geometries. For components such as the tail, carbon fiber is laid up onto the foam to increase the rigidity of the component. This carbon fiber foam-core part is used in the tail due to its ability to withstand tail-strikes. The leading edge of the wing was constructed using carbon fiber foam-core for a similar reason. Fuselage molds are shown in Figure 32.



Figure 32: Bonding Fuselage Molds



6.1.3 Composites

The team has experimented with composite materials for the past 3 years and has benefited greatly from the excellent strength-to-weight ratios they provide. As mentioned in Section 6.1.2, molds for composites can be quickly fabricated using XPS foam and a hot-wire foam CNC cutter.

The main body of the fuselage is constructed with Lantor Soric core material sandwiched between two layers of carbon fiber for the main body of the fuselage. Additives such as bonding agents and foam core can be included in composites to increase strength, mitigate inconsistencies, and create a uniform surface finish.

6.1.4 Additive Manufacturing

3D printing allows for the creation of custom parts at decreased cost and downtime as opposed to ordering them through a 3rd party vendor. In addition, they allow for the creation of a part with increased accuracy compared to other manufacturing methods discussed. However, a downside to the use of 3D printed parts is their weight, making it impractical for widespread use on the airplane. This manufacturing method is ideal for creating small parts that are too complex for other manufacturing methods to produce. Airplane components using 3D parts include the tail mount and nose landing gear straps.

6.2 Manufacturing Processes Selected

6.2.1 Wing

The wing surfaces are formed over an internal structure of foam, balsa, basswood, and plywood. The leading edge of the wing is comprised of carbon fiber laid up over an XPS foam core as shown in Figure 33.



Figure 33: Carbon Fiber, Foam-Core Leading Edge

The main wing structure contains 0.125 in (0.318 cm) basswood leading and trailing edge shear webs. The main ribs are composed of 0.0625 in (0.158 cm) balsa wood while the ribs located above the fuselage and on the wingtips are made of plywood. The ribs and shear webs are fitted together using opposing slots which allow each rib to be spaced evenly and accurately while allowing the design to be easily manufactured. After the leading edge is cured and trimmed, 2-Ton epoxy is used to fix the aft surface of the leading edge to the leading edge shear web. This assembly can be seen in Figure 34.



Figure 34: Main Wing Assembly

Plywood trays are installed on the inside of the main wing structure to hold the servos and both ESCs. This ensures the security and serviceability of these components. For all control surfaces, a sheet of 0.0312 in (0.0794 cm) balsa wood is fitted over the trailing edge of the surface. A layer of MonoKote plastic shrink wrap is fitted around the entire structure of the wing and control surfaces, and nylon pin hinges are used to join the control surfaces to the main wing structure. This combination of internal structures and outer skin provides the aerodynamic qualities outlined in Section 4.2.

6.2.2 Tail

All tail components are carbon fiber, foam core composites. XPS foam cores are created using the aforementioned foam cutter in Section 6.1.2. Laser-cut basswood end caps are adhered to the ends of the tail components using a foam-safe Cyanoacrylate (CA) adhesive to protect the foam from damage. Two carbon fiber spars of outer diameter 0.430 in (1.09 cm) are installed along the span of the stabilizers for increased strength and rigidity. Spackle is applied to the stabilizers at locations of imperfections to improve the surface finish before the composite occurs. A pre-measured and epoxy-saturated piece of 88-gram spread tow plain weave carbon fiber is prepared. Before the application of the uncured composite, a thin layer of epoxy is applied to the piece to prevent delamination. The saturated pieces of carbon fiber are applied to the XPS foam parts and a squeegee is used to help adhere the carbon fiber to the foam and remove the excess epoxy, decreasing the overall weight of the piece. Once the tail pieces are cured, the horizontal and vertical stabilizers are attached to a 3D printed tail mount via 2-Ton epoxy. The spars of each stabilizer fit into their respective hole on the tail alignment piece. Once all of the pieces have cured to the tail alignment piece, the assembly of the tail is mounted to the boom via lashing. The lashing is completed using 6k carbon fiber tow and 2-Ton epoxy. The rudder and elevator are then hinged allowing for appropriate deflection and servos are installed.

6.2.3 Fuselage

The main body of the fuselage is a carbon fiber composite with a Lantor Soric core produced from an XPS foam mold as seen in Figure 32 in Section 6.1.2. The nose cone and tail cone are made out of fiberglass for the ease of manufacturing. Fiberglass is more compatible with complex curves like the nose and tail cone shape and does not interfere with radio connection between the receiver and transmitter. The main body fuselage molds are cut by a hotwire CNC cutter. 2in (5.08 cm) sections of foam are cut and glued together using non-foaming Clear Gorilla Glue. The molds are sanded and then reinforced by two layers of fiberglass composite. After the fiberglass reinforcement is cured, the molds are sanded again to a smooth finish to reduce the number of surface imperfections and provide better continuity between the mold sections. This reinforcement provides strength and re-usability to the molds. They are then coated in 6 layers of Polyvinyl



alcohol, a water-based plastic that leaves behind a wax-like material after it dries. This acts as a mold-release to aid in the removal of parts. The fuselage is formed by laying up two separate mold halves that are later attached. Each half is comprised of two layers of 3-ounce carbon fiber and 1 ply of Lantor Soric core material. The fuselage also has a 1-ply strip of Kevlar aramid inlaid in the fuselage composite along the length of the airplane to increase structural rigidity. Rectangular pieces of carbon fiber, Lantor Soric foam core, peel ply and breather are measured and fitted to the molds with minimal excess. Once the composite materials are measured and cut, a vacuum bag is prepared for after the composite is complete. The composite materials are placed on a flat surface sandwiched between two sheets of a polyester film (Mylar) to contain the epoxy. A pre-measured amount of epoxy is spread over the smooth surface, between the Mylar sheets. Squeegees are used to spread the epoxy over the entirety of the composite surface and pushing away excess preventing the addition of any unnecessary weight due to excess epoxy. The material is cut, Mylar is removed from both sides, and the material placed and fitted within the mold. This process is repeated for each of the remaining material sheets in a carbon-Soric-Kevlar-carbon order. Once all the layers are in the mold, a layer of peel ply is added to assist with the composite removal from the vacuum bag once the cure is complete. A layer of breather is added on top of the peel ply to absorb excess epoxy during the curing process. Once that is complete, the mold consisting of the wetted composite materials, peel ply and breather is placed into the prepared vacuum bag and is pressurized to 15-20 psi for 12-16 hours as seen in Figure 35.



Figure 35: Carbon Fiber Fuselage Layup in Vacuum Bag



6.2.4 Landing Gear

The main landing gear is laid up on an XPS foam mold made by a hotwire CNC cutter reinforced with fiberglass. Several layers of mold-release wax are applied to the wooden mold to ensure the complete separation of the gear and mold after the curing process. Next, five layers of plain weave carbon fiber are applied to the mold and followed by a single layer of Kevlar. Each layer is soaked with epoxy after it is applied. Next, a balsa core of 0.0625 in (0.159 cm) thickness is applied to the composite followed by an additional six layers of plain weave carbon fiber. The complete composite is 0.180 in (4.57 mm) thick as per the design. The nose landing gear is created from 0.1570 in (0.404 cm) diameter steel rod and is bent by hand with the assistance of a table vice. Holes are drilled through the fuselage, large enough for the steel rod to go all the way through. It is attached to the airplane via two 3D printed landing gear straps on the front bulkhead. Two collets are used to secure the rod on either side of the top of the fuselage. The front wheel is held in place with a pair of wheel collets, one on either side of the wheel.

6.2.5 Servos

The airplane's wing servos are secured in place using laser cut plywood trays as referenced in Section 6.2.1 which allow for quick and easy replacement and maintenance. These trays are placed into specific sections of the wing and secured into place with 2 mm screws. The tail servos are installed into the foam structure of the tail surfaces using a low temperature hot glue. The rudder servo arms protrude perpendicular to the center line of the airplane, while the elevator arm protrudes from the upper surface for increased reliability during pitch up.

6.3 Summary

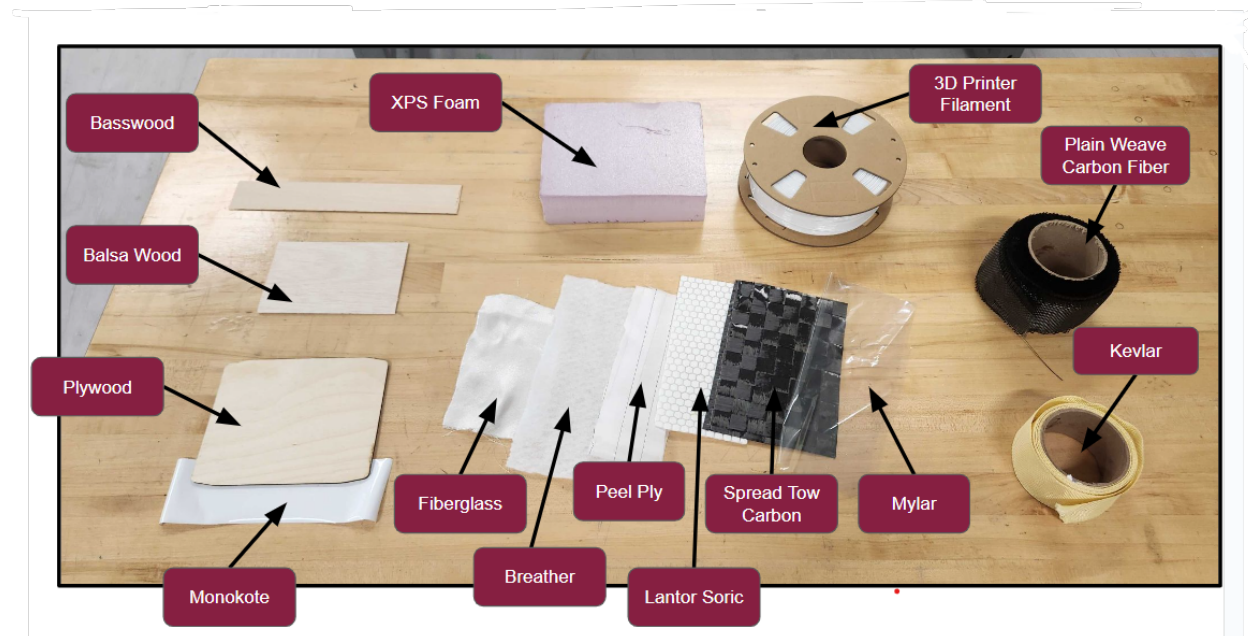


Figure 36: THE Construction Materials



Table 28: Summary of Manufacturing Processes and Material Organized by Airplane Subdivision

Manufacturing Summary			
Airplane Subdivision	Component	Material/Brand	Procedures
Wings	Leading Edge	XPS Foam	Hotwire CNC Cut
		Bass Wood (1/16")	Laser Cut
	Spar	Carbon Fiber	Purchased
		Balsa Wood (1/16" & 1/32")	Laser Cut
	Main Body & Control Surfaces	Bass Wood (1/16")	Laser Cut
		Bass Wood (1/8")	Laser Cut
		Plywood (1/8")	Laser Cut
		Skin	Monokote
Carbon Fiber	Wet Layup		
Fuselage	Bulkheads	Plywood (1/8")	Laser Cut
	Skin	Carbon Fiber	Wet Layup
		Lactor Soric	
		Fiberglass	
		Kevlar	
Tail	Core	XPS Foam	Hotwire CNC Cut
	Endcaps	Bass Wood (1/16")	Laser Cut
	Skin	Carbon Fiber	Wet Layup
Landing Gear	Core	Balsa Wood (1/16")	Wet Layup
	Skin	Carbon Fiber	
	Reinforcement	Kevlar	
Electronics & Propulsion System	Motors	Scorpion A-4220-540	Purchased
	Propellers	Aeronaut Folding 14x9 & 17x9	Purchased
	Batteries	Thunderpower Rampage 6s 2250 mA/h 70c & 5s 2250 mA/h 70c	Purchased
	ESCs	Cobra 100A	Purchased
	Wiring	Servo wires	Soldering
		12 AWG propulsion wires	
Fuses	100 Blade Fuse	Purchased	
Mission 2 Equipment	Gurney	PETG	3D Printing
	Medical Supply Cabinet	Lead weights	Purchased
		Plywood (1/8")	Laser Cut
Mission 3 Equipment	Passenger Fastener	PETG	3D Printing
		Magnets	Purchased

6.4 Manufacturing Milestones

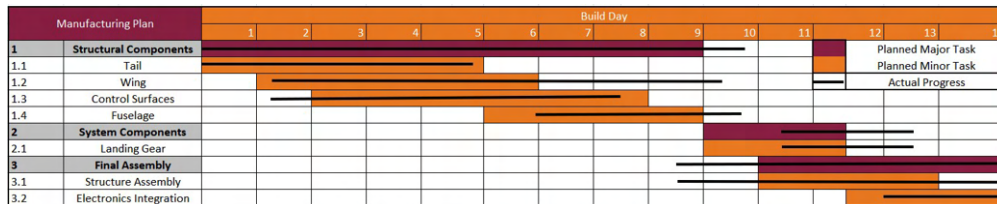


Figure 37: Manufacturing Plan



7 TESTING PLAN

All tests are conducted to prove successful completion of all aspects of competition missions.

7.1 Testing Objectives

Overall

- Takeoff in 20 ft (6.10 m) with max payload
- Complete M_2 with 6.00 lbs (26.7 N)
- Complete M_3 with 52 passengers and fly for 5 minutes

Propulsion

- Static test for each configuration to verify the takeoff requirement of 1.44 T/W
- Spektrum data analysis to confirm airplane top speed predictions of 117.0 ft/s (35.6 m/s) for M_2 , and 88.0 ft/s (26.8 m/s) M_3
- Test battery packs to ensure capacity ratings of 2700 mAh 5S2P for M_1 , a 2250 mAh 6S2P for M_2 , and 2250 mAh 5S2P for M_3 is sufficient for flight

Wing

- Tip test at max loading case (M_2 configuration) to verify maximum deflection for the spar and boom
- Rotate from parked configuration and check secure mounting
- Break test of the wing to verify structural analysis

Ground Mission

- Timing of GM to simulate competition

Landing Gear

- MTOW load test to validate the expected deflection of landing gear
- Ground handling test to ensure the airplane rolls straight for takeoff
- Drop the airplane from 2 ft (0.61 m) to ensure landing gear strength

7.2 Sub-System Testing

7.2.1 Propulsion Testing

Static Performance Testing

A static thrust test was conducted to validate the predicted performance of the propulsion system. The team constructed a custom thrust stand consisting of a load cell and an Arduino that was used to collect static thrust data. This thrust stand was calibrated using standard laboratory weights. The results of the test are discussed in Section 8.1.1.

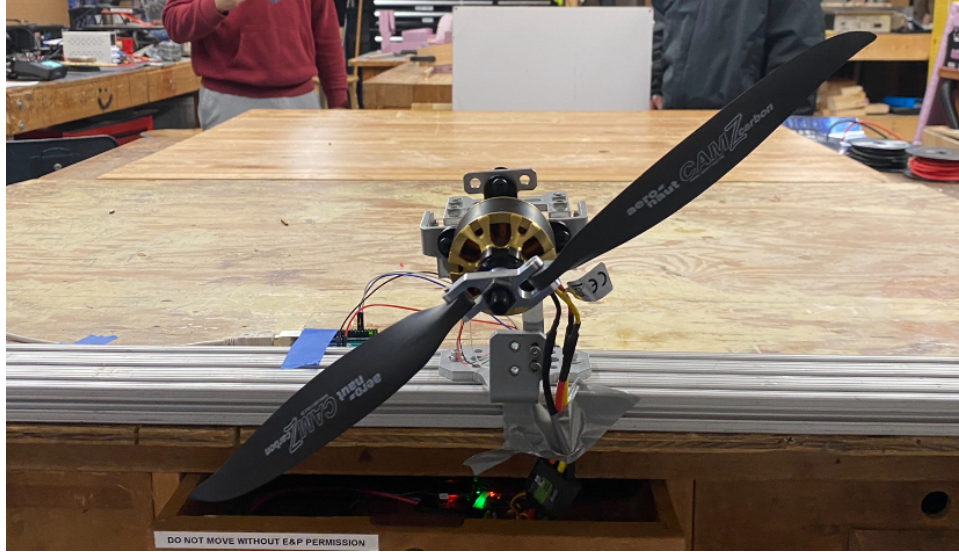


Figure 38: Thrust Stand

Dynamic Performance Testing

A Spektrum GPS module was used during test flights to provide accurate in-air data. The GPS module provides telemetry on airspeed and altitude. The Spektrum AR14400T receiver collects data on battery voltage, motor RPM, ESC temperature, and g-forces. This data was compared post-flight to the analysis performed on MotoCalc for performance verification. The results of the test are discussed in Section 8.1.1.

Range Testing

A range test was completed to test the interference of the carbon fiber fuselage with the communication from the transmitter to the receiver. The test was conducted at 150ft (45.7m) while in reduced power mode. The test validated the communication range of the transmitter which helps mitigate risk to the airplane and spectators.

7.2.2 Structural Testing

To validate FEA simulations, the spar and boom underwent physical load tests. These tests were set up using the same boundary conditions used in the respective FEA simulations mentioned in Section 5.2. Clamps acted as the fixed point boundary conditions and standard weights were used as the force boundary conditions. The load test for THE's spar can be seen in Figure 39.

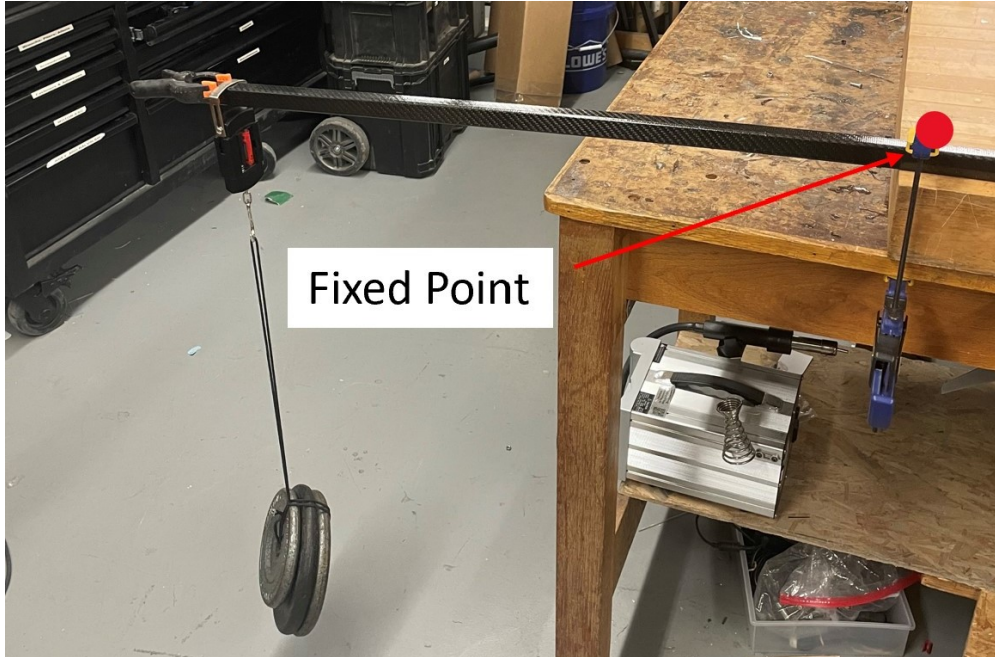


Figure 39: Spar load test

For the tail boom, a similar test was conducted, this time including the second fixed point as mentioned in Section 5.2.2. This setup can be seen in Figure 40.

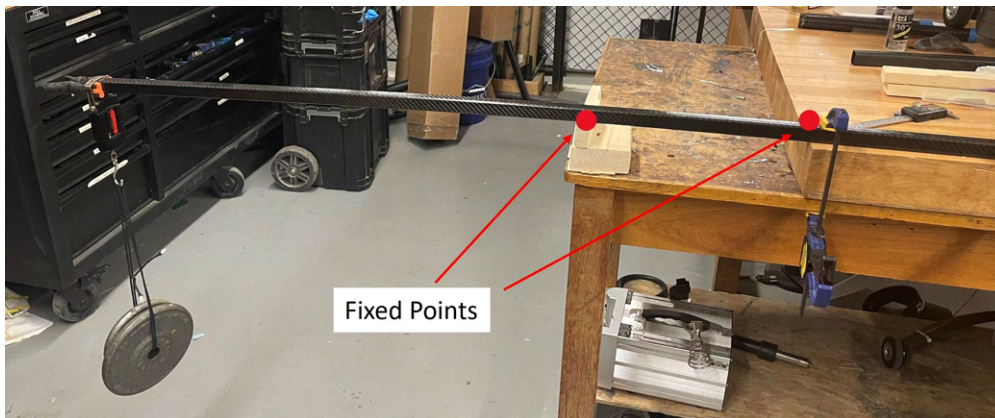


Figure 40: Boom load test

7.3 Flight Test Schedule and Flight Plan

Flight testing is crucial to the success of THE as it validates the design and build of both the airplane and sub-systems. As shown in Table 29, testing was scheduled over several months to ensure each component was successfully working as expected before improving the design for competition. Results of every test flight were evaluated using flight computer data along with pilot communication to fully understand the performance of THE.



Table 29: Flight Test Plan and Schedule

Testing Plan	Sep				Oct				Nov				Dec				Jan				Feb				Mar				Apr			
	1	2	3	4	1	2	3	4	1	2	3	4	1	2	3	4	1	2	3	4	1	2	3	4	1	2	3	4	1	2	3	4
Subsystem Testing																																
Motor and Propeller																																
Structures																																
Battery																																
AV1 Flight Test																																
Design Validation																																
Payload Flight																																
AV2 Flight Test																																
Design Validation																																
Payload Flight																																
Speed Test																																
Ground Mission																																
AV3 Flight Test																																
Design Validation																																
Antenna Flight																																
GM																																
M1																																
M2																																
M3																																
Competition Mock Flight																																
M1																																
M2																																
M3																																
GM																																

7.4 Flight Checklist

The team used a flight test checklist to ensure crew safety and proper documentation of flight test results as shown in Figure 41.

		Current Conditions														
Preflight	Date	%			Weather		%			%			%			
	Time	%			Wind Speed (kts)	%	Direction	%			Temperature	%				
	Battery	Configuration			°F	Start Voltage	Charge Cycle (amps/time)			Comments						
	Propulsion	%			%			%			%			%		
	Receiver Pack	%			%			%			%			%		
	Transmitter	%			%			%			%			%		
	Mission Profile	GND	1	2	3	Custom										
	Aircraft															
	AV #:	%			Propeller	%			# Syringes	%			Syring Weight	%		
	Mass (lb)	%			CG (in)	%			# VVPs	%			VVP Weight	%		
Flight Approvals	Chief Engineer			%	Safety Officer			%	Pilot			%				
Flight Goals																
1)	%			%			%			%			%			
2)	%			%			%			%			%			
		Test Procedure														
Flight	1. Prep aircraft per preflight Checklist															
	2. Arm, Throttle / Prop Direction / control check															
	3. Set High rate, altitude hold, climb to ~100 ft															
	a. VO Starts Timer at throttle up															
	b. PIC calls full throttle															
	4. Flaggers call passing point on radio and pilot turns (3 laps for M1/M2 and max laps for M3)															
a. PIC calls turn start & complete for turns and 360°																
b. Flaggers call after initial pass and when abeam again																
5. Attempt landing																
6. Spotter calls (min):																
		1	2	3	4	5	6	7	8	8.5	9	9.5	10	11	12	13
Flight Notes																
Post Flight																
Post Flight	Flight Notes															
	Takeoff Range		Voltage				°F	Number of Laps			Voltage Post Discharge			Flight Time		
	Battery	Voltage		°F		Cap Discharged	Voltage Post Discharge		Comments							
	Propulsion	%			%			%			%			%		
	Receiver Pack	%			%			%			%			%		
	Transmitter	%			%			%			%			%		
	Pilot's Comments															
		%			%			%			%			%		
		%			%			%			%			%		

Figure 41: Flight Test Checklist



8 PERFORMANCE RESULTS

8.1 Demonstrated Performance of Key Sub-Systems

8.1.1 Propulsion

Using the methods described in Section 7.2.1, experimental variables for static thrust, airspeed, battery voltage and endurance were obtained. These data points were compared to the MotoCalc analysis. The results for the static thrust test are shown in Figure 42.

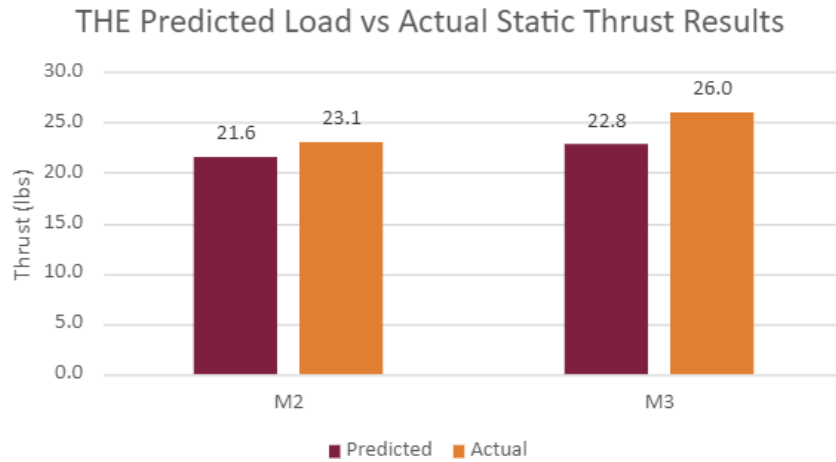


Figure 42: 2023-24 DBF @ VT Static Thrust

MotoCalc analysis slightly underpredicted the values for static thrust, which is consistent with historical DBF data. The static thrust of 23.1 lbs (102.3 N) and 26.5 lbs (117.9 N) exceed the required T/W of 1.44 for MTOW in 20.0 ft (6.1 m). Telemetry data recorded from the Spektrum GPS module indicated a maximum speed for M_2 as 120.2 ft/s (36.7 m/s) and M_3 as 105.6 ft/s (32.2 m/s).

8.1.2 Structures

The results from the physical structural testing is compared with the simulated results in Figure 43

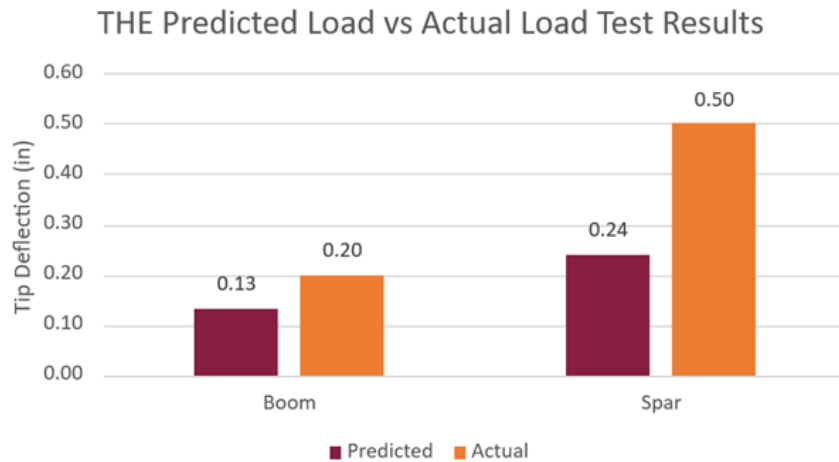


Figure 43: Predicted vs Actual Structural Test



The actual results for tip deflection were larger than expected, but were still within acceptable bounds.

8.1.3 Controllability

No issues were reported with airplane control. Control limits were never reached and the airplane handling qualities proved more than sufficient for the pilot in all flight missions.

8.2 Demonstrated Flight Performance of Completed Airplane

8.2.1 Test Matrix

Table 30 is a test matrix of all the flight tests the team has performed as of February 23, 2024. A total of 5 flight tests were performed with two air vehicles between November 2023 and February 2024. At the time of writing, AV2 has only been flight tested once. AV2 took off in 35 ft (10.7 m) at 16.77 lb (75.6 N) in the propulsion configuration for M_1 and M_3 .

Table 30: Flight Test Matrix

Vehicle Iteration	Flight Test #	# of PAX	Lap Time (s)	Flight Time (m:ss)	Objective(s)	Result
AV1	1	---	---	4:26	•Show AV1 airworthiness	•Showed the airplane to have good handling qualities and high control authority •Revealed a propeller clearance issue •Plane requires visual cues so pilot can tell orientation
	2	---	---	4:09	•Pilot Practice •Trim the airplane	•Pilot requires lower rates on the transmitter •Trim deflections found to be acceptable
	3	---	44.8	3:44	•Demonstrate M1	•Able to make 20 ft takeoff in M1 configuration
	4	52	40	1:55	•Demonstrate M3	•Plane could not takeoff in 20 ft in M3 configuration
AV2	5	---	---	1:40	•Show AV2 airworthiness •Make 20 ft takeoff	•Revealed a tail authority issue •35 ft takeoff distance at MTOW

The team tested the wing rotate mechanism after flight test to find ways to refine the design. The team found that bolts on top of the fuselage interfered with the wing rotate mechanism. The team plans to design the system with different bolts to eliminate this interference. Additionally, nuts on the inside of the fuselage broke away from the wing mount mechanism while putting the wing back into the flight configuration. The team will find a different method of holding the nuts in place for the next air vehicle. AV2 in the parked configuration is shown in Figure 44.

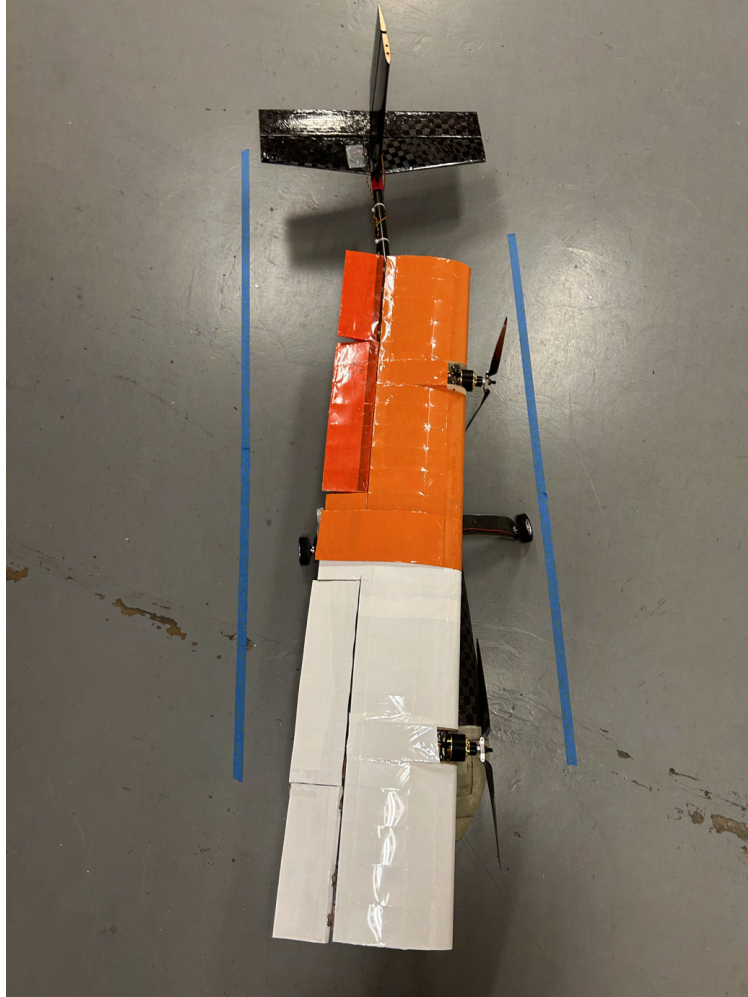


Figure 44: AV2 in the Parked Configuration

8.2.2 Flight Testing Findings

Though AV2 did not meet the takeoff requirement, the team took away some key findings from the maiden test flight. THE takes off at 21.2 mph (9.47 m/s), this value is significantly lower than the 30.0 mph (13.4 m/s) the team assumed in all performance calculations. This was determined to be a result of the combination of drooped ailerons and blown lift effect, neither of which were accounted for in analyses due to modelling complexity. During takeoff it was determined that THE had trouble rotating. An examination of the flight video revealed that as soon as the nose gear left the ground, the airplane lifted off. On takeoff, a manufacturing defect also caused THE's right flap to fail and remain deployed for the entirety of the flight.

Considering the observations from this flight test, the team determined that the high takeoff distance was due to a tail authority issue. The team plans to upsize the elevator and move the main gear closer to the center of gravity to allow for a quicker takeoff rotation. Once in the air, AV2 flew for 1 minute and 40 seconds. Post flight checks revealed that 36% of the battery capacity was used. This shows that THE has enough battery capacity to fly for 5 minutes in M_1 and M_3 . Based on these flight testing results, DBF @ VT is confident that THE will be able to successfully complete all three flight missions and produce highly competitive scores. AV2 and AV1 are shown in Figure 45.



Figure 46: Team Members at the First AV1 Flight Test



Figure 45: From Left to Right: AV2 and AV1



References

- [1] "AIAA, "2023-24 Design, Build, Fly Rules," Reston, VA, 2021. Available: https://www.aiaa.org/docs/default-source/uploadedfiles/aiaadbfr/resources/dbf-rules-2024-final.pdf?sfvrsn=a235c9f7_20. [Accessed 2023]."
- [2] The MathWorks Inc., *MATLAB*. [Online]. The MathWorks Inc., Available: <https://www.mathworks.com/>. [Accessed 2024].
- [3] "SOLIDWORKS 2023-24", Dassault Systemès SOLIDWORKS Corp. Available: <https://www.solidworks.com/>. [Accessed 2024].
- [4] "Autodesk Fusion", Autodesk Available: <https://www.autodesk.com/products/fusion-360/overview?term=1-YEAR&tab=subscription>. [Accessed 2024].
- [5] "XFLR5" [ONLINE]. Available: <http://www.xflr5.tech/xflr5.htm>. [Accessed 2023].
- [6] "'Athena Vortex Lattice," [Online]. Available: <http://web.mit.edu/drela/Public/web/avl/>. [Accessed 2023].
- [7] "M. H. Sadraey, Airplane Design, A Systems Engineering Approach, John Wiley Sons, 2013."
- [8] Flying qualities of piloted aircraft. <https://engineering.purdue.edu/>. Available: https://engineering.purdue.edu/~andrisan/Courses/AAE490F_S2008/Buffer/mst1797.pdf. [Accessed 2024]
- [9] APC Propellers Performance Data [Accessed 2024] <https://www.apcprop.com/technical-information/performance-data/>
- [10] "MotoCalc," [Online]. Available: <http://www.motocalc.com/>. [Accessed 2023].
- [11] Roskam, J. 09 Airplane flight dynamics and Automatic Flight Controls.pdf. Available: https://edisciplinas.usp.br/pluginfile.php/5616491/mod_resource/content/1/09_Airplane%20Flight%20Dynamics%20and%20Automatic%20Flight%20Controls.pdf. [Accessed 2024]
- [12] M. Müller", *eCalc - propCalc*. [Online]. Available: <https://www.ecalc.ch/motorcalc.php>. [Accessed 2023].